RECONFIGURABLE AND MULTI-FUNCTIONAL

ANTENNAS

By

GHAITH ELSANOSI M. MANSOUR

A Thesis submitted to the College of

Engineering and Physical Sciences, University

of Birmingham, for the degree of

DOCTOR OF PHILOSOPHY

School of Electronics, Electrical, & Computer Engineering,

University of Birmingham, Edgbaston,

Birmingham, B15 2TT,

U.K.

UNIVERSITY OF BIRMINGHAM

University of Birmingham Research Archive

e-theses repository

ABSTRACT

This thesis describes a research into multi-frequency and filtering antennas. Several novel antennas are presented, each of which addresses a specific issue for current and future communication systems, in terms of multi-frequency operation, and filtering capability. These antenna designs seem to be good candidates for implementation in future multiband radios, cognitive radio (CR), and software defined radio (SDR). This approach is of a great utility since it allows the wireless terminal to operate in different frequency bands. The filtering antenna provides an additional filtering action which greatly improves the noise performance and reduces the need for filtering circuitry in the RF front end.

Two types of frequency reconfigurable antennas are presented. One is tunable left-handed loop over ground plane and the second is slot-fed reconfigurable patch. The operating frequency of the left handed loop is reconfigured by loading varactor diodes whilst the frequency agility in the patch is achieved by inserting switches in the coupling slot. The length of the slot is altered by activating/deactivating the switches. The ability of theses antennas to switching between different frequencies makes them of a great utility when multiple standards/services to be performed by the same receiver.

Compact microstrip antennas with filtering capabilities are presented in this thesis. The antennas are designed, based on filter synthesis approach, to function as a bandpass filter. Two filtering antennas are presented. Whilst the first one consists of three edge-coupled patches, the second filtering antenna consists of rectangular patch coupled to two hairpin resonators. The proposed filtering antennas combine radiating and filtering functions by providing good out of band gain suppression.

DEDICATION

This thesis is dedicated to

My beloved Parents

and

My beloved Siblings

ACKNOWLEDGEMENTS

PUBLICATIONS

Journal Papers:

1. **Ghaith Mansour,** Peter S. Hall, Peter Gardner, and M.K.A Rahim "Slot-fed switched patch antenna for multiple frequency operation", Progress in Electromagnetic Research PIERS C, vol.36, pp.91-104, 2013.

2. **Ghaith Mansour,** M. J. Lancaster, Peter S. Hall, Ekasit Nugoolcharoenlap, and Peter Gardner, "Design of filtering microstrip antenna using filter synthesis approach", Submitted to Progress in Electromagnetic Research, PIERS 2013.

Conference Papers:

1. **Ghaith Mansour**, Peter S. Hall, Peter Gardner, and M.K.A. Rahim, "Switchable multiband coplanar antenna", *Loughborough Antenna & Propagation Conference LAPC, 14-15 Nov 2011*, pp.1-4.

2. **Ghaith Mansour**, Peter S. Hall, and Peter Gardner, "Circular loop antenna loaded by left handed ladder network", National Union for Radio Science URSI, Leicester, 12 January 2011.

3. **Ghaith Mansour**, Peter S. Hall, Peter Gardner, and M.K.A. Rahim "Tunable slot-loaded patch antenna for cognitive radio", *Loughborough Antenna & Propagation Conference LAPC, Nov 2012*, pp.1-4.

TABLE OF CONTENTS

LIST OF ACRONYMS

MFA	Multi-Functional Antenna
EM	Electromagnetic
AIA	Active Integrated Antenna
RF	Radio Frequency
CR	Cognitive Radio
SDR	Software Defined Radio
QoS	Quality of Service
LHTL	Left-Handed Transmission Line
RHTL	Right-Handed Transmission Line
CRLHTL	Composite Right/Left Handed Transmission Line
MTM	Metamaterial
DPS	Double Positive
ENG	ε-Negative
MNG	μ-Negative
DNG	Double Negative
UWB	Ultra Wide Band
TEM	Transverse Electromagnetic
RHCP	Right Hand Circular Polarization
LHCP	Left Hand Circular Polarization
AR	Axial Ratio
TLM	Transmission Line Model
MOM	Method of Moment
PIFA	Planar Inverted F Antenna
DVB-H	Digital Video Broadcasting Handheld
E-GSM	Extended Global System for Mobile Communications
ESA	Electrically Small Antenna
SMD	Surface Mounting Device
PCB	Printed Circuit Board
CPW	Coplanar Waveguide

MEMS	Micro Electromechanical Systems
BPF	Bandpass Filter
FBW	Fractional Bandwidth
IMD	Inter-Modulation Distortion
CQ	Cascaded Quadruplet
RL	Return Loss
VSWR	Voltage Standing Wave Ratio
BW	Bandwidth

LIST OF FIGURES

XI

XIV

LIST OF TABLES

CHAPTER I

INTRODUCTION

1.1. Background

In modern communication systems, it is required to integrate various functions into a single component to achieve requirements such as low cost, low loss, and compact size. To meet these requirements, multifunctional antennas (MFA's) have been presented. MFA can be defined as an electromagnetic (EM) radiating or receiving element that provides additional functions, which might include multiple bands, reconfiguration, filtering, and active devices. For example, a frequency reconfigurable antenna is able to tune its operating frequency over a wide bandwidth, which eliminates the need for multiple antennas dedicated to different wireless services. Thus, the cost and the size of the wireless system are reduced. Similarly, an integrated module with filtering and radiating functions will greatly simplify and reduce the size and the cost of the system. Such a module is known as a filter-antenna or 'filtenna'. The filtenna aims to exhibits superior out of band gain suppression and flat in-band gain. Thus, the need for bandpass filter in the RF front end is eliminated. Another way of achieving multifunctionality is by employing Active Integrated Antennas (AIA's) which provide built-in functions such as switching, oscillation, mixing, or amplification. These additional features can be realized by utilizing active devices in the antenna such as diodes and transistors. Reconfigurable antennas and filtering antennas are two types of multi-functional antennas that are presented in this thesis.

1.2. Frequency Reconfigurable Antennas

Reconfigurable antennas emerged many years ago and received considerable attention and innovation. Reconfiguration of an antenna is obtained by redistributing the currents in the antenna's aperture [1]. These effects are achieved by different methods such as switching and structural modifications.

To support diverse applications such as communications, surveillance, and navigation, many wireless systems require multiple antennas that work at different frequency bands and polarizations. These antennas are normally placed at different locations on a wireless platform, such as radar, or satellite base station for better communication quality [2]. The use of multiple antennas is strongly undesirable because it increases the size and the cost of the system. In addition, the electromagnetic interference between adjacent antennas may degrade the performance of the system. An antenna that can be reconfigured to provide multiple functions, such as operating in different frequencies, producing different radiation patterns or switching the polarization, will eliminate the need for multiple antennas and results in a reduction in the number of antennas used. Reconfigurable antennas can be classified based on their functions into frequency reconfigurable antennas, radiation reconfigurable antennas, and polarization reconfigurable antennas.

Reconfiguring the resonant frequency of an antenna aims to having a single multi-functional antenna that supports a small terminal for many services. The frequency reconfiguration could be achieved by changing the operating frequency of the antenna, while keeping the radiation properties unchanged. Different reconfiguration mechanisms can be used to achieve frequency reconfigurability, such as relying on movable parts such as RF micro electromechanical systems MEMS, [3] or the integration of solid state devices such as varactors and PIN diodes [4-5]. The selection

of the reconfiguration method presents a trade-offs in performance, complexity, and device lifetime.

One significant challenge that frequency reconfigurable antenna try to meet is covering several frequency bands with a single efficient antenna. Such an antenna may not cover all bands simultaneously, but it could provide dynamically selectable narrow instantaneous bandwidths and would have better efficiency than a conventional multiband or wideband antenna. Furthermore, the narrow instantaneous frequency response decreases the need for filtering in the RF front end, due to the superior out-of-band suppression it provides over multiband or wideband antennas. Thus, the antenna provides great versatility and flexibility to wireless terminal to operate in several frequency bands. In addition, it provides pre-filtering at the RF front end resulting in reduced interference levels at the receiver.

Cognitive radio (CR) is one of the applications which are driving the development of frequency reconfigurable antennas. CR systems aim to improve the utilization of the spectrum by interacting with the environment in a dynamic way [6]. It was developed to be a solution for the problem of limited spectrum resource and low efficiency in spectrum utilization. The spectrum bands are assumed to be owned by primary users and whenever these bands are not occupied, secondary users can utilize them as long as the quality of service (QoS) of the primary user is not degraded [7]. The RF architecture of the CR system, shown in figure 1.1, consists of a searching antenna that keeps monitoring the wireless channel to search for unused frequency bands, and a transmitting/receiving antenna to perform the communication within the unused channel [8]. The communicating transmit/receive antenna is required to be frequency-agile and capable of tuning its operating frequency to the selected frequency band.
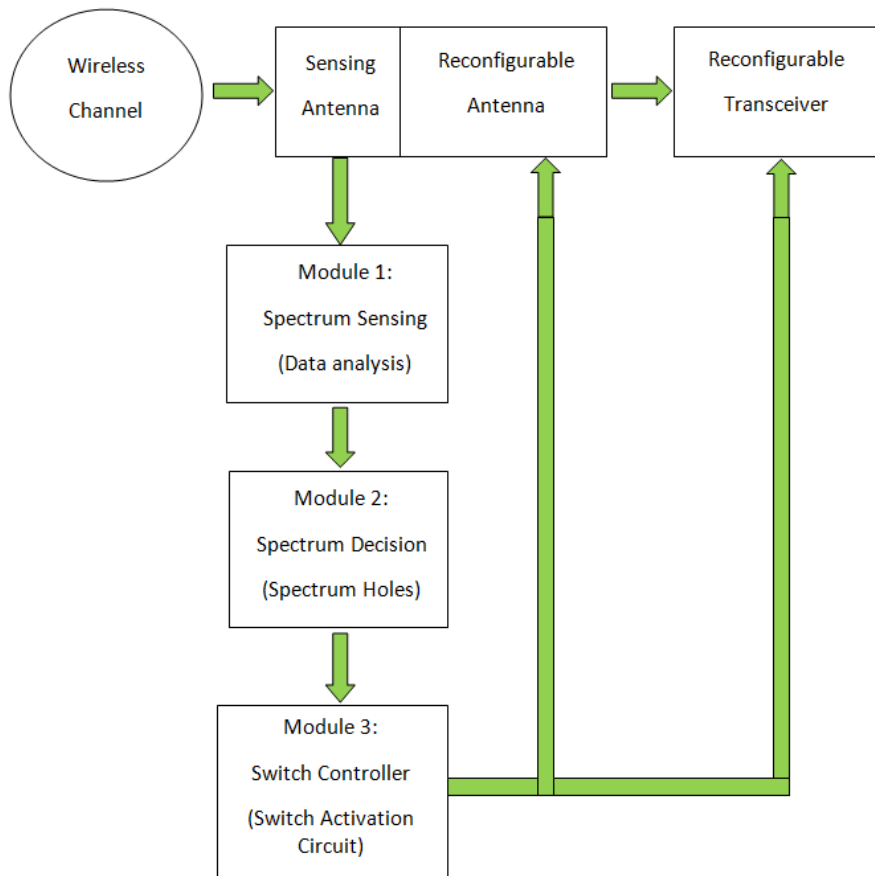
Figure 1.1: A cognitive radio system [6]

.

1.3. Filtering Antennas

The antenna and the bandpass filter are key components in the RF front end. They are conventionally designed separately and connected using 50 Ω transmission lines. The RF filter is normally placed after the antenna to reject spurious signals that are received by the antenna as shown in figure 1.2. Due to the trend to reduce the size and the cost in circuit design, it is strongly desirable to integrate the bandpass filter and the antenna into a single component that achieves filtering and radiating functions simultaneously, such filtering antenna reduces the pre-filtering requirement and improves the noise performance. In addition, the integration helps in reducing the

4

signal transmission path and therefore avoids picking up additional noise. The filtering antenna exhibits filter-like frequency response (return loss). Similarly, the realized gain of the filtering antenna is similar to the insertion loss of the filter. The frequency response of the realized gain is of an importance in the design of filtering antennas. The response is required to be highly selective with good skirt selectivity (fast roll-off) at the edges of the operating band. It is usually compared to conventional antenna in order to demonstrate the filtering capabilities. The design of filtering antenna represents trade-offs in functionality, complexity, and size. For example, a filtering antenna composed of multiple coupled resonators exhibit a lower in-band gain due to the losses of the high Q resonators. However, the high out-of band high of band gain suppression it provides often offsets the degraded in-band gain. Co-design approaches to incorporate the filter and the antenna have been presented. This integration approach reduces the size of the filtering antenna. It also reduces the transition loss between the filter and the antenna. The filtering antenna has been implemented in different topologies [9-10].
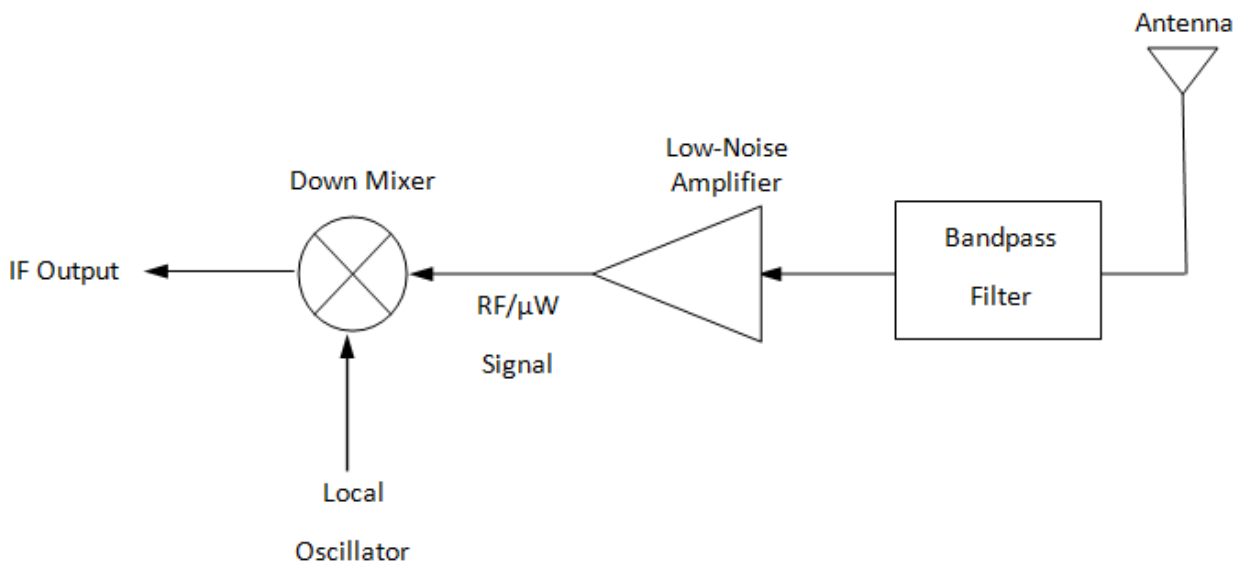
Figure 1.2: RF receiver

1.4. Objective of the Project

The primary object of this research is to design multifunctional antennas that can begin to approach the requirements for the systems described above. The work has been split into two areas as follows:

1. Design of frequency reconfigurable antennas to meet the following requirements:

    i. The antenna is able to tune its resonant frequency to different frequency bands to serve different wireless services. Thus, it eliminates the need for multiple antennas to cover each of the different services.

    ii. The antenna exhibits narrow instantaneous frequency response that is dynamically controlled. Thus, the antenna achieves the frequency agility and superior out-of-band gain suppression resulting in a reduction in the filtering requirement in the RF front end.

    iii. The antenna exhibits stable and well-shaped radiation pattern and good gain over the operating bandwidth.

    iv. The structure of the antenna is compact and small in size.

2. Design of filter-antenna 'filtenna' to meet the following requirements:

    i. The antenna exhibits flat in-band gain and superior out-of-band gain suppression such that the structure combines radiation and filtering functions into a single component.

    ii. Stable and well-shaped radiation pattern.

    iii. Compact structure and small size.

1.5. Contributions of the Thesis

Several novel antennas are presented in this thesis. These antennas address different issues for modern communication systems. The proposed switchable patches are capable of switching between wide ranges of discrete frequencies, which makes them of a great utility when multiple standards to be performed by the same receiver. Many of the reconfigurable patches presented in the literature suffer from disadvantages such as switching between limited number of frequency bands and/or unstable radiation patterns. Tunable LH over ground plane, which is another frequency reconfigurable antenna, is presented. The resonant frequency of the antenna can be tuned over a bandwidth of 1.88:1 by adjusting varactors diodes. The main disadvantage of the previously reported LH antennas is the need for a feeding balun. The balun circuit introduces additional losses and causes some spurious resonances. The LH loop presented in this thesis avoids the need for balun by using SMA connector soldered to the ground plane underneath. Compact filtering microstrip antennas are also presented in this thesis. Co-design of filter and antenna is fully described. The proposed antennas exhibit good filtering capabilities by providing superior out-of-band gain suppression.

1.6. Layout of the Thesis

The thesis is composed of six chapters. An overview of each chapter is given below:

Chapter 1 provides an introduction to the project. The systems that potentially require frequency reconfigurable and filtering antennas are discussed. In addition, the motivation and the objective of the thesis are presented.

In chapter 2 the background of multifunctional antennas is discussed. The literature review covers reconfigurable antennas and filter antennas are discussed. Previous related works are summarized and presented.

A tunable Left-Handed (LH) loop antenna over ground plane is presented in chapter 3. The antenna is loaded with three LH cells; each LH cell consists of two series capacitors and one shunt inductor. The resonant frequency can be tuned by varying the capacitance. Initially, the antenna was fabricated and measured using fixed (lumped) capacitors. Afterwards, the fixed capacitors were replaced by varactor diodes. Biasing circuitry for the varactors was designed such that the impedance mismatch and spurious radiation is minimized. In order to detune the unwanted modes, a highpass filter was designed to be integrated with the antenna.

Reconfigurable microstrip patch antennas for multiple frequency operation are presented in Chapter 4. The resonant frequency of the antenna can be easily reconfigured by utilizing switches/varactors in the coupling slot. Switchable patches using PIN diodes are designed. Three prototypes of switchable patches are presented. The first two utilize two switches and one capable of switching between two and four frequency bands respectively. The third prototype incorporates four switches and is capable of switching between ten frequency bands. A tunable patch antenna using a varactor diode is also presented. The resonant frequency of the antenna is tuned by varying the capacitance of the varactors.

Chapter 5 introduces compact filter-antennas for wireless systems. Two structures using microstrip implementation are presented. The first structure is a third order edge-coupled patches. The patches are fed using coupling a slot. The second structure was initially designed as a third order hairpin line bandpass filter. Then, the last resonator and the load resistance of the filter were replaced with a radiating patch.

The proposed structures exhibit flat in-band gain and superior out-of-band gain suppression.

In chapter 6 some important conclusions derived from the research study are summarised. Also, some possible future work is suggested.

References:

[1] Constantine A. Balanis, Modern Antenna Handbook, 2nd ED. New York, USA: John Wiley & Sons, Inc.2008.

[2] Eng Kock Lim, and Kwok Waleung, Compact Multifunctional Antennas for Wireless Systems, New York, USA: John Wiley & Sons Inc. 2012.

[3] R Al-Dahleh, C. Shafai, and L. Shafai, "Frequency Agile Microstrip Patch Antenna Using Reconfigurable MEMS Ground Plane," Microwave OPTICAL Technol. Lett., vol.43, pp64-67, October 2004.

[4] N. Behdad and K. Sarabani, "Dual-band Reconfigurable Antenna with Very Wide Tunability Range", IEEE Transaction on Antennas and Propagation, vol.52, pp.409-416, February 2004.

[5] C. Luxey, L. Dussopt, J. L. Le Sonn and J.M. Laheurte, "Dual Frequency Operation of CPW-fed antenna controlled by pin diodes", Electron. Lett.6 January 2000, vol36,pp.2-3

[6] Y. Tawk, J. Costantine, and C. G. Christodoulou, "Rotatable Reconfigurable Antenna for Cognitive Radio Applications," Radio and Wireless Symposium (RWS), pp.158-161, 16-19Jan.2011.

[7] P. S. Hall, P. Gardner, J. Kelly, E. Ebrahimi, M. R. Hamid, F. Ghanem, F. J. Herraiz-Martinez, and D. Segovia-Vargas, "Reconfigurable antenna challenges for future radio systems", Antennas and Propagation, 2009. EuCAP 2009. 3rd European Conference on 23-27 March 2009, pp. 949-955.

[8] Y. Tawk and C. G. Christodoulou, "A new reconfigurable antenna design for cognitive radio," IEEE Antennas and Propgation Letters, vol.8, 2009.

[9]   C. K. Lin and s. j. Chung, "A compact edge-fed filtering microstrip antenna with 0.2 db equal-ripple response," in Proc. 39th Eur. Microw. Cof., 2009, pp.378-380.

[10]   Wei-Jun Wu, Ying-Zeng Yin, Shao-Li Zuo, Zhi-Ya Zhang, and Jiao-Jiao Xie "A new compact filter-antenna for modern wireless communication systems," IEEE Letters on Antennas and Propagation, vol10, pp.1131-1134, 2011.

CHAPTER II

LITERATURE REVIEW

This chapter presents a review of the literature in three topic areas studied in later chapters of this thesis. Section 2.1 reviews wire antennas with left-handed (LH) loading. Reconfigurable antennas are presented in Section 2.2. The literature review of filtering antennas is presented in Section 2.3. The basic theory and parameters of antenna are presented in Appendix B.

2.1. Wire Antennas with Left-handed Loading

This section explains the theory of metamaterials and their application to wire antennas. In 2.1.1, the concepts of metamaterials and left handed transmission lines are explained. Section 2.1.2 explains the operation of wire antennas such as dipole and loop. The concept of LH loaded wire antennas along with few designs reported in the literature are presented in section 2.1.3.

2.1.1. The Concept of Metamaterials

This section explores the properties of metamaterials and the LH transmission lines.

2.1.1.1 The Metamaterials Definition and Properties

Metamaterials are electromagnetic materials fabricated to achieve unusual properties not available in nature. In figure 2.1 different materials are classified based on their constitutive parameters: permittivity ε and permeability μ [1].

Most of the materials available in nature, such as dielectric materials, have positive parameters ($\varepsilon > 0$ and $\mu > 0$). Therefore, they are called double positive materials, (DPS). Other materials which have negative permittivity and positive permeability (ε

< 0 and μ > 0) are called epsilon-negative materials, (ENG). Plasmas, for instance, exhibit these properties over certain frequency range. On the other hand, materials such as ferrites, with positive permittivity and negative permeability ($\varepsilon > 0$ and $\mu < 0$) are known as μ-negative materials, (MNG). Finally, materials with both negative constitutive parameters ($\varepsilon < 0$ and $\mu < 0$) are known as double-negative materials, (DNG). These materials are not available in nature but can be produced artificially.

It worth mentioning that electromagnetic waves can only propagate through DPS and DNG materials. In the DPS material, the magnetic field (H), electric field (E), and the propagation vector (β) form a right-handed triplet, as shown in figure 2.2a. That is why it is known as Right-handed (RH) material. In RH materials, the propagation constant β is positive which results in forward wave propagation. However, the propagation in DNG material follows the left handed rule, which implies that H, E, and β form left-handed triplet as shown in figure 2.2b. Consequently, the propagation constant β is negative ($\beta < 0$) and the wave propagation is backward. Thus, the DNG materials are called left handed materials.
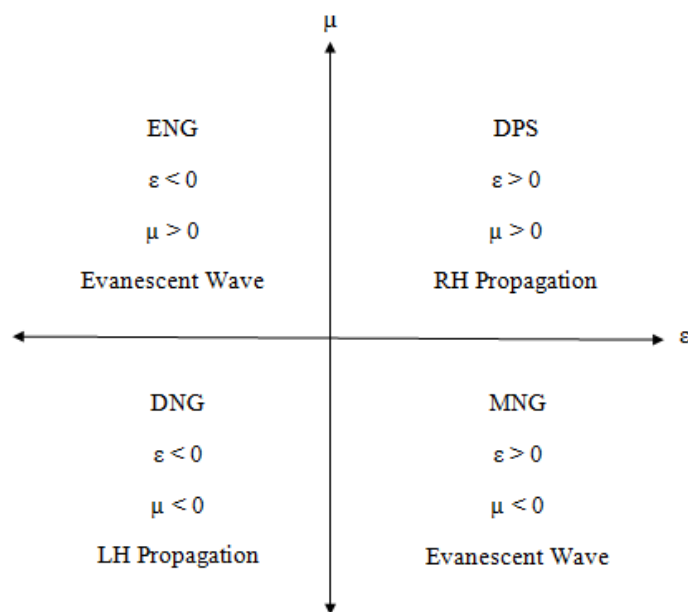
Figure 2.1: The classification of materials based on the constitutive parameters.

The history of metamaterials started in 1967 with the Russian physicist Viktor Veselago, who predicted their existence and he described them as substances with simultaneously negative values of permittivity ε and permeability μ [2]. He also studied the unusual properties of the LH materials which are:

- Frequency dispersion of constitutive parameters

- Negative refraction at the interface between LH and RH medium

- Reversal of Doppler Effect

- Reversal of Snell's law
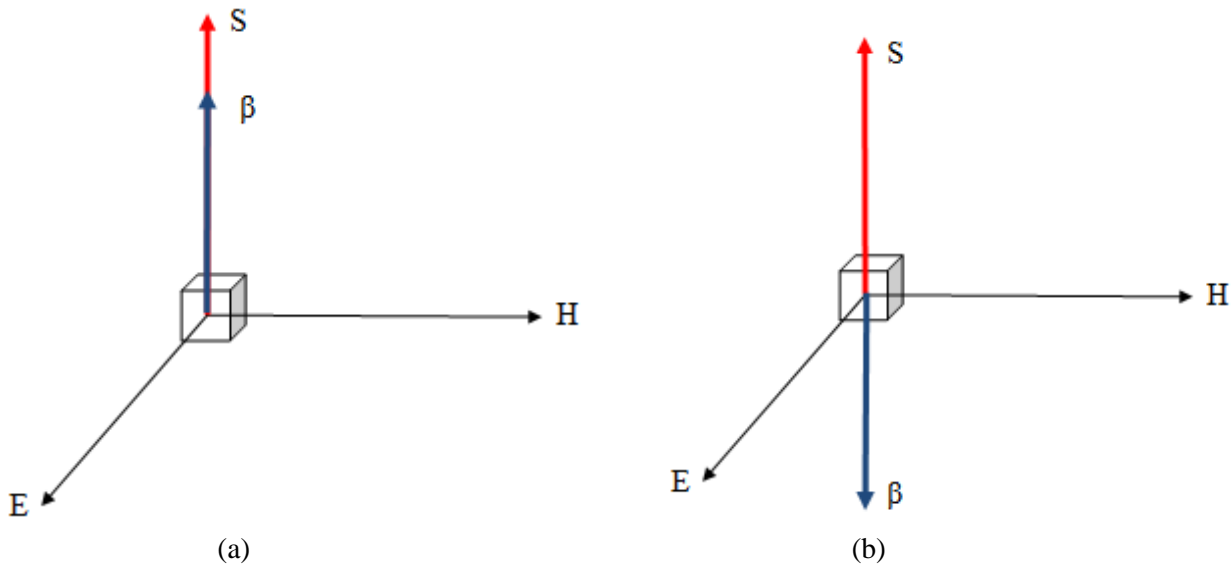
Figure 2.2: E, H, β, and S vectors: (a) RH material; (b) LH material.

2.1.1.2 Left-handed Transmission Lines

One popular approach for achieving planar metamaterials is the dual transmission line approach. It is based on line that allows the propagation of backward waves. This approach was presented in [3, 4] and has been used to develop novel microwave structures [5].

A conventional right handed lossless line can be modelled as an array of unit cells, each consists of two series inductances, L_R, and shunt capacitances, C_R, as shown in figure 2.3a. Theoretically, the dual of such cells supports the propagation of backward waves. Thus, the dual consists of series capacitances (C_L) and shunt inductances (L_L) and known as left handed transmission line as shown in figure 2.3b.
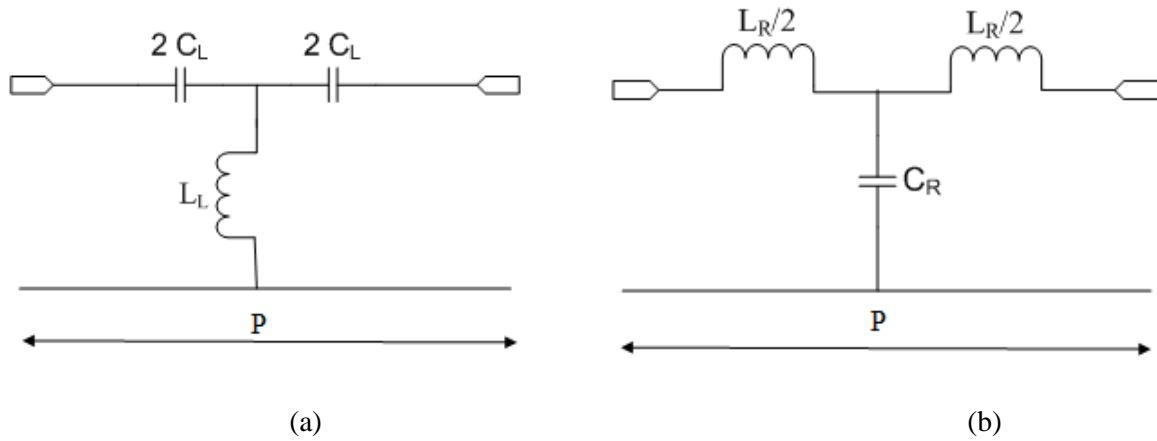
Figure 2.3: Unit cells for: (a) RH TL; (b) LH TL.

The line can be analyzed using the theory of periodic structures [6] where the structure is either infinite or has matched ports. The phase constant β and the Bloch characteristic impedance Z_B can be obtained from

$$\cos(\beta p) = 1 + \frac{Z_{sc}(\omega)}{Z_{sh}(\omega)} \tag{2.1}$$

$$Z_B = \sqrt{Z_{Se}(\omega)[Z_{se}(\omega) + 2Z_{sh}(\omega)]} \tag{2.2}$$

where Z_{se} and Z_{sh} are the series and the shunt impedances of the unit cells respectively and p is the length of its period. Thus, the parameters for the right and left handed transmission lines can be readily determined from

$$\beta_{RH} = \frac{1}{p}\cos^{-1}\left[1 - \frac{L_R\,C_R}{2}\,\omega^2\right] \tag{2.3}$$

$$Z_{BRH} = \sqrt{\frac{L_R}{C_R}}\left(1 - \frac{\omega^2}{\omega_{CRH}^2}\right) \tag{2.4}$$

15

$$B_{LH} = \frac{1}{P}\cos^{-1}\left[1 - \frac{1}{2\,L_L C_L \omega^2}\right] \qquad (2.5)$$

$$Z_{BLH} = \sqrt{\frac{L_L}{C_L}\left(1 - \frac{\omega_{cLH}^2}{\omega^2}\right)} \qquad (2.6)$$

where ω_{cRH} and ω_{cLH} are the cutoff frequencies for the right and left handed lines respectively. The cutoff frequencies are similar to those of a lowpass and highpass filters, as given in:

$$\omega_{CRH} = \frac{2}{\sqrt{L_R C_R}} \qquad (2.7)$$

$$\omega_{CLH} = \frac{1}{2\sqrt{L_L C_L}} \qquad (2.8)$$

Transmission is possible in the frequency ranges within which the phase constant and characteristic impedance are real numbers. From (2.7) and (2.8) it can be seen that the dispersion is present in both lines. However, this equivalent circuit is only valid for frequencies satisfying $\omega \ll \omega_{cRH,}$ such that the unit cell period is smaller than the guided wavelength ($p \ll \lambda_g$). Using this assumption, the expressions (2.3) and (2.4) can be approximated by the well known non-dispersive expressions

$$\beta_{RH}(\omega) = \omega\sqrt{L_R' C_R'} \qquad (2.9)$$

$$Z_{BRH} = \sqrt{\frac{L_R'}{C_R'}} \qquad (2.10)$$

where C_R' and L_R' are the per unit length capacitance and inductance of the line which can be calculated as $L_R' = L_R/p$ and $C_R' = C_R/p$. The approximation of the long wavelength limit can be applied to the LH TL

$$\beta_{LH}(\omega) = \frac{-1}{\omega\sqrt{L_L' C_L'}} \qquad (2.11)$$

and

$$Z_{BLH} = \sqrt{\frac{L'_L}{C'_L}} \qquad (2.12)$$

Where L'_L and C'_L are the inductance and capacitance of the transmission line per unit length. They can be computed as $L'_L = L_L\, p$ and $C'_L = C_L\, p$. Figure 2.4 shows the dispersion diagrams. As can be seen in the figure, the phase constant is always positive in the right handed case. However, a negative phase constant is observed in the left handed transmission line. The negative phase constant in the left handed medium explains the backward wave propagation.

The group and phase velocities of the lines can be obtained from the propagation constant:

$$v_p = \frac{\omega}{\beta} \qquad (2.13)$$

and
$$v_g = \frac{\partial \omega}{\partial \beta} \qquad (2.14)$$

For the right handed case, we find

$$v_{pRH} = \frac{1}{\sqrt{L'_R\, C'_R}} = v_{gRH} \qquad (2.15)$$

whereas the phase and group velocities in the left handed case are:

$$v_{pLH} = -\omega^2 \sqrt{L'_L\, C'_L} \qquad (2.16a)$$

and
$$v_{gLH} = \frac{1}{\omega^2 \sqrt{L'_L C'_L}} \qquad (2.16b)$$

From equation (2.15) it can be seen that the phase velocities are positive in the right handed medium. On the other hand, the phase velocity is negative for left handed medium as can be seen in (2.16a). The group velocity is positive in both mediums. The effective constitutive parameters can be calculated as:

$$\varepsilon = \frac{Y'_{sh}}{j\,\omega} \qquad (2.17a)$$

$$\mu = \frac{Z'_{se}}{j\omega} \tag{2.17b}$$

where Y'_{sh} and Z_{se} are the shunt admittance and series impedance per-unit length. The

parameters for the right handed line are:

$$\varepsilon_{RH} = C'_R \tag{2.18a}$$

$$\mu_{RH} = L'_R \tag{2.18b}$$

and for the left handed are

$$\varepsilon_{LH}(\omega) = \frac{-1}{\omega^2 C'_L} \tag{2.19a}$$

$$\mu_{LH}(\omega) = \frac{-1}{\omega^2 C'_L} \tag{2.19b}$$

From (2.19) it can be seen that the constitutive parameters are negative for the left

handed case, which shows the double negative characteristic of the medium.

(a)   (b)
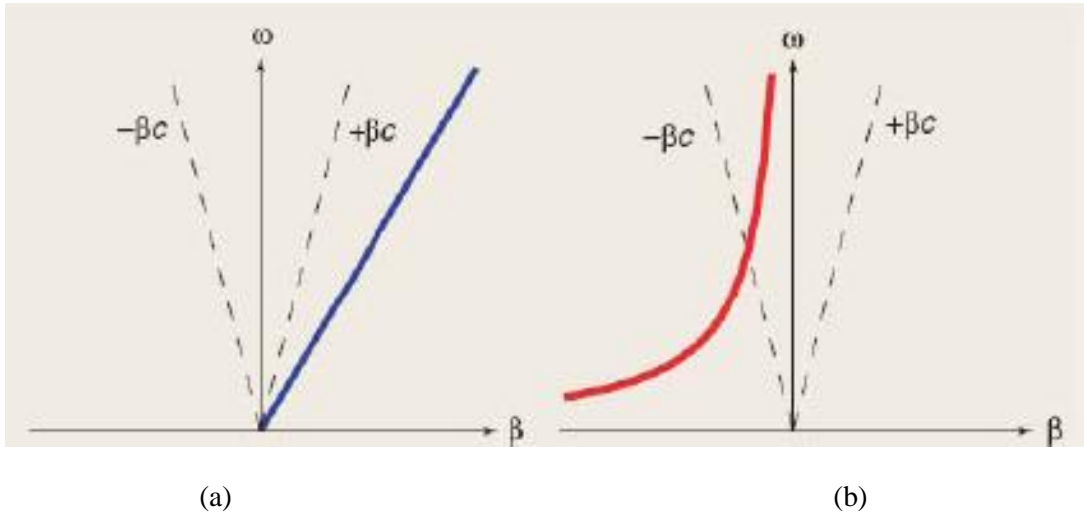
Figure 2.4: The dispersion diagram for TLs: (a) RH; (b) LH [1]

Realizing pure left handed line is not possible practically. The easiest method is by

periodically loading a conventional right handed host line with left handed unit cells

(i.e. series capacitors and shunt inductors). This structure is known as a composite

right/left handed transmission line (CRLH TL). This model was introduced in [1]. The

18

equivalent circuit for this composite line is shown in figure 2.5a. The dispersion relation can be calculated

$$\beta = \frac{1}{p}\cos^{-1}\left(1 - \frac{1}{2}\left[\frac{\omega_L^2}{\omega^2} + \frac{\omega}{\omega_R^2} - (\frac{\omega_L^2}{\omega_{se}^2} + \frac{\omega_L^2}{\omega_{sh}^2}]\right)\right) \tag{2.20}$$

where

$$\omega_R = \frac{1}{\sqrt{L_R C_R}} \tag{2.21a}$$

$$\omega_L = \frac{1}{\sqrt{L_L C_L}} \tag{2.21b}$$

are introduced for simplicity and

$$\omega_{se} = \frac{1}{\sqrt{L_R C_R}} \tag{2.22a}$$

$$\omega_{sh} = \frac{1}{\sqrt{L_L C_L}} \tag{2.22b}$$

are the series and shunt resonance frequencies respectively. The dispersion relation is shown in figure 2.5b.

The characteristic impedance of the composite line can be calculated

$$Z_{BCRLH} = Z_{BLH} \sqrt{\frac{\left(\frac{\omega}{\omega_{se}}\right)^2 - 1}{\left(\frac{\omega}{\omega_{sh}}\right)^2 - 1}} \tag{2.23}$$

Unlike the right and left handed lines, the characteristic impedance of the composite line is frequency dependent, as can be seen in (2.23). Therefore, it can be only matched at single frequency.

The effective constitutive parameters can be calculated from (2.17)

$$\varepsilon_{CRLH}(\omega) = \frac{C_R}{p} - \frac{1}{\omega^2 L_L p} = \varepsilon_{RH} + \varepsilon_{LH}(\omega) \tag{2.24a}$$

$$\mu_{CRLH}(\omega) = \frac{L_R}{p} - \frac{1}{\omega^2 C_L p} = \mu_{RH} + \mu_{LH}(\omega) \tag{2.24b}$$
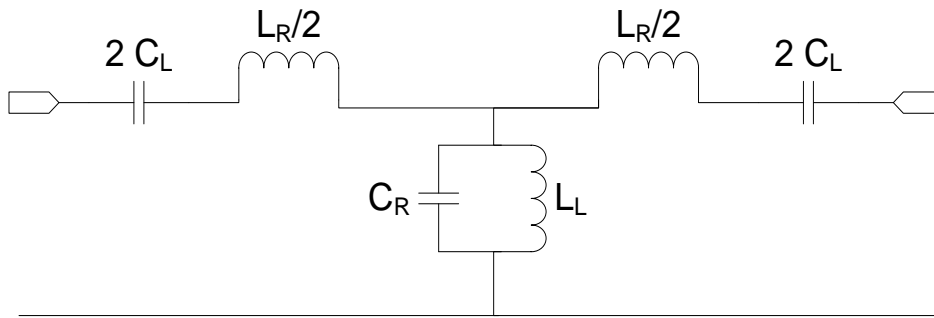
(a)
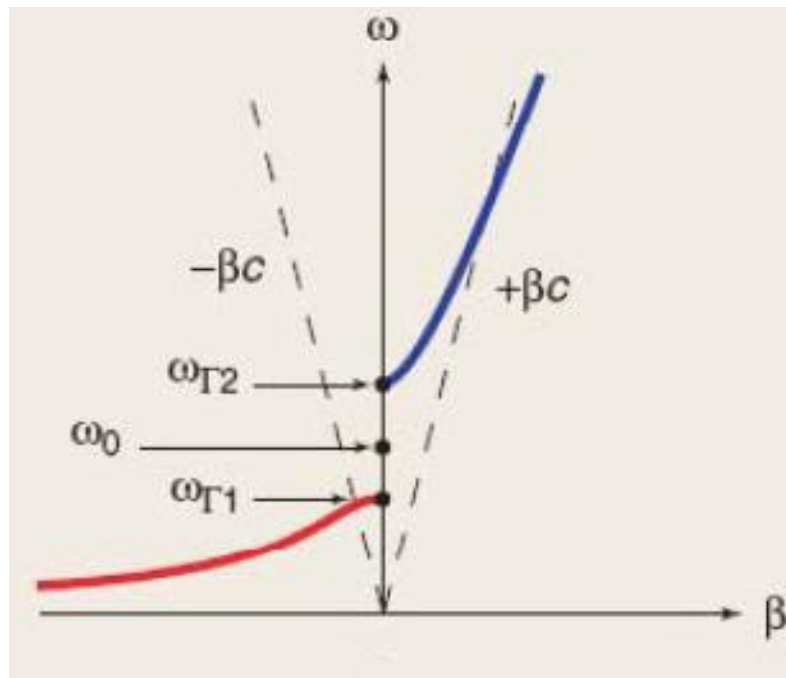
(b)

Figure 2.5: The CRLH TL: (a) an equivalent circuit;

(b) the dispersion diagram [1].

In order to realize a composite right/left handed line, a conventional host line is periodically loaded with lumped or distributed left handed components, C_L and L_L. The host line can be planar transmission line, such as microstrip line, stripline, or coplanar waveguide (CPW). The choice of lumped or distributed elements the components represents trade off in size, ease of manufacturing and performance. A

line using the geometry of a coplanar line was proposed by the group of Caloz and Itoh in 2002 [7] and it has been used in many applications such as [8]. The line is periodically loaded with interdigital capacitors and grounded stubs. While the capacitors act as series components, C_L, the grounded stubs act as shunt inductors, L_L as shown in figure 2.6. The right handed components are realized through the conventional action of the line. Thus, the capacitance C_R is provided by the plane parallel capacitor formed between the ground plane and metallization strips, and the inductance L_R is achieved by the current in the elements in the interdigital capacitor. The line, which is composed of 24 unit cells, is printed on RT Duroid substrate 5880 with dielectric constant $\varepsilon r = 2.2$ and thickness h = 1.57 mm. Parameter extraction method was used to find the left and right handed parameters for the unit cell and found to be $L_L = 3.4$ nH, $C_L = 0.7$ pF, $L_R = 2.5$ nH, and $C_R = 0.5$ pF. The dimensions of the unit cells, shown in figure 2.5 b, are: width p = 6.1 mm, $w_c = 2.4$ mm, $l_c = 5.0$ mm, $w_s = 1.0$ mm, $l_s = 8.0$, and five pairs of digits with widths 0.15 mm and spacing of 0.1 mm.
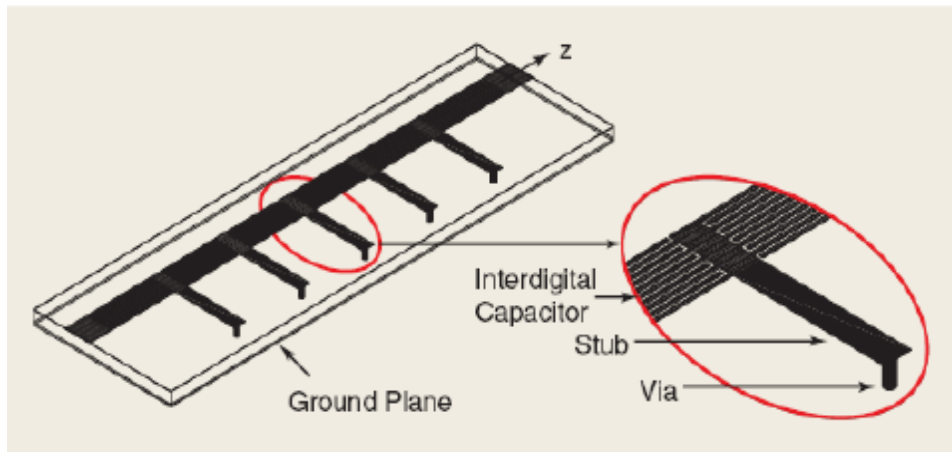
(a)
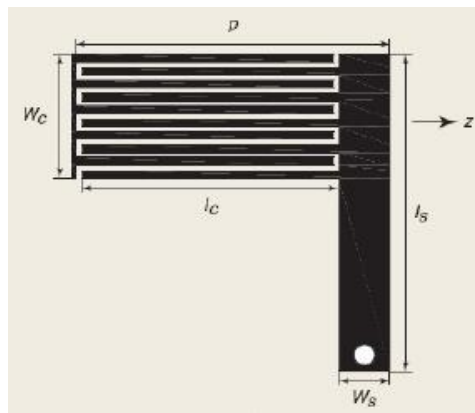
(b)
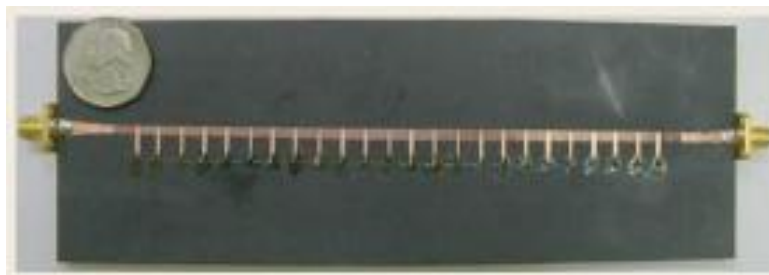
(c)

Figure 2.6: Microstrip implementation of CRLH TL [8]: (a) structure;
(b) unit cell; fabricated prototype.

A composite line implemented using coplanar waveguide was presented by Eleftheriades group at University of Toronto in [9]. Whilst the shunt inductors, L_L, were achieved by narrow lines connecting the centre conducting strip to the coplanar

ground planes, the series capacitors, C_L, were achieved by etching gaps in the CPW centre conductor as shown in figure 2.7.
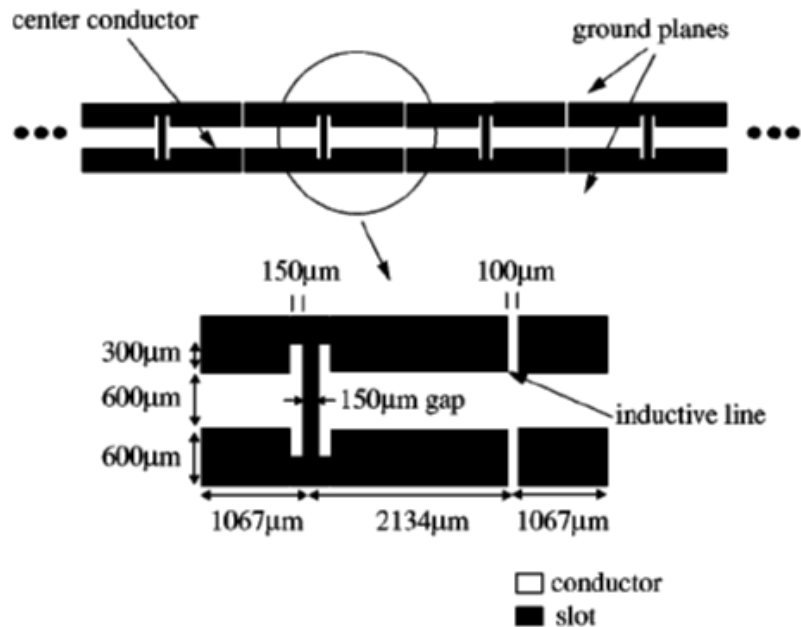
Figure 2.7: CPW implementation of CRLH TL [9]

2.1.2. Conventional Wire Antennas

Wire antennas, linear or curved, are of the simplest, oldest, and the most versatile antennas for many applications, in addition to having ease of fabrication. Examples of wire antennas include dipole, loop, monopole, helix, log-periodic dipole array (LPDA), and Yagi-Uda.

2.1.2.1 Dipole Antennas

Dipole is of the simplest and the most commonly used wire antennas. It was developed by Heinrich Rudolph Hertz around 1886 [9]. As shown in figure 2.8, the dipole consists of two equal length conducting wires. It can be considered as an open-end two wire transmission line.
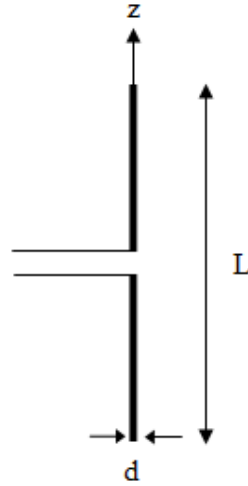
Figure 2.8: The geometry of dipole antenna.

The reflection coefficient, for an open ended transmission line, at the end is 1. The current distribution through the line can be calculated as [14]:

$$I(z,t) = \frac{1}{z_0}\left(A_1 e^{j(\omega t - \beta z)} - A_2 e^{j(\omega t + \beta z)}\right) = \frac{2}{z_0} A_1 \sin(\omega t)\sin(\beta z) \qquad (2.25)$$

This distribution is a standing wave with current peaks at $z = \lambda/4 + n\,\lambda/2$, where n is an integer. If the diameter of the dipole is very small (thin dipole), it can be approximated by this equation:

$$I(z) = \begin{cases} I_0 \sin(\beta(l - z)) & 0 \le z \le l \\ I_0 \sin(\beta(l + z) & -l \le z \le 0 \end{cases} \qquad (2.26)$$

where I_0 denotes the maximum current. Therefore, the current along the dipole is a time-varying wave. From (5.26) we conclude that the current is

- zero at the end of the dipole;

- $I_0 \sin(\beta l)$ at the feed position (centre of the dipole)

The characteristics of different length dipoles are summarized in table 2.1. The radiation pattern of an antenna can be calculated if the time-varying current is known using the equation

24

$$E(r) = -j\omega\mu \int j(r') \frac{e^{-j\beta.|r-r'|}}{4\pi\,|r-r'|}\,dv' + \frac{1}{j\omega\varepsilon}\nabla\left(\nabla\int J(r')\frac{e^{-j\beta\,|r-r'|}}{4\pi\,|r-r'|}\,dv'\right) \qquad (2.27)$$

By replacing the current density in (2.27) by (2.26) gives

$$E(r) = \left(-j\omega\mu + \frac{\nabla\,\nabla.}{j\omega\varepsilon}\right) \int_{-l}^{l} zI(z)\frac{e^{-j\beta r + j\beta z\,\cos\theta}}{4\pi r}\,dz \qquad (2.28)$$

The radiated electric filed can be obtained, after some mathematical operations, which

is

$$E_\theta \simeq j\eta\,\frac{I_0 e^{j\beta r}}{2\pi r}\left(\frac{\cos(\beta l\,\cos\theta)-\cos(\beta l)}{\sin\theta}\right) \qquad (2.29)$$

Where η is the intrinsic impedance. The electric field is shown in table 2.1.

The magnetic field can be obtained as

$$H_\Phi = \frac{E_\theta}{\eta} \simeq j\,\frac{I_0 e^{j\beta r}}{2\pi r}\left(\frac{\cos(\beta l\,\cos\theta)-\cos\beta l)}{\sin\theta}\right) \qquad (2.30)$$

Therefore, the average power density is

$$S_{avg} = \frac{1}{2}\,Re\,(E\,X\,H^*) = \hat{r}\,\frac{\eta\,I_0^2}{8\pi^2 r^2}\left(\frac{\cos(\beta l\,\cos\theta)-\cos(\beta l)}{\sin\theta}\right)^2 \qquad (2.31)$$

The radiation intensity can be obtained as

$$U = r^2 S_{av} = \frac{\eta\,I_0^2}{8\pi^2}\left(\frac{\cos(\beta l\,\cos\theta)-\cos(\beta l)}{\sin\theta}\right)^2 \qquad (2.32)$$

When βl is too small (βl < π/4), then, cos (βl) $\simeq 1 - (\beta l)^2/2$ and we have

$$\left(\frac{\cos(\beta l\,\cos\theta)-\cos(\beta l)}{\sin\theta}\right) = \frac{1}{2}\,(\beta l)^2\sin\theta$$

Therefore, for short dipole, the electric field and radiation efficiency are given by

$$E_\theta \simeq j\eta\,\frac{I_0 e^{j\beta r}}{2\pi r}\,(\beta l)\,\sin\theta \qquad (2.33)$$
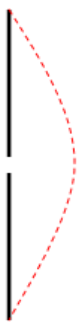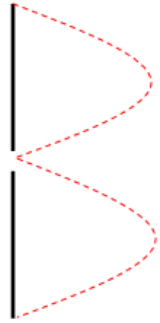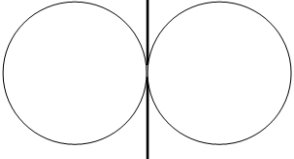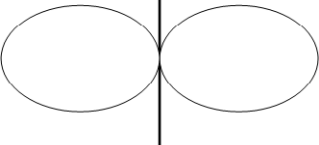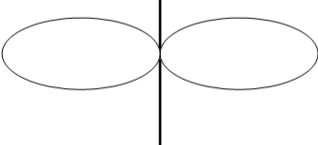
$$U = \frac{\eta\,I_{in}^2}{32\pi^2}\,(\beta l)^2\sin\theta \qquad (2.34)$$

where the input current of the dipole, I_{in}, is equal to $I_0 \sin\beta l$.

The half wavelength dipole is popular and widely used for many reasons which can be listed as [10]:

- It exhibits an omnidirectional radiation pattern in the H plane, which is desired in many wireless applications

- It exhibits a reasonable directivity (2.15 dBi)

- The input impedance is approximately 73 Ω , which can be matched to 50 Ω line

Table 2.1: the characteristics of different length dipoles

Dipole length (l)	$\lambda/10$	$\lambda/2$	λ
Current distribution			
Radiation pattern (E field)			
Directivity (dBi)	1.5	1.64	2.4
Input resistance	R: very small jx: capacitive	R: $\simeq$ 73 Ω jx $\simeq$ 0 Ω	R: $\simeq$ very large jx $\simeq$ 0 Ω

2.1.2.2 Loop Antennas

Loop is another simple and versatile wire antenna. It consists of metal wire of appropriate cross section that emits and receives radio energy. It can take different configurations such as rectangular, square, circular, and elliptical. Planar loops exhibit directional radiation patterns with a deep null which are similar to those of dipole antennas with E and H planes interchanged. While the dipole can be considered as a transmission line with an open end, the loop can be considered as a short-ended transmission line.

If the circumference of the loop is less than λ/4, it is considered as a small loop. It has been reported that a small loop is equivalent to an infinitesimal magnetic dipole which is perpendicular to the plane of the loop [10]. The small loop has large and constant current but a small voltage. Thus, it has a small input resistance. Consequently, the small loop is an inefficient radiator. Increasing the perimeter or the number of turns represent two effective strategies to increase the radiation resistance of the loop. The radiation pattern of a small loop is similar to that of a short dipole except that the polarization is in the plane of the loop. Figure 2.9 shows a loop antenna and its corresponding dipole.
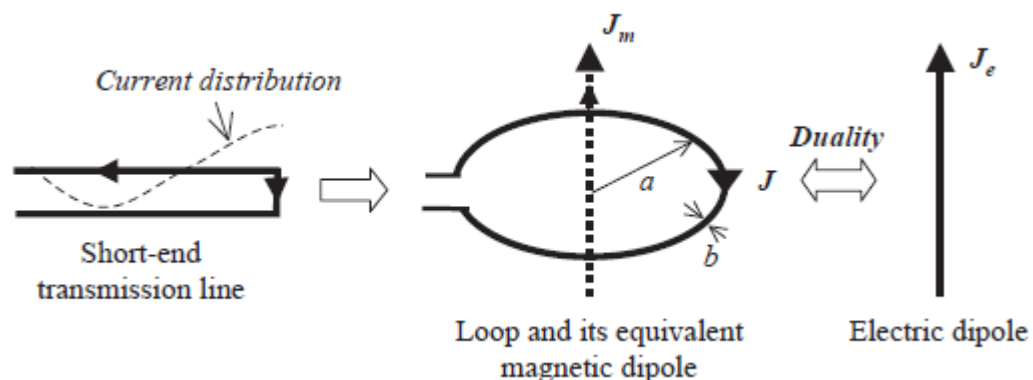
Figure 2.9: Small loop and its equivalent dipole [10].

A large loop is a multiple of a half or full wavelength. Unlike the small loop, the large loop doesn't exhibit a uniform (constant) current distribution. Therefore, it has different properties. It is been shown that when the circumference of the loop is close to the wavelength, the maximum directivity is perpendicular to the plane of the loop.

A unique loop antenna was presented by Alford in [11]. It exhibits good advantages such as good radiation efficiency, omnidirectional pattern and horizontal polarization. This was achieved by the feeding method as shown in figure 2.10. The two centre conductors are fed with currents that are equal in magnitude and opposite in direction and therefore cancel each other. Thus, the currents in the four sides will be travelling in the same direction. The loop has a uniform current distribution but large circumference of approximately one wavelength.
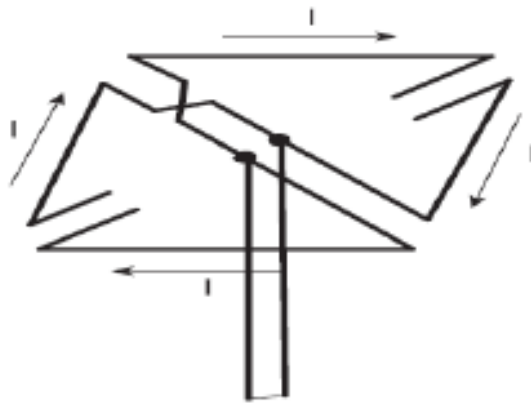
Figure 2.10: Alford loop antenna [11].

2.1.3. Left-Handed Wire Antennas

Antenna miniaturization is one of the most interesting topics in modern antenna design. Electrically small antennas, such as the dipole, are inefficient radiators because of their small resistance and large reactance. Therefore, they are difficult to match to the power source. An external circuit that matches the impedance of the antenna to the source is used [12]. However, the total size of the systems increases and the antenna can be no longer considered as electrically small. Recently, many wire antennas with left handed loading have been developed at the University of Birmingham. These antennas are electrically small, internally matched, and frequency reconfigurable. In addition, the left handed components provide new features which are described in this section.

Dipole antennas based on metamaterial lines were presented in [13-14]. The dipole is loaded by a left handed ladder network. The network is a periodic structure composed of unit cells. Each cell consists of two series capacitors and one shunt inductor as shown in figure 2.11. While the capacitors are placed in the feed side of the ladder, the inductors are placed in the interconnections between the wires. The operating frequency and the input impedance of the antenna are controlled using the loading elements (C_L and L_L), and independent of the size of the antenna. Therefore, size reduction and internal matching can be easily achieved. The relationship between the resonance number n, the length L, and the wavelength λ is given by:

$$L = n \; \frac{\lambda_a}{2} \qquad (2.35)$$

The dipole has resonant modes with negative indices. The number of the left handed modes depends on the number of the unit cells. Higher order modes appear at lower frequencies, in a way that is opposite to the conventional (right handed) modes. A dipole with N cells will have the following potential modes in the left handed region:

n = -N+1, -N+2, ..., 0. The resonant frequencies do not follow a linear ratio. A unique

feature in these antennas is that in the left handed region as the frequency decreases,

the wavelength of the current decreases.
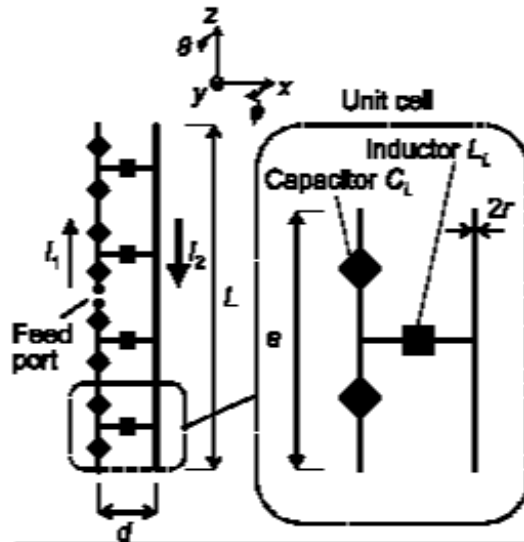
(a)
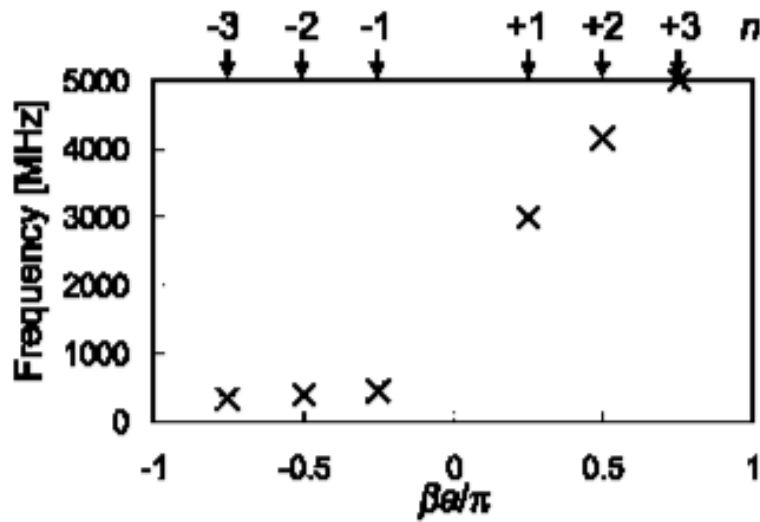
(b)

Figure 2.11: Configuration of LH dipole: (a) geometry; (b) relationship
between frequency, phase constant, and mode number [13].

30

In [13] the dipole is loaded with 4 LH cells. Three LH modes are observed which are n = -1, -2, and -3. These modes have one, two, and three standing wave peaks respectively. The n = -1 mode is well matched in this prototype. The antenna achieves a figure of eight radiation pattern.

Left handed dipoles with different implementation, based on distributed elements, were presented in [14]. They are implemented using interdigital capacitors and meandered inductors. A prototype dipole, with N = 4 unit cells, worked in the n = -1 mode, at 547 MHz, with total size of only 0.18 λ_0. The antenna has gain of – 3.9 dB and bandwidth of 1.7%. A meandered dipole, with 18 unit cells, is shown in figure 2.12a. It operates at the n = -9 mode, as shown in figure 2.12b, with a polarization orthogonal to a conventional dipole. The size of the antenna is 0.77 λ_0 at 643 MHz with a gain of -11.7 dB.

Another implementation using distributed elements is presented in [15]. While the capacitors are realized using parallel plates, the inductors are realized using spiral lines. The dipole is composed of 4 LH cells and operating in the n = -1 mode which resonates at 487MHz. The antenna has a small size of only 0.16 λ_0 at the resonant frequency. A detailed study on the efficiency of the left handed dipoles was presented in [16].

The even modes are not excited in the dipoles since they are anti-resonant and thus only odd modes are excited. In order to obtain geometry with even modes, the left handed loop antenna was developed, [17]. It is based on the same left handed unit cells used in the dipoles. As shown in figure 2.13a, the loop is loaded with 4 cells. Whilst the capacitors are placed in the outer wire, the inductors are placed in the interconnections between the wires. A balun is used in the feed network. The circumference of the loop is approximately one wavelength at 500 MHz. The n = 0

31

mode resonates at 500 MHz with a gain of 0.3 dBi and efficiency above 90%. The antenna produces an omnidirectional radiation pattern in the plane of the loop. For a loop with N unit cells, the excited modes are n = -N, -N+2, ..., -0, +2, ... A varactor loaded loop, in which the chip capacitors were replaced by varactor diodes, was also presented, [18-19]. This approach enables switching between the n = 0 and n = +2 modes at the same frequency (546 MHz) which results in two orthogonal radiation patterns.

(a)

(b)
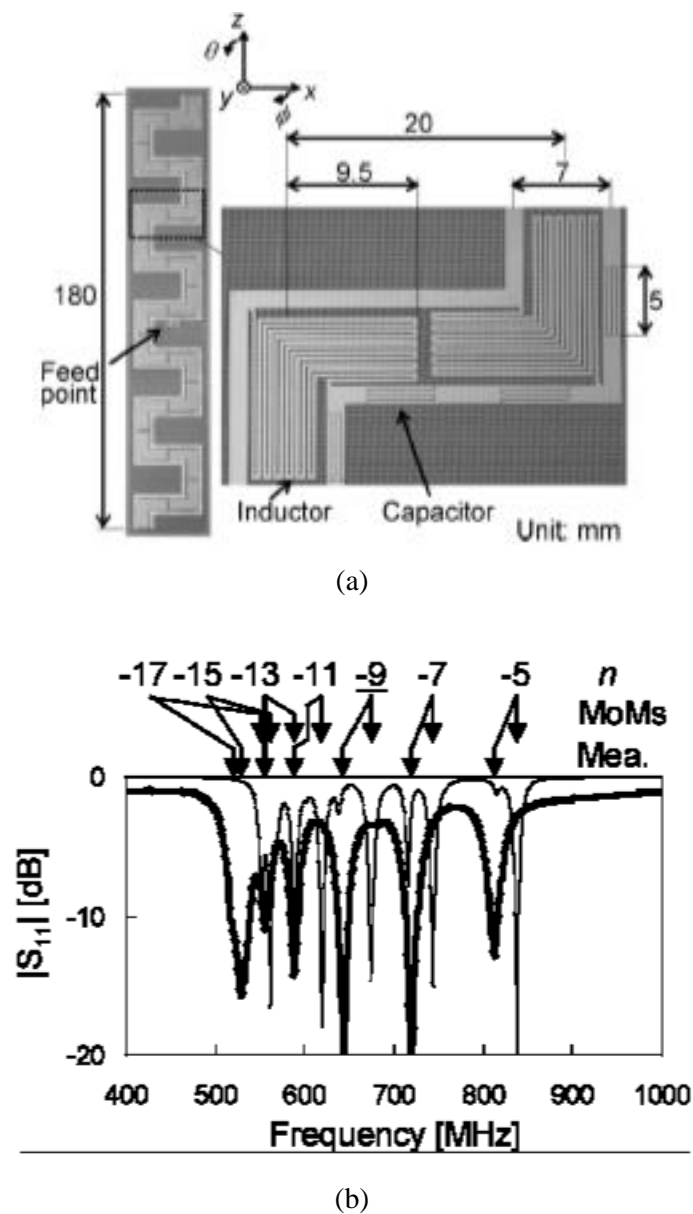
Figure 2.12: Printed meandered LH dipole: (a) configuration;
(b) measured reflection coefficient [14].
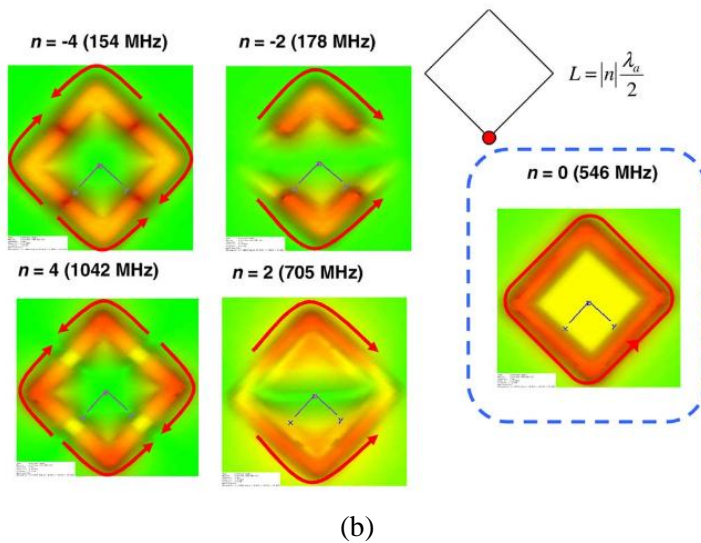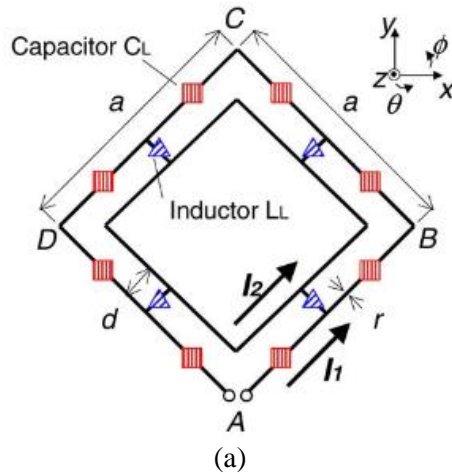
Figure 2.13: LH loop antenna: (a) configuration;
(b) current distribution for even modes [17].

The main disadvantage of the antennas discussed above is the need for a feeding balun. The balun circuit introduces some additional losses, causes some spurious resonances, and increases the total size of the antenna. In order to avoid the use of the balun, left handed loop and monopole antennas mounted over a ground plane have been presented, [20].

The left handed monopole is formed of two parallel lines printed on a dielectric substrate, mounted over a ground plane, as shown in figure 2.14a. While the outer conducting strip is connected to the feed, the other one is shortened to the ground. The

antenna is composed of two LH cells. The input impedance and the resonant frequency are controlled using the loading elements (inductors and capacitors). Each mode in the monopole corresponds to a standing wave on the monopole that satisfies the conventional resonance numbering relationship of equation (2.30). The $n = -1$ and $n = -3$ modes are excited in the monopole, which have current distribution of one and three quarter wavelengths, respectively. Both modes produce an omnidirectional radiation pattern. The $n = -1$ mode can be tuned by varying the capacitors. The resonant frequency decreases from 0.87 GHz to 0.7 GHz as the capacitance C_L is increased from 0.5 pF to 5.0 pF as shown in figure 2.14b.
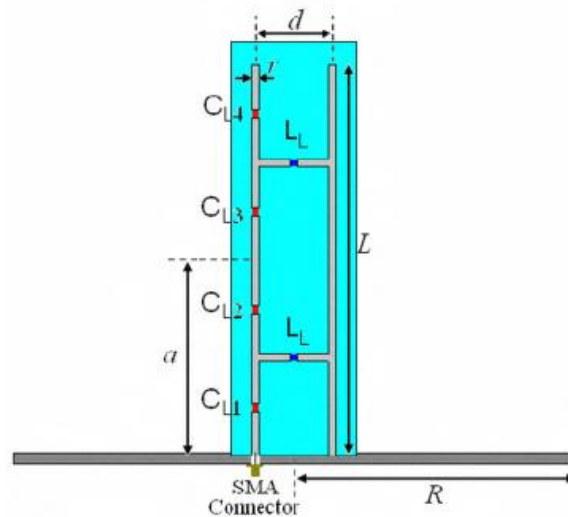
(a)
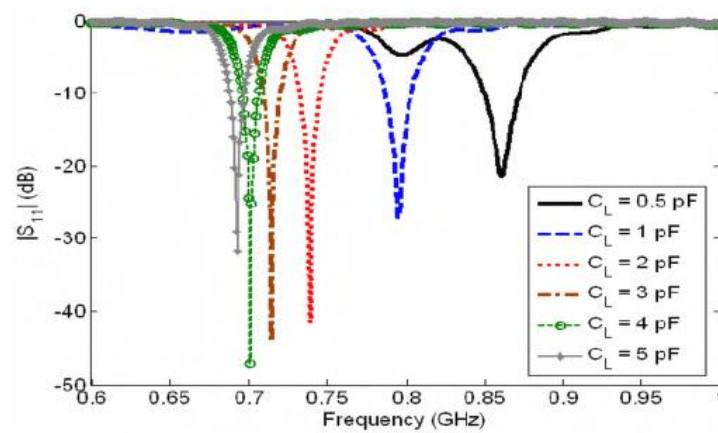
(b)

Figure 2.14: LH monopole over ground plane: (a) configuration;
(b) S_{11} for different values of C_L [20].

34

The left half-loop over a ground plane is shown in figure 2.15a. It consists of two strips that are folded and short-circuited. While one end of the outer strip is connected to the feed, the other end is shortened to the ground. The inner strip is connected to the ground. The even modes, -6, -4, -2, 0, .. are excited. The resonant frequency of the n = 0 mode is well matched over wide range and can be tuned by varying the loading capacitance as shown in figure 2.15b. The achievable tuning range is 1.6:1 considering the -10 dB matching.
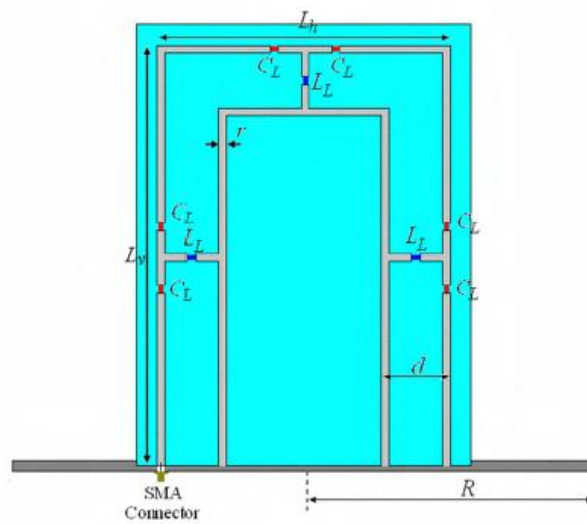
(a)
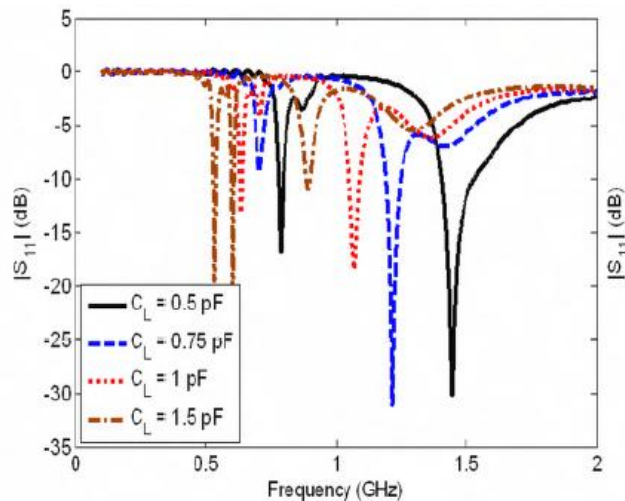
(b)

Figure 2.15: Tunable LH loop over ground plane: (a) configuration;
(b) reflection coefficient for different values of C_L [20].

In order to achieve electronically tunable antennas, the left handed monopole and half-loop have been implemented using varactor diodes [21]. The capacitors were replaced by varactor diodes which represent voltage controlled capacitance. Also, biasing circuitry was included in the design to control the varactors.

2.2. *Reconfigurable Antennas*

Reconfigurable antennas have emerged many years ago and have received great attention. Reconfiguration can be achieved by re-distributing the currents on the antenna or the electromagnetic fields in the antenna's aperture. There are different mechanisms to achieve reconfigurability such as switching and material tuning [22]. Practically, the additional capabilities the reconfigurable antennas support should offset the complexity and the cost of the reconfiguration. Application systems that drive the development of reconfigurable antennas include Cognitive Radio (CR), multi-functional wireless devices, and ultra-wideband (UWB) systems. The development of the reconfigurable antenna is highly dependent on the performance of the semiconductor diodes and switches. This section addresses the operation of reconfigurable antennas and it also presents some case studies to show the potential of such antennas.

2.2.1. Pattern Reconfigurable Antennas

Radiation pattern reconfigurability represents an effective strategy to reinforce the signal in the desired directions. In addition, noise and electronic jamming can be avoided by utilizing a pattern reconfigurable antenna.

Employing an array of antennas (e.g. phased array) is a common method to achieve radiation pattern manipulation. Figure 2.16 shows an array of N elements. The

elements have the same amplitude but different phase where each succeeding element has β progressive phase lead current excitation relative to the proceeding one.

By multiplying the array factor F of the isotropic source by the field of single element, The total field can be obtained. The array factor, F, is given by [23]

$$F = 1 + e^{+j(kd\cos\theta+\beta)} + e^{+2j(kd\cos\theta+\beta)} + \dots. + e^{+j(N-1)(kd\cos\theta+\beta)} \qquad (2.36)$$

where K is the wave vector of the incident wave, β is the phase excitation difference, and d is the separation of elements. The field can be controlled by adjusting the d and/or β. Therefore, the radiation pattern reconfigurability can be achieved.
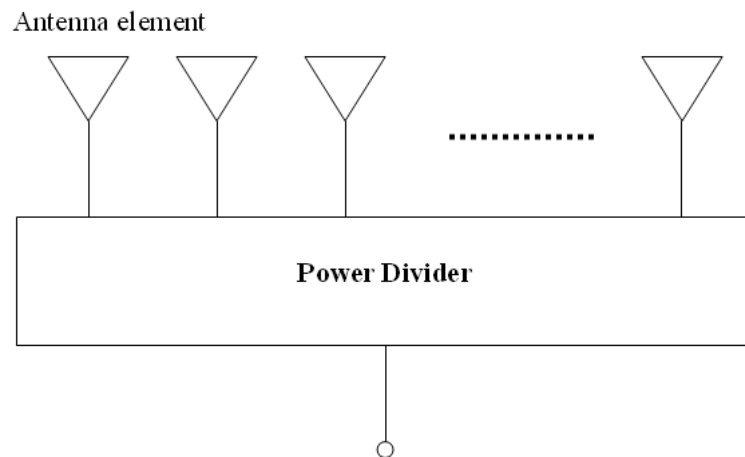
Fig. 2.16 Structure of N-element linear array

An electrically small pattern reconfigurable Yagi antenna is presented in [24]. It consists of a driver and two directors which are located at opposite sides of the driver as shown in figure 2.17a. The pattern can be controlled by using two PIN diodes with one PIN diode at the bottom of each director. The operation is based on activating at time. If switch one is activated, the beam will be steered towards the direction of director 1. When the switch 2 is activated, the beam will be steered towards director 2 as shown in figure 2.17b

(a)

— switch 1: on, switch 2: off
--- switch 1: off, switch 2: on
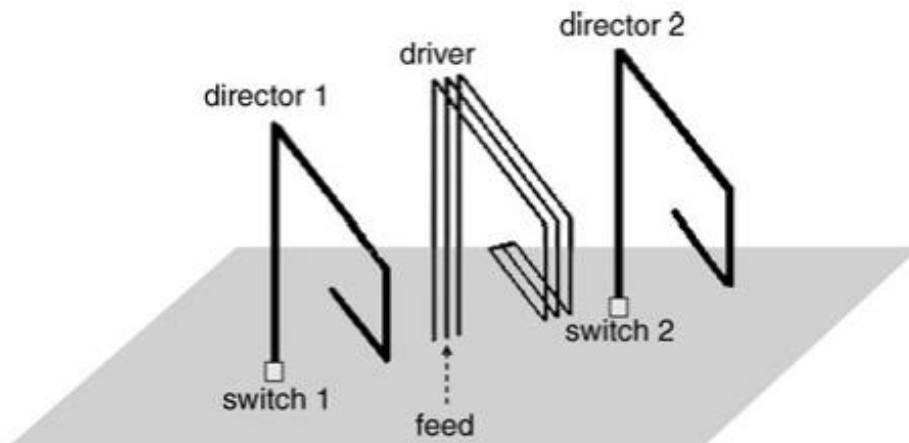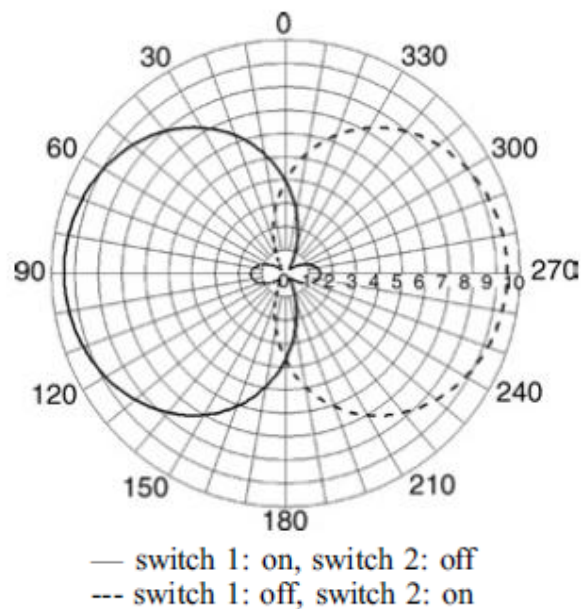
(b)

Figure 2.17: Pattern reconfigurable Yagi antenna: (a) the structure; (b) the radiation patterns

In azimuth plane [24]

Another simple pattern reconfigurable antenna is presented in [25]. The antenna, shown in figure 2.18, is a combination of monopole and dipole antennas. By controlling three switches which are utilized in the antenna, the antenna can operate as either monopole with omnidirectional pattern or dipole with directional pattern.

(a)

(b)
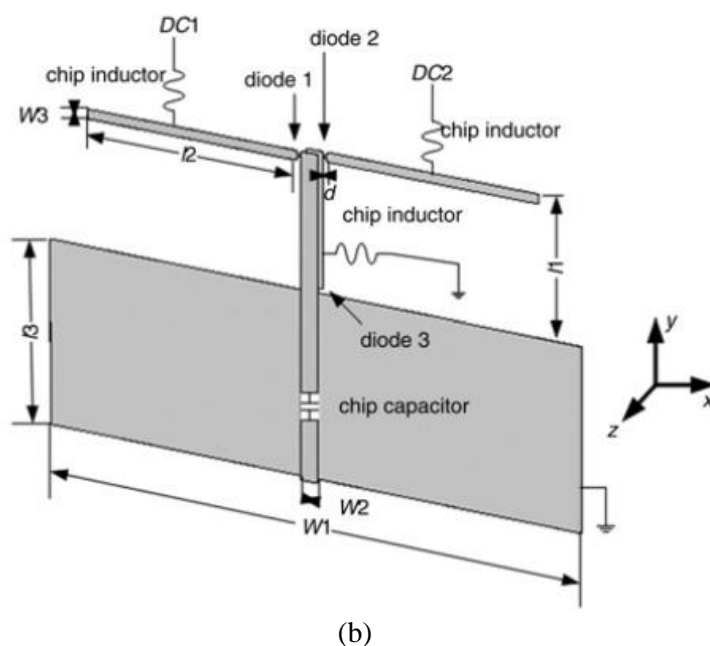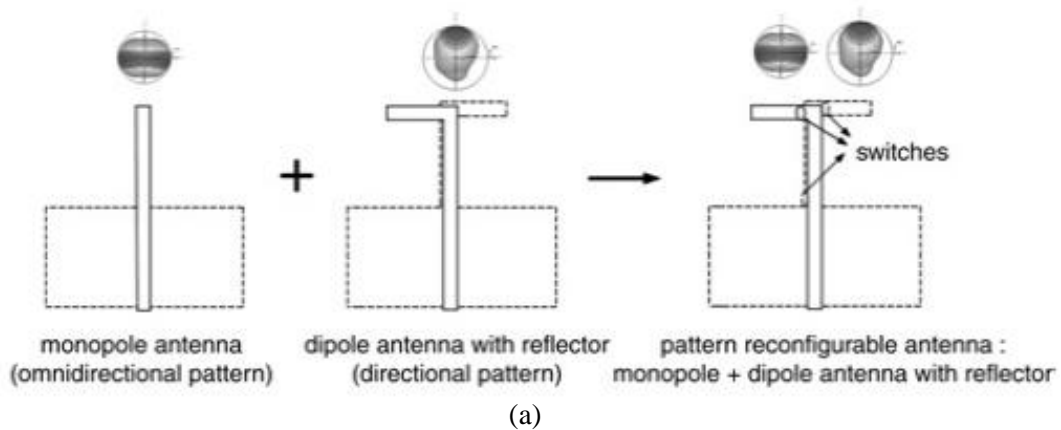
Figure 2.18: Pattern reconfigurable antenna: (a) different operations.
(b) Structure of the antenna [25].

A radiation reconfigurable wideband circular array antenna is presented in [26]. It consists of an array of eight TEM horns fed through eight reconfigurable bandstop filters and a power splitter, as shown in figure 2.19a. The TEM horn array is shown in figure 2.19b. When all ports are excited by the same signal (amplitude and phase), the antenna produces an omnidirectional pattern. However, a pattern notch is created when an element is disconnected as shown in figure 2.19c.

(a)

(b)
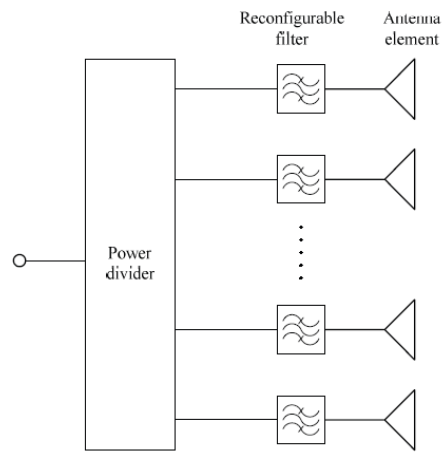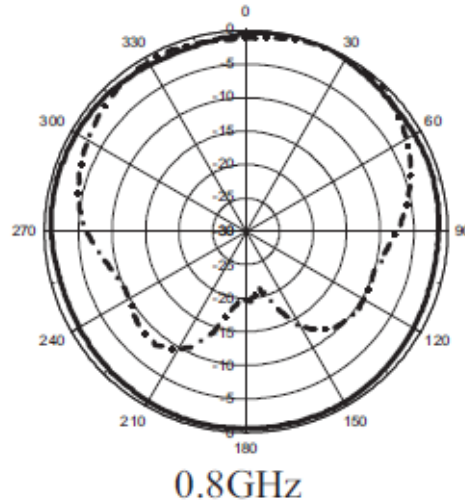
0.8GHz

(c)

Fig. 2.19: Pattern reconfigurable wideband circular array antenna:

(a) the antenna fed through reconfigurable bandstop filter;

(b) prototype of the TEM circular array; (c) measured radiation pattern at 0.8 GHz [26].

2.2.2. Polarization Reconfigurable Antennas

Polarization reconfigurable antennas are used to mitigate the fading caused by multipath propagation environment. They have found application in applications such as adaptive multiple-input multiple-output which allows the dynamic change of the radiating properties of each antenna according to the fast changing channel conditions. A polarization reconfigurable patch is presented in [27]. The patch, with a single feed, is capable of achieving right hand circular polarization (RHCP) and left hand circular polarization (LHCP). Two orthogonal slots are etched in the patch and two PIN diodes are inserted in the slots as shown in figure 2.20. By controlling the switches the antenna can switch between RHCP and LHCP. The operating frequency of the antenna is at 4.64 GHz with a 3-dB axial ratio bandwidth of 3%.
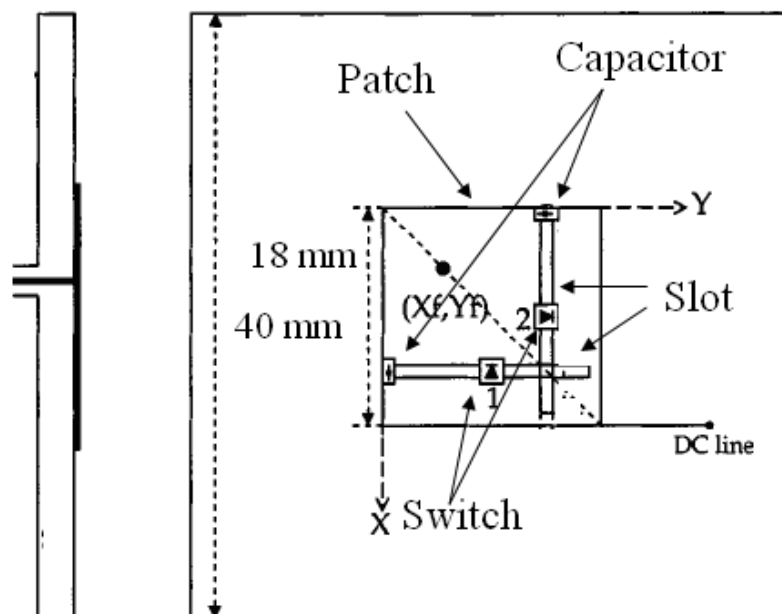
Fig. 2.20 Structure of a patch antenna with switchable slots
for RHCP/LHCP [27]

Another polarization reconfigurable antenna is presented in [28]. The antenna consists of a circular patch fed by an open-end coplanar waveguide (CPW) through a diagonal slot. Two PIN diodes are inserted across the coupling slots which have 45° inclination to the CPW open end, as shown in figure 2.21. A bias voltage is applied through the divided ground plane and DC isolation capacitors are soldered across the slits. By activating one pair of switches at time, the antenna can switch between RHCP and LHCP. The antenna resonates at 5.8 GHz with a measured 3 dB axial ratio bandwidth of 1.8%.

(a)

(b)
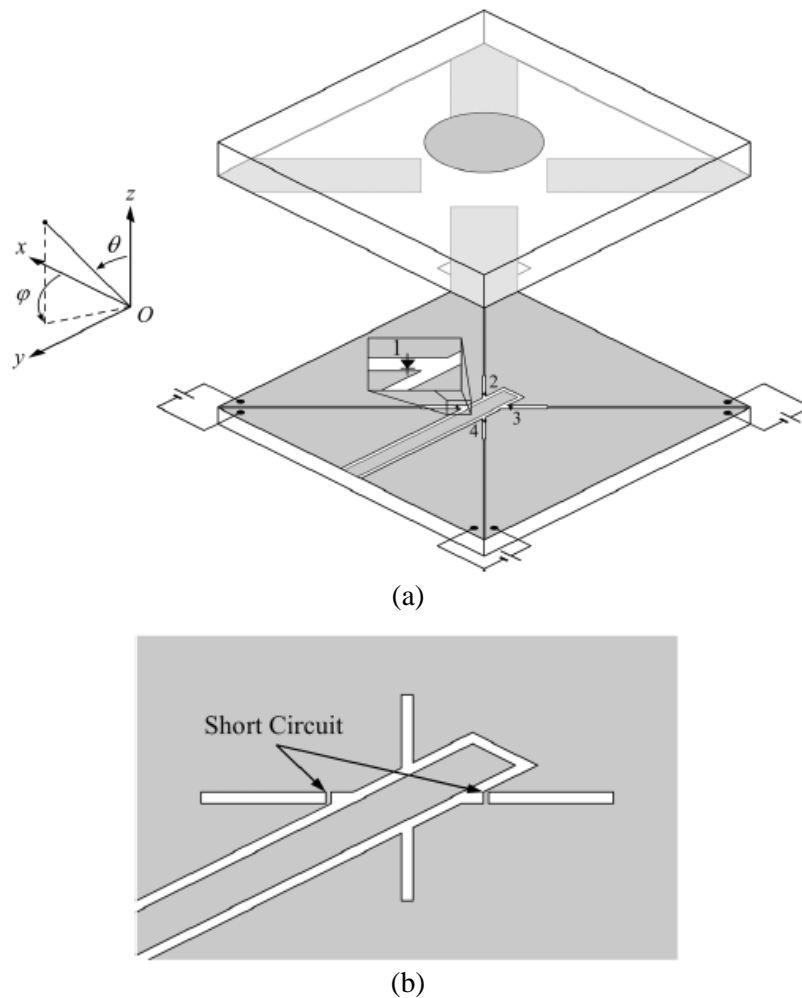
Figure 2.21: Polarization reconfigurable circular patch: (a) structure of the antenna; (b) location of the short circuit [28].

2.2.3. Frequency Reconfigurable Antennas

Due to the rapid development of the wireless communications industry, mobile wireless terminals are required to cover multiple services scattered over wide frequency range. In order to support these services, wideband antennas which cover all frequency bands can be used. However, this solution suffers from drawbacks. Firstly, the wideband antenna can't be miniaturized because the bandwidth is limited by the physical dimensions according to the well known relationship between Q and bandwidth. Secondly, since the antenna receives unwanted frequencies, a filtering network will be required. In addition, there is a variation in the radiation properties over the wide operating frequency range. On the other hand, a frequency reconfigurable antenna appears as a promising solution to this problem. Although the reconfigurable antenna can't cover all bands at the same time, it will provide dynamically selectable narrow bandwidths. The narrowband instantaneous frequency response reduces the filtering requirement in the RF front end. The frequency reconfigurable antenna is thus capable of changing the resonant frequency while maintaining continuity in the other parameters such as radiation pattern and polarization.

The frequency reconfigurability can be enabled by using different mechanisms, such as material tuning and switching. System control is then applied to reconfigure the resonant frequency. The selection of reconfiguration method presents trade-offs in performance, complexity, and cost. The functionality that the frequency reconfigurable antenna provides should offset the complexity and the cost of the reconfiguration. There are many ways for achieving the frequency reconfigurability, including:

- Switching between different external matching circuits

- Changing the properties of the substrate (i.e. the permittivity or the height)

- Utilizing switches/varactors to alter the resonance length

- Mechanical reconfiguration, such as RF MEMS

2.2.3.1 Frequency Reconfigurable Antennas using Switches

In the early days, semiconductor switches were not available. Therefore, reconfigurable antennas were fabricated using mechanical switches. Due to the rapid development of semiconductor and photoconductor technologies, reconfigurable antennas can now be easily manufactured using one of these switches. To achieve frequency reconfigurability, switching components are used. The PIN diode is the most commonly used switching device. It has several advantages such as good reliability, low insertion loss, high switching speed, small size, and low cost. The operation of the PIN diode requires a dc bias voltage to control it. Figure 2.22 shows the equivalent circuit of the PIN diode in the on and off states. When it is turned on (forward biased), it can be represented by a forward resistance R_S and a package inductance L_S. As shown in figure 2.22, the reverse biased PIN diode (off state) can be represented by a large reverse resistance R_P and a capacitance C_T. The on and off states of ideal switches are short and open circuits respectively. The quality factor (Q) of the PIN diode decreases as the frequency increases. Therefore, the switch exhibits higher insertion loss at higher frequencies, which can degrade the gain of the reconfigurable antenna.

A switchable slot antenna was presented in [30]. The antenna consists of an S-shaped slot fed by a microstrip line, printed in the opposite side of the dielectric substrate, as shown in figure 2.23. The slot is loaded with a series of PIN diode switches in order to change its effective electrical length and therefore tune the operating frequency.

Four switches are inserted across the slot to tune the resonant frequency from 540 MHz to 950 MHz. When any switch is activated, the slot is shortened at the position of that switch, resulting in decreased the slot length and increased resonant frequency. Table 2.2 shows the measured and calculated resonant frequencies for different switch states.

(a)

(b)
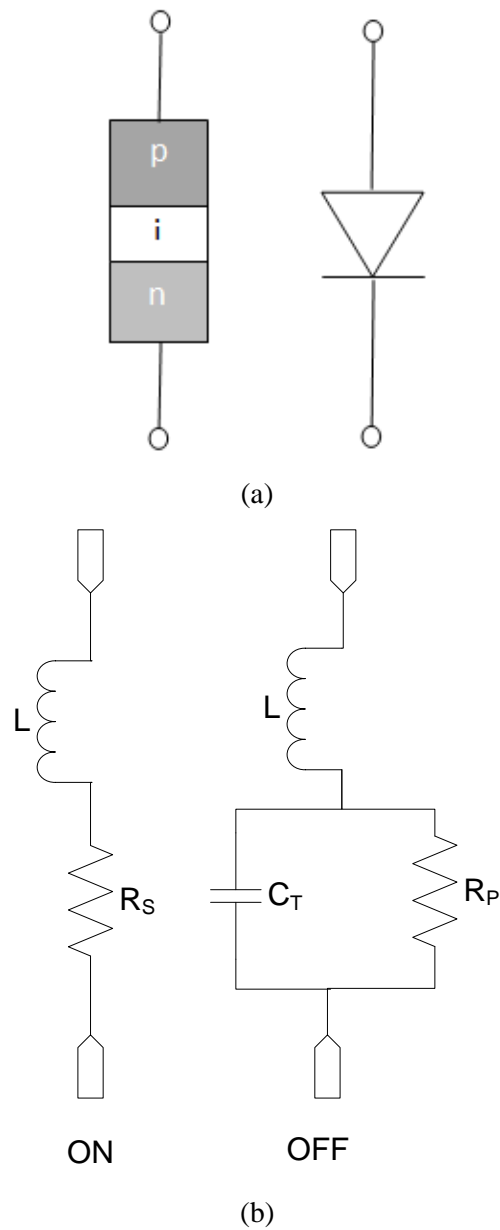
Figure 2.22: The PIN diode switch (a) structure and symbol; (b) equivalent circuit [29]
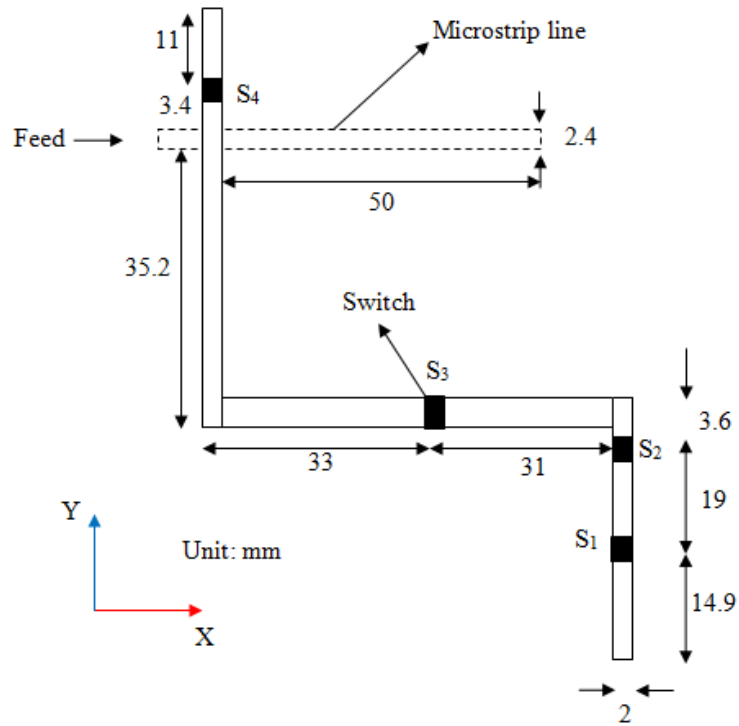
Figure 2.23: The switchable S-shaped slot antenna [30].

Table 2.2: The measured and simulated resonance frequencies of the switchable
S –shaped slot antenna [30]

TLM Fr (MHz)	MOM Fr (MHz)	Measurement Fr (MHz)	Switch configuration
542	561	537	1, 2, 3 = OFF 4 = ON
596	627	603	1, 4 = ON 2, 3 = OFF
688	711	684	2, 4 = ON 1, 3 = OFF
1002	950	887	2, 3 = ON 1, 4 = OFF

A frequency reconfigurable Yagi antenna was presented in [31]. The antenna is capable of switching the resonant frequency between 2.4 GHz and 5.78 GHz frequency bands.

46

Initially, two independent Yagi antennas operating at these frequencies were designed separately. Afterwards, the two antennas were superimposed in the same plane in order to achieve reconfigurable Yagi using switches as shown in figure 2.24. When the switches are off (on), the antenna operates at 5.78 (2.4) GHz.
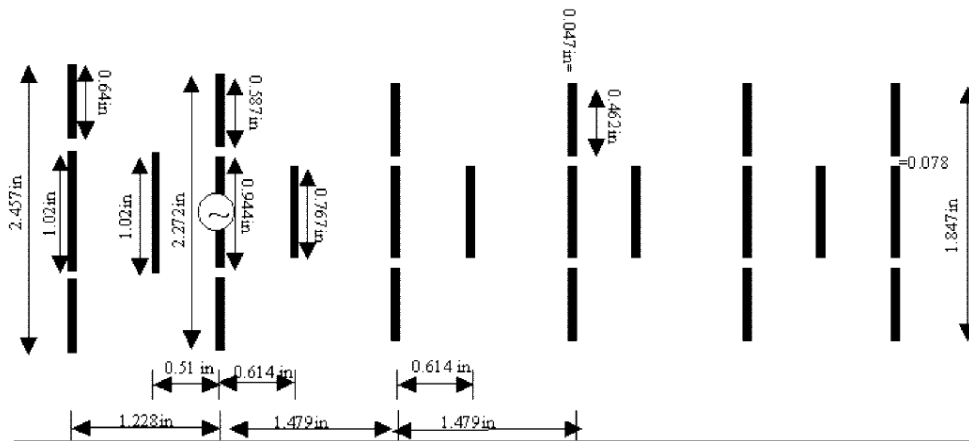
(a)
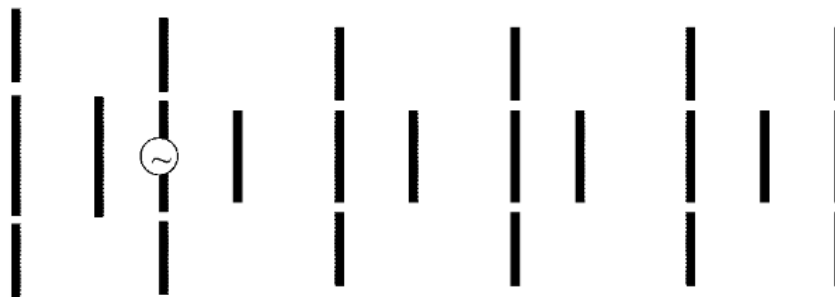
(b)
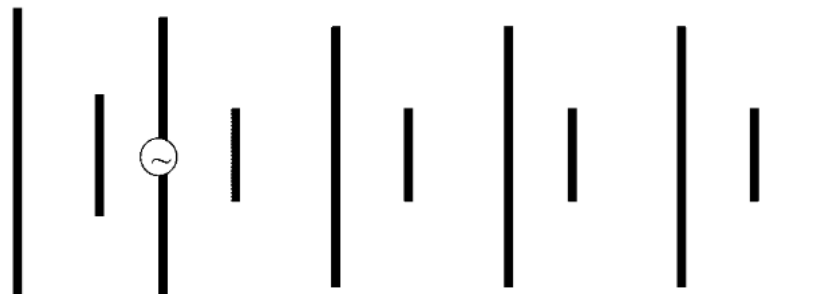
(c)

Figure 2.24: The reconfigurable Yagi antenna: (a) geometry;
(b) Yagi at 2.4 GHz with switches on; (c) Yagi at 5.78 GHz switches off [31].

47

An interesting switchable patch antenna is presented in [32]. The antenna is a circular patch with a sectoral slot of an angle of 30°. The slot is shunted at different positions using PIN diodes as shown in figure 2.25a. The resonant frequency of the antenna can be switched between three distinct frequency bands depending on the states of the PIN diodes as shown in figure 2.25b. When both diodes are off, the antenna resonates at 1.78 GHz. When diode 1 is on, the antenna resonates at 2.065 GHz. When both diodes are on, the antenna resonates at 2.29 GHz.
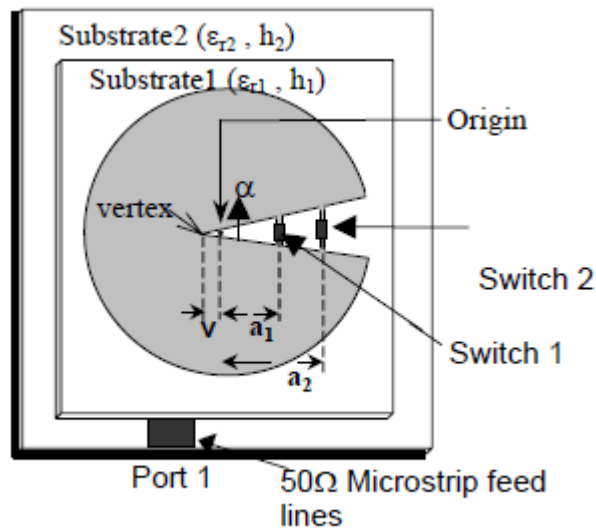
(a)
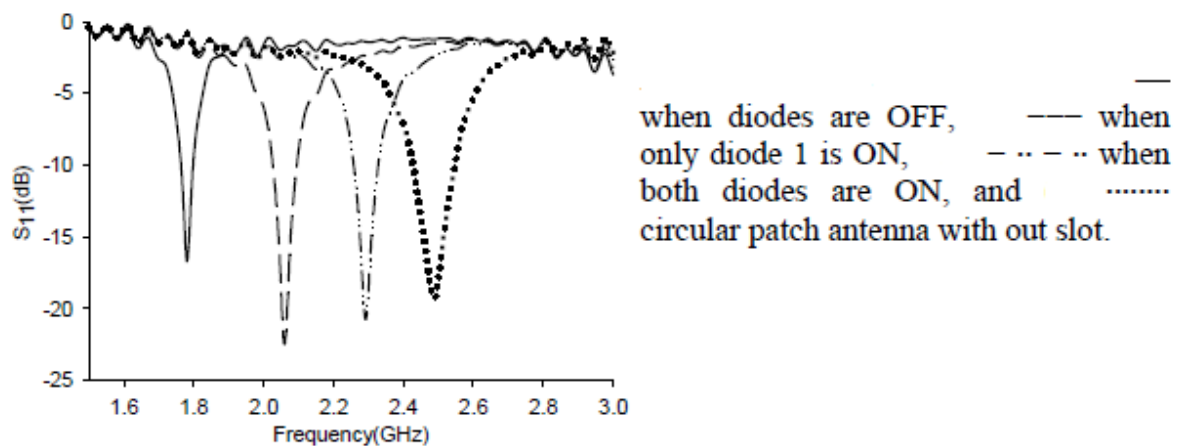
(b)

Figure 2.25: The switchable circular patch antenna: (a) geometry;
(b) the resonant frequency for different states of the PIN diodes [32].

Ref. [33] describes a Vivaldi antenna capable of operating in wideband or narrowband modes. Four pairs of switchable ring slots are etched to change the wideband operation into a narrow band as shown in figure 2.26. When all the ring slots are decoupled from the tapered slot, the antenna exhibits a wideband resonance covers from 1 to 3.2 GHz. A narrowband operation is obtained when the lower, middle, or upper ring slots are coupled. In narrow band mode, three sub bands, low band 1.1 GHz, midband 2.25 GHz, and upper band 3.1 GHz are obtained.
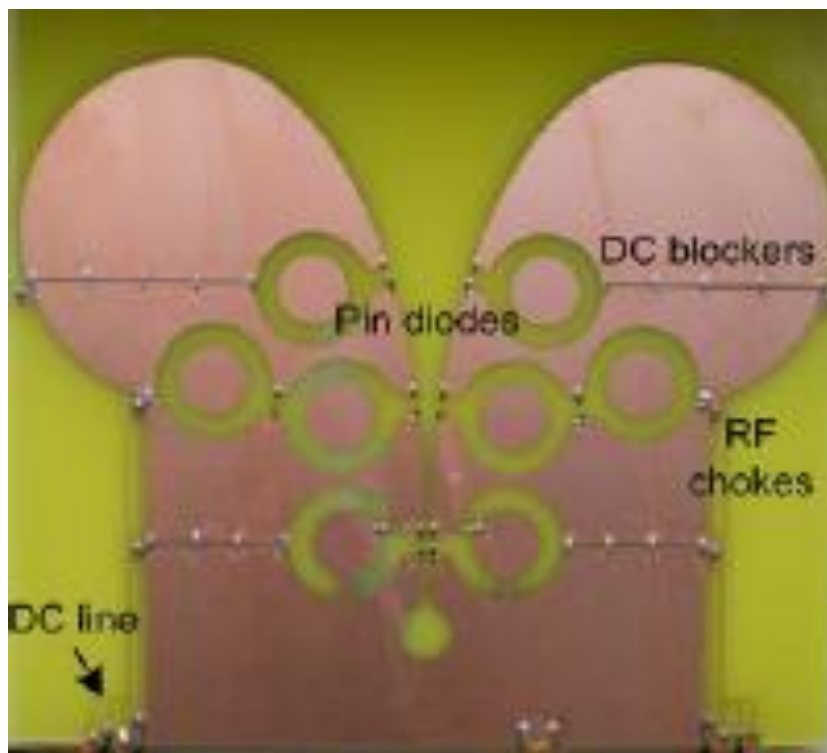
Figure 2.26: Frequency reconfigurable Vivaldi antenna [33].

Reconfigurable printed dipole capable of selecting between several frequency bands is presented in [34]. The antenna, shown in figure 2.27, uses a harmonic trap in order to eliminate the higher order modes. The harmonic trap is an open circuited stub with length of $\lambda/4$ at the frequency $3f_0$. The operating frequency can be switched between seven frequency bands by using six switches in each dipole arm.
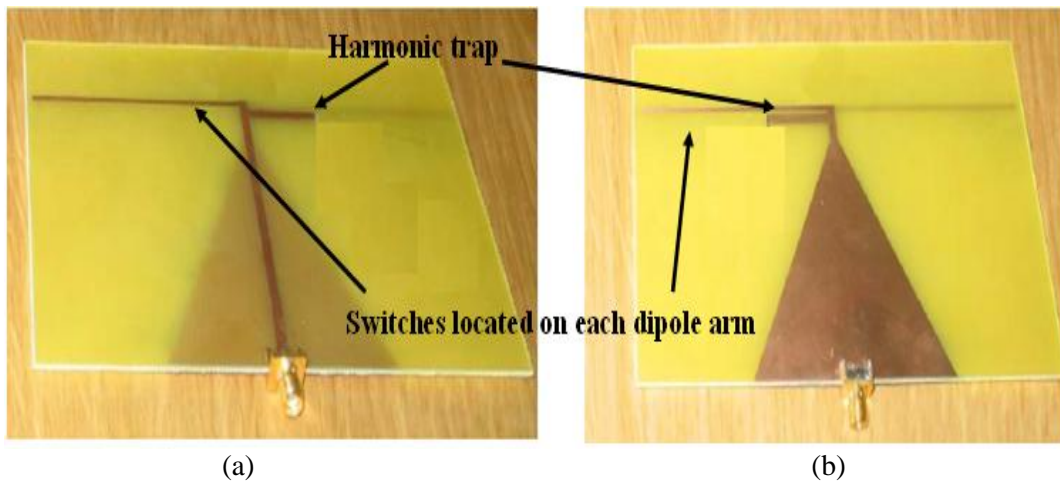
Figure 2.27: Frequency reconfigurable dipole antenna: (a) front side;
(b) back side [34].

The last example of switchable antennas is a single port chassis antenna presented in [35]. The antenna utilizes 17 matching circuits to cover from 76 MHz to 2500 MHz. In addition, 5 matching circuits are used to cover from 470 MHz to 2500 MHz. As shown in figure 2.28, the antenna consists of a coupling element which excites the chassis antenna and tuning circuit to optimize the coupling. Switches are used to connect/disconnect different matching circuits.
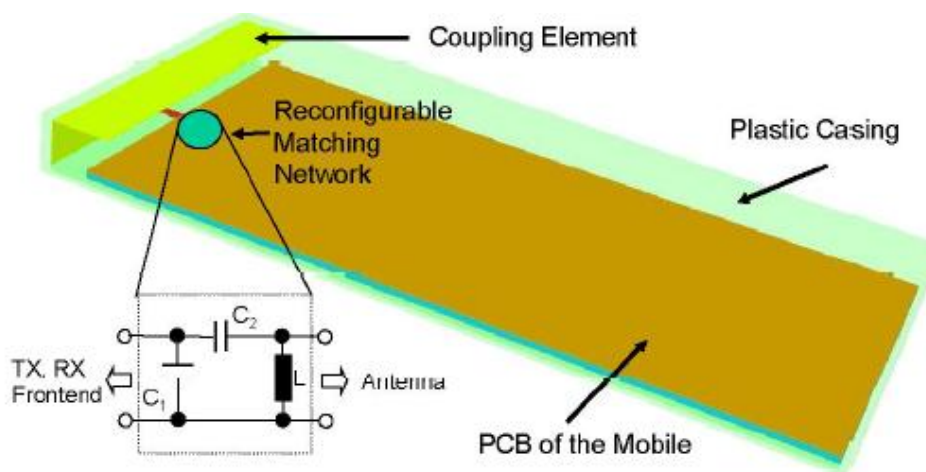
Figure 2.28: Structure of the chassis antenna [35].

2.2.3.2 Frequency Reconfigurable Antennas using Varactor Diodes

The varactor diode, widely used as a variable capacitor, has a capacitance that varies with bias voltage, thus providing an electronically tunable reactive element [6]. Varactor diodes are usually made of silicon or gallium arsenide semiconductors. An equivalent circuit of a reverse biased varactor diode is shown in figure 2.29. The junction capacitance depends on the junction bias voltage v, according to

$$C_j(V) = \frac{C_0}{\left(1 - \frac{V}{V_0}\right)^{\gamma}} \tag{2.37}$$

where C_0 and V_0 are constants and γ is an exponent that varies between 1/3 and 5 depending on the semiconductor doping profile used in the diode. The used of varactor diodes implies the design of biasing circuit to provide the bias/control voltage for the varactor diodes.
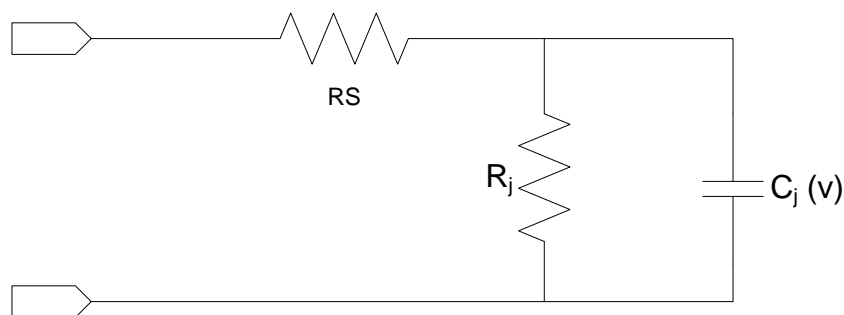
Figure 2.29: Equivalent circuit of reverse biased varactor diode [6].

Many reconfigurable antennas using varactor diodes are available in the literature. A few examples are presented here and more examples are presented in appendix A.

A simple example of an electronically tunable antenna is the varactor tuned planar inverted F antenna (PIFA). A variable capacitor is connected between the edge of the radiating element and the ground. The position at which the varactor is located has the

highest electric field magnitude. Therefore, it results in the widest possible resonant frequency tuning ratio [10].
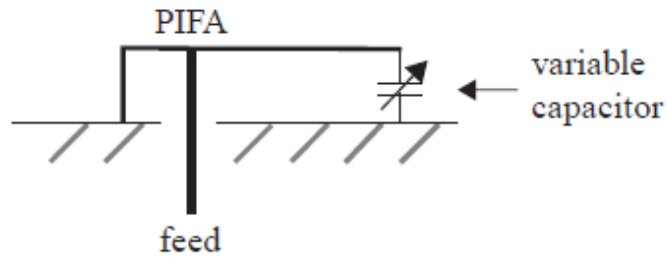
Figure 2.30: A side view of a tunable PIFA [10].

A simple tunable microstrip antenna is presented in [36]. The antenna consists of a rectangular patch divided into two sections that are connected using varactor diodes as shown in figure 2.31. The antenna incorporates 6 varactor diodes. The resonant frequency decreases from 2300 MHz for C = 0 pF to 1500 MHz for C = 15 pF. The achievable tuning range is 1.53:1.

(a)   (b)
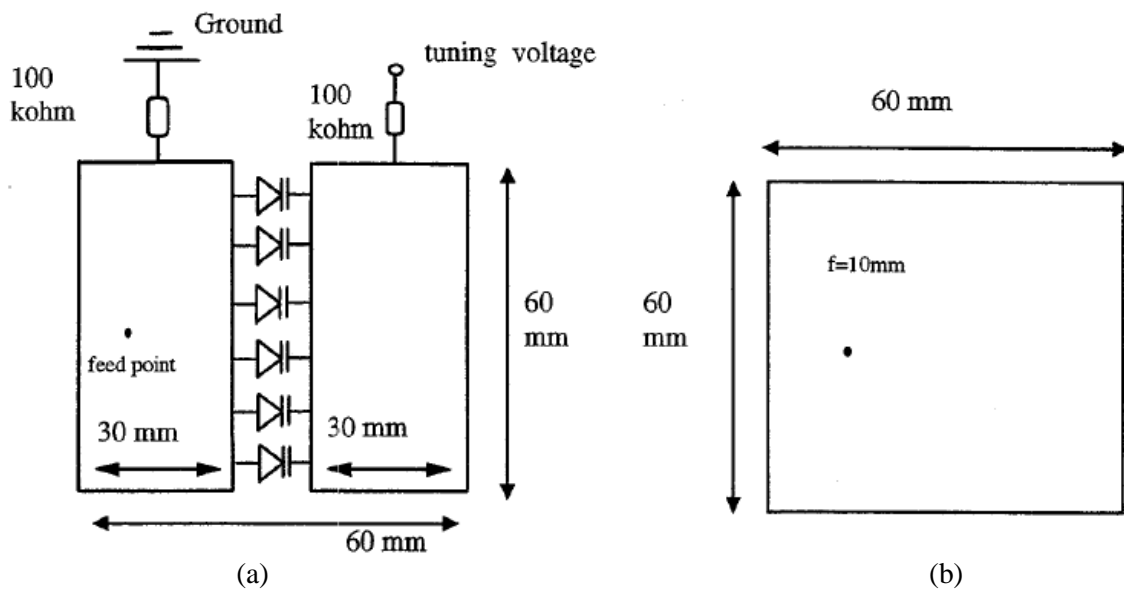
Figure 2.31: the electronically tunable patch: (a) varactor biasing details;

(b) the patch and feed details [36].

Another tunable patch is presented in [37]. The antenna consists of a rectangular patch loaded with varactor diodes at its radiating edge. A meandered slot is etched along the non radiating edge of the patch as shown in figure 2.32. By varying the capacitance of the varactor diodes, the resonant frequency can be tuned from 1.79 GHz to 2.71 GHz.
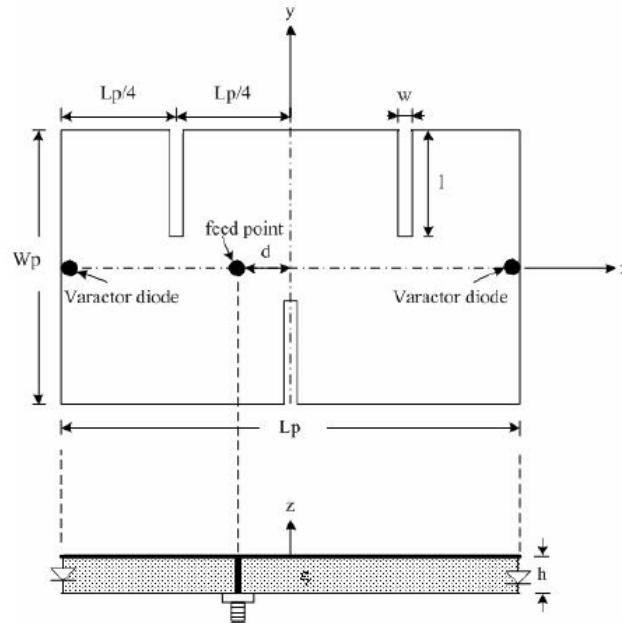
Figure 2.32: The varactor loaded meandered patch [37].

An interesting dual band tunable slot antenna is presented in [38]. The antenna, shown in figure 2.33, uses two varactor diodes to independently tune two matched impedance frequency bands. The frequency of one band can be fixed and the other frequency tuned over wide frequency range. In addition, both bands can be tuned simultaneously if desired. An equivalent circuit of the antenna, shown in figure 2.30b, has been used to obtain the positions of the varactor diodes in order to achieve the widest tuning range.

(a)

(b)

(c)
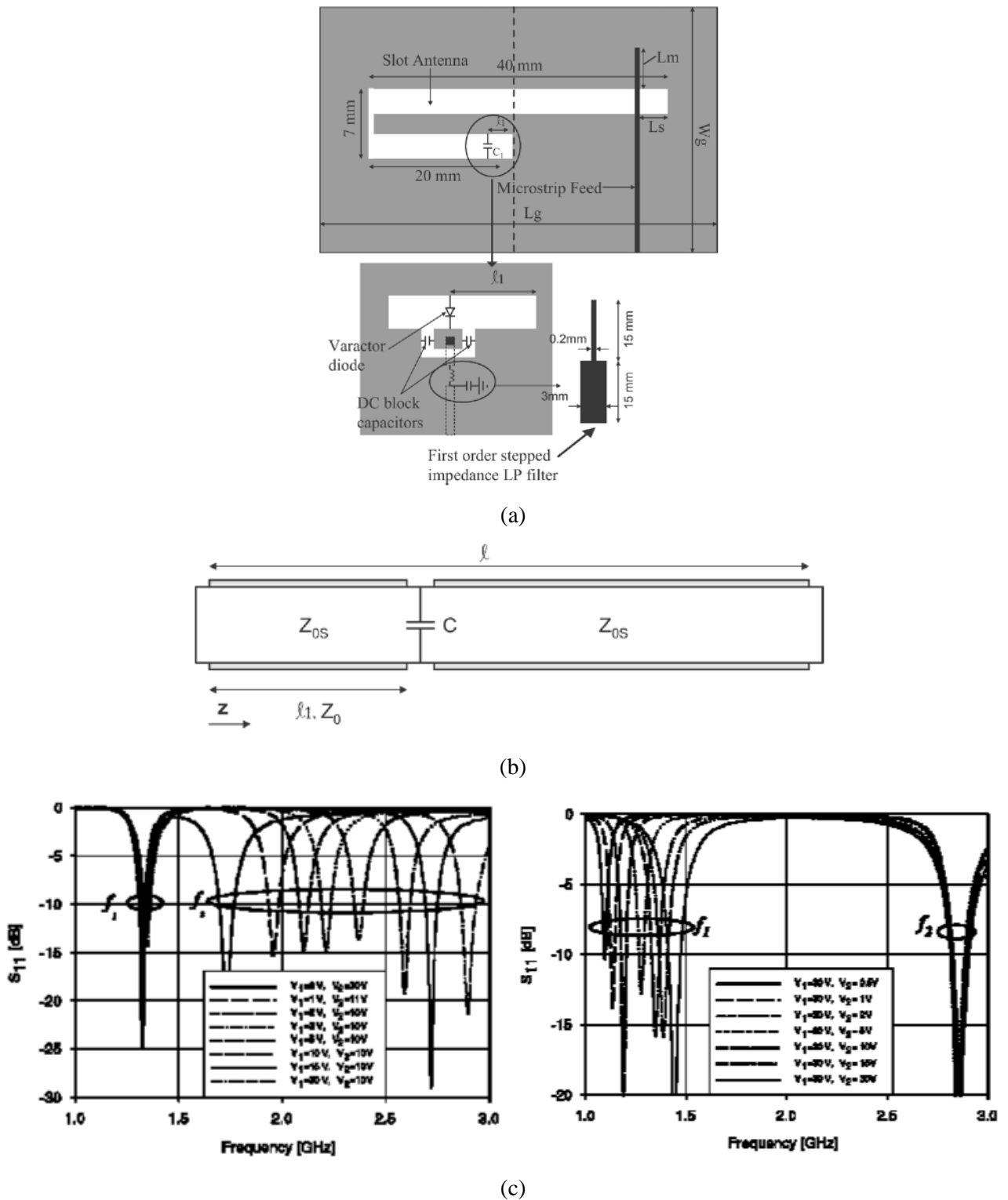
Figure 2.33: The dual band tunable slot antenna: (a) geometry of the antenna;

(b) transmission line model of the slot antenna;

(c) reconfiguration of the upper band (left) and lower band (right) [38].

A two port chassis antenna capable of covering the DVB-H and EGSM-900 bands simultaneously is presented in [39]. One tunable antenna is dedicated for the DVB-H band while the other is for the EGSM band. An external matching circuit made of varactor in series with an inductor is used to achieve the DVB-H band. A filter is also used in order to filter out the EGSM TX to the DVB-H antenna.
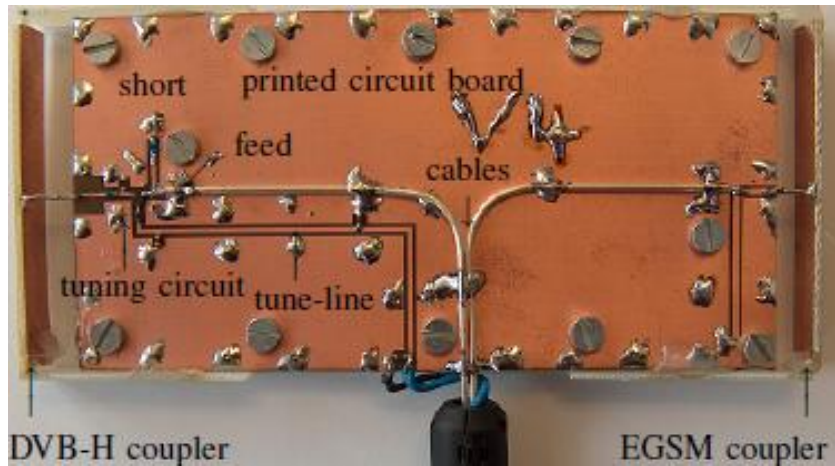
Figure 2.34: The structure of two port chassis antenna [39].

A compact system for cognitive radio (CR) is presented in [40]. The system is based on two antennas printed on the same substrate as shown in figure 2.35a. The total size of the substrate is 60 mm x 60 mm. The first antenna is printed monopole which has wideband operation. The other antenna is tunable narrow band left handed antenna. While the monopole provides a wideband operation from 1.75 to 3 GHz, the other antenna provides a tunable narrowband resonance that can be tuned by varying the capacitors from 1.5 GHz to 3.0 GHz as shown in figure 2.35b.

(a)

(b)

(c)

Figure 2.35: The proposed system for CR terminal: (a) structure;
(b) port 1 with wide band operation; (c) port 2 with tunable narrow band [40].

56

A reconfigurable microstrip patch antenna is presented in [41]. The antenna is composed of four sub-patches connected to one feed line as shown in figure 2.36. Each sub-patch produces a single band. In order to tune the resonant frequency, variable capacitors are placed at the input of the sub-patches. The tuning range extends from 0.92 GHz to 2.98 GHz.
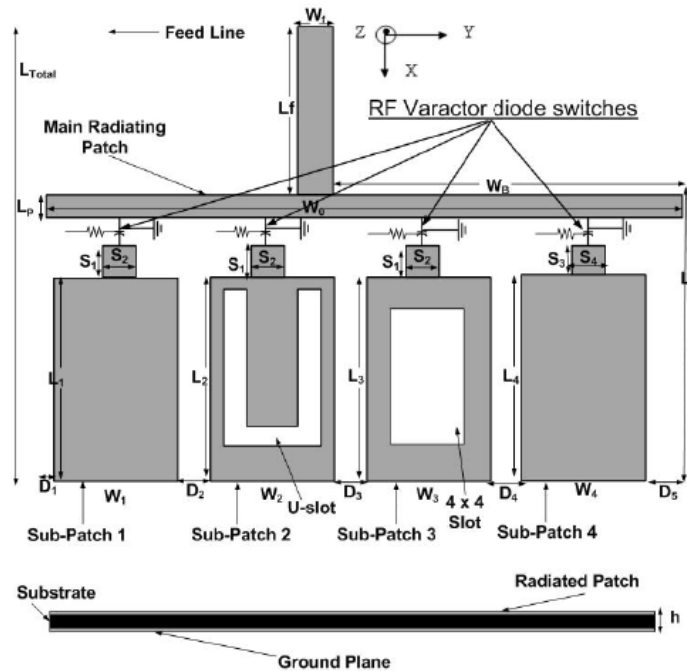
Figure 2.36: The structure of the reconfigurable antenna [41].

2.3. Filtering Antennas

In recent years there has been great advancement in antenna design. One of the focus areas is the design of filtering antennas, which have recently received increasing attention. This section presents and summarizes several research works on the filtering antenna design using a filter synthesis approach. Also, the operation of microwave resonators and the design of bandpass filters using synthesis method are reviewed.

2.3.1. Microwave Bandpass Filters

The microwave bandpass filter is an array of coupled resonators which are tuned to the same frequency. Part of the signal entering the first resonator is stored as the resonance mode of the resonator and the rest of it follows to the next resonator. Storage and flow of signal continues until the signal reaches the load where it is absorbed.

2.3.1.1 Microwave Resonators

The microwave resonator can be defined as a structure that contains oscillating electromagnetic fields [42]. Figure 2.37 shows some configurations of microstrip resonators. The resonator shown in figure 2.37a is known as a quarter wavelength resonator since it is $\lambda/4$ long at the fundamental resonant frequency. Higher order modes exist at higher frequencies when $f = (2n - 1) f_0$ for $n = 2, 3, ...$ The half wavelength resonator, shown in figure 2.37b, is another distributed line resonator. The resonator is $\lambda_{g0}/2$ long at its fundamental resonant frequency. Higher order resonances exist at $f = nf_0$ for $n = 2, 3, ...$ Figure 2.37c shows the ring resonator. The fundamental resonance for the ring resonator occurs when its circumference $2\pi r = \lambda_{g0}$. The higher order modes exist at $f = n f_0$. For a half wavelength microstrip resonator, the electric field is maximum at the open ends and minimum at the centre. However, the maximum magnetic field intensity is at the centre of the resonator.

The microstrip resonator can be shaped into any geometry such as U shape (hairpin resonator), or C shape (open loop resonator). Varying the shape of the resonator will not cause the field distributions to vary. Figure 2.38a shows the electric field distribution for a half wavelength U-shaped (hairpin) microstrip resonator, it can be seen that the maximum electric field intensity is at the open ends whereas the maximum magnetic field intensity is at the centre as shown in figure 2.38b.
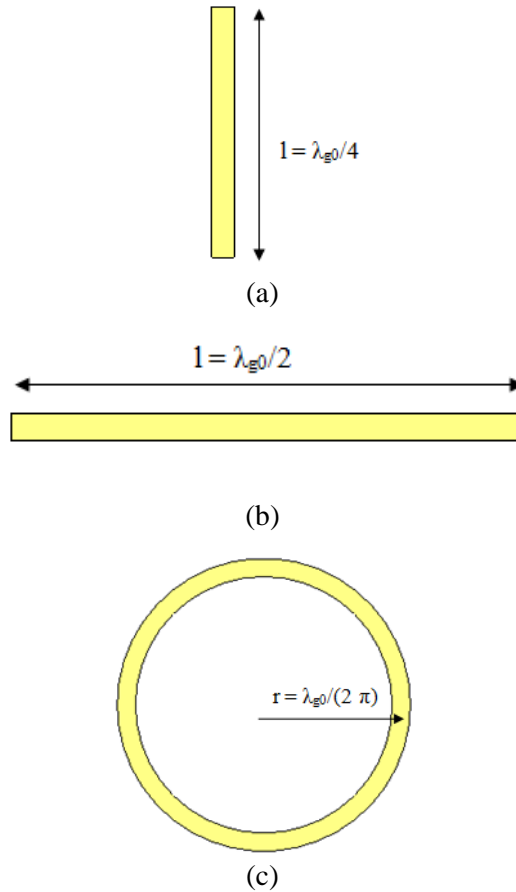
Figure 2.37: Some commonly used microstrip resonators:

(a) quarter wavelength resonator; (b) half wavelength resonator; (c) ring resonator.
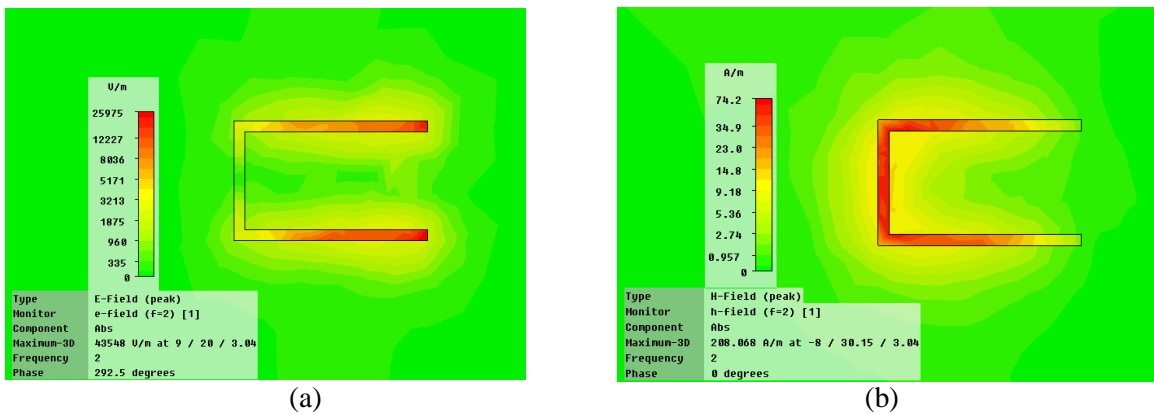
Figure 2.38: The field distribution of the hairpin half wavelength resonator:

(a) E field; (b) H field.

Figure 2.39 shows some typical coupling structures of coupled microstrip resonators. The electric coupling can be obtained if the open ends of the coupled resonators are closely placed as shown in figure 2.39a. If the centres of the coupled resonators are closely placed, as shown in figure 2.39b, the magnetic coupling can be achieved. For the coupled resonators shown in figure 2.39c and 2.39d, the electric and magnetic fields at the coupled sides have comparative distributions. Therefore, both electric and magnetic coupling exist. In this case, the coupling is known as a mixed (electromagnetic) coupling [42].

In practical filter design, it is desirable to compute the unloaded quality factor Q_u of the resonator. This will help to predict if the required insertion loss can be achieved or not. A general definition of Q_u that is applicable to any resonator is

$$Q_u = \frac{Time-average\ energy\ stored\ in\ the\ resonator}{Average\ power\ lost\ in\ the\ resonator} \tag{2.38}$$

For a microstrip resonator, the losses are usually due to the dielectric, conductor, and radiation. The unloaded Q is the sum of these losses together, resulting in

$$\frac{1}{Q_u} = \frac{1}{Q_c} + \frac{1}{Q_d} + \frac{1}{Q_r} \tag{2.39}$$

where Q_c, Q_d, and Q_r are the conduction, dielectric, and radiation quality factors respectively.
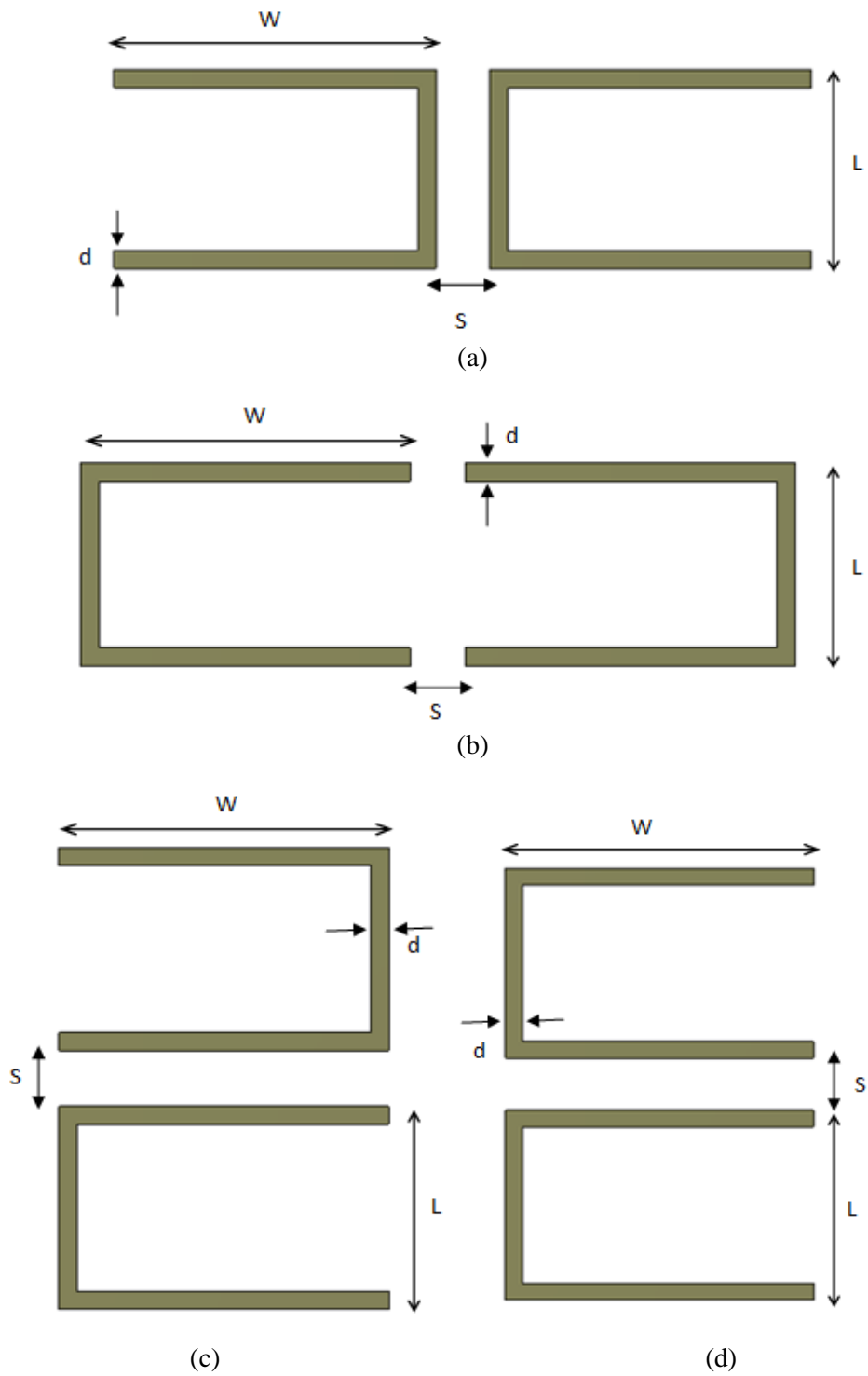
Figure 2.39: Typical coupling structures of coupled Hairpin resonators with: (a) Magnetic coupling; (b) Electric coupling; (c-d) Mixed coupling

2.3.1.2 Bandpass Filter Synthesis Using the Coupling Coefficients Method

This section describes a filter synthesis method used in this thesis. It allows the direct calculation of the coupling coefficients. This method is flexible and it is based on electromagnetic simulations. It is well described in [42].

When designing a filter using the synthesis method and employing EM simulation, it is computationally efficient to break the filter down into different parts that are simulated separately. The simulations are performed to find the physical dimensions that give the desirable coupling coefficients. This simulation based method is efficient for narrowband filter design.

In order to illustrate the synthesis method, the design of three-pole microstrip bandpass filter is considered. The filter is composed of three half wavelength open loop resonators as shown in figure 2.40. Figures 2.41 and 2.42 illustrate the synthesis concept. Figure 2.41a shows experimental/simulation set up to work with the input/output resonators. The resonator is excited at port 1 using a tapped line at a location denoted by t. Port 2 must be weakly coupled in order to minimize the coupling effects. Figure 2.41b shows the simulated frequency response of the structure. The external quality factor can be calculated from the resonant frequency and the 3-dB bandwidth as follows:

$$Q_e = \frac{f_0}{\Delta f} \tag{2.40}$$

The coupling between two adjacent resonators can be extracted using the arrangement shown in figure 2.42a. The coupling is controlled by the spacing S. Figure 2.42b shows typical simulated frequency response for the coupled resonators. Two resonant peaks, which are due to the mode split, can be observed. The coupling coefficient can be extracted using the equation

$$M_{i,\,i+1} = \frac{f_2{}^2 - f_1{}^2}{f_2{}^2 + f_1{}^2} \qquad\qquad (2.41)$$
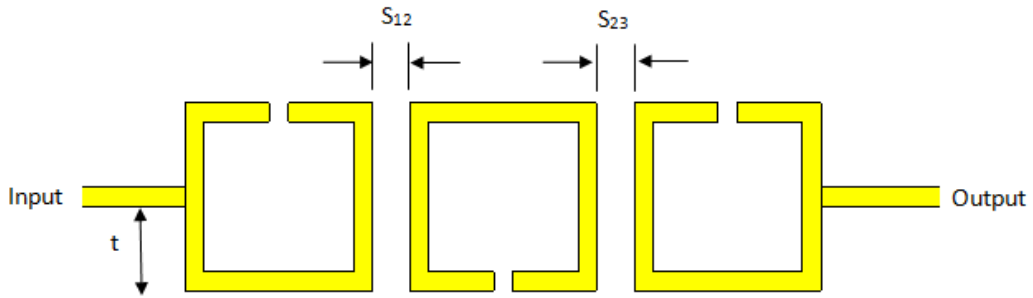
Figure 2.40: Three-pole microstrip bandpass filter
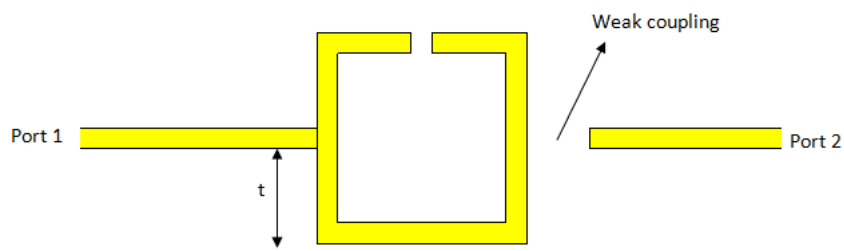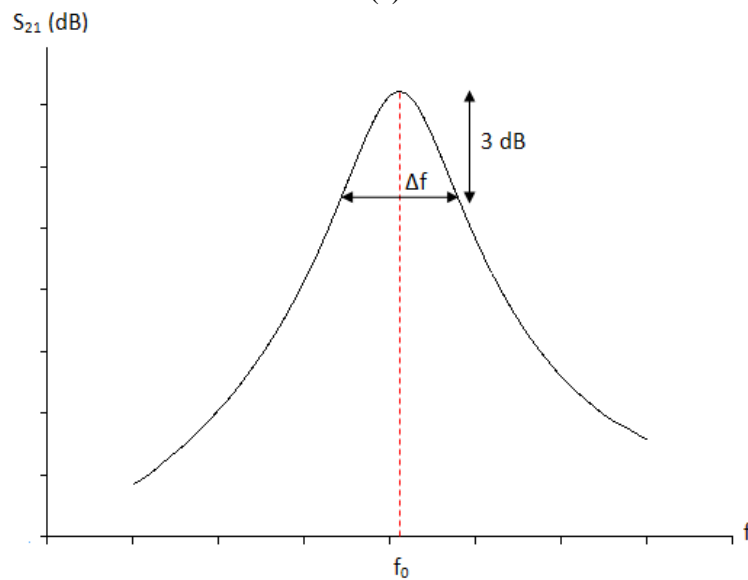
Figure 2.41: The extraction of the external quality factor (a) simulation set up;
(b) the amplitude response of S_{21}.

(a)

(b)
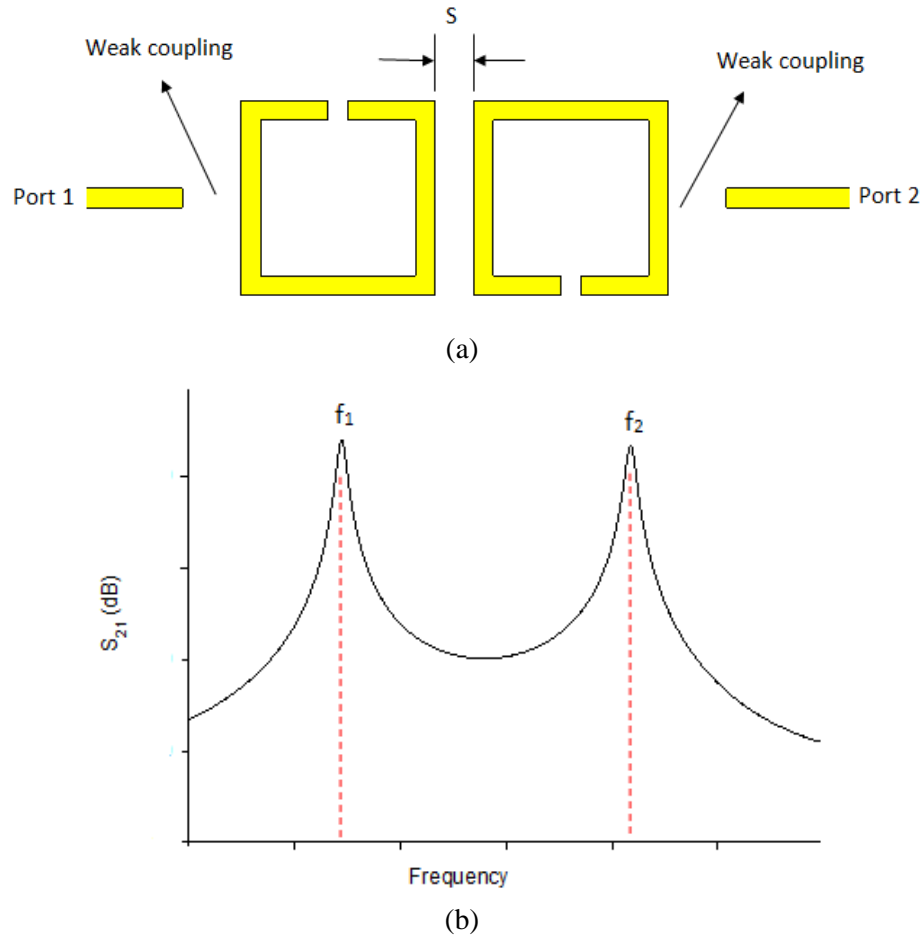
Figure 2.42: The extraction of the coupling coefficient (a) simulation set up;

(b) the amplitude response of S_{21}.

2.3.2. Co-Design of Filter and Antenna

The filtering antennas have received great attention. This section presents and summarizes several research works on the filtering antenna design using filter synthesis approach.

A compact edge-fed filtering microstrip antenna is presented in [43]. The antenna is designed based on the synthesis process of the bandpass filter. Initially, a lumped element filter with 0.2 dB equal ripple response and a fractional bandwidth of 4% at 12 GHz is designed. The filter consists of two parallel LC resonators with resonance frequency at 12 GHz are connected by a π-circuit admittance inverter as shown in

figure 2.43a. Afterwards, the lumped elements are realized using microstrip elements. The first stage of the filter, the parallel LC circuit, is realized by a half wavelength microstrip resonator. The parallel RLC circuit (C_2, L_2, and R_2) is realized by a patch antenna. Figure 2.43b shows the simulated and measured performance of the antenna.

(a)

Dimension of the antenna. $W_p = 7.9$ mm, $l_p = 5.97$ mm, $W_0 = 1.17$mm, $l_1 = 3.415$ mm, $l_2 = 3.05$ mm, $g_1 = 1.1$ mm, $g_2 = 0.9$ mm, and $g_3 = 0.965$ mm.

(b)

(c)
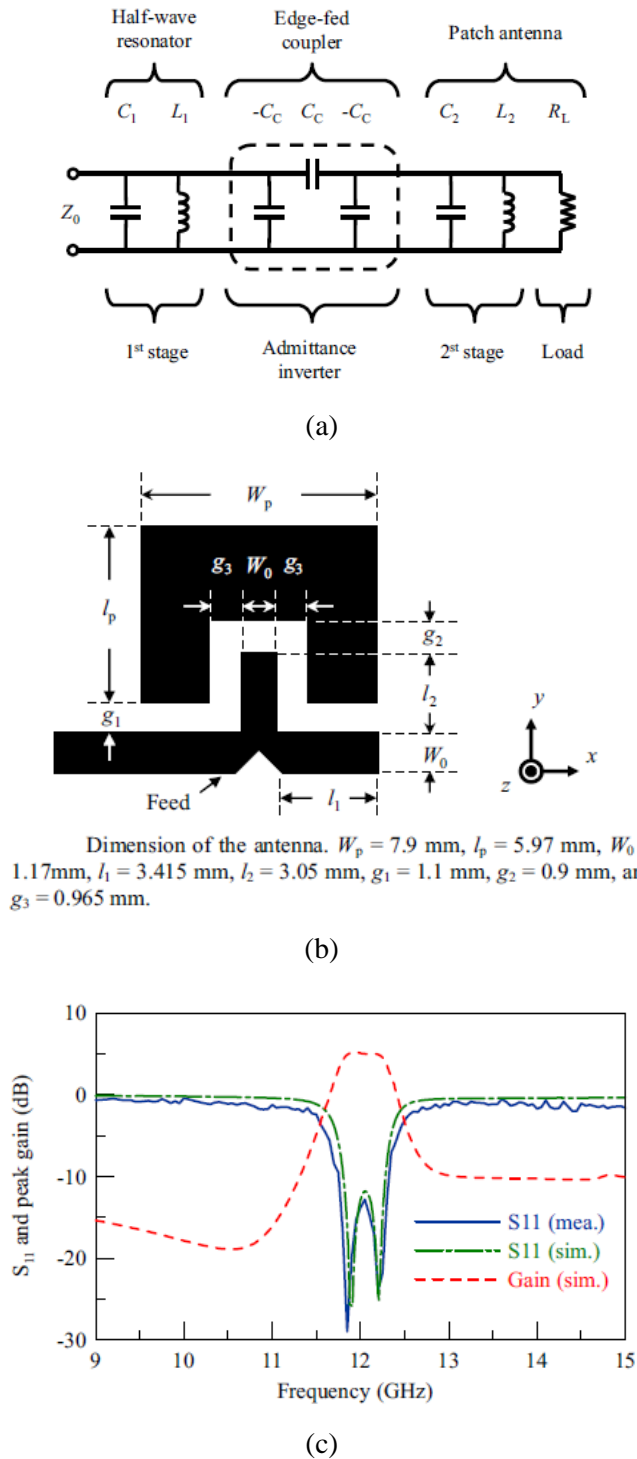
Figure 2.43: The filtering microstrip antenna: (a) equivalent circuit; (b) structure of the antenna; (c) simulated and measured performance [43].

A printed filtering antenna with selectivity enhancement is presented in [44]. Based on co-design approach, a meander line antenna and a quarter wavelength resonator are integrated to form the filtering antenna as shown in figure 2.44a. The quarter wavelength resonator acts as a shunt resonator with a high capacitance and introduces two transmission zeros for selectivity enhancement.
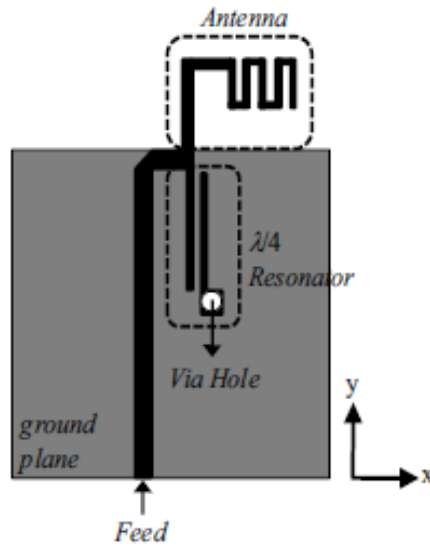
(a)
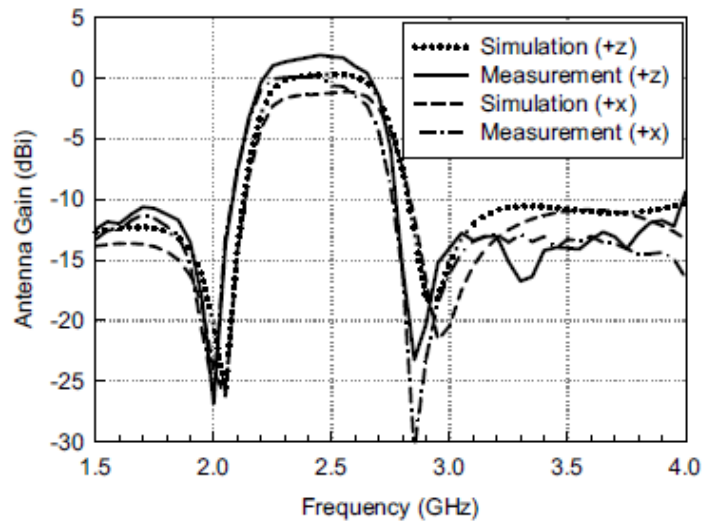
(b)

Figure 2.44: The printed filtering antenna: (a) the structure
Of the antenna; (b) the measured and simulated gain [44].

66

Ref. [45] presents a filtering microstrip antenna with quasi-elliptic gain response. The antenna, as shown in figure 2.45, consists of three parts, the U-shaped patch, T-shaped resonator, and the microstrip feed line. The U-shaped patch acts a radiating element as well as the last resonator of the filter. The broadside gain of the antenna has two broadside radiation nulls at the band edges for improving the selectivity.

(a)

(b)
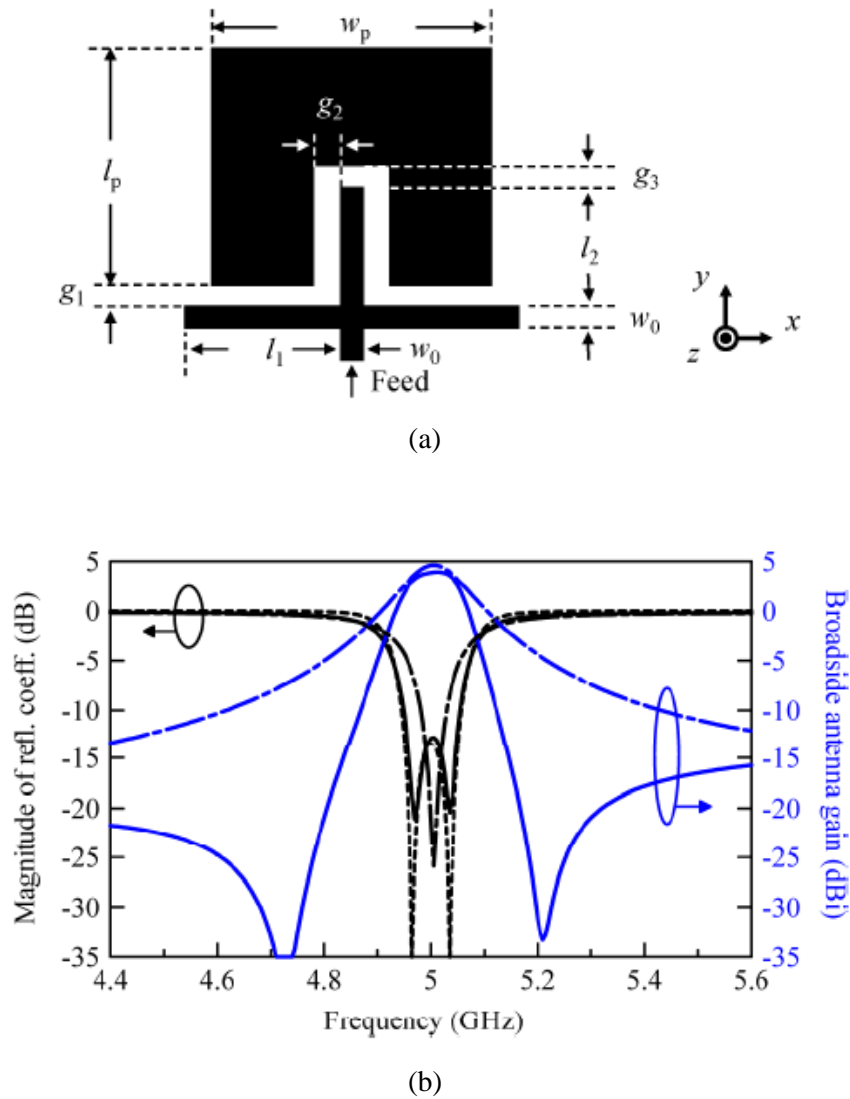
Figure 2.45: The filtering microstrip antenna: (a) the structure;
(b) the simulated and measured performance [45].

A filtering microstrip array is presented in [46]. The array is a combination of filtering antenna elements and filtering feed network. Thus, the array antenna has the return loss response and the gain response just like a bandpass filter. The radiating elements and the feeding circuitry function as a third order bandpass filter. While the feeding network, which consists of power dividers and baluns, provides the first two stages of the filter, the microstrip patch provides the last stage (i.e. resonator) in the filter. The antenna array, shown in figure 2.46, is designed to have a fractional bandwidth of 3% at a midband frequency of 5 GHz with Chebyshev response with passband ripple of 0.3 dB.

Figure 2.46: The filtering microstrip array [46].

A Yagi antenna with frequency domain filtering performance is presented in [47]. The antenna, shown in figure 2.47a, is designed to function as a bandpass filter. The external quality factor, Q_e, is controlled by the spacing between the driven element and the adjacent parasitic element. As the spacing decreases, Q_e increases. The spacing between the driven element and the first director and reflector is less than

68

0.12 λ, which improves the loaded Q factor of the antenna. The separation and the size of the directors and reflectors are optimized to suppress the out of-band gain. Figure 2.47b shows the performance of the filtering Yagi antenna.
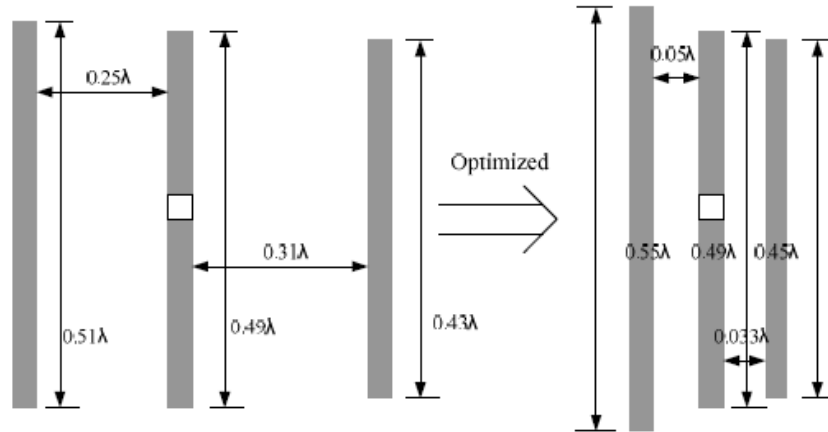
(a)
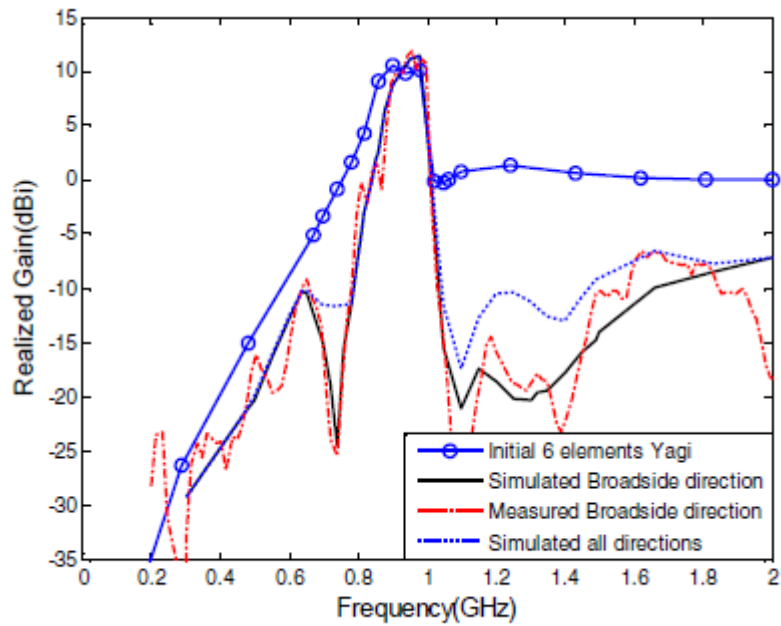
(b)

Figure 2.47: The filtering Yagi antenna: (a) the geometry;
(b) simulated and measured realized gain [47].

Another filtering microstrip antenna is presented in [48]. The antenna, shown in figure 2.48, consists of a coupled line, two open loop resonators, and Γ-shaped patch. The elements together function as a third order bandpass filter with 0.1 dB equal ripple response and FBW = 13% at 2.45 GHz.
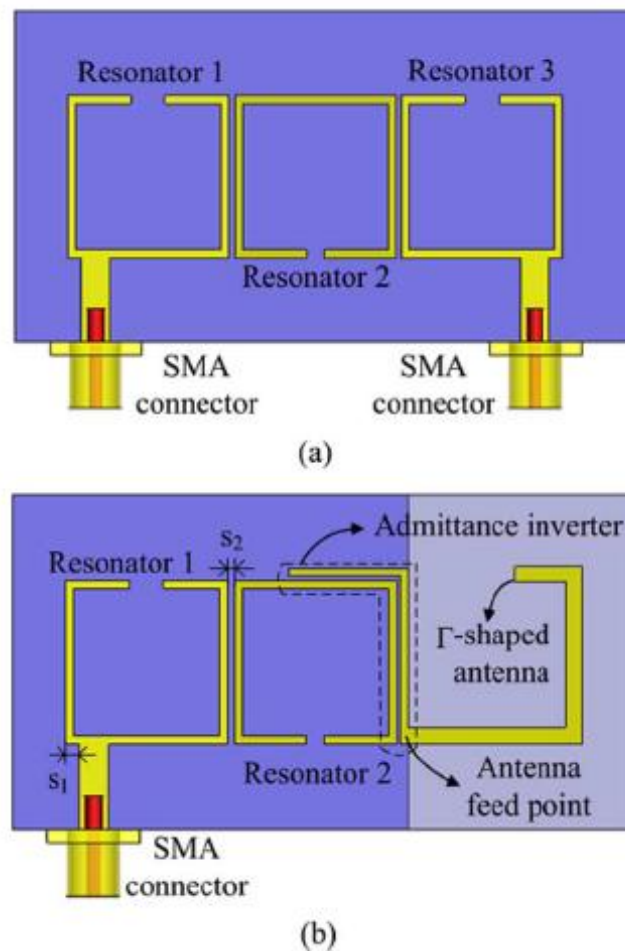
Figure 2.48: The Γ-shaped filtering antenna: (a) three-pole microstrip filter; (b) integrated filter-antenna [48].

Reference [49] represents a well-designed waveguide slot antenna with an integrated filter. The design process starts by designing a five-pole waveguide bandpass filter. The filter is composed of five cavity resonators as shown in figure 2.49. The filter is developed into an antenna by replacing the last resonator by a waveguide slot. The

radiation Q of the waveguide slot is equal to the external quality factor at the input. Therefore, the filtering characteristics are preserved.

(a)

(b)
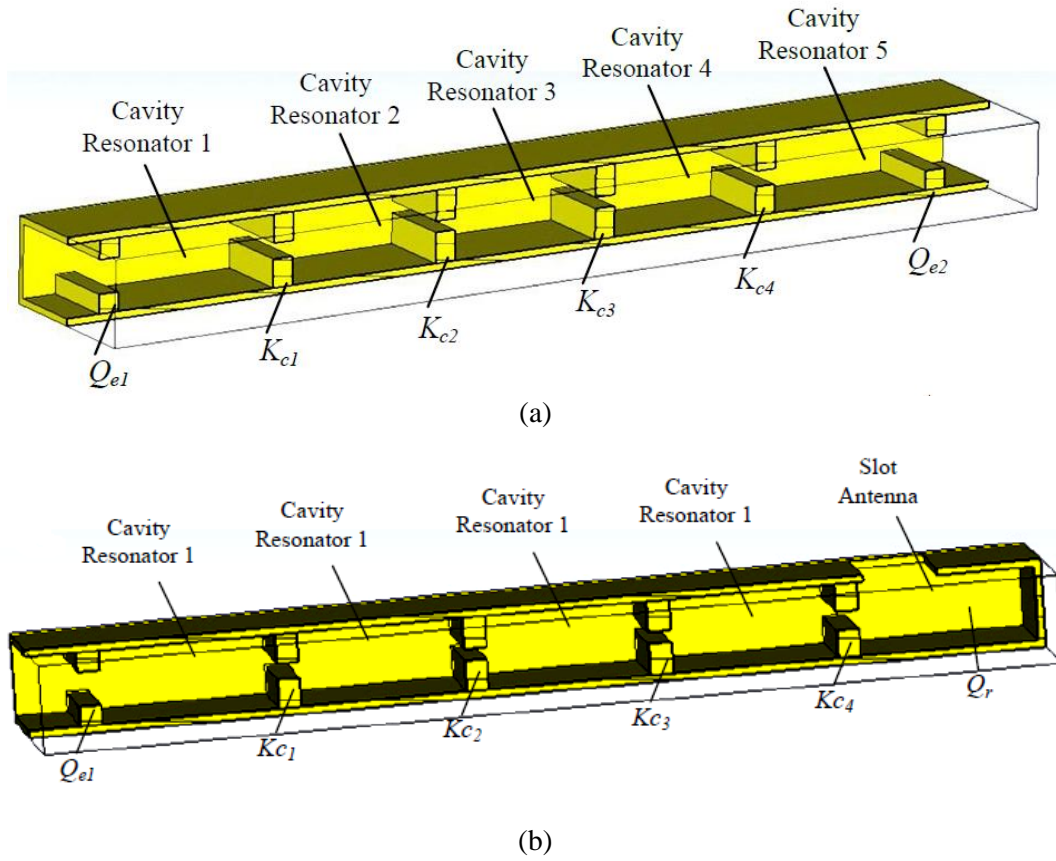
Figure 2.49: Waveguide slot antenna with integrated filter: (a) five-pole waveguide bandpass filter; (b) waveguide slot antenna with integrated filter [49].

References:

[1]   C. Caloz and T. Itoh, Electromagnetic Metamaterials: Transmission Line Theory and Microwave Applications. Ney York, NY, USA:IEEE-Wiley, 2004

[2]   V. Veselago, "The electrodynamics of substances with simultaneously negative values of ε and μ," Soviet Physics Uspekhi, vol.10, no.4, pp.509-514, 1968.

[3]   A. K. Iyer and G. V. Eleftheriades, "Negative refractive index metamaterials supporting 2-d waves," in 2002 IEEE-MTT International Microwave Symposium Digest. vol.2, Seattle, WA, USA, June 2002, pp.412-415.

[4]   A. A. Oliner, "A periodic-structure negative-refractive-index medium without resonant elements," in 2002 IEEE-AP-S USNC/URSI National Radio Science Meeting, San Antonio, TX, USA, June 2002, p.41.

[5]   G. V. Eleftheriades and K. G. Balmain, Negative-Refraction Metamaterials: Fundamentals Principles and Applications. Hoboken, NJ, USA: IEEE-Wiley, 2005.

[6]   D. Pozar, Microwave Engineering, 2nd Edition, John Wiley and sons Inc., New York. 2005.

[7]   C. Caloz, A. Sanada, and T. Itoh, "Microwave applications of transmission-line based negative refraction index structures," in Asia-pacific Microwave Conference, vol.3, Seoul, Korea, November 2003, pp.1708-1713.

[8]   A. Grbic and G. V. Eleftheriades, "Experimental verification of backward wave radiation from a negative refractive index metamaterial," Journal of Applied physics, vol.92, no.9, pp.5930-5935, November 2002.

[9]   H. R. Hertiz, Electric Wves, London: Macmillan, 1893; Dover, 1962.

[10]   Y. Huang and Kevin Boyle, Antennas from Theory to Practice, Wiley-Blackwell, 2008.

[11]   A. Alford and A. Kandoian, "Ultra-high frequency loop antenna," Electrical communication, vol.18, pp.255-265, 1940.

[12]   G. S. Smith, "Efficiency of electrically small antennas combined with matching networks," IEEE Transaction on Antennas and Propagation, vol. AP-40, no.5, pp.369-373, MAY 1977.

[13]   H. Iizuka, P.S .Hall, and Lucas Borja, "Dipole antenna with Left-handed Loading," IEEE Antennas and Wireless Propagation letters, vol.5, pp.483-485, 2006.

[14]   H. Iizuka and P. S. Hall, "Left-handed dipole antennas and their implementations," IEEE Transactions on Antennas and Propagation, vol.55, pp.1246-1253, May 2007.

[15]   Q. Liu, P. S. Hall, and Lucas Borja, "Dipole with left handed loading with optimized efficiency," in second European Conference on Antennas and Propagation (EuCAP 2007), Edinburgh, UK, November 2007.

[16]   Q. Liu, P. S. Hall, and A. Lucas Borja, "Efficiency of electrically small dipole antennas loaded with left handed transmission lines," IEEE Transactions on Antennas and Propagation, vol.3009-3017, no.10, p.57, October 2009.

[17]   A. Lucas Borja, P. S. Hall, Q. Liu, and H. Iizuka, "Omnidirectional loop antenna with left handed loading," IEEE Antennas and Propagation Letters, vol.6, pp.495-498, 2007.

[18]   P. S. Hall and Q. Liu, "Dual-mode reconfigurable loop antenna with left handed loading," in metamaterials 2008, PAMPLONA, Spain, September 2008.

[19] Q. Liu and P. S. Hall, "Varactor-loaded left handed loop antenna with reconfigurable radiation pattern," IEEE International Symposium on Antennas and Propagation, Charleston, UAS, 2009.

[20] F. J. Herraiz-Martinez, P. S. Hall, Qing Liu, and D. Segovia-Vargas, "Tunable left-handed monopole and loop antennas," IEEE Antennas and Propagation Society, International Symposium, pp.1-4, APSURSI 2009.

[21] F. J. Herraiz-Martinez, P. S. Hall, Qing Liu, and D. Segovia-Vargas, "Left-handed wire antennas over ground plane with wideband tuning," IEEE Transaction on Antennas and Propagation, vol.59, pp.1460-1471, May 2011.

[22] C. A. Balanis, Modern Antenna Handbook, John Wiley & Sons, Inc, 2008.

[23] C. A. Balanis, Antenna Theory, 3rd edition, Analysis and Design, John Wiley & Sons, Inc, 2005.

[24] S. Lim and H. Ling, "Design of electrically small pattern reconfigurable Yagi antenna," Electronics Letters, vol.43, no.24, 22 Nov. 2007, pp.3-4.

[25] W. S. Kang, J. A. Park, and Y. J. Yoon, "Simple reconfigurable antenna with radiation pattern," Electronics Letters, vol.44, no.3, 31 Jan 2008, pp.182-183.

[26] Z. P. Wang, P. S. Hall, J. Kelly, and P. Gardner, "TEM horn circular array for wide band radiation pattern notch reconfigurable antenna system," LAPC 2010, Loughbrough Antennas & Propagation Conference, 2010, 8-9 Nov. 2010, Loughbrough, UK, pp.365-367.

[27] F. Yang, and Y. Rahmat-Samii, "A reconfigurable patch antenna using switchable slots for circular polarization diversity," IEEE Microwave and Wireless Components Letters, vol.12, no.3, March 2002, pp.96-98.

[28] H. Assist, L. Cirio, M. Grzeskowiak, J. M. Laheurte, and O. Picon, "Reconfigurable circularly polarized antenna for short-range communication

systems," IEEE Transactions on Microwave Theory and Techniques, vol.54, no.6, June 2006, pp.2856-2863.

[29]   Eng Hock Lim and Kwok Wa Leung, Compact Multi-functional Antennas, John Wiley & Sons, Inc, 2012.

[30]   D. Pcroulis, K. Sarabandi, and L.P.B. Katehi, "Design of reconfigurable slot antennas," IEEE Transaction Antennas Propagation, vol.53, pp.645-654, Feb. 2005.

[31]   P. F. Wahid, N. A. Ali, and B. C. Deloach, Jr. "A reconfigurable Yagi antenna for wireless communications", Microwave Opt. Tech. Lett., vol.38, no.2, pp.140-141, July 2003.

[32]   Das Krishna, C. K. Aanandan, P. Mohanan, K. Vasudeban, "Electrically switchable circular microstrip antenna with sector-slot for multiple frequency operation," Antennas and Propagation Society International Symposium 2006, APSURSI 09, pp.4277-4280, 2006.

[33]   M. R. Hamid, P. S. Hall, P. Gardner, and F. Ghanem, "Frequency reconfigurable Vivaldi antenna," Proceedings of the fourth European conference in Antennas and Propagation (EuCAP) 2010.

[34]   A. Mirhamali, P. S. Hall, and M. Soleimani, "Wideband reconfigurable printed dipole antenna with harmonic trap," IEEE international workship on Antenna technology small antennas and novel metamaterials, pp.188-191, 2006.

[35]   D. Manteuffel, M. Amold, "Considerations for reconfigurable multi-standard antennas for mobile terminals," International workshop on antenna technology: small antennas and novel metamaterials, iwat, pp.231-234, 2008.

[36]   N. Fayyaz, S. Safavi-Naeini, E. Shin, N. Hodjat, "Novel electronically tunable rectangular patch antenna with one octave bandwidth," IEEE Canadian Conference on Electrical and Computer Engineering. Vol.1, pp.25-28. 1998.

[37]   Junying Liu, Jinping Zhang, Weidong Wang, and Dongjin Wang, "Compact reconfigurable microstrip antenna for multi-band wireless applications," IEEE International Symposium on Microwave Antenna and Propagation and EMC Technologies for Wireless Communications, pp.608-611, 2007.

[38]   N. Behdad and K. Sarabandi, "Dual-band reconfigurable antenna with a very wide tenability range," IEEE Transactions on Antennas and Propag., vol.52, pp.409-416, February 2004.

[39]   L. Huang, and P. Russer, "Tunable antenna design procedure and harmonics suppression methods of the tunable DVB-H antenna for mobile applications," European conference on Wireless Technologies, 2007, pp.304-307, 8-10 Oct. 20007.

[40]   F. J. Herraiz-Martinez, P. S. Hall, and D. Segovia-Vargas, "Application of the Left handed half loop antenna with wideband tuning to a cognitive radio terminal," European Conference on Antennas and Propagation EuCAP, pp.1-4, April 2010.

[41]   H. F. Abutarboush, R. Nilavalan, K. M. Nasr, H.S. Al-Raweshidy, and D. Budimir, "Widely tunable multiband reconfigurable patch antenna for wireless applications," European Conference on Antennas and Propagation, EuCAP, pp.1-3, 2010

[42]   Jia-Shen Hong and M. J. Lancaster, Microstrip Filters for RF/Microwave Applications, 2nd Edition, John Wiley and sons Inc., New York. 2011.

[43]   Chin-Kai Lin and Shyh-Jong Chung, "A compact edge-fed filtering microstrip antenna with 0.2 dB equal ripple response," European Microwave Conference EuMC 2009, pp.378-380.

[44]   C. T. Chuang and S.J. Chung, "New printed filtering antenna with selectivity enhancement," in Proc. 39th Eur. Microw. Conf., vol.9, pp.747-750.

[45]   Chin-Kai Lin and Shyh-Jong Chung, "A compact filtering microstrip antenna with quasi-elliptic broadside antenna gain response," IEEE Antennas and Wireless Propagation Letters, vol.10, pp.381-384, 2011.

[46]   Chin-Kai Lin and Shyh-Jong Chung, "A filtering microstrip antenna array," IEEE Trans. Microw. Theory Tech., vol.59, no.11, pp.2856-2863, Nov.2011.

[47]   Z. P. Wang, P. S. Hall, and P. Gardner, "Yagi antenna with frequency domain filtering performance," IEEE Antennas and Propagation Society International Symposium APSURSI, pp.1-2, July 2012.

[48]   Wei-Jun Wu, Ying-Zeng Yin, Shao-Li Zuo, Zhi-Ya Zhang, and Jiao-Jiao Xie, "A new compact filter-antenna for modern wireless communication systems," IEEE Antennas and Wireless Propagation Letters, vol.10, pp.1131-1134, 2011.

[49]   Yang Y., and M. J. Lancaster, "Waveguide Slot Antenna with Integrated Filters," the 32 European Space Agency Workshop, 2010.

CHAPTER III

TUNABLE LEFT-HANDED CIRCULAR LOOP ANTENNA

Electrically small antennas (ESA) have recently received great attentions. Due to their very large reactance, ESAs are difficult to match, and a considerable effort is needed to design a matching circuit to match the impedance [1]. In addition, the matching circuit increases the total size of the antenna which is contrary to the overall goal of miniaturization. Wire antennas such as dipoles, monopoles, and loops are very popular radiators. The printed version of these antennas offers additional advantages such as low cost, low profile, and ease of fabrication. However, these antennas cannot meet some requirements of modern systems such as small size and multi-frequency operation. A design approach of wire antennas based on the metamaterial transmission line is presented to achieve positive features such as size reduction and multi-frequency operation.

Metamaterial transmission lines (TLs) represent the dual performance of conventional right handed (RH) TLs. In left handed (LH) TLs, the electric, magnetic, and propagation vector form a LH triplet. Consequently, the phase and group velocities are anti-parallel and wave propagation is backward [2]. The equivalent circuit of an infinitesimal RH TL is a series inductance and shunt capacitance. However, the equivalent circuit for the LH TL is series capacitance and shunt inductance [3].

Recently LH dipole antennas have been presented [4-5]. These antennas are electrically small with internal matching. The antennas are based on the metamaterial transmission line approach using a LH ladder network. The ladder network is a periodic structure of LH unit cells where each cell consists of two series capacitors

(C_L) and shunt inductor (L_L). The dipole consist of two wires, the capacitors are placed in the feed wire and inductors are placed in the connections between the wires. The LH loading elements provide the new features of modes with negative indices. The resonant frequency and the input impedance of the LH dipoles depend on the loading element but not the size of the antenna. LH wire antennas using distributed elements of meandered inductor and interdigital capacitor are presented in [6]. A detailed study of the efficiency of these antennas has been presented in [7].

The even modes are not excited in the LH dipoles because they are anti-resonant in the dipolar geometry. Only the odd modes are excited. LH loops are presented as a solution to excite the even modes [8-9]. The zeroth order mode, n = 0, has exceptional characteristics of uniform current in both amplitude and phase. The LH loops are based on the typical LH ladder network with series capacitors and shunt inductors. For a loop composed of N cells, the excited modes are –N, -N+2... 0, N+2,.. Tunable LH monopole and LH half-loop antennas over a ground plane were presented in [10-12]. These antennas are small with wide tuning bandwidth. The resonant frequency of the antennas is controlled using the capacitance of the LH cells. The LH monopole achieves a bandwidth of 1.33:1 whereas the loop achieves a tuning bandwidth of 1.64:1.

This chapter presents a tunable LH loop antenna. The circular loop is located over a ground plane and loaded with three LH unit cells. Each unit cell is composed of two series capacitors, and one shunt inductor. The resonant frequency and the input impedance are controlled using the loading components. The n = 0 mode is excited and it is tuned by varying the lumped capacitors (C_L). This mode has a uniform current distribution both in magnitude and phase which gives a rise to a directional pattern orthogonal to the ground plane. The antenna was initially implemented by

lumped capacitors and inductors. Afterwards, the lumped capacitors were replaced by varactor diodes. The achievable tuning bandwidth is 1.88: 1 and it extends from 0.99 GHz to1.86 GHz. The antenna exhibits directional pattern with maximum directivity orthogonal to the ground which is maintained within the tuning bandwidth. The antenna exhibits good gain. The wide tuning bandwidth is useful to cover a large number of wireless services, such as GSM, GPS, PCS, UMTS, Wi-Fi, and Bluetooth. All the simulation results presented in this chapter were performed using the time domain solver in CST Microwave Studio$^{®}$. The S_{2P} file representing the chip capacitors and inductors were imported from the pre-defined vendor library in Microwave Office, from Applied Wave Research.

3.1. *Tunable LH Loop Antenna*

In this section simulations and measurements are given for a LH loop antenna that operated at different frequencies by changing fixed capacitors in the loop.

3.1.1 Design and Operation

The antenna, as shown in Figs. 3.1, is LH loop over a ground plane. The antenna is formed of two circular strips printed on Taconic substrate TLY-5 of thickness h = 0.5 mm and dielectric constant ε_r = 2.2. The width of the substrate is W_s = 58 mm and the length L_s = 52 mm. One end of the outer strip is connected to the feed and the other is connected to the ground plane. However, both ends of the inner strip are connected to the ground. The antenna is a periodic structure whose unit element is the LH cell. Each cell consists of two series capacitors (C_L) and one shunt inductor (L_L). Whilst the capacitors are placed in the outer strip, the inductors are placed in the

interconnections between the strips. The antenna is placed over a ground plane of width $W_g = 80$ mm, length $L_g = 80$ mm and thickness $h_g = 0.8$ mm.

The antenna is a left-handed structure whose resonant frequency depends on the components of the left-handed cells. Each mode has a standing wave which satisfies the equation:

$$L = |n| \frac{\lambda_a}{4} \qquad (3.1)$$

where L is the total length of the loop, λ_a is the guided wavelength of the standing wave, and n is the resonance number.

Only even modes are excited in this structure. The $n = 0$ mode is excited. This mode is well matched over a wide bandwidth. For a LH loop antenna with N unit cells, the modes $n = -2N, -2N+2, -2N+4, ..., 0, 2 ...$ can be excited. In the proposed antenna, the modes -6, -4, -2, 0 are excited.

The resonant frequency of the modes can be tuned by varying the capacitors. Whilst the inductors are kept fixed at $L_L = 10$ nH, the capacitors are varied from 0.3 to 1.2 pF. The resonant frequency decreases as the loading capacitance increases. Chip inductors from Coilcraft and ceramic chip capacitors from ATC were used. The S parameter files representing these components are extracted from the pre-defined vendor library in Microwave Office design suite[®]. The simulation includes the parasitic components in the surface mounted components. Therefore, the degradation in the circuit performance due to the parasitic elements can be calculated.
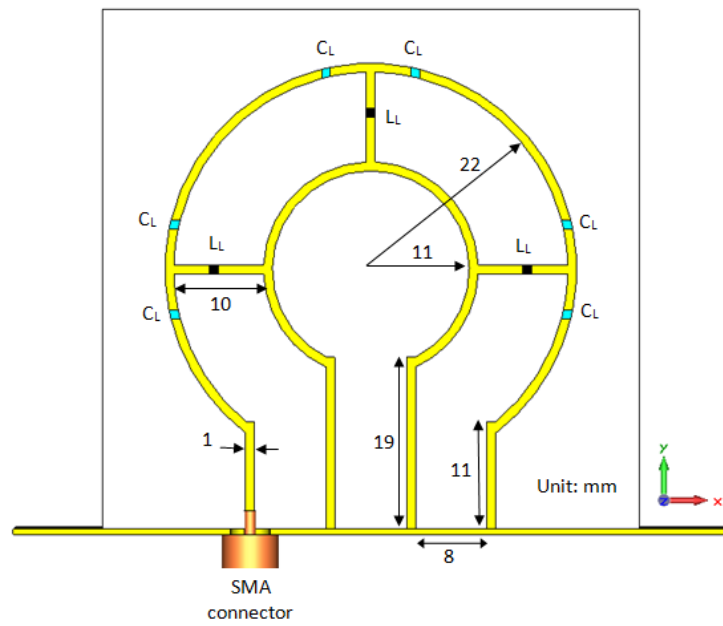
(a)
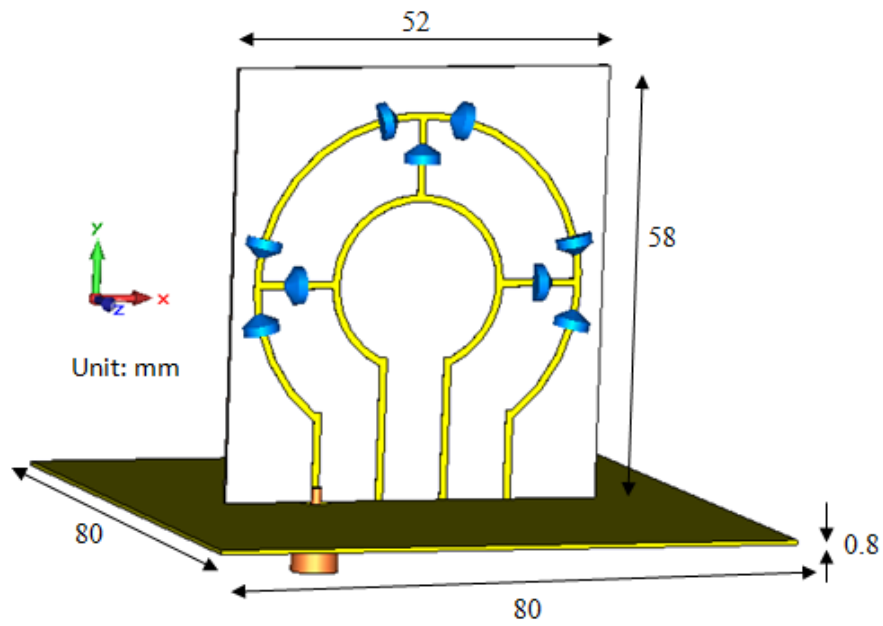
(b)

Figure 3.1: The LH circular loop antenna over ground plane:

(a) front view; (b) 3D view.

3.1.2. Simulation and Measurement Results

As noted earlier, simulations were performed with CST Microwave Studio[®] and Microwave Office[®], from Applied Wave Research. Figure 3.2 shows the simulated and measured reflection coefficient for $C_L = 0.8$ pF. The n = 0 mode resonates at 1. 17 GHz. The magnitude of the reflection coefficient at this resonance is -21 dB. Modes with negative indices are also excited. The n = -6 mode resonates at 0.62 GHz. The n = -2 and n = -4 modes are only weakly excited and they can be observed in the phase characteristic of the reflection coefficient. The resonance mode can be identified by looking at the current distribution as explained below. The zeroth order mode is well matched over wide frequency range, as shown in figures 3.3 and 3.4, where the resonant frequency decreases as the capacitance C_L increases. The achievable tuning range is 1.88:1 and it extends from 0.99 GHz to 1.86 GHz for a – 10 dB return loss. Two prototypes have been fabricated and measured, using 0.5, and 0.8 pF chip capacitors.

The discrepancy between the simulated and measured result is mainly due to the tolerances of the dielectric substrate. Other factors include the etching accuracy, the soldering and the metallization thickness.
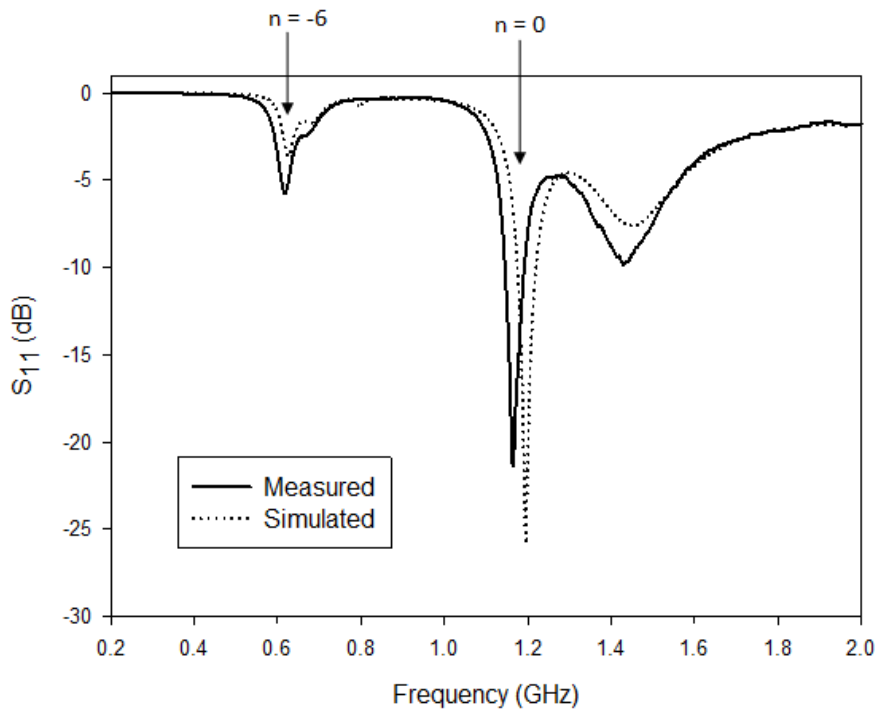
(a)
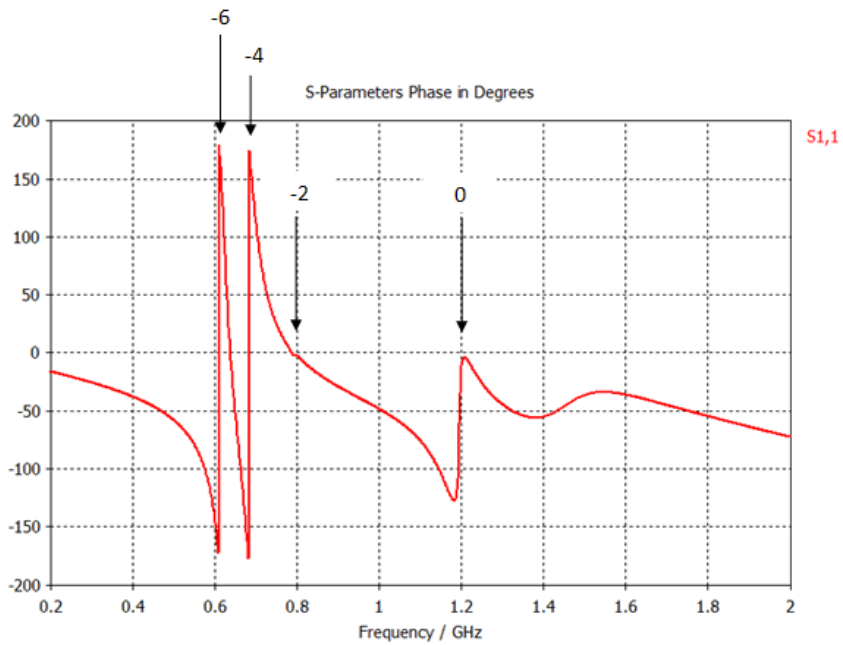
(b)

Figure 3.2: The simulated reflection coefficient for $C_L = 0.8$ pF.

(a) amplitude; (b) phase.

84
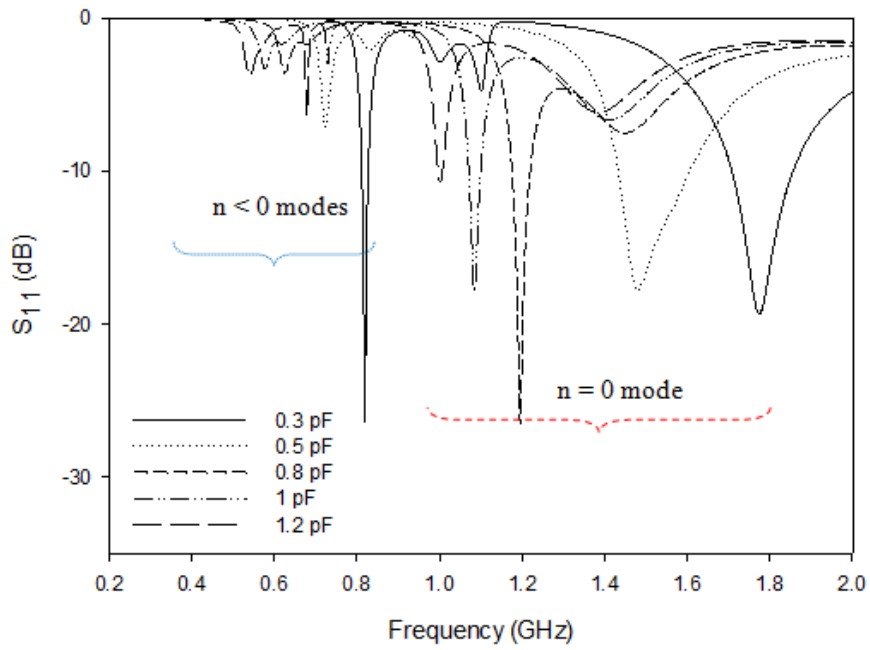
Figure 3.3: The simulated reflection coefficient vs the capacitance C_L.
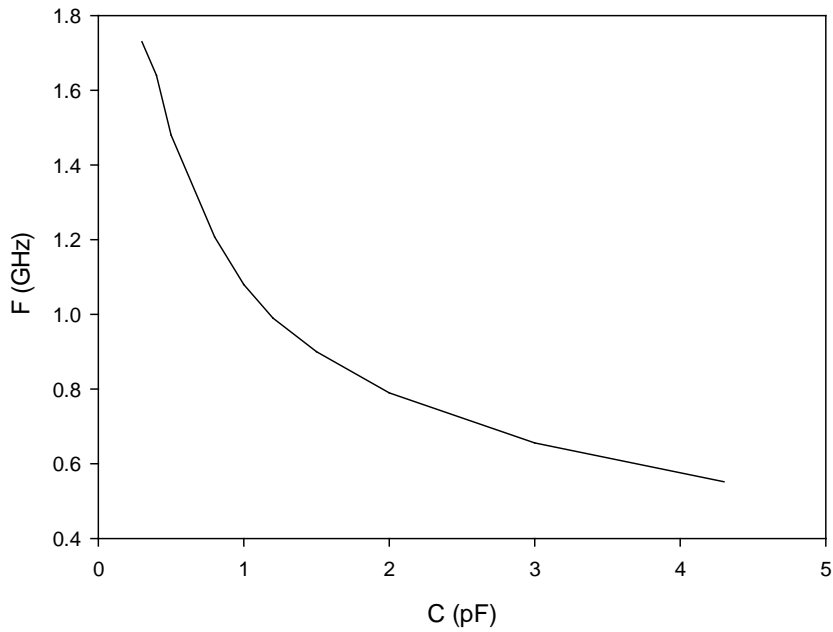
Figure 3.4: The dependence of the resonance frequency on the loading capacitance C_L.

85

The surface mounting devices (SMD) used in the antenna, the lumped capacitors and the inductors, will have an effect on the total performance. The parasitic resistances of these elements will cause some power losses and degrade the total efficiency of the antenna. The parasitic inductance or capacitance, however, might cause some shift in the resonance frequency. In order to include the effects of the parasitic components, manufacturer data was employed in the simulation. The S_{2p} files of the elements were extracted from the pre-defined vendor library in AWR software package. Chip capacitors from AVX® and inductors from Coilcraft® were used.

The $n = 0$ mode is well matched in the proposed antenna. It has a unique feature of uniform current distribution in both amplitude and phase. This mode gives a rise to a directional radiation pattern with maximum directivity orthogonal to the ground plane as shown in figure 3.5b. Furthermore, the radiation pattern maintains the same shape within the operating bandwidth. Modes with negative indices (-6,-4,-2) exist at frequencies lower than the zeroth order mode. The $n = -6$ mode has a current distribution with six quarter wavelengths in the loop as shown in figure 3.6a. This mode produces an omnidirectional pattern in the plane of the ground plane (xz) as shown in figure 3.6b. The mode $n = -4$ has a current distribution with four quarter wavelengths in the loop. The radiation pattern of this mode is an omnidirectional pattern in the plane of the loop as shown in figure 3.6d. Similarly, the $n = -2$ mode has a current distribution of two quarter wavelengths in the loop which produces an omnidirectional pattern in the plane of the ground plane as shown in figure 3.6f.

<div align="center">(a)   (b)</div>
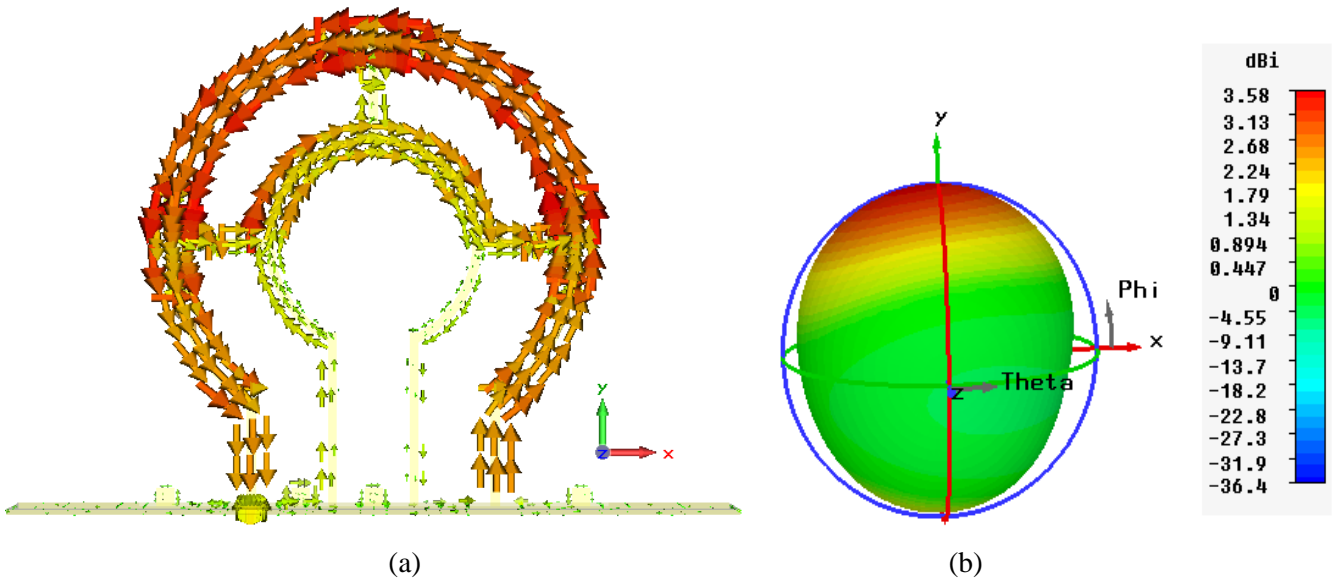
Figure 3.5: n = 0 mode at 1.17 GHz: (a) the current distribution; (b) the radiation pattern.

The radiation of the proposed LH loop antenna has been simulated and measured for different capacitance values. Unlike conventional loop antennas, the proposed antenna produces a directional pattern when operating in the n = 0 mode. Figure 3.7 shows the simulated and measured radiation pattern in the xy and yz planes. The maximum directivity is orthogonal to the ground plane. The cross polarization levels are below -10 dB. The radiation pattern has also been simulated and measured at 0.62 GHz, for n = -6 mode, as shown in figure 3.8.

(a)

(b)

(c)

(d)

(e)

(f)
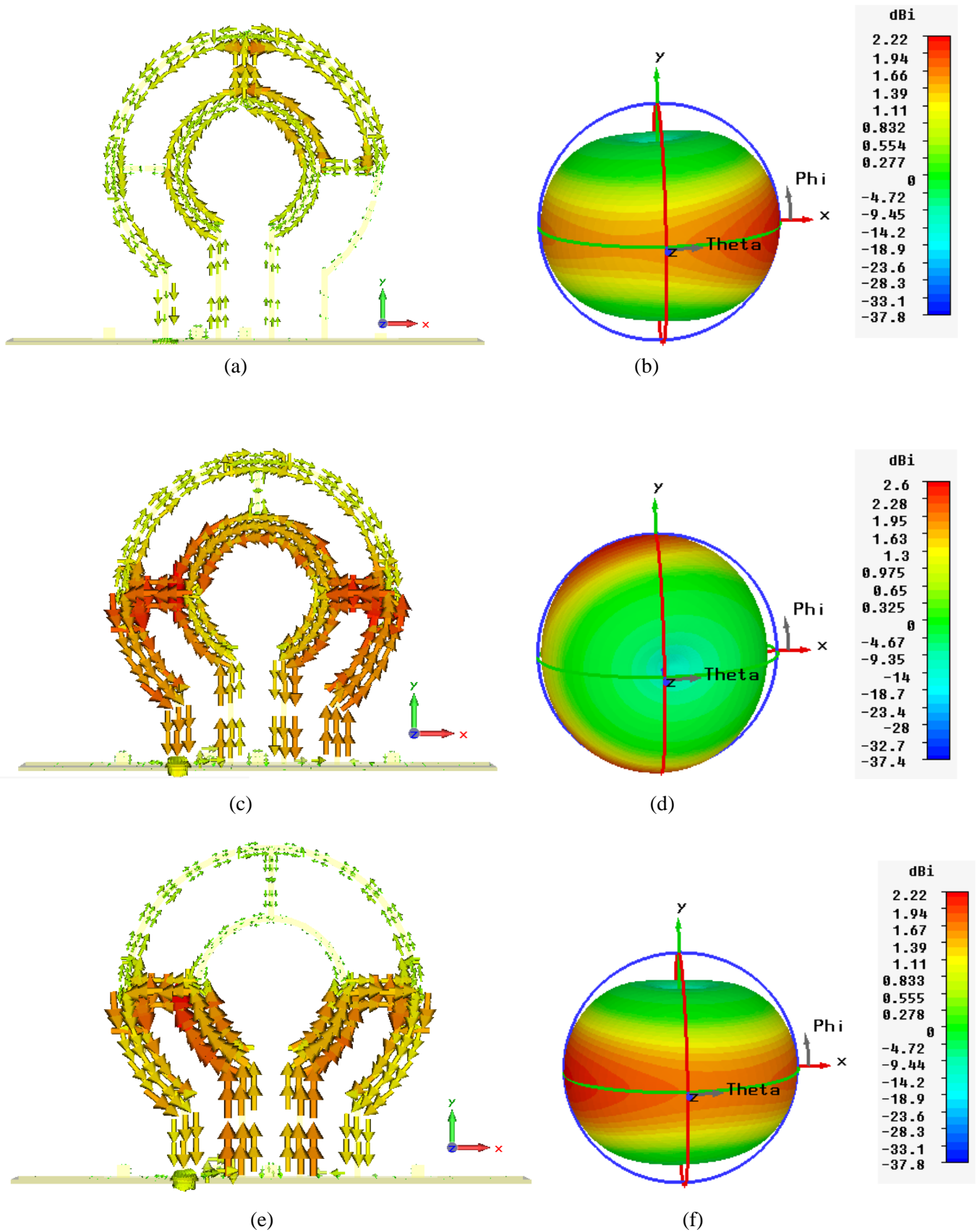
Figure 3.6: The current distributions in the LH loop for the modes: (a) n = -2; (c) n = -4; (e) n = -6. The simulated radiation patterns for the LH modes: (b) n = -2; (d) n = -4; (f) n = -6.
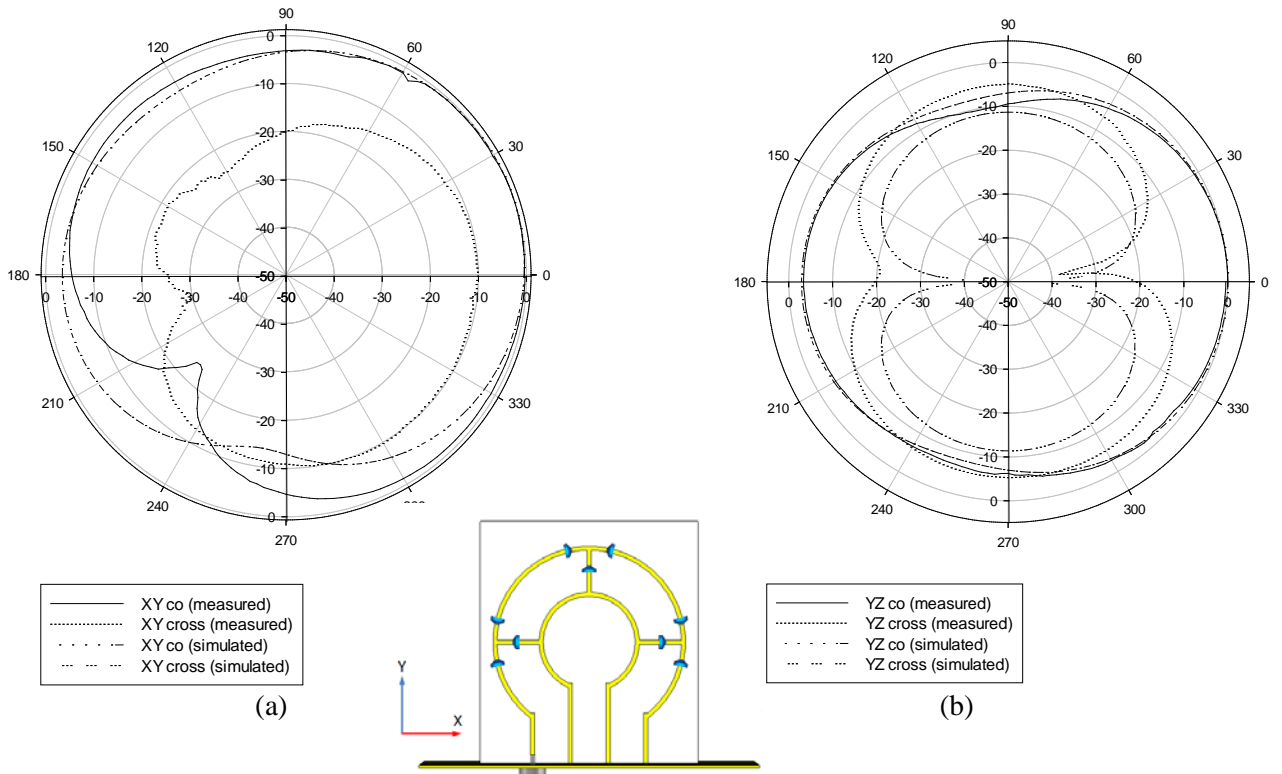
Figure 3.7: The simulated and measured radiation pattern for the n = 0 mode
at 1.2 GHz: (a) xy plane; (b) yz plane

(c)

(d)
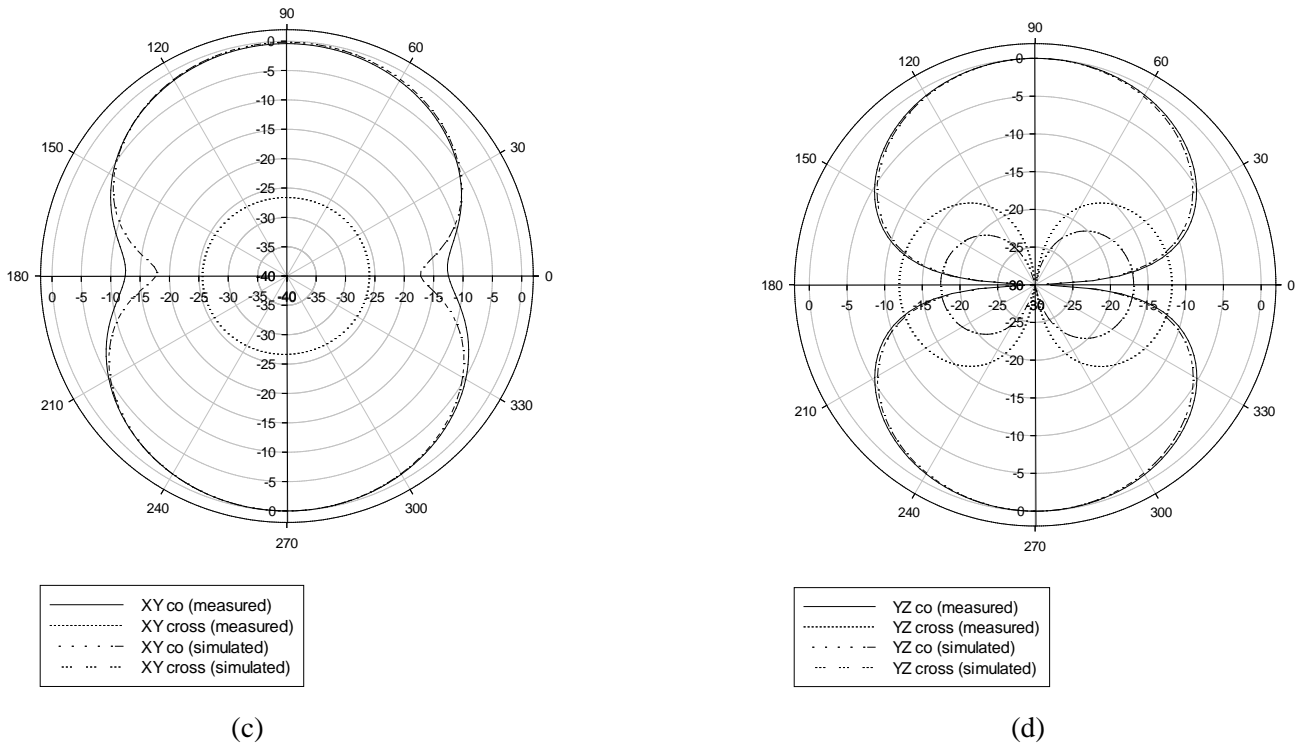
Figure 3.8: The simulated and measured radiation pattern for the n = -6 mode
at 0.63 GHz: (a) xy plane; (b) yz plane.
(Radial units are dB. Circumferential scale is in degrees).

The realized gain of the proposed antenna has been simulated and measured. Figure 3.9 shows the simulated realized gain versus frequency for the n = 0 mode. It shows the minimum simulated realized gain within the tuning bandwidth is 2.6 dBi. The realized gain has been measured for two prototypes with 0.5 and 0.8 pF capacitors as shown in figure 3.10. For the prototype with 0.5 pF capacitors, the n = 0 mode resonates at 1.47 GHz. The measured and simulated realized gains at this frequency are 3.7 and 4.14 dBi respectively. Due to the losses associated with the SMA connectors and cables used in the gain measurements, the measured gain is less than the simulated one. Also the alignment of the antenna is critical in order to ensure that the peak gain is being measured. The gain of the standard gain antenna has a tolerance of ±0.5 dB, which adds some error to the measurement. Figure 3.11 shows the radiation efficiency of the modes n = -6, -4, and 0. As can be seen in the figure, the n = 0 mode is the most efficient mode with radiation efficiency above 30 %. Figure 3.12 shows a fabricated prototype of the LH loop antenna.
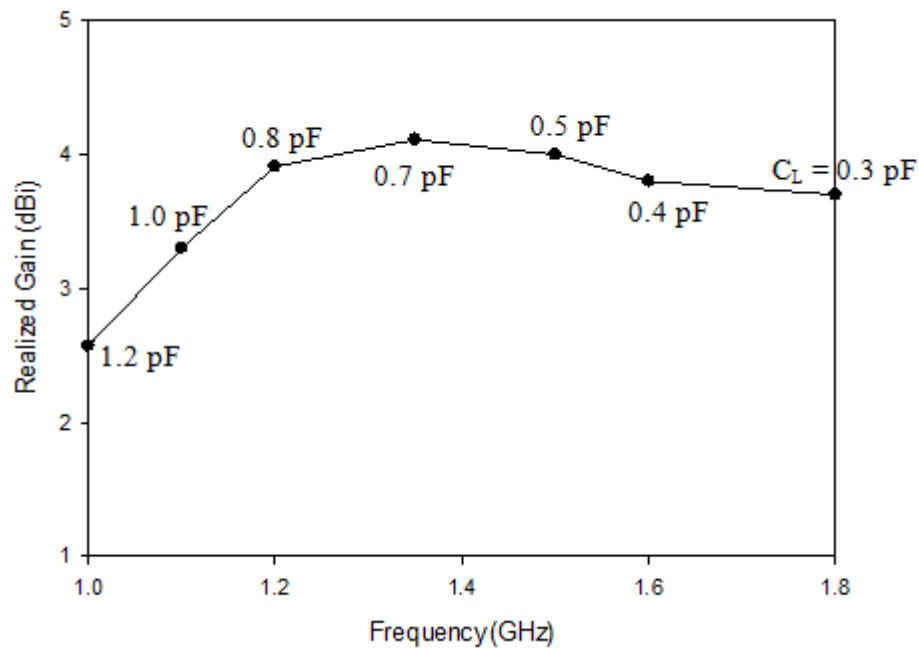
Figure 3.9: The simulated realized gain for the n = 0 mode within the tuning bandwidth.
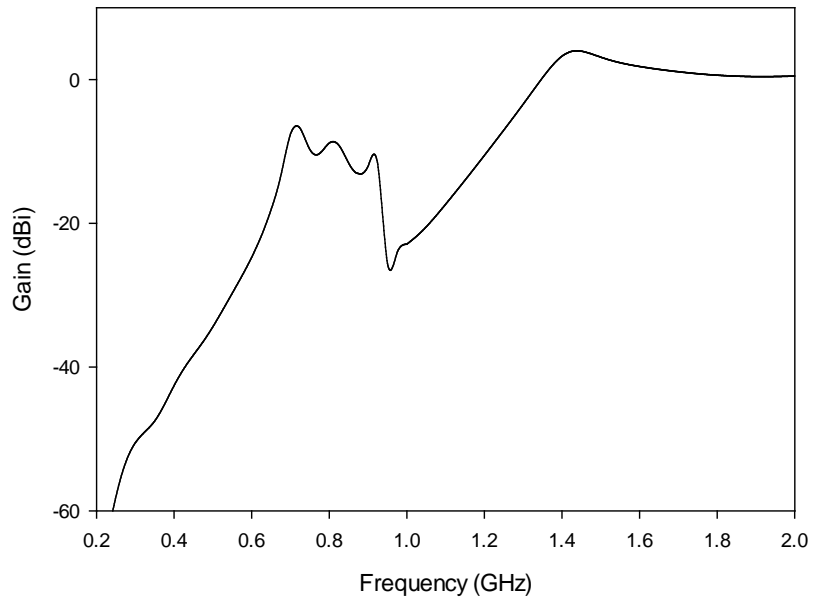
(a)
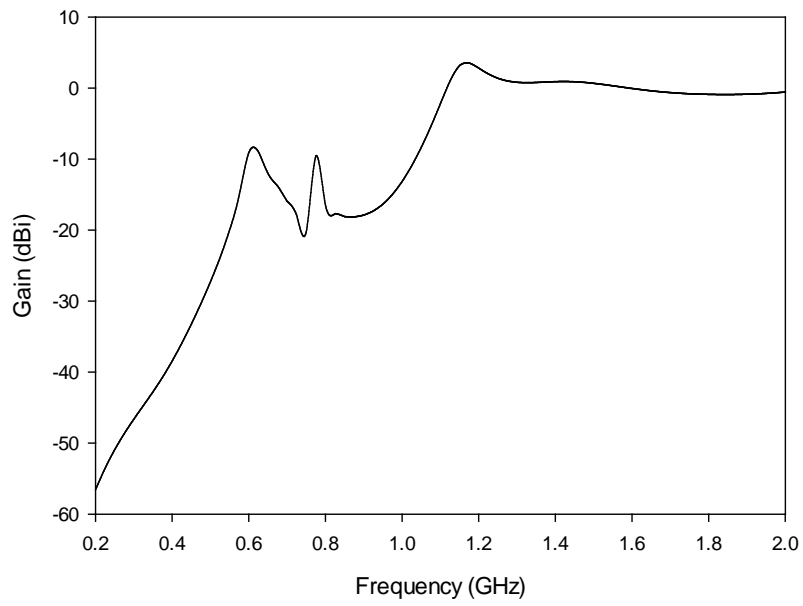
(b)

Figure 3.10: The measured realized gain: (a) $C_L = 0.5$ pF;

(b) $C_L = 0.8$ pF.
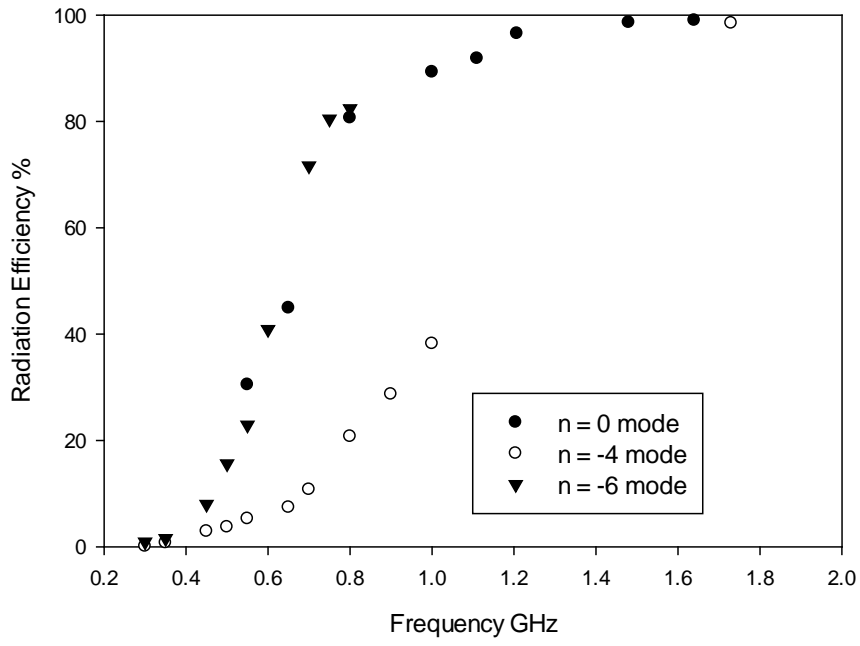
Figure 3.11: The simulated radiation efficiency for different modes.

Figure 3.12: Picture of the fabricated circular LH loop antenna over ground plane.

3.2.   Varactor-Tuned LH Loop Antenna

Since the resonant frequency of the LH loop antenna depends on the value of the loading capacitors, an electronically tunable antenna can be developed if the fixed capacitors are replaced by variable ones. In practice, the easiest way to implement variable capacitors is to use varactor diodes. Figure 3.13 shows the circular LH loop implemented with varactor diodes. The bias voltages of the varactors (V_b) are supplied through 0.4 mm, high impedance, lines printed at both sides of the loop. 10 kΩ resistors (R_c) from multicomp are used as RF chokes and connected across the bias lines. They represent very high impedance for the RF energy. Thus, they mitigate the leakage of the RF signal in the bias lines. 39 pF DC isolation/blocking capacitors (C_b) were used in the design in order to isolate the DC and RF components. They provide low impedance (capacitive reactance) such that the RF signal passes across them without reflection. The isolation capacitors also used to avoid damaging the vector network analyzer (VNA) by blocking the DC signal from flowing through the SMA connector. While one end of each varactor diode is connected to the bias line, the other end is connected to the copper plate underneath. The copper plate acts as a common ground for the RF and DC components. The end of the bias lines is widened in order to facilitate soldering them to the wires.

3.2.1. Details of the Varactor Diodes

The varactor diodes are widely used to implement variable capacitors. They provide junction capacitance that varies with bias voltage, thus providing an electronically tunable reactive element [13]. SMV1231 silicon varactor diodes from Skyworks® were used in the presented antenna. The diode has a voltage controlled capacitance

which decreases from 2.35 to 0.47 pF as the bias voltage increases from 0 to 15v as shown in Table 3.1. The diode has positive features such as high capacitance ratio, and low series resistance. The varactor diode is reverse biased where the positive terminal of the power supply is connected to the cathode of the diode.

Table 3.1: the capacitance vs the reverse bias voltage for SMV1231 varactor diodes

V_b (v)	0	1	2.5	4.0	6.5	10	15
C (pF)	2.35	1.58	1.09	0.794	0.59	0.497	0.466
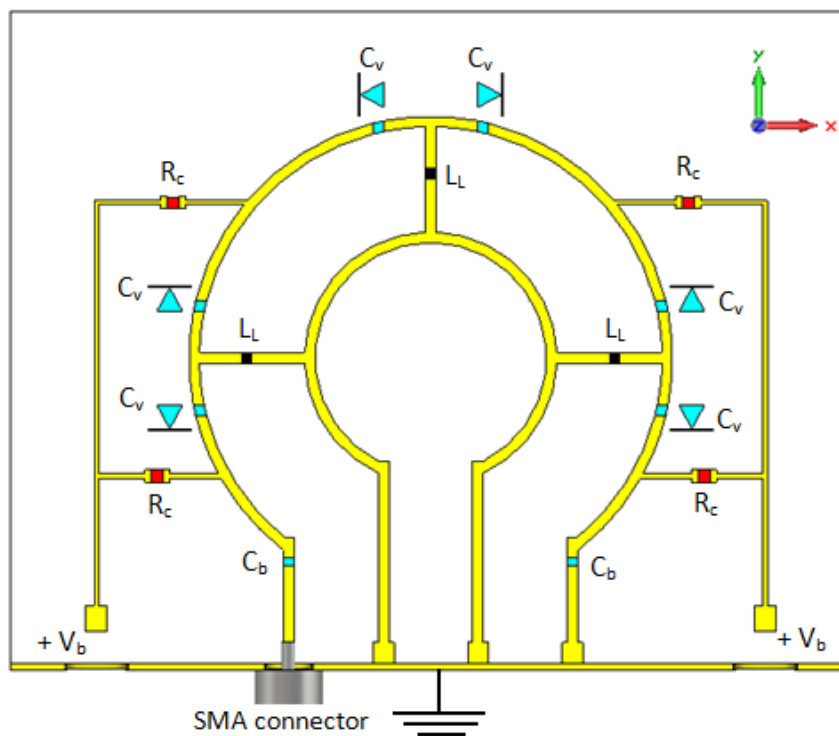
Figure 3.13: The varactor-tuned LH circular loop antenna.

(Dimensions are the same as the LH loop of figure 3.1)

3.2.2. Simulation and Measurement Results

Simulations were performed with CST Microwave Studio® and Microwave Office®. Figure 3.14a shows the simulated and measured reflection coefficient for bias voltage of 15 v, which implies a varactor capacitance of C_v = 0.47 pF. The simulation result exhibits a resonance at 1.53 GHz for the n = 0 mode. The magnitude of the reflection coefficient at this resonance is -28 dB. A small shift was observed in the measured result towards 1.48 GHz. The magnitude of the reflection coefficient at this resonance is -22 dB. Modes with negative indices are also excited. Figure 3.14b shows the measured S_{11} for different bias voltages. It can be seen that the resonant frequency is tuned from 1.53 GHz for V_b = 15 v to 0.91 GHz for V_b = 1.5 v. The achievable tuning range, considering the – 10 dB impedance matching, is 1.7:1. The tuning range is smaller than the simulated one because of the limited capacitance range of the varactor diode.

The radiation efficiency of the n = 0 mode has been simulated. Table 3.2 summarizes the simulated radiation efficiency, and realized gain for different bias voltages. The efficiency is higher than 45% within the operating bandwidth within which the antenna is well-matched.

  Improper design of the biasing circuitry may cause some spurious radiation and therefore it degrades the radiation properties of the reconfigurable antenna. In order to demonstrate the radiation properties of the proposed antenna, the radiation pattern has been measured and simulated for different bias voltages. The proposed antenna maintains the same radiation shape within the operating bandwidth. Figure 3.15 shows the simulated and measured radiation pattern for V_b = 15 v and 4 v at 1.53 GHz and 1.18 GHz respectively. The cross polarization levels in the direction of propagation are well below -15 dB. The well-shaped radiation patterns indicate that

95

the biasing circuitry has a small spurious radiation. Therefore, the radiation pattern of the varactor tuned loop is not degraded.

(a)

(b)
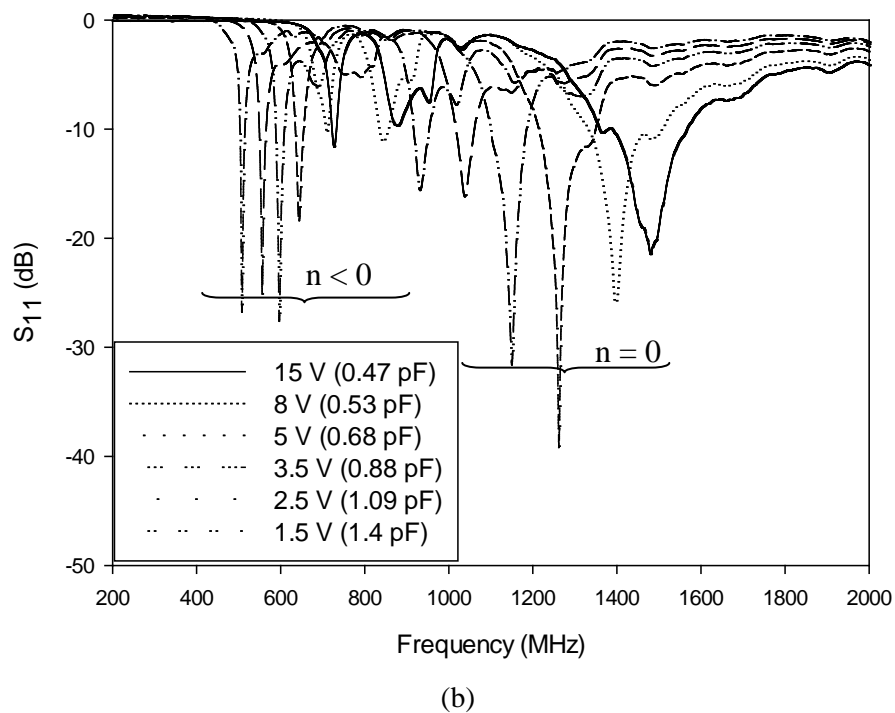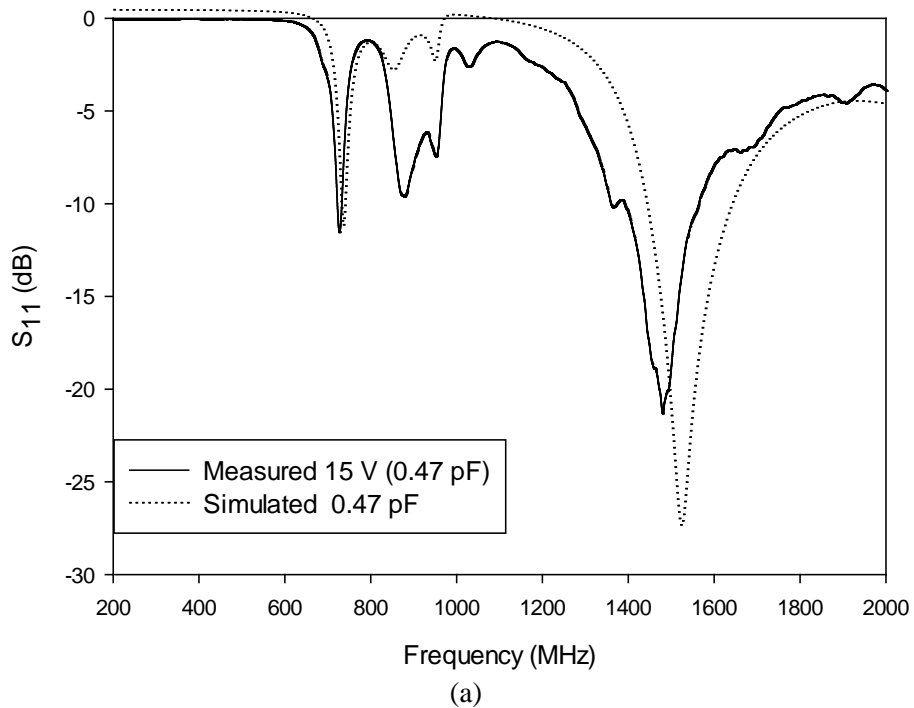
Figure 3.14: (a) The simulated (0.47 pF) and measured (15v) reflection coefficient; (b) the measured reflection coefficient for different bias voltages.
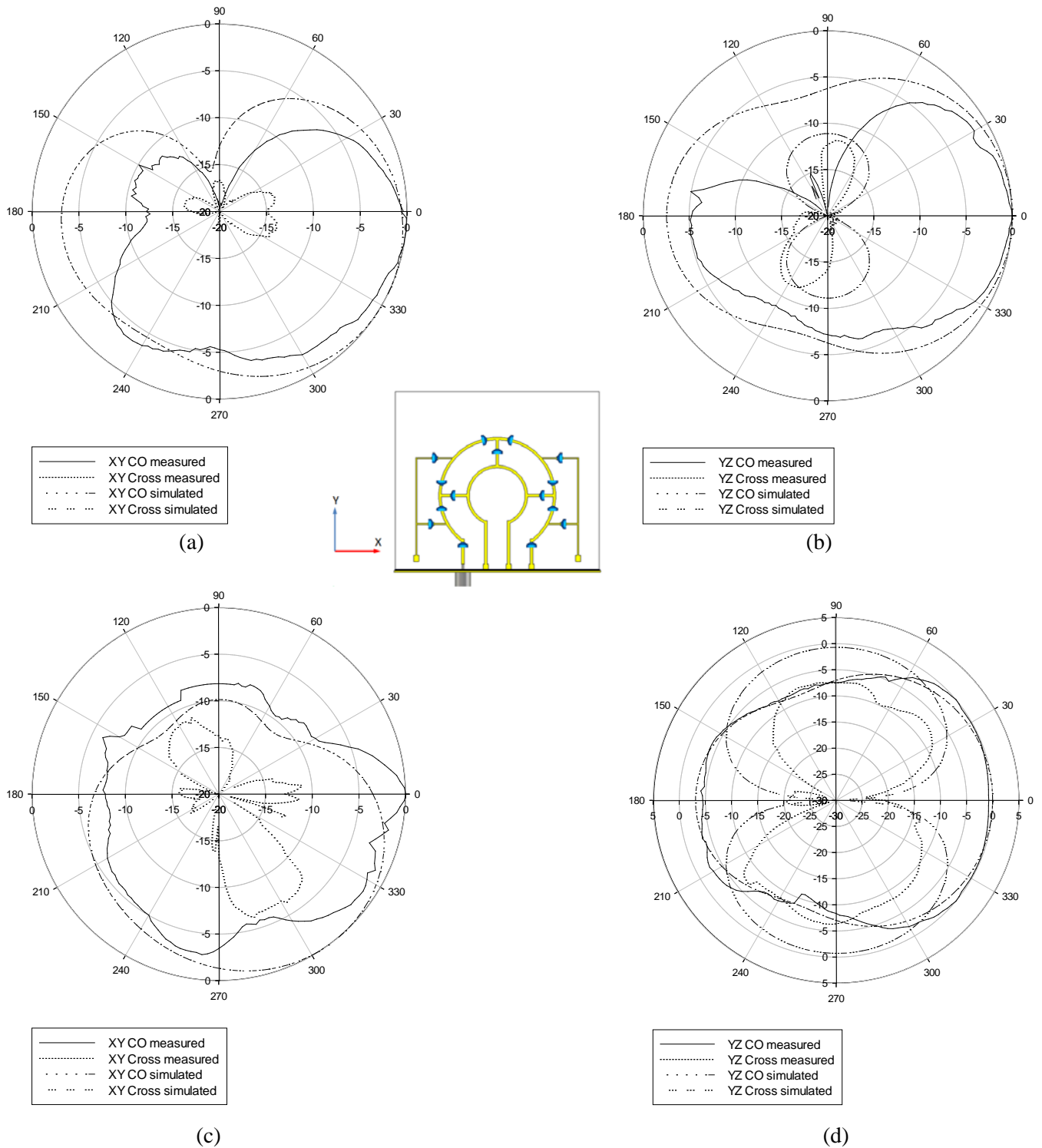
Figure 3.15: The simulated and measured radiation pattern for the n = 0 mode:

at 1.2 GHz (4 v): (a) xy plane; (b) yz plane;

at 1.53 GHz (15 v): (c) xy plane; (d) yz plane.

(Radial units are dB. Circumferential scale is in degrees)

Table 3.2: The simulated (measured) radiation efficiency and realized gain for different bias voltages

V_b (v)	15	5	4	2.5	1.5
f_0 (GHz)	1.52	1.3	1.18	1.04	0.93
η_{rad} (%)	89.1	84.3	75.6	60.56	54.5
Gain (dBi)	3.24 (3.0)	3.08	2.41 (2.1)	1.37	-0.18

The realized gain has been measured for the prototypes with 0.5 and 0.8 pF. Figure 3.17a shows the measured gain for $C_L = 0.5$ pF. Whereas the peak gain is 3.0 dBi measured at 1.48 GHz, the simulated one is 3.24 dBi. The peak gain for $C_L = 0.8$ pF is 2.1 dBi measured at 1.28 GHz which is smaller than the simulated gain of 2.4 dBi.
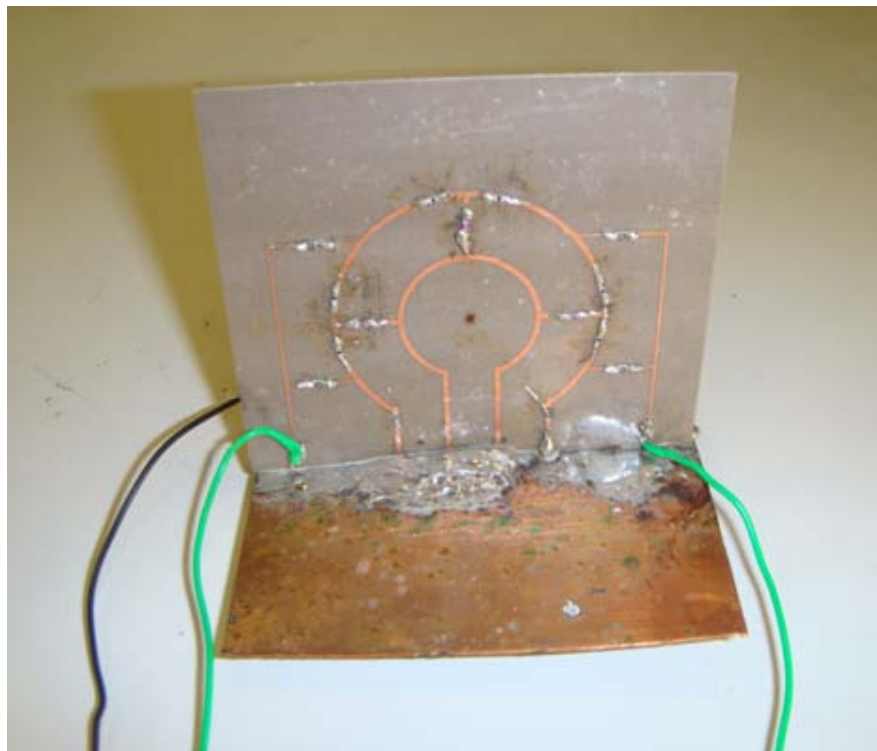
Figure 3.16: The varactor-tuned LH circular loop antenna.
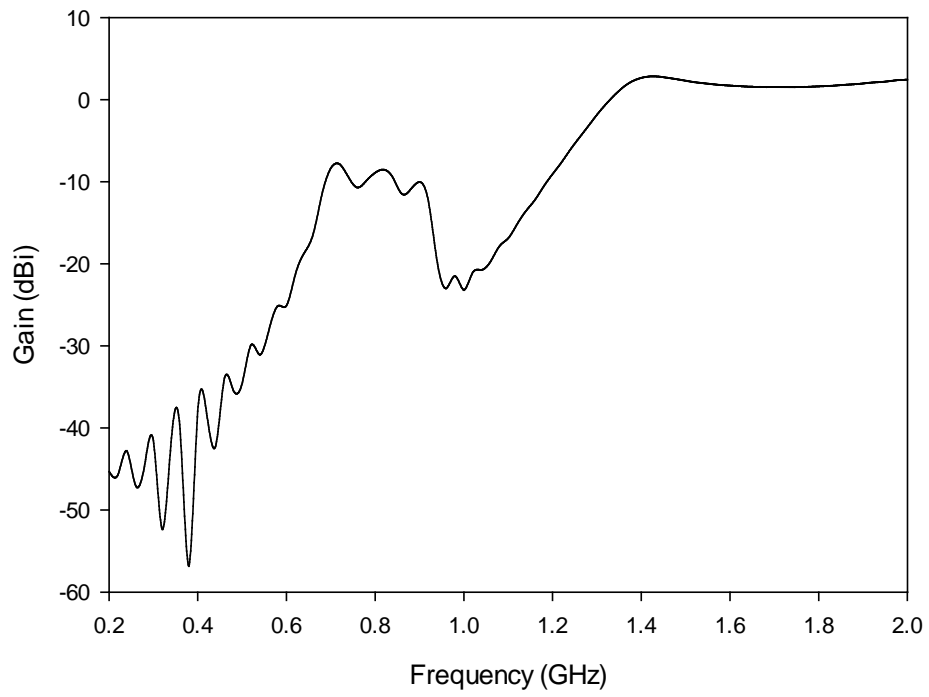
(a)
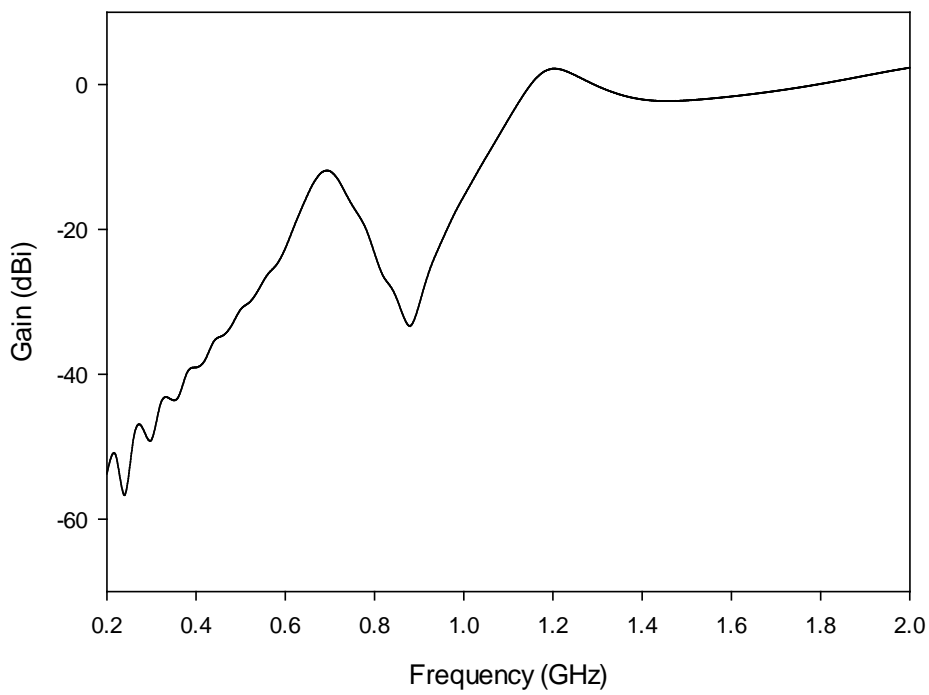
(b)

Figure 3.17: The measured realized gain: (a) $C_L = 0.5$ pF;

(b) $C_L = 0.8$ pF.

3.3. LH loop with single mode operation

In order to filter out the unwanted modes, a LH loop with filtering capability is designed. The low efficiency LH modes at lower frequency are suppressed and the n = 0 mode is maintained since it is highly efficient and well matched over wide frequency range as shown in section 3.1.2.

Since the unwanted modes exist at lower frequencies, a highpass filter (HPF) will be designed to detune these modes. A lumped element HPF is integrated in the antenna. The filter consists of five elements (n = 5), three series capacitors and two shunt inductors. The cut off frequency is chosen to be at the lower edge of the tuning range of the n = 0 mode. A five pole Chebychev lowpass prototype with a passband ripple of 0.1 dB is chosen. The lowpass prototype parameters, given for a normalized lowpass cutoff frequency $\Omega_c = 1$, are $g_0 = g_6 = 1$, $g_1 = g_5 = 1.1468$, $g_2 = g_4 = 1.3712$, $g_3 = 1.9750$.

The practical highpass filter with a cut off frequency at 0.9 GHz and 50Ω terminals can be obtained by applying the transformation to the lowpass prototype shown below [14]. However, this approach is not effective since it does not consider losses, and discontinuities. An effective method is to use the optimizer available in the circuit simulator of microwave office. The lumped elements are represented by discrete ports in CST simulation and the result is exported as touchstone file (S parameter) to the microwave office. The optimizer is run with the goals:

From 0.2 to 0.9 GHz: $S_{21} < - 30$ dB (stopband)

From 1.0 to 2.0 GHz: $S_{21} > - 0.5$ dB (passband)

After several runs, the required result was obtained. The values for the lumped capacitors and inductors were found to be: $C_1 = 2.1$ pF, $L_2 = 4.4$ nH, $C_3 = 1.7$ pF, $L_4 = 4.2$ nH, $C_5 = 2.3$ pF. In the highpass filter, each element in the lowpass prototype is

replaced by one of the opposite type. The optimized performance of the filter is shown in figure 3.19.
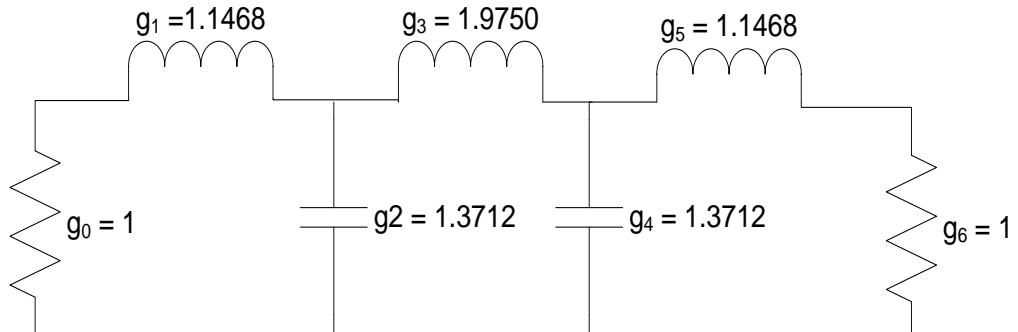
Figure 3.18: Chebyshev lowpass prototype with passband ripple of 0.1 dB.
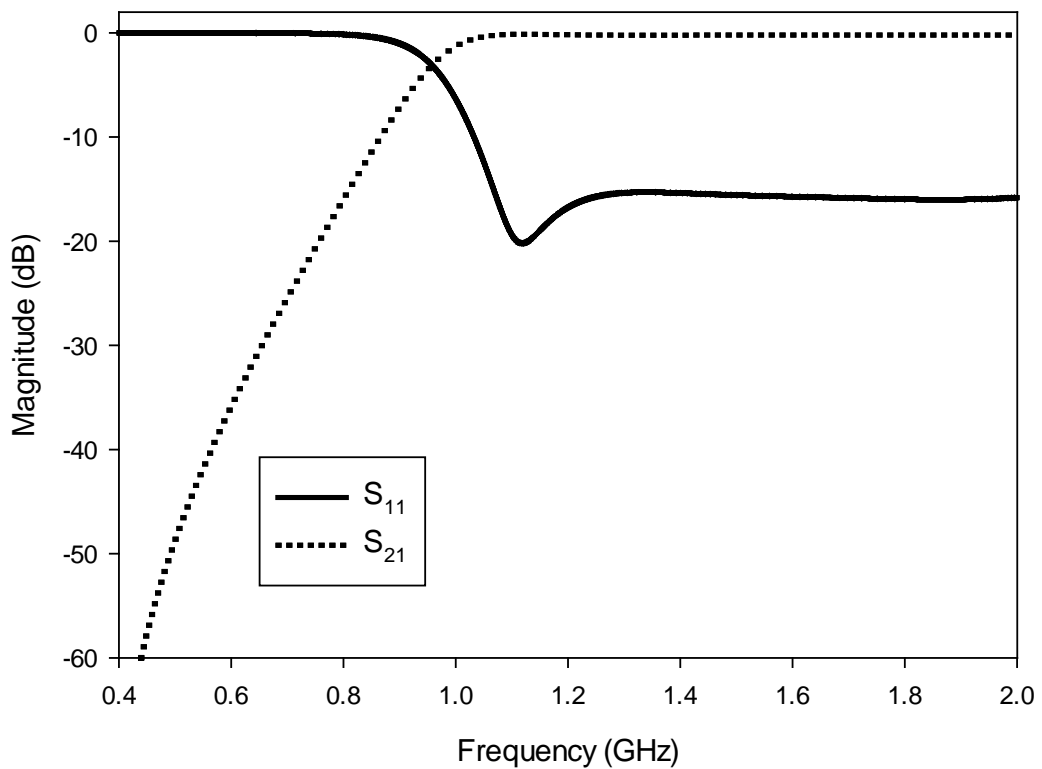
Figure 3.19: The simulated performance of the highpass filter.

Figure 3.20 shows the structure of the antenna with the HPF integrated. All the dimensions of the antenna are maintained as in figure 3.1. A small copper strip is printed on the opposite side of the substrate to act as ground plane for the filter and it is soldered to the copper plate underneath.

In order to demonstrate the filtering capability of the antenna, its performance is compared with the LH loop shown in figure 3.1. Figure 3.21 shows the simulated S_{11} for the structures for C_L =0.5 pF. It can be seen that the lower LH modes are not excited in the S_{11} result of the filter antenna. That is because they exist inside the stopband of the filter. For instance, the n = -6 mode which resonates at 0.73 GHz, can be observed in the S_{11} result of the LH loop antenna but it is not excited in the filter-antenna. It can also be seen that the integration of the BPF causes a slight shift in the resonance frequency. The resonance frequency of the n = 0 mode is shifted from 1.5 GHz to 0.9 GHz as the loading capacitance is increased from 0.5 to 1.2 pF. The tuning range, considering the – 10 dB return loss, is 1.6:1. Figure 3.23 shows the simulated and measured radiation pattern of the antenna.

(a)   (b)
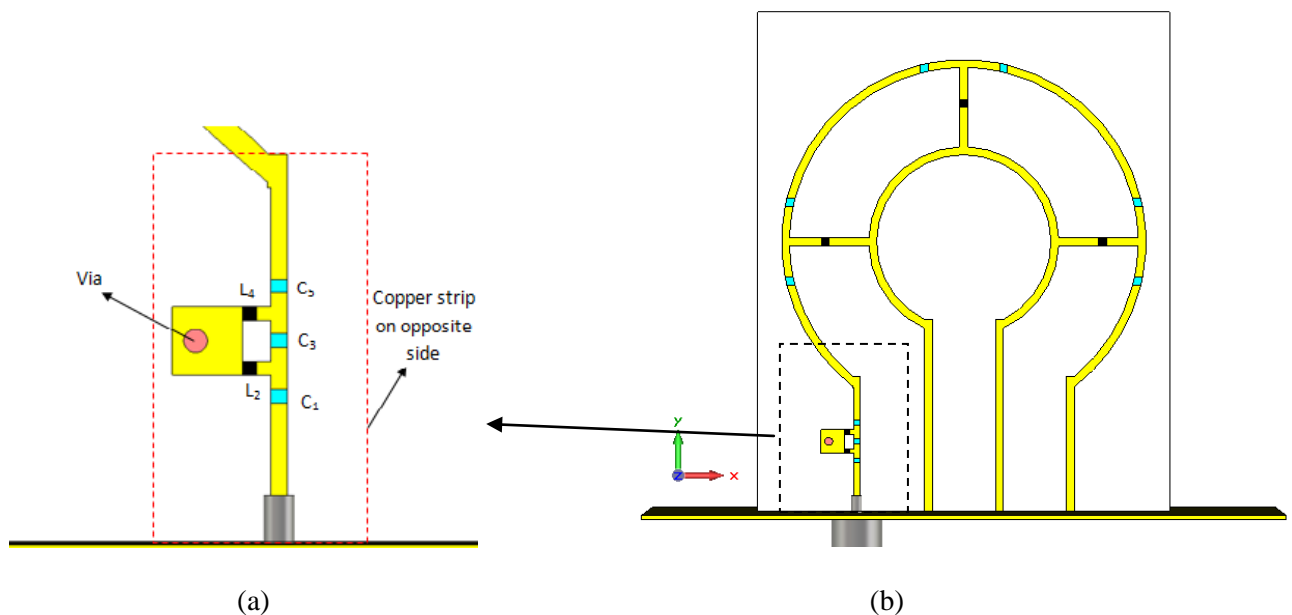
Figure 3.20: The structure of the LH loop antenna integrated with HPF.
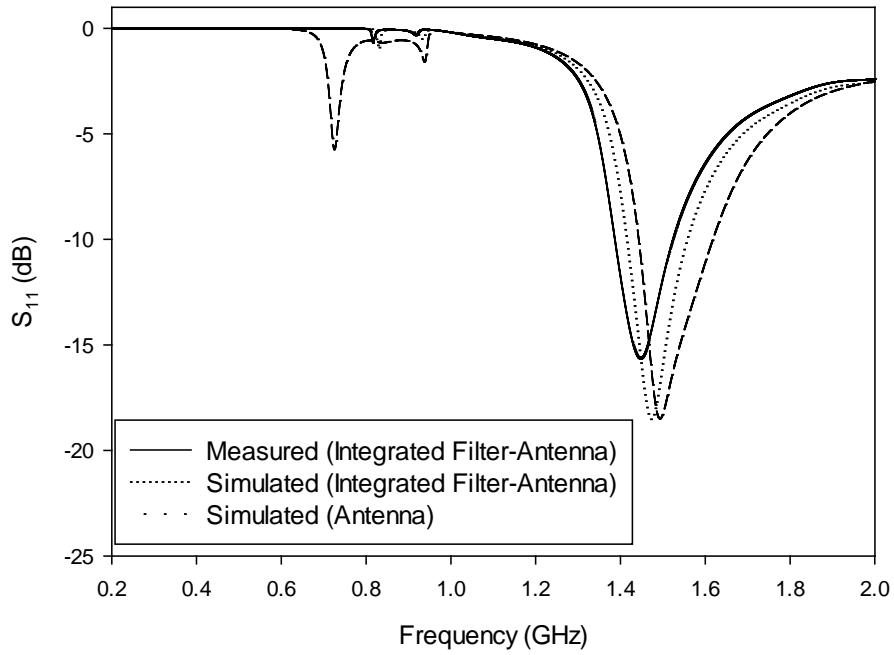
Figure 3.21: The simulated and measured S_{11} for $C_L = 0.5$ pF.
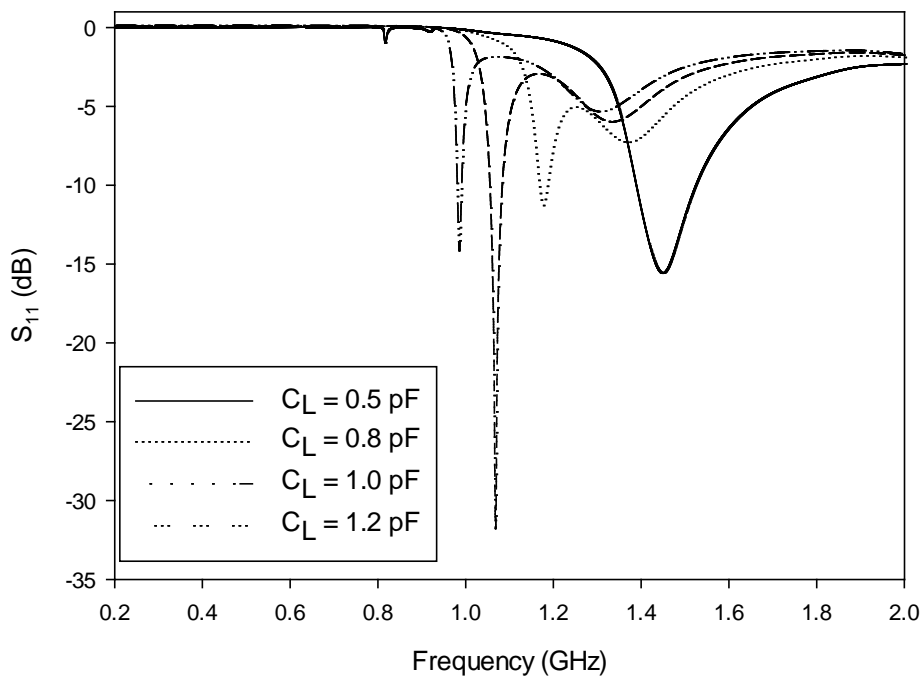
Figure 3.22: The simulated S_{11} vs the capacitance C_L

(a)

(b)
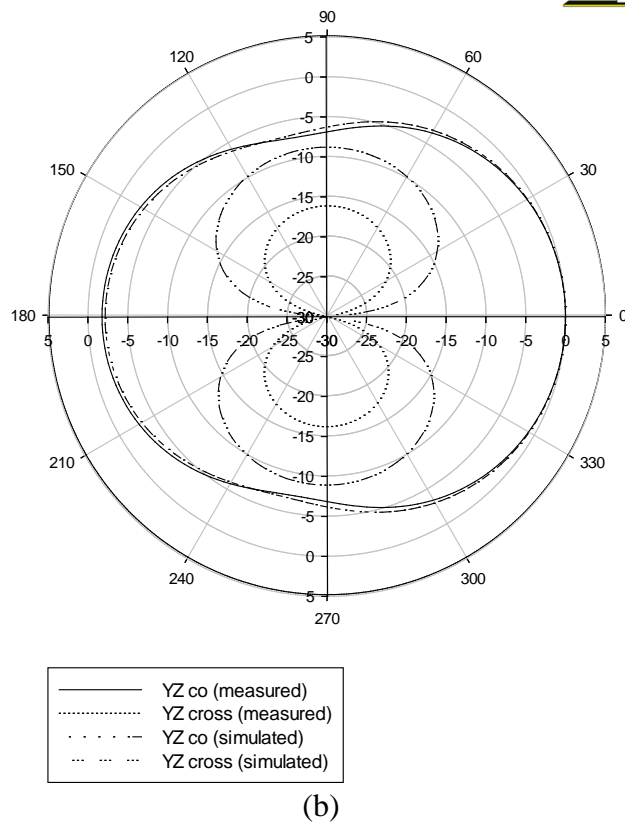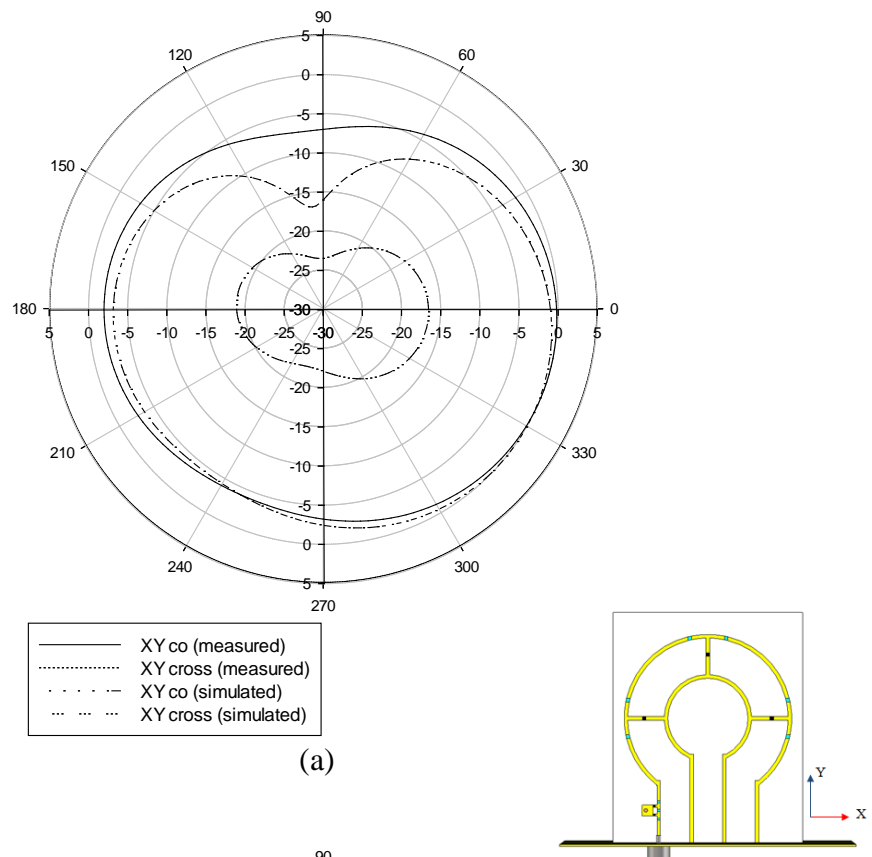
Figure 3.23: The simulated and measured radiation pattern for the n = 0 mode

For C_L = 0.5 pF at 1.47 GHz: (a) xy plane; (b) yz plane.

(Radial units are dB. Circumferential scale is in degrees)

The realized gain of the antenna is higher than 2 dBi within the operating bandwidth. The antenna exhibits less gain than the LH loop shown in section 3.1 due to the losses of the elements added in this prototype. Table 3.3 summarizes the radiation efficiency and realized gain for the integrated filter-antenna.

Table 3.3: The simulated (measured) radiation efficiency and realized gain
of the integrated filter-antenna.

C_L (pF)	0.5	0.8	1.0	1.2
f_0 (GHz)	1.47	1.17	1.07	0.98
η_{rad} (%)	98.21	94.33	90.82	87.2
Gain (dBi)	3.16 (2.8)	3.35	3.10	2.02
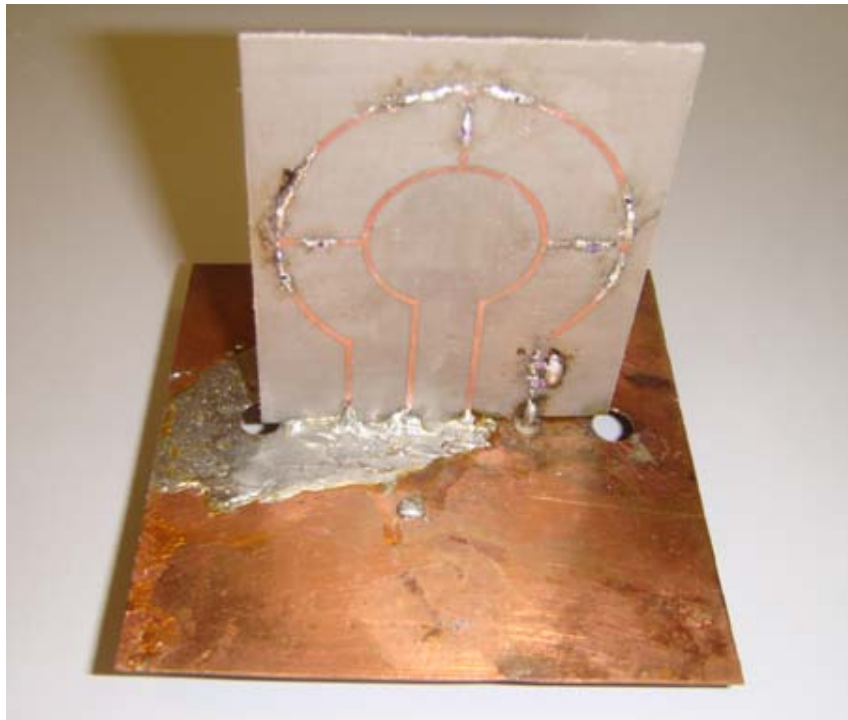
Figure 3.24: The LH loop antenna integrated with HPF.

3.4. Conclusion

LH printed circular loop antenna over ground plane is presented. The antenna exhibits the positive features of LH wire antennas such as size reduction, internal matching, and unique radiation properties. The size is further reduced due to the presence of the ground plane underneath (image theory). The circular half-loop antenna provides the $n = 0$ mode which has uniform current distribution. Consequently, it produces a directional radiation pattern with maximum directivity orthogonal to the ground plane. It is also well matched over wide frequency range. The resonance frequency of the antenna is tuned by varying the lumped capacitors. The achievable tuning range is 1.88:1 and it extends from 0.99 GHz to 1.86 GHz. Two prototypes were fabricated and measured using 0.5 and 0.8 pF. The realized gain is above 2.1 dBi within the tuning range. An electronically tunable antenna is developed by replacing the fixed chip capacitors with varactor diodes (variable capacitors). This design involves designing biasing circuitry to provide the control voltage to the varactors and to isolate the DC and RF components. The varactor tuned loop achieves tuning range of 1.7:1 and it extends from0.91 to 1.53 GHz. The realized gain is above 1.37 dBi within the tuning range. A tunable loop with filtering features was designed in order to filter out the unwanted low efficiency LH modes at lower frequencies. A lumped highpass filter was integrated in the antenna. The structure maintains only the desirable mode of $n = 0$ which is well matched from 0.9 GHz to 1.5 GHz.

References:

[1]   G. S. Smith, "Efficiency of electrically small antennas combined with matching networks," IEEE Transactions on Antennas and Propagation, vol. AP-40, no. 5, 369-373, May 1977.

[2]   V. Vesalgo, "The electrodynamics of substances with simultaneously negative values of ε and μ," Soviet Physics Uspekhi-User, vol.10, pp.509-514, 1968.

[3]   C. Caloz and T. Itoh, Electromagnetic Matamaterials: Transmission Line Theory and Microwave Applications. New York: Wiley, 2004.

[4]   H. Iizuka, P. S. Hall, and Lucas Borja, "Dipole antenna with left-handed loading," IEEE Antennas and Wireless Propagation Letters, vol.5, pp.483-485, 2006.

[5]   H. Iizuka and P. S. Hall, "Left-handed dipole antennas and their implementations," IEEE Transactions on Antennas and Propagation, vol.55, no.5, pp.1246-1253, May 2007.

[6]   Q. Liu, P. S. Hall, and A. Lucas Borja, "Dipole with Left-handed loading with optimized efficiency," in second European Conference on Antennas and Propagation (EuCAP), Edinburgh, UK, Novemebr 2007.

[7]   Q. Liu, P. S. Hall, and A. Lucas Borja, "Efficiency of electrically small dipole antennas loaded with left handed transmission lines," IEEE Transactions on Antennas and Propagation, vol.57, no.10, pp.3017-1253, October 2009.

[8]   A. Lucas Borja, P. S. Hall, Q. Liu, and H. Iizuka, "Omnidirectional loop antenna with left handed loading," IEEE Antennas and Wireless Propagation Letters, vol.6, pp.495-498, 2007.

[9]   P. S. Hall and Q. Liu, "Dual mode reconfigurable loop antenna with left handed loading," in Metamaterials 2008, Pamplona, Spain, September 2008.

[10] F. J. Herraiz-Martinez, P. S. Hall, Qing Liu, and Daniel Segovia-Varagas, "Left-handed wire antennas over ground plane with wideband tuning", IEEE Transactions on Antennas and Propagation, vol.59, no.5, pp.1460-1471, May 2011.

[11] F. J. Herraiz-Martinez, P. S. Hall, Qing Liu, and Daniel Segovia-Varagas, "Tunable left-handed monopole and loop antennas", Antennas and Propagation Society International Symposium APSURSI, pp.1-4, June 2009.

[12] Ghaith Mansour, P. S. Hall, and Peter Gardner, "Circular loop antenna loaded by left-handed ladder network", International Union for Radio Science URSI, January 2011.

[13] D. Pozar, Microwave Engineering, 2nd Edition, John Wiley and Sons Inc., New York, 2005.

[14] Jia-Sheng Hong, and M .J. Lancaster, Microstrip Filters for RF/Microwave Applications, New York, USA: John Wiley & Sons, 2001.

CHAPTER IV

SLOT-FED RECONFIGURABLE PATCH ANTENNAS

FOR MULTI-FREQUENCY OPERATION

This chapter presents a reconfigurable microstrip patch antenna concept for multi-frequency operation. The antenna is fed by a coplanar waveguide (CPW) via a capacitive coupling slot, which enables an easy reconfigurability of the resonant frequency by incorporating switches loaded in the coupling slot. Switchable patches are proposed in section 4.3. The resonant frequency of the antenna can be tuned by activating/deactivating the switches. Three prototypes are presented. The first two incorporate two switches and are capable of switching between two and four frequency bands over frequency ranges of 1.36:1 and 1.23:1 respectively. The third prototype incorporates four switches and is capable of switching between sixteen frequency bands, over frequency range of 1.5:1. A tunable version is presented in section 4.4, which allows tuning of the resonant frequency by utilizing switches and capacitors in the coupling slot. The achievable tuning bandwidth is 1.7:1 and it extends from 1.39 GHz to 2.36 GHz. The proposed structures have a compact and simple biasing circuit. Simulations and measurements show that the proposed antennas demonstrate excellent impedance matching, well-shaped and stable radiation patterns and good gain at all operating frequencies.

The antennas presented in this chapter were simulated using the time domain solver (transient solver) in CST Microwave Studio®. The S-parameter files for the PIN diode switches were obtained from the manufacturer's website. The S-parameter files for the DC blocking capacitors were imported from the predefined vendor's library in

Microwave Office software package®. These S_{2p} files were exported to the circuit simulator in CST MWS.

4.1. Objective

New technologies are emerging in communication systems, such as cognitive radio (CR) and software-defined radio (SDR), which add new opportunities and challenges to antenna design. Covering multiple frequency bands with a single and efficient antenna is quite significant challenge. Employing frequency reconfigurable antenna that has the ability to switching between different frequencies seems a promising solution. Such an antenna would not cover all bands simultaneously, but would provide narrow instantaneous bandwidths that can be selected in a dynamic way. It also would have higher efficiency than a wideband or multi band antenna. An intrinsically narrowband antenna with dynamically controlled frequency response easily achieves frequency agility. In addition, the narrow instantaneous frequency response eliminates the need for filtering circuitry in the RF front end. Thus, the reconfigurable antenna provides high out of band gain suppression as compared to multi-band or wideband antennas.

Reconfigurable patches are good candidates for wireless communications due to their ability to improve the system's capacity by adjusting the resonant frequency, radiation pattern and polarization modification [1]. To achieve reconfigurability in an antenna, RF switching devices such as semiconductor, photoconductor switches, micro-electromechanical system (MEMS) switches can be used. The PIN diode switch is widely used in microwave circuits because of its good reliability, high switching speeds, compact size, low insertion loss, and its ability to handle high currents. Various designs for switchable patch antennas are presented in the literature.

Switchable patch antennas with PIN diodes loaded in the radiating element were presented in [2-8]. This is normally achieved by etching slots at appropriate positions in the radiating patch. In order to achieve different resonances, the length of the slot is adjusted by inserting switches. In the case of electromagnetic coupling, switchable patches have been realized by placing the PIN diode switches in the feeding network or the coupling slot [9-14]. Alternatively, the frequency reconfigurability can be achieved by using varactor diodes [15-17]. A tunable dual-band microstrip antenna is presented in [15]. By adding a parasitic strip parallel to the square patch, the dual-band operation is obtained. The two resonant frequencies are then tuned using a varactor diode inserted between the patch and the strip. A patch antenna with wide and tunable bandwidth is presented in [16]. The patch is divided into three parts (sub-patches). In order to tune the resonant frequency, varactor diodes are inserted in the gaps between the sub-patches. Dual frequency operation in [17] is achieved by perturbing the fundamental resonant mode of the patch using a C slot, splitting it into two distinct modes, frequency tuning is obtained by using a varactor diode. Tunable patches with the varactor diodes located at the radiating edges of the patch [18-21]. This leads to widening the tuning range since the electric field is maximum at the centre of the radiating edge. Tunable patch with varactor diode placed at the non-radiating edge is presented in [22]. A slot might be etched in the radiating patch, through which the varactor diodes can be connected as presented in [23-24]. Many of the antennas reported in the literature suffer from limitations such as the ability to only switch between a limited number of frequency bands, or exhibiting multiband resonances. Antennas with multi-resonances are not desirable as a filtering network will be needed to filter out unwanted frequencies. The proposed antennas overcome all these limitations.

The design of frequency reconfigurable patch antenna, allowing easy reconfigurability of the frequency band of operation, is the main objective in this chapter.

4.2. Capacitively Coupled Patch

The antenna as shown in figure 4.1 consists of a rectangular patch printed on the top of the substrate and a thin slot etched, opposite to the patch, in the ground plane. The slot is capacitively fed by a coplanar waveguide. The radiating patch was designed using transmission line calculations [25-26] to operate at 2.4 GHz. The antenna is printed on Taconic TLC32 substrate of thickness h=1.6 mm and dielectric constant ε_r=3.2. The patch width is W_p=41 mm and length L_p=30 mm, the ground plane and the substrate have a width of Wg=100 mm and a length L_g=100 mm. The coplanar waveguide is designed to have 50Ω characteristic impedance. The width of the conducting strip is 4 mm and the gap between the conducting strip and the ground plane is 0.5 mm.
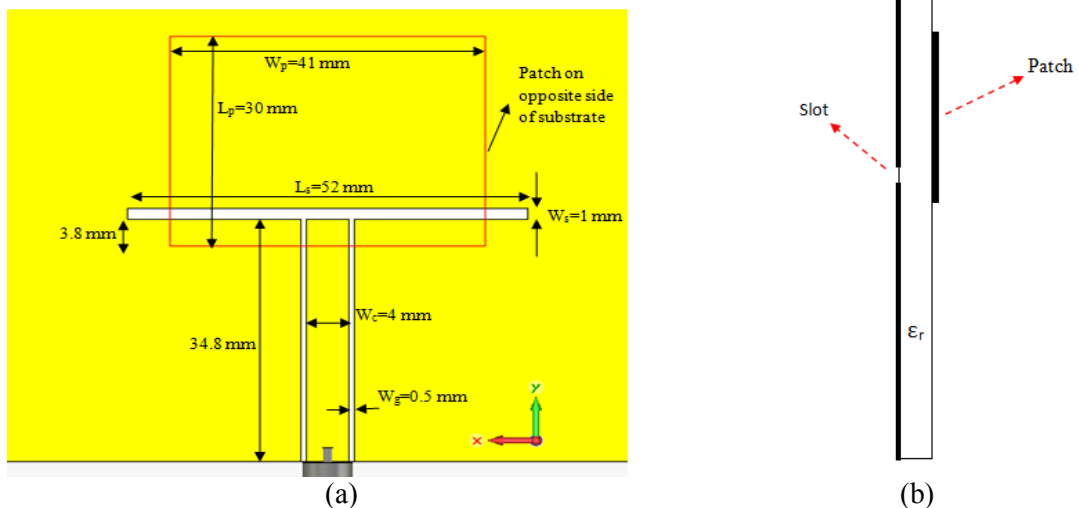
Figure 4.1: The structure of capacitively coupled patch: (a) bottom view; (b) side view

As these antennas are symmetrical with respect to the feeding CPW line, no CPW even mode can propagate in the CPW line [27]. This simplifies both theoretical studies, where only the propagation of CPW odd mode to be considered, and measurements, which don't require bond wires along the feeding line to achieve ground equalization.

The length of the coupling slot affects the resonance frequency but has only a small effect on the return loss. The resonant frequency decreases by increasing the slot length as reported in [27-28]. Thus, the resonance frequency can be tuned by changing the length of the slot. The proposed prototypes have different slot lengths (L_s) but the same slot width (W_s) of 1mm. PIN diodes are inserted across the slot to effectively alter its length.

4.3.   Switchable Patches

Three prototypes are presented in this section. The first prototype is shown in figure 4.2a. It uses two PIN diodes that are symmetrically located in 40 mm length slot and are 23 mm apart. In order to obtain diode biasing, two parallel thin slots are etched in the ground plane. Thus, two DC-isolated conducting strips are created. The strips, as shown in figure 4.2, are parallel to the CPW. They are connected to the power supply through metal wires to provide a path for the DC current. The area above the coupling slot provides a common ground for the DC and RF components. Four 27 pF DC isolation capacitors are soldered across the bias slots 10 mm apart. The capacitors are used to isolate the RF and the DC components. They provide low capacitive reactance such that the RF signal will pass through them with little loss or reflection. The PIN diodes are inserted across the coupling slot. The anode terminal of the diode is soldered to the lower edge of the coupling slot which is connected to the positive terminal of the power supply. However, the cathode terminal is soldered to the upper

113

edge of the slot which is connected to the negative terminal of the power supply. This configuration leads to excellent RF continuity and DC isolation.

The antenna prototype 1 is capable of switching between two frequency bands. Since two PIN diodes are used, and each diode could be either on or off, There are (2^2) 4 possible combinations and consequently 4 corresponding frequency bands. However, only two distinct bands are achievable in this prototype. Either both switches on or both of them off. The switches can't be independently biased because the PCB end launch connector shortens the conducting strips attached to the switches. In the prototype 2, shown in figure 4.2b, the biasing circuitry has been modified to allow the switches to be independently biased. An extra thin slot of 0.3 mm width is added parallel to the CPW between the CPW and one of the switches. Also, the switches have been located at asymmetrical positions so that activating one of them results in different frequency band. Thus, the number of achievable frequency bands is increased to four.

(a)   (b)
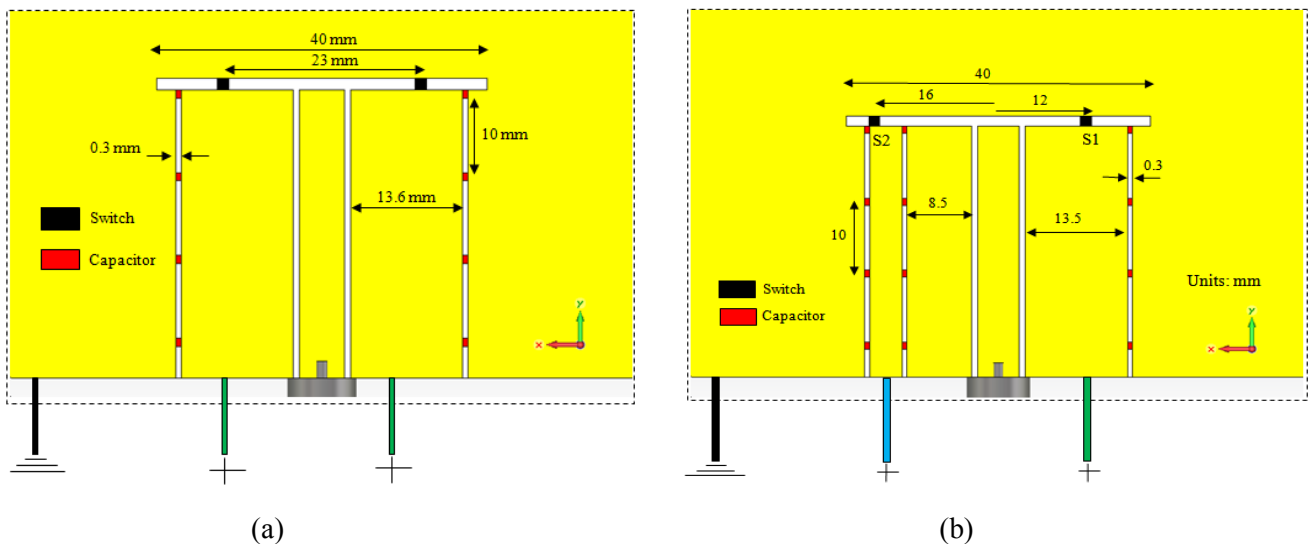
Figure 4.2: Bias and switch details of antenna of figure 4.1: (a) prototype 1; prototype 2 (Figures are not to scale)

In order to increase the number of frequency bands, the number of switches might be increased. A switchable patch with four switches is proposed in prototype 3 of figure 4.3. The biasing circuitry of the diodes is similar to the prototype 1. An extra two slots parallel to the CPW are etched in the ground plane resulting in extra conducting strips parallel to the CPW. These strips provide current paths for the two PIN diodes added in this layout. The switches are asymmetrically located and independently biased.
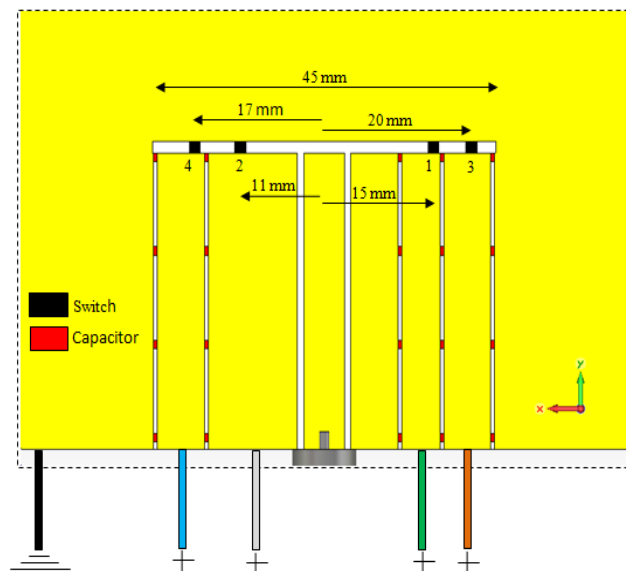
Figure 4.3: Bias and switch details of prototype 3

4.3.1. Details of the PIN Diodes

In early days of reconfigurable antennas, semiconductor switches were not available commercially. Therefore, many frequency reconfigurable antennas were implemented using mechanical switches. These switches exhibit low loss, but they don't provide fast switching. Semiconductor and MEMS switches appeared as alternative to the mechanical switches. A PIN diode can be used as switch in the design of reconfigurable antenna to achieve the reconfigurable frequency capability. PIN diodes are the widely used switching devices for RF and microwave systems. They have

several positive features, such as low insertion loss, good reliability, high switching speed and low cost. BAR50-02V silicon PIN diodes from Infinion® were used in the proposed antennas. Their operating frequency range extends from 10 MHz to 6 GHz. They have low forward resistance and low capacitance at zero volts reverse bias. The PIN diode is a current dependant RF resistor, the resistance decreases as the forward current increases. In order to minimize the parasitic resistance of the PIN diode, a 100 mA current (maximum current rating) is applied to the diodes for the forward biased case. The reverse biased voltage applied to the PIN diodes is 0 V. Current limiting resistors are used to avoid damaging the diodes and the DC voltage source. By controlling the biasing voltage, the switches can be turned on or off. Real components that include parasitic elements will change the performance of the antenna. They introduce loss causing a reduction in the total efficiency. S_2p files for the on and off state of the diode were extracted from the manufacturer's website [29]. The S_2p file for the DC blocking capacitors was extracted from the predefined vendor's library in Microwave Office software package®. These files were imported into the circuit simulator of CST MWS where the simulations were performed.

4.3.2. Simulation and Measurement Results

4.3.2.1 Resonance Properties

The proposed structures were simulated using the time domain solver in CST Microwave Studio®. The proposed prototypes have been fabricated and measured using an HP8722D vector network analyzer (VNA). Figure 4.4 shows the simulated reflection coefficient versus the slot length (L_S) for the capacitively coupled patch shown in figure 4.1. The slot length is increased from 14 mm to 50 mm while the slot

116

width is kept fixed at 1 mm. The resonance frequency decreases from 2.6 GHz to 1.4 GHz as the slot length is increases from 14 to 52 mm. This result gives an indication of the possible switching bandwidth. As can be seen in figure 4.4, the magnitude of the reflection coefficient remains below -10 dB ($|S_{11}| < $ -10 dB) for a wide range of slot lengths. Therefore, it is possible to switch the resonant frequency between many frequency bands by placing switches in the coupling slot to alter its length.
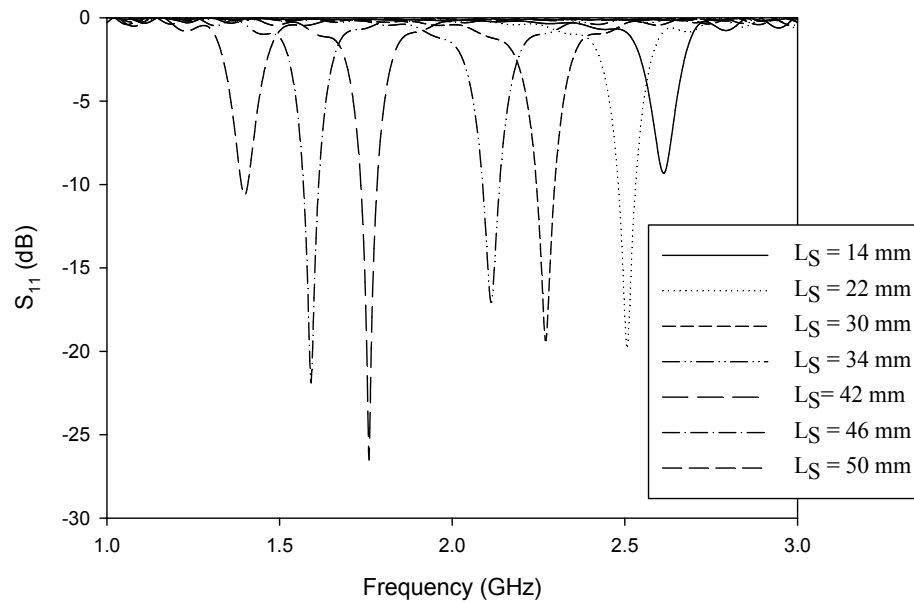
Figure 4.4: Simulated S_{11} for different slot lengths

The simulated and measured reflection coefficient for the prototype 1 is shown in figure 4.5. The simulation result for the switches on exhibits a resonance at 2.32 GHz. The magnitude of the reflection coefficient at this resonance is -14 dB. The -10 dB impedance bandwidth is about 2.58%. A small shift was observed in the measured result towards 2.48 GHz. The lower band is obtained when both switches are off. The simulation result for this case exhibits a resonance at 1.82 GHz. The magnitude of the reflection coefficient at this resonance is -18 dB. The -10 dB return loss bandwidth is about 3.04%. The measured result shows a narrow band resonance at 1.83 GHz.

Table 4.1: Different states of the PIN diodes and corresponding frequency bands of prototype 1

Switches	Freq Meas (Sim)	BW (measured)
OFF	1.83 (1.82) GHz	2.18 %
ON	2.48 (2.32) GHz	2.22%
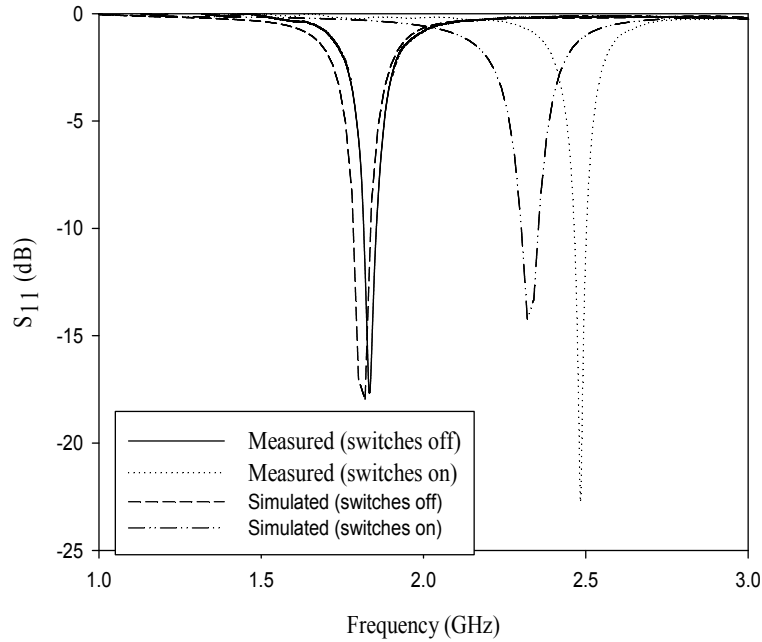
Figure 4.5: Simulated and measured reflection coefficient for different switch states for the prototype 1

The measured reflection coefficient for the prototype 2 is shown in figure 4.6. This prototype is capable of switching between four frequency bands. The measured result shows that the resonant frequency can be switched between 1.83, 1.96, 2.07, and 2.25 GHz. The achievable switching range extends from 1.83 to 2.25 GHz with a switching ratio of 1.23:1. The -10 dB measured bandwidth is above 1.7 %. The results are summarized in table 4.2.

Table 4.2: Different states of the PIN diodes and corresponding frequency bands of prototype 1

Switches		Frequency (GHz)		BW % Measured
1	2	measured	simulated	
OFF	OFF	1.83	1.80	2.46
OFF	ON	1.96	1.92	2.54
ON	OFF	2.07	2.04	1.7
ON	ON	2.25	2.16	2.22
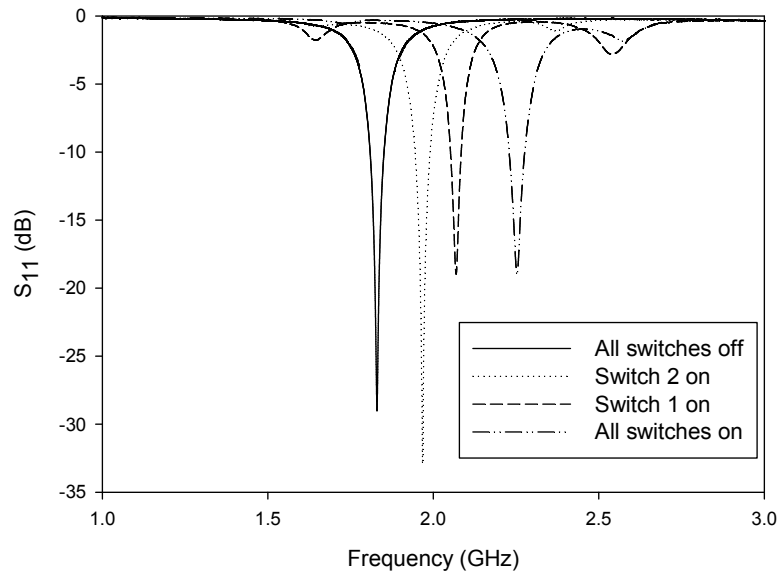
Figure 4.6: Measured reflection coefficient for different switch states for the prototype 2

Many factors can contribute to the discrepancy between the simulated and measured results. The position of the switch is thought to be the most significant factor. A difficulty in placing the switches in the right positions was experienced while fabricating the antennas. The deviation from the intended positions is estimated to be up to ± 2 mm. A small shift in the PIN diode position will cause a shift in the resonant frequency. Other factors cause the difference between the measured and simulated results include the etching accuracy, the dielectric substrate tolerances. In addition, the wires soldered to the ground plane have a small effect on the measured result.

The third prototype, shown in figure 4.3, utilizes four PIN diodes. The measured reflection coefficient is shown in figure 4.7. The measured result shows that it is capable of switching between eight distinct frequency ranges. It is noticeable that some combinations result in resonances at the same frequency and that is mainly because they produce almost the same slot length. For instance, activating switches 1 and 4 results in a resonance close to the same frequency obtained by activating switches 2, 3, and 4 which is about 1.95 GHz. Thus, the number of distinct frequency bands is reduced from 16 to 8. The main advantage of this structure is the excellent matching for all possible combination of diode biasing. The frequency bands and corresponding states of the PIN diodes are summarized in table 4.3.
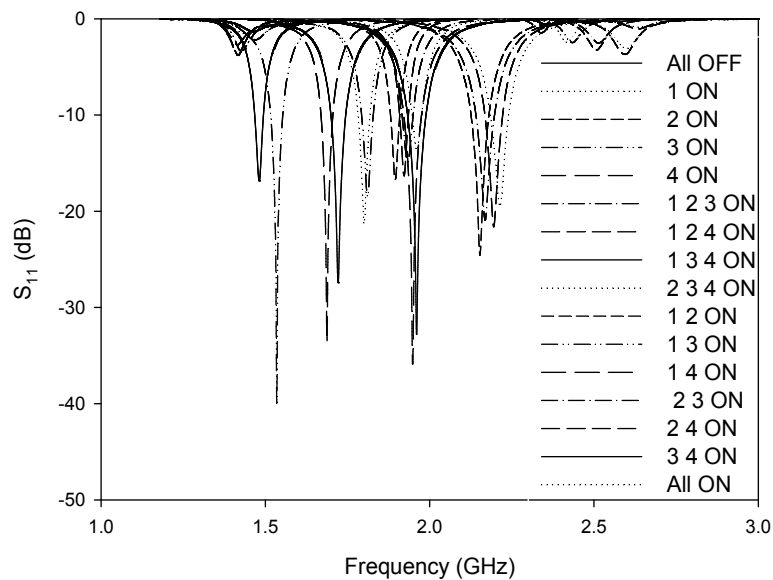
Figure 4.7: Measured reflection coefficient for different switch states for the prototype 3

Table 4.3: Different states of the PIN diodes and corresponding frequency bands of the prototype 3

Switch Band	1	2	3	4	Frequency (GHz)		BW %	
					meas	sim	meas	sim
1	OFF	OFF	OFF	OFF	1.48	1.5	2.03	2.75
2	OFF	OFF	OFF	ON	1.69	1.66	2.37	2.58
3	OFF	OFF	ON	OFF	1.54	1.56	2.61	2.62
4	OFF	OFF	ON	ON	1.72	1.72	2.76	2.89
5	OFF	ON	OFF	OFF	1.9	1.86	1.58	1.78
6	OFF	ON	OFF	ON	1.92	1.9	1.56	1.72
7	OFF	ON	ON	OFF	1.93	1.9	1.81	2.11
8	OFF	ON	ON	ON	1.96	1.94	1.68	2.05
9	ON	OFF	OFF	OFF	1.8	1.72	2.22	2.43
10	ON	OFF	OFF	ON	1.95	1.86	3.08	3.3
11	ON	OFF	ON	OFF	1.81	1.74	2.07	2.53
12	ON	OFF	ON	ON	1.96	1.88	3.06	3.32
13	ON	ON	OFF	OFF	2.15	2.02	2.79	2.94
14	ON	ON	OFF	ON	2.2	2.08	2.73	2.89
15	ON	ON	ON	OFF	2.17	2.04	2.76	3.03
16	ON	ON	ON	ON	2.22	2.1	2.7	3.02

4.3.2.2 Radiation Properties

The radiation patterns of the proposed antennas have been simulated and measured in different frequency bands. The proposed antennas produce a directional pattern with maximum directivity orthogonal to the patch. The radiation patterns in H (xz) and E (yz) planes for the antenna prototype 1 are shown in figure 4.8.

(a)   (b)
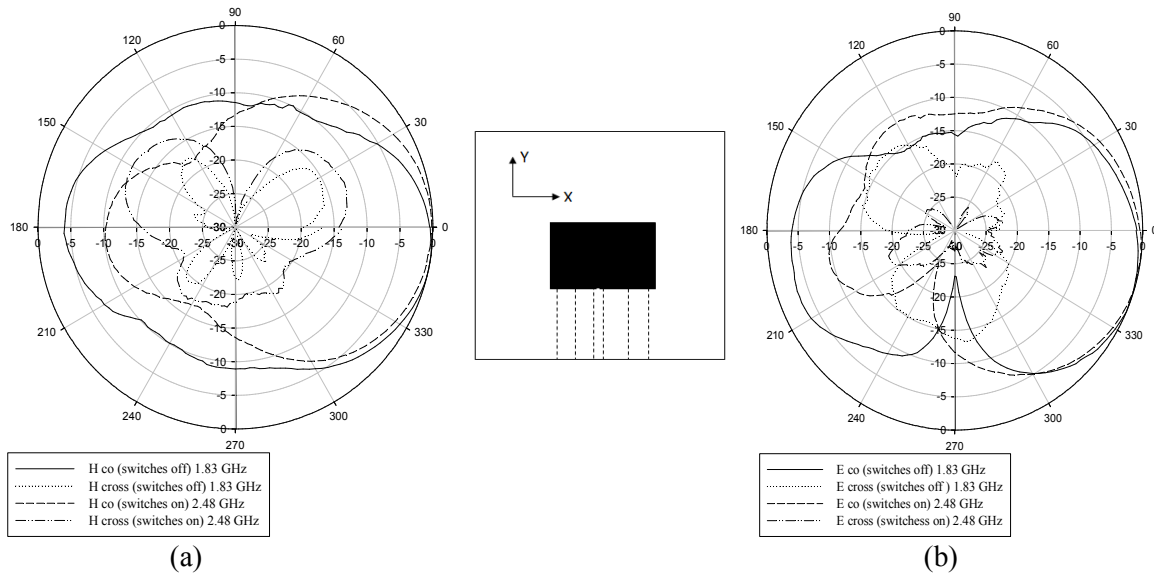
Figure 4.8: The normalized measured radiation pattern for prototype 1: (a) XZ plane;
(b) YZ plane
(Radial axis in dB, circumferential axis in degrees)

(a)   (b)
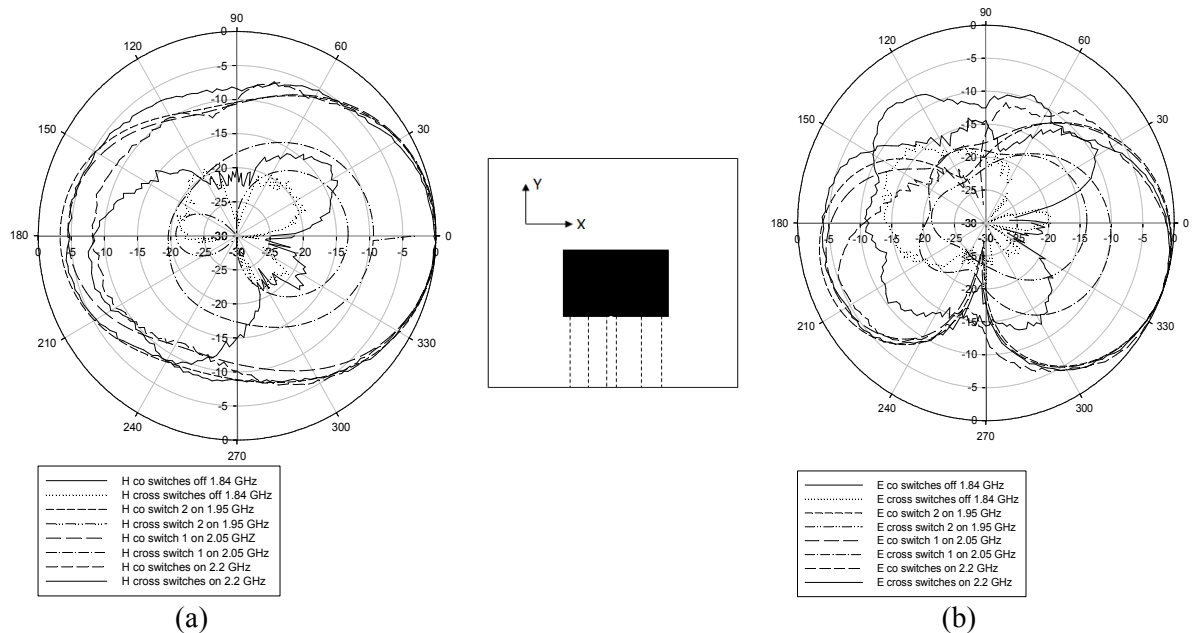
Figure 4.9: The measured radiation pattern prototype 2: (a) XZ plane; (b) YZ plane
(Radial axis in dB, circumferential axis in degrees)

The operating bands resulting from asymmetric slots (activating one switch) exhibit higher cross polarization levels. Nonetheless, the levels remain below -10 dB. As can be seen in figure 4.9, the frequency bands 2 and 3 have higher cross polarization levels. This is mainly due to the asymmetry in the structure since it is obtained by activating one switch (either 1 or 2) and therefore asymmetrical slot length. The prototype 3 shows very similar patterns as can be seen in figure 4.10. The measured radiation patterns show that the proposed antennas have stable and well-shaped radiation patterns over the operating bands. That is due to the fact that the biasing circuitry and switching diodes are arranged in the feeding structure rather than the radiating structure (the patch). Therefore, frequency reconfigurability is achieved without degrading the radiation properties.
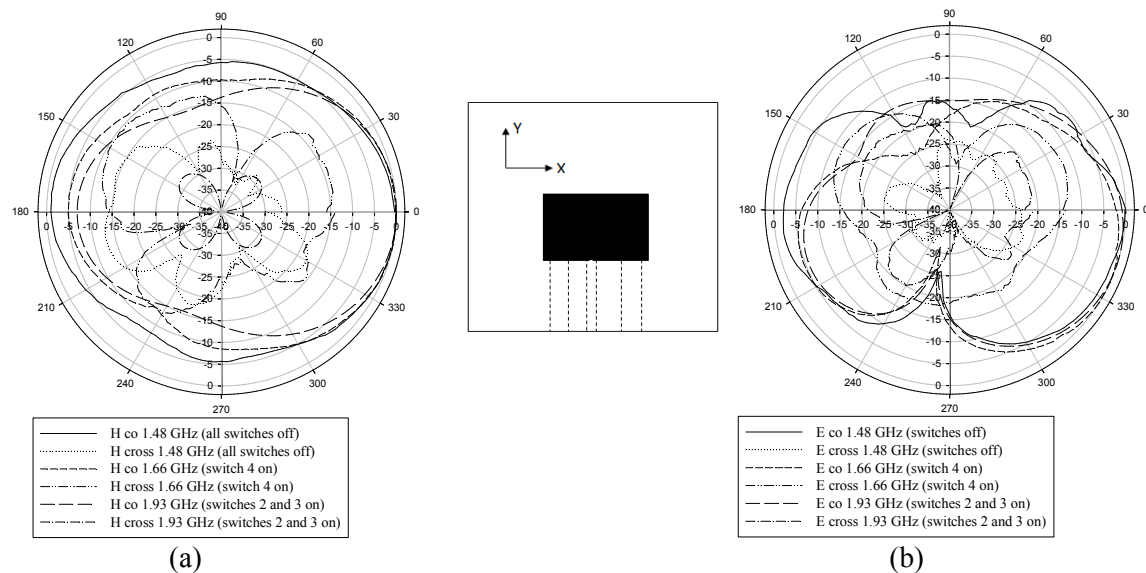
Figure 4.10: The measured radiation pattern prototype 3: (a) XZ plane;

(b) YZ plane

(Radial axis in dB, circumferential axis in degrees)

4.3.2.3 Surface Current Analysis

The surface currents are obtained from the magnetic fields in CST Microwave Studio®. Figure 4.11a shows the surface current plot for the antenna prototype 1 at 1.8 GHz (switches off). The figure shows strong current is flowing along the edges of the coupling slot. The surface current plot at 2.12 GHz (switches on) is shown in figure 4.11b. It can be seen that some of the current is flowing through the switch. When the switch is off mode, the RF currents on the ground flow around the slot, resulting in a relatively long current path as shown in figure 4.11a. Therefore, the antenna resonates at a low frequency. However, when the switch is activated (on), some of the RF current flow through the switch as shown in figure 4.11b. In this case, the current path is shorter so that the antenna resonates at higher frequency.

(a)   (b)
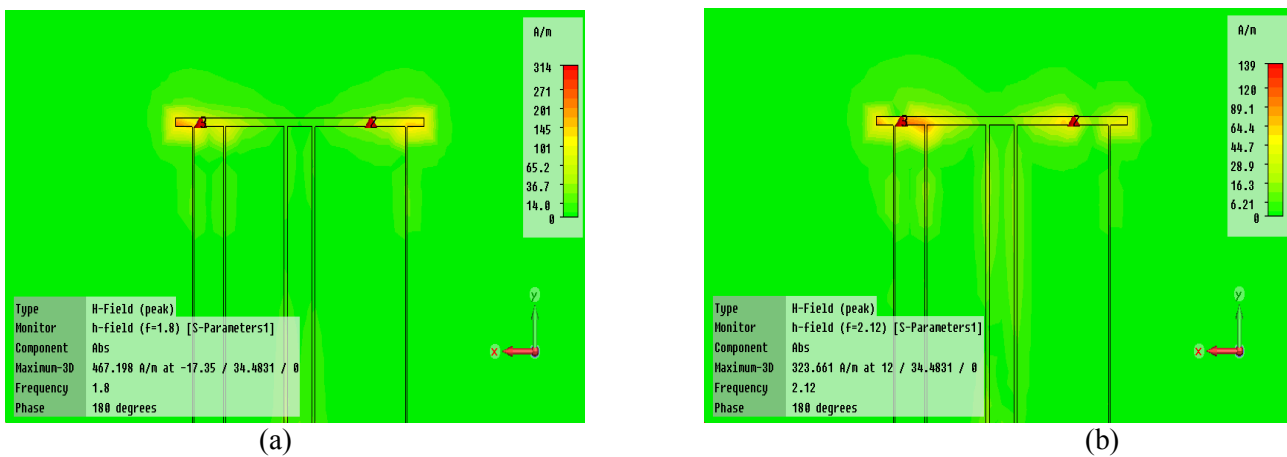
Figure 4.11: The surface current plot for the antenna prototype 2:
(a) switches off; (b) switches on

4.3.2.4 Realized Gain and Efficiency

The gain has been simulated and measured in different frequency bands for the proposed antennas. The prototype 1 has the highest gain levels. The gain of the lower

operating band is 4.12 dBi measured at 1.83 GHz. While the gain for the higher operating band is 4.81 dBi measured at 2.48 GHz. The results are summarized in table 4.4. The realized gain and the radiation efficiency for the prototype 2 are summarized in table 4.5.

The proposed antennas exhibit stable radiation properties within the operating bandwidth. Utilizing PIN diodes and DC blocking capacitors in the antenna will degrade its radiation efficiency and gain. Since these components include parasitic resistors, they will cause power loss. The prototype 1 exhibits the highest radiation efficiency (above 65%) compared to other prototypes. This is due to the fact that less number of components is used. Thus, increasing the number of the PIN diodes to 6 or 8 in order to achieve more frequency bands will further decrease the efficiency of the antenna. It can be seen that the measured gain is 1 to 2 dB less than the simulated. This could be due to the losses of the conductors and cables used in the measurement. Practically, the SMA connector introduces an insertion loss of 0.15 to 0.2 dB [30]. The alignment of the antenna could also introduce some losses. If the measured antenna is not well-aligned with the transmitting antenna, the measured gain will not be the maximum gain. The quality factor (Q) of the PIN diode is usually low at high frequencies (less than 3 at 10 GHz) [30]. This explains the decrement in the radiation efficiency as the frequency increased. It can be seen that the radiation efficiency decreases as the frequency increases. The measured gain for the prototypes 1 and 2 are shown in figures 4.12 and 4.13 respectively. The realized gain and the radiation efficiency for the prototype 3 are summarized in table 4.6.
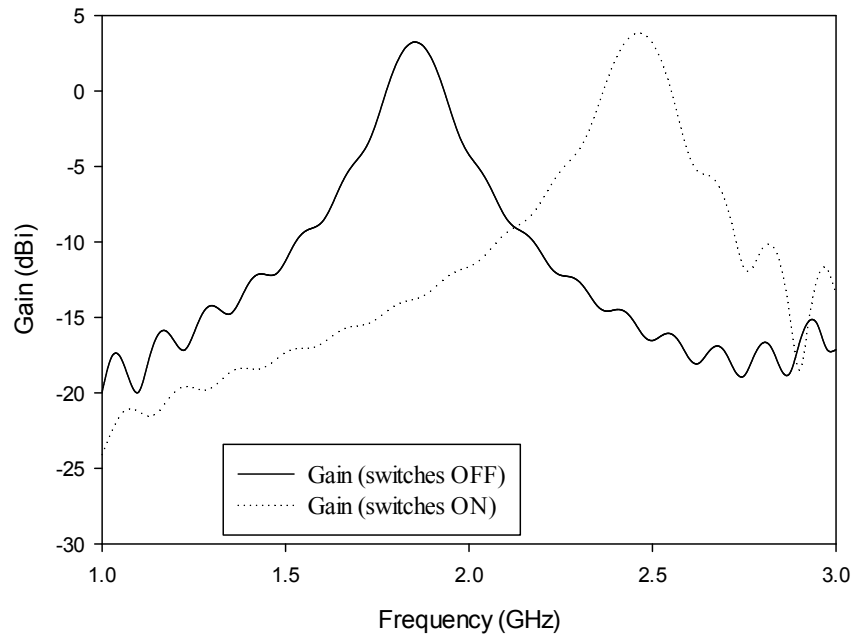
Figure 4.12: The measured gain for prototype 1

Table 4.4: The simulated directivity, radiation efficiency and the realized gain of the prototype 1

Switches	Directivity (dBi) simulated	Realized Gain (dBi)		Radiation Efficiency (%) simulated
		simulated	measured	
OFF	6.03	4.11	3.2	65.6
ON	7.54	4.81	3.8	55.4

Table 4.5: The simulated directivity, radiation efficiency and the measured realized gain of the prototype 2

Operating band	Directivity (dBi)	Realized Gain (dBi)		Radiation Efficiency (%)
		simulated	measured	
1	6.05	4.26	3.4	66.6
2	6.35	4.08	3.1	60.46
3	6.84	4.27	3.2	56.6
4	6.96	4.3	3.5	54.88
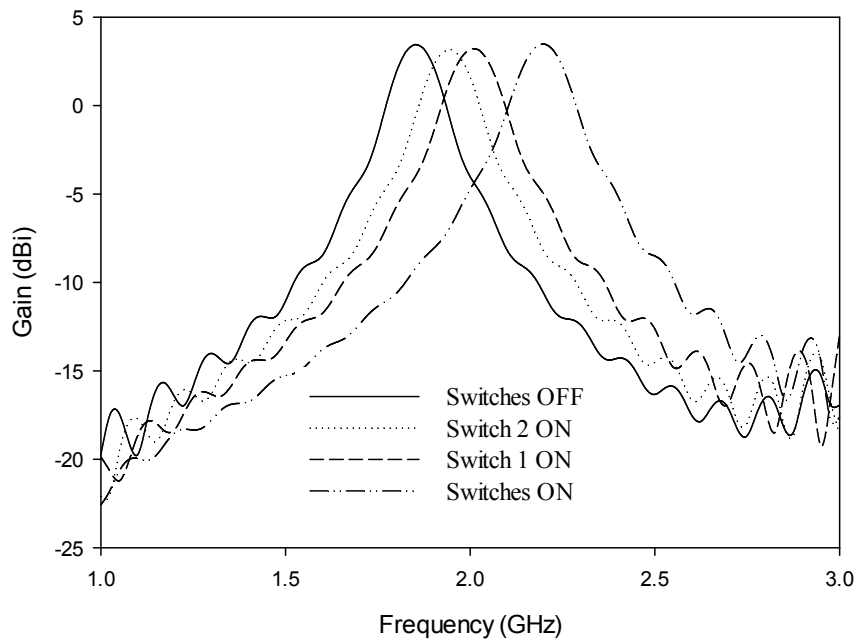
Figure 4.13: The measured gain for prototype 2

(a)   (b)
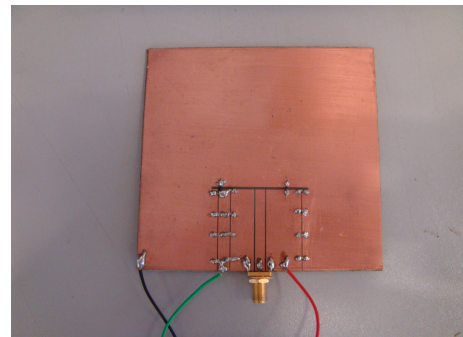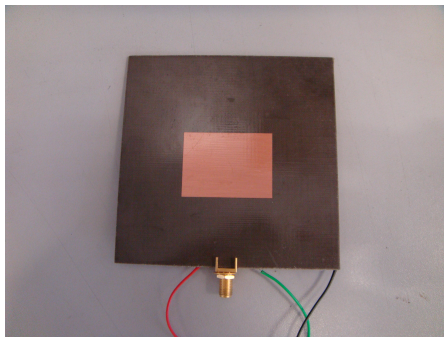
Figure 4.14: Antenna prototype 2: (a) top view;

(b) bottom view

Table 4.6: The simulated directivity, radiation efficiency and
the measured realized gain of the prototype 3

Operating band	Directivity (dBi)	Realized Gain (dB)		Radiation Efficiency %
		simulated	measured	
1	4.94	1.53	1.1	48.23
2	5.34	1.96	1.35	49.52
3	5.1	1.97	1.5	50.96
4	5.81	2.06	1.75	43.28
5	6.31	2.72	2.1	47.38
6	6.58	3.2	2.85	49.25
7	6.57	2.81	2	43.69
8	6.77	3.24	2.9	45.51
9	5.46	2.35	1.8	52.67
10	6.46	2.42	1.8	40
11	5.57	2.63	2.1	54.21
12	6.54	2.6	2	40.76
13	7.04	2.99	2.58	40.4
14	7.16	3.32	2.7	41.96
15	7.09	3.15	2.8	41.25
16	7.21	3.54	3	43.23

4.4. Tunable Patches

A tunable microstrip patch antenna for cognitive radio applications is presented in this section. The antenna has the same structure as the switchable patch presented in section 4.3.

4.4.1. Design and Operation

Reconfiguring the antenna's operating frequency is achieved by adding tuning capacitors in the coupling slot. The resonant frequency of the antenna can be tuned by activating/deactivating the switches and/or varying the capacitors. The switches are controlled using the bias voltages. The achievable tuning bandwidth is 1.7:1 and it extends from 1.39 GHz to 2.36 GHz. The antenna has a compact structure and simple biasing circuit. The proposed antenna was simulated and measured where electromagnetic simulations were found to agree with measurements. The proposed

antenna shows excellent impedance matching, well-shaped pattern and good gain within the tuning bandwidth.

In addition to the PIN diodes, two tuning capacitors are placed in the coupling slot as shown in figure 4.15. The capacitors are symmetrically located around the CPW and 12 mm apart. In the absence of the tuning capacitors the antenna will be switching between two distinct frequencies: 1.81 GHz (switches off) and 2.39 GHz (switches on). The tuning capacitors, which could be implemented by varactor diodes, are added to allow tuning the resonant frequency. The resonance frequency decreases as the capacitance increases. Thus, the antenna provides a continuously tunable bandwidth.

From simulations it was found that a narrow tuning range will be obtained if only the capacitors are used. Thus, combining switches with varactors results in wider tuning range.

The position of the capacitors represents a trade-off between the tuning range and the gain. Inserting the capacitors near the open ends of the coupling slot will have a large effect on the return loss but only a small effect on the resonance frequency. Thus, a narrow tuning range is achieved. However, placing them near the centre of the slot will have a large effect on the resonance frequency but only a small effect on the return loss (as desirable). The RF current has a larger magnitude at the centre of the coupling slot than the ends. Therefore, placing the capacitors at the centre of the slot will cause high losses because large current flows through their parasitic resistance resulting in lower realized gain.
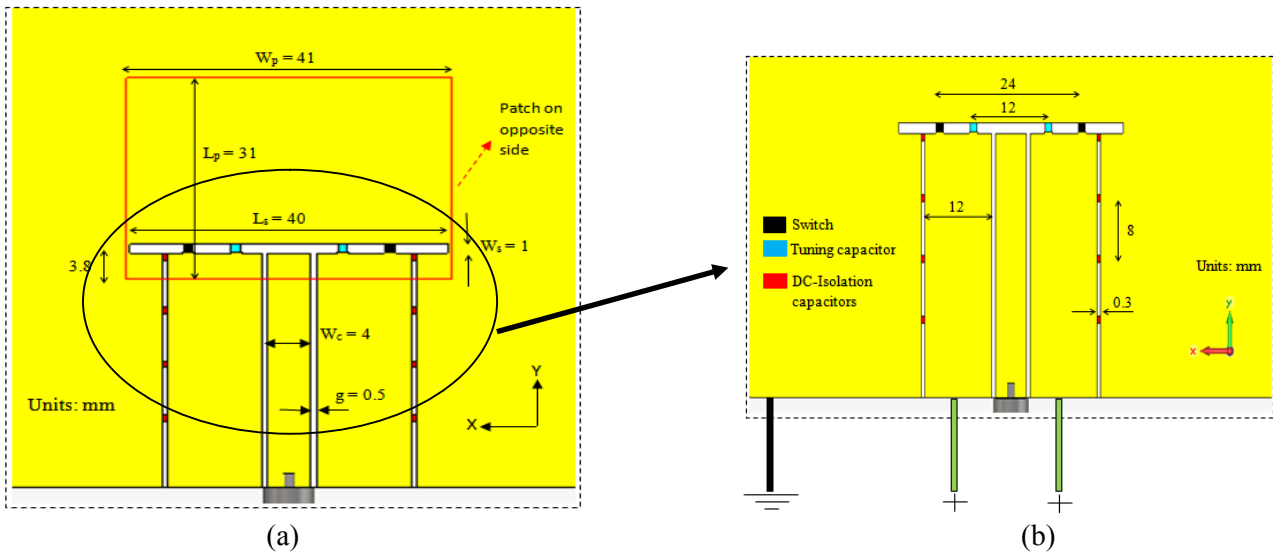
Figure 4.15: The structure of the tunable patch: (a) the antenna structure;
(b) the biasing circuitry arrangement

4.4.2. Simulation and Measurement Results

4.4.2.1 Resonance Properties

Figure 4.16 shows the measured reflection coefficient versus the capacitance. When

the switches are turned on, the antenna resonates at 2.36 GHz. The resonant frequency

decreases to 1.8 GHz by increasing the capacitance from 0.1 to 1.2 PF. Likewise,

when the switches are off, the antenna resonates at 1.8 GHz which decreases to 1.39

GHz by increasing the capacitance. Thus, the antenna provides a continuously tunable

narrowband resonance. The tuning range, considering the -10 dB return loss, extends

from 1.39 to 2.36 GHz with a tuning ratio of 1.7:1. The operation of the antenna is

summarized in table 4.7. The tuning bandwidth is thus divided into two overlapping

frequency bands. The upper (lower) band correspond to the switches being activated

(deactivated). While the state of the switches determines the operating band, the value

of the tuning capacitors determines the resonant frequency within that band.
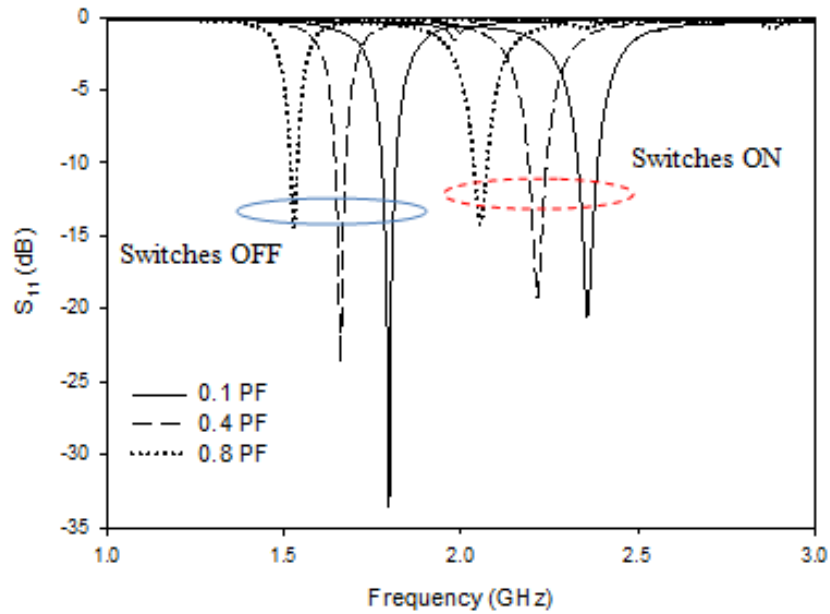
Figure 4.16: The measured reflection coefficient vs. the capacitance

Table 4.7: The measured and simulated resonant frequency vs. the capacitance

C (PF)	F_o (GHz)			
	Switches ON		Switches OFF	
	simulated	measured	simulated	measured
0.1	2.23	2.36	1.76	1.8
0.4	2.07	2.22	1.6	1.65
0.8	1.93	2.06	1.49	1.53
1.2	1.8	___	1.39	___

4.4.2.2 Radiation Patterns

The radiation pattern of the proposed antenna has been simulated and measured at different frequencies. The radiation patterns in the H (xz) and E (yz) plane are shown in figure 4.17. The radiation pattern is stable and well shaped with cross polarization levels below -15 dB. Good agreement is found between simulated and measured radiation patterns.

131
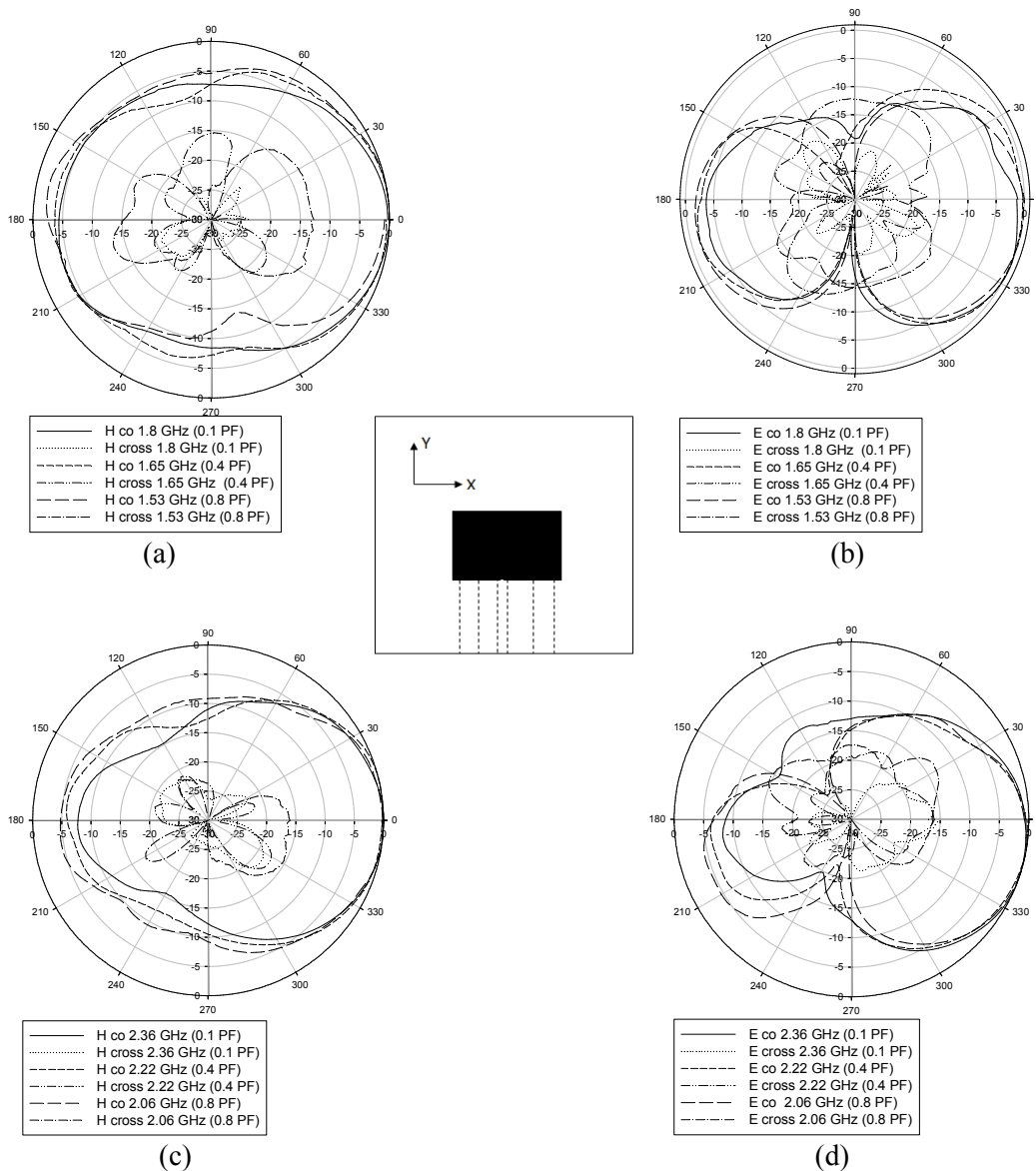
Figure 4.17: Measured radiation pattern: (a) H plane (lower band); (b) E plane (lower band); (c) H plane (upper band); (d) E plane (upper band)

(Radial axis in dB, circumferential axis in degrees)

Table 4.8 shows the radiation efficiency and the realized gain of the antenna. It is noticeable that the radiation efficiency is low within the upper band (switches on) and that is due to the parasitic (forward) resistance of the PIN diodes. While the off state of the PIN diode can be modelled by a capacitance, the off state can be modelled by a small resistance. Therefore, the switch will cause more losses when it is activated.

132

Using the PIN diodes and tuning capacitors will degrade the performance of the antenna. The parasitic resistance of these components will cause power loss and therefore, it will reduce the total efficiency.

Table 4.8: Simulated radiation efficiency and measured realized gain

C (PF)	Switches off		Switches on	
	Realized gain (dB)	Radiation efficiency %	Realized gain (dB)	Radiation efficiency %
0.1	4.16	67.14	4.72	54.09
0.4	3	61.46	3.16	42.12
0.8	1.9	54.65	1.76	34.9
1.2	0.52	47.25	0.11	28.54
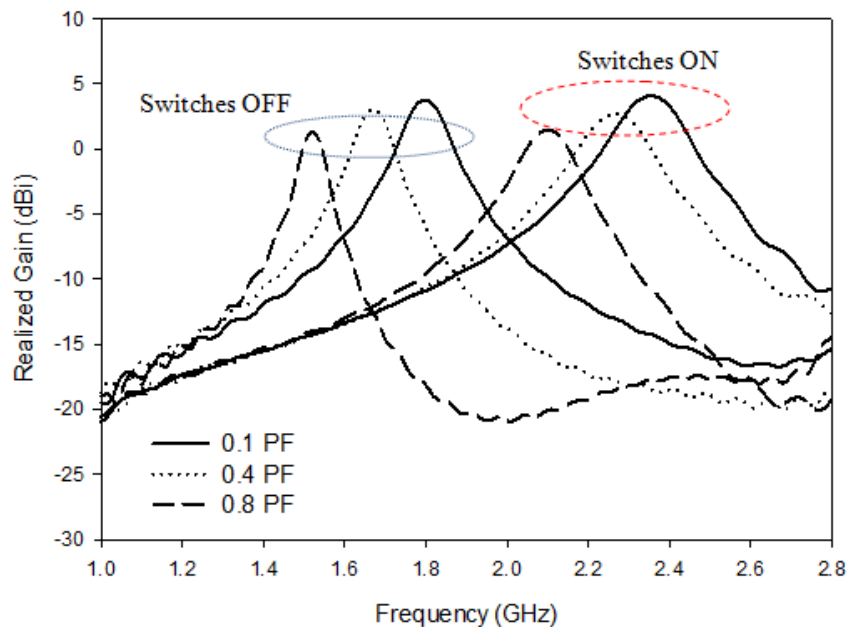
Figure 4.18: The measured realized gain vs the capacitance

4.5. Conclusions

A switchable multi-band reconfigurable patch antenna is proposed. The operating frequency can be switched between different frequency bands by activating PIN diodes loaded in the coupling slot. Three prototypes were designed, simulated, fabricated and measured. The first two prototypes incorporate two switches and

capable of switching between two and four frequency bands over frequency ranges of 1.36:1 and 1.23:1 respectively. The third prototype utilizes four switches and capable of switching between eight distinct frequency bands, over frequency range of 1.5:1. The proposed antennas show very good impedance matching, well-shaped radiation patterns and good gain over all operating bands. Tunable patch is also presented in which frequency agility is achieved by combining switches and capacitors inserted in the coupling slot. The resonant frequency of the antenna can be shifted over a wide tuning range. The tuning range extends from 1.39 GHz to 2.36 GHz. The proposed antenna exhibits stable radiation patterns and reasonable gain within the operating bandwidth. The ability of the proposed antennas to easily select of wide range of discrete frequencies makes them of interest when multiple standards to be processed by the same receiver. Single passive antenna with multi-resonance or wideband characteristics is a solution. However, this solution suffers from a drawback since the antenna receives other non desired frequencies and some filtering network is required to cancel the undesirable frequencies. The narrow instantaneous frequency response makes the antenna good candidate for the cognitive radio applications.

References:

[1]   Fan Young, and Yahia Rahmat-samii "Patch Antennas with Switchable Slots (PASS) in wireless Communications: Concepts, Designs, and Applications" *IEEE Antennas and propagation Magazine, vol. 47, NO.2, April 2005.*

[2]   Das Krishna, C.K. Anandan, P. Mohanan, K. Vasudeven, "Electronically switchable circular microstrip antenna with sector-slot for multiple frequency operation," Antennas and Propagation Society International Symposium, 2006. APSURSI 09.IEEE, 2006, pp. 4277-4280.

[3]   Manoj Singeh, Ananj Manojan Basu, and Shiban K. Koul, "Switchable frequency bands microstrip antennas," IEEE international workshop on antenna technology, 2009, IWAT 2009, pp.1-4.

[4]   I. Tekin and M. Knox, "Reconfigurable dual band microstrip antenna for software defined radio applications," IEEE international conference on wireless information technology and systems (ICWIST), 2010, pp.1-4.

[5]   Ya-chi Liu, and Kai Chang, "Multiband frequency reconfigurable antenna by changing the microstrip connecting element position," Antennas and propagation society international symposium, ASPURI 2009, PP.1-4.

[6]   Y. J. Sung, B. Y. Kim, T. U. Jang, and Y. S. Kim, "Switchable triangular microstrip patch antenna for dual frequency operation," Antennas and propagation society international symposium, 2004, vol.1, pp.265-268.

[7]   Zammit J. A., Muscat A., "Tunable microstrip antenna using switchable patches", Loughbrough antenna and propagation conference LAPC 2008, pp.233-236.

[8]   Nanbo Jin, Fan Yang, and Y. Rahmat Samii, "A novel patch antenna with switchable slot (PASS): dual frequency operation with reversed circular

polarizations" IEEE transactions on antennas and propagation, vol.54, pp.1031-1034, 2006.

[9]   Saed M., "Reconfigurable broadband microstrip antenna fed by coplanar waveguide," progress in electromagnetic research, vol. 55, 227-239, 2005.

[10]   J. M. Laheurte, "Switchable CPW-fed Slot Antenna for Multifrequency Operation", Electron. Lett.6 December 2001, vol37.

[11]   C. Luxey,L. Dussopt,J.L. Le Sonn and J.M. Laheurte, "Dual-frequency operation of CPW-fed antenna controlled by pin diodes", Electron. Lett.6 January 2000, vol36. P.2-3

[12]   H.F.A. Tarboush, S. Khan, R. Nilavan, H. S. Al-rawshidy and D. Budimir, " Reconfigurable wideband patch antenna for Cognitive Radio" Loughbrough Antenna and Propagation Conference LAPC 2009,pp 141-144.

[13]   C.Y.D. Sim, T.Y. Lin, and J. S. Row, "Aperture-coupled Antenna with Switchable Polarisation and Frequency Agility" Electron. Lett.6 December 2009, vol45.

[14]   Ghaith Mansour, Peter S Hall, Peter Gardner, and MKA Rahim, "Switchable multi-band coplanar antenna," Loughbrough *Antennas and Propagation Conference, LAPC, 14-15 Nov 2011,* pp.1-4.

[15]   Sung Y. J. "Simple tunable dual-band microstrip patch antenna", Electron. Lett., vol.45. pp. 666-667, 2009.

[16]   Baylis S.; Aguilar S.; Weller T.;"Wide Bandwidth Varactor-Tuned Patch Antenna," Electron. Lett. Vol.45,pp816-818,2009

[17]   S.V. Shynu, G. Augustin, CK. Aanandan, and K. Vasusevan, "C-Shaped slot loaded reconfigurable microstrip antenna," Electron. Lett.16 March 2006, vol. 42. no6.

[18]   G. Le Ray, M. Hamidi and J.P. Daniel, "Frequency agile slot-fed patch antenna", Electronics Letters, vol.32,no1,pp2-3,Jan1996

[19]   B.R Holland, R Ramadoss, S. Paneley and P. Agrwal, "Tunable coplanar patch antenna using varactor", Electronic Letters, vol42,no6,pp319-321, March 2006

[20]   P. Bharita and I.J. Bahal, "A frequency agile microstrip antenna", Proceedongs of APS, vol.20, pp. 304-307, May 1982.

[21]   Sami H. Al-charchafi, and Martin Frances," Electronically tunable microstrip patch antennas", Antennas and Propagation Society Symposium, vol.1, pp. 304-307, June 1998.

[22]   Eisuke Nishiyama, and Tatsuo Itoh," Widely tunable stacked microstrip antenna using varactor diodes" Asia Pacific Microwave Conference APMC, pp. 1-4, 2008.

[23]   R.B. Waterhouse, and N.V. Shuley, "Full characterisation of varactor-loaded probe-fed rectangular microstrip patch antennas", IEE Proceedings of Microwaves, Antennas and Propagation, vol.141, no5, pp. 367-373, Oct1994.

[24]   Fayyaz N., Safavi-Naeini S., Shin E., Hodjat N., "A novel electronically tunable rectangular patch antenna with one octave bandwidth", IEEE Canadian conference on Electrical and Computer Engineering, vol.1, pp.5-28, 1998

[25]   Constantine A. Balanis, *Antenna theory: Analysis and Design*.2nd Ed. New York, USA: John Wiley& Sons, Inc. 1997.

[26]   Garg, R., Bhartia, P., Bahl, I., Ittipiboon, A., Microstrip antenna design handbook, Artech House, Inc, 2001.

[27]   L. Giauffrat and J.M. Laheurte, "Parametric study of the coupling aperture in cpw fed microstrip antennas", IEE Proc. Microwaves, Antennas and Propagation, pp. 169-174, 1999

[28]   L. Giauffret , J.M. Laheurte , and A. Papiernik "Study of Various Shapes of the Coupling Slot in CPW-fed Microstrip Antennas" *IEEE Trans. Antennas and Propag.,* vol. 45, issue 4, 1997, pp. 642-647.

[29]   http://www.infenion.com

[30]   Eng Kock Lim, and Kwok Wa Leung, Compact Multifunctional Antennas for Wireless Systems, New York, USA: John Wiley & Sons Inc. 2012.

[31]   Ghaith Mansour, Peter S. Hall, Peter Gardner, and M.K. Abd Rahim, "Tunable Slot-Loaded Patch Antenna for Cognitive Radio," Loughbrough *Antennas and Propagation Conference,* LAPC, Nov 2012, pp.1-4.

[32]   Ghaith Mansour, Peter S. Hall, Peter Gardner, and M.K. Abd Rahim, "Slot-Fed Switched Patch Antenna for Multiple Frequency Operation", Progress in Electromagnetic Research PIERS C, vol.36, pp.91-104, 2013.

CHAPTER V

DESIGN OF FILTERING MICROSTRIP ANTENNAS

BASED ON BANDPASS FILTER SYNTHESIS

In wireless communication systems, the antenna and the filter are the key components. While the antenna transmits and receives signals, the bandpass filter (BPF) selects signals in the operating band and rejects spurious (out-of-band) signals. Due to the increasing trend towards simplicity and miniaturization, it is desirable to integrate the filter and the antenna into a single component that achieves filtering and radiating functions simultaneously, known as a filtering antenna or "filtenna". The filtenna reduces the pre-filtering requirement and improves the noise performance of the system. Many filtering antennas, in different topologies, have been designed using a filter synthesis approach, in which the antenna acts as the last resonator in the filter. Filtering antennas have been implemented in different forms including the rectangular patch [1], circular patch [2], patch array [3], Γ-shaped antenna [4], slot dipole [5], monopole antenna [6], inverted-L antenna [7], Yagi antenna [8], dielectric resonator antenna [9] and waveguide slot antenna [10].

This chapter presents some novel compact filtering microstrip antennas for wireless communication systems. A novel design of edge-coupled patch filter antenna is presented in section 5.1. The structure consists of array of three edge-coupled microstrip patches. The antenna array was designed to function as a third order bandpass filter with Chebyshev response with -20 dB return loss. The filter is designed to have a fractional bandwidth (FBW) of 5% at midband frequency of 2.0

GHz. In section 5.2, a compact filtering microstrip antenna with different design is presented. The antenna is designed to function as a third order bandpass filter with FBW = 0.029 at a midband frequency of 2.0 GHz. A Chebyshev lowpass prototype with a passband ripple of 0.043 dB is chosen. The antenna consists of a coupled line, two hairpin resonators, and rectangular patch. The patch acts not only as radiating element, but also as the last resonator of the bandpass filter. The design process starts with designing a simple three-pole hairpin microstrip bandpass filter. A filtering antenna action is achieved by replacing the third resonator and the output line in the filter by a radiating patch. The radiation quality factor of the patch is equal to the external quality factor at the input. Therefore, the filter characteristics are preserved. The proposed filtering microstrip antennas exhibit good out-of-band gain suppression, flat in-band gain response, good selectivity at the band edges, and well-shaped radiation patterns. All of the structures presented in this chapter were simulated using the transient solver (time domain solver) in CST Microwave Studio[®].

5.1. Radiating Edge-Coupled Patch Filter Antenna

A novel microwave structure that combines filter and antenna functions is presented in this section. The structure consists of an array of three edge-coupled microstrip patches. The patches are aperture fed, and printed on stacked substrates. The array antenna was designed using filter theory to function as three-pole bandpass filter at midband frequency of 2.0 GHz.

5.1.1. Antenna Design and Structure

Fig. 5.1 illustrates the structure of the antenna. It consists of an array of three microstrip patches printed on stacked substrates, two of which are aperture fed, with an open-ended microstrip line printed on a lower inverted substrate to excite the patch through a coupling slot in the ground plane. The slot-coupling or aperture-coupling technique is used to avoid soldered coaxial connections, and to avoid the radiation from coplanar line feeds that interfere with the patch radiation [11]. Each patch resonator is approximately half wavelength long at the midband frequency. The coupling from one patch to another is through the gap between adjacent radiating edges and therefore it is capacitive [12]. The dimensions in figure 5.1 indicated by variables are determined using the synthesis method described in section 5.1.2. The microstrip bandpass filter is designed to have a fractional bandwidth (FBW) of 5% at a midband frequency of 2.0 GHz. A three-pole Chebychev lowpass prototype with -20 dB return loss is chosen whose equivalent circuit is shown in figure 5.2. Having obtained these specifications, the bandpass design parameters can be calculated [12],

$$Q_{e1} = \frac{g_0 \cdot g_1}{FBW} \qquad\qquad Q_{en} = \frac{g_n \cdot g_{n+1}}{FBW} \qquad\qquad (5.1)$$

$$M_{i,\,i+1} = \frac{FBW}{\sqrt{g_i \cdot g_{i+1}}} \qquad\qquad (5.2)$$

141

where Q_{e1} and Q_{en} are the external quality factors of the input and the output resonators. $M_{i,i+1}$ is the coupling coefficient between the adjacent resonators i and i+1. The coupling coefficients were found to be, $Q_{e1} = Q_{e3} = 17$ and $M_{12} = M_{23} = 0.052$. Taconic substrate RF35-30 with relative dielectric constant of $\varepsilon_r = 3.5$ and thickness of h = 1.52 mm was used. A design approach, to extract the array dimensions from the coefficients, employing full-wave electromagnetic (EM) simulations is described.

(a)

(b)

(c)
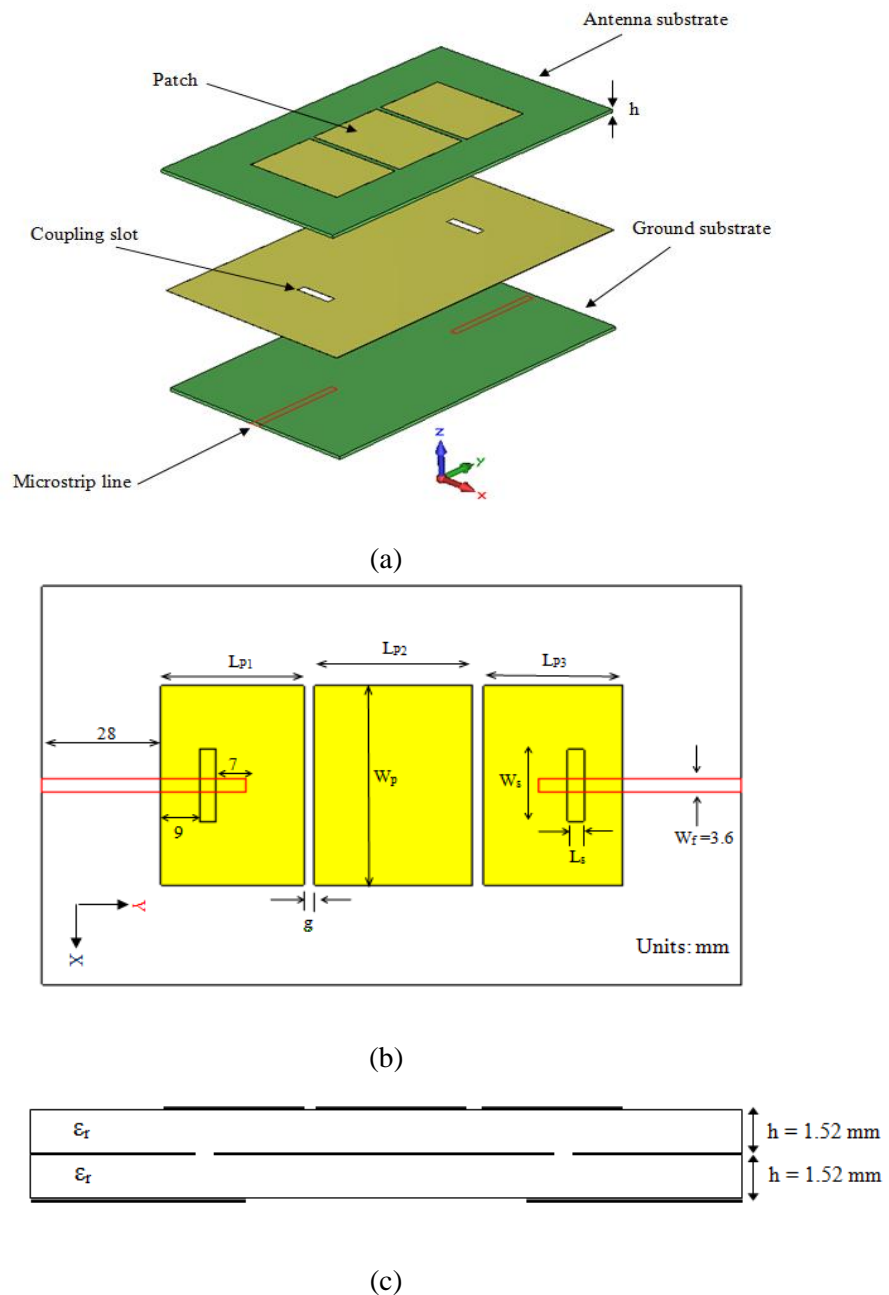
Figure 5.1: Layout of three-pole edge coupled patches filter;
(a) 3-D view (b) top view (c) side view
(All dimensions shown by a variable name are determined by the synthesis method).
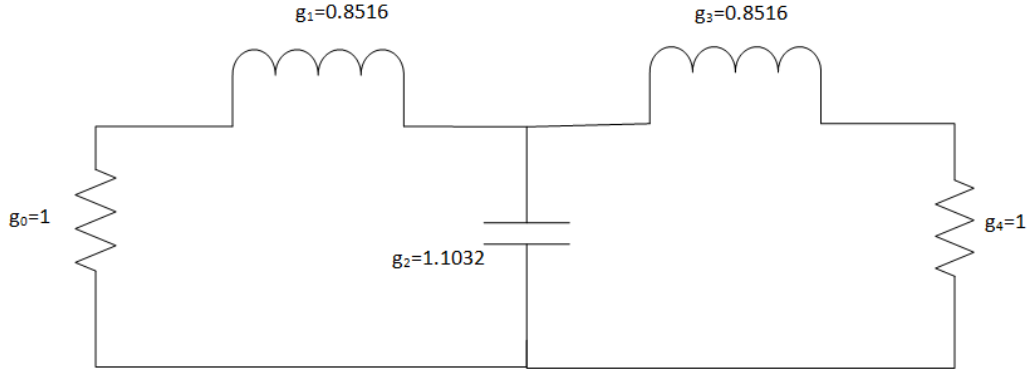
Figure 5.2: Three-pole Chebyshev lowpass prototype with -20 dB return loss.

While designing a microstrip filter, it is very useful to plot the performance of the filter based on the coupling matrix calculations. This performance can be used as a reference, such that the simulated results will be optimized to meet it. The general coupling matrix is important for representing filter topologies. Since the presented filter is composed of three resonators (n = 3), the coupling matrix will be of third order (3x3).

The general coupling matrix is given by [12]:

$$[A] = [q] + P [U] - j [m]$$

Or written in full,

$$A(P) = \begin{bmatrix} 1/q_{e1} & 0 & 0 \\ 0 & 0 & 0 \\ 0 & 0 & 1/q_{e3} \end{bmatrix} + P \begin{bmatrix} 1 & 0 & 0 \\ 0 & 1 & 0 \\ 0 & 0 & 1 \end{bmatrix} - j \begin{bmatrix} 0 & m_{12} & 0 \\ m_{21} & 0 & m_{23} \\ 0 & m_{32} & 0 \end{bmatrix} \qquad (5.3)$$

where q_{e1} and q_{e3} are the scaled external quality factors, given by

$$q_{ei} = FBW \cdot Q_{ei} \qquad (5.4)$$

m_{ij} are the normalized coupling coefficients

$$m_{ij} = \frac{M_{ij}}{FBW} \qquad (5.5)$$

143

and P is the complex frequency variable

$$P = \frac{j}{FBW} \left(\frac{\omega}{\omega_0} - \frac{\omega_0}{\omega} \right) \tag{5.6}$$

Having obtained the coupling matrix of the filter, the scattering parameters, S_{11}, and S_{21}, can be calculated directly from (5.7) and (5.8)

$$S_{11}(P) = 1 - 2[1/q_e]A(P)_{1,1}^{-1} \tag{5.7}$$

$$S_{21}(P) = 1 - 2[1/\sqrt{q_{e1}.q_{e3}}]A(P)_{3,1}^{-1} \tag{5.8}$$

Figure 5.3 shows the scattering parameters of the filter based on the coupling matrix calculation. It can be seen that the level of the return loss is − 20 dB in the passband. Three reflection zeros are observed in the return loss result. Two of them are located at the edges of the passband at 1.95 and 2.0 GHz and the third is located at the midband frequency of 2.0 GHz. It is worth mentioning that this performance might not be realizable, since it doesn't take into account losses, spurious radiation, and unwanted couplings.
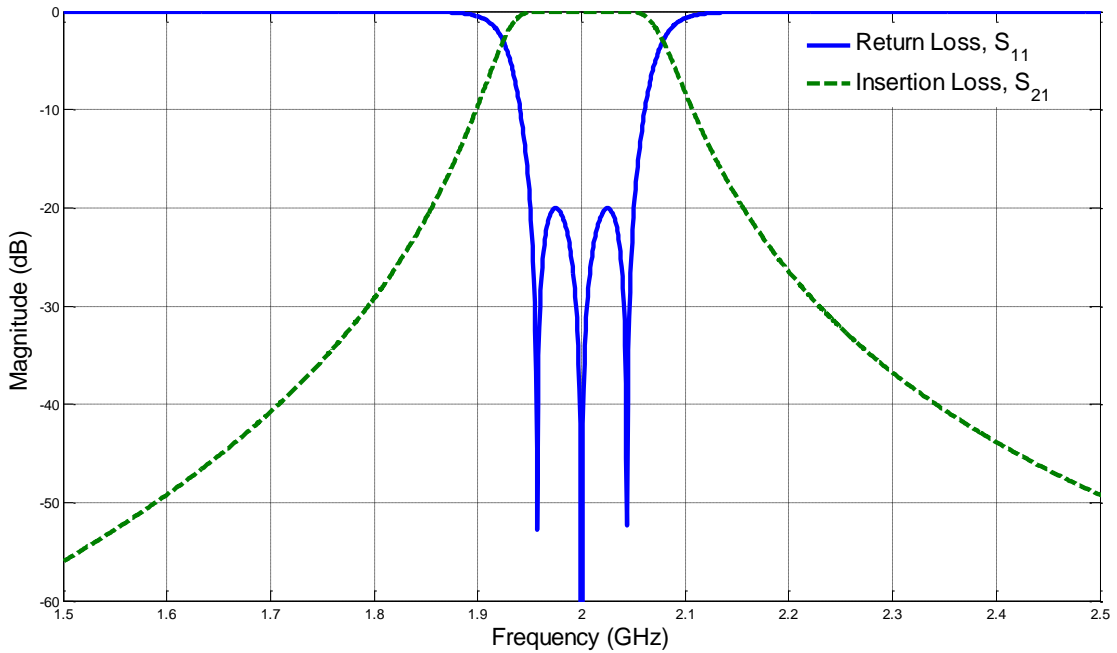
Figure 5.3: The filter performance based on the coupling matrix calculations.

Since the filter is synchronously tuned, such that all resonators resonate at the same frequency, namely, the midband frequency of the filter, then $M_{11} = M_{22} = M_{33} = 0$. The filter is directly coupled, and it is assumed that there is no cross coupling, $M_{13} = M_{31} = 0$.

5.1.2. Extraction of the Design Parameters

When a microstrip filter is designed using EM simulations, it is computationally efficient to break the filter down into different parts that are simulated separately by the simulator. The simulations are performed to find the physical dimensions that give the desired design parameters according to the prescribed coupling matrix. The different parts of the filter are then combined to obtain the overall filter response. This simulation based method is efficient for narrowband filter designs. The three-pole edge coupled patches filter is designed based on the coupling matrix given in (5.3).

Using the parameter extraction technique, full-wave EM simulations were carried out to extract the radiation quality factor of the patch Q_r, and the coupling coefficients for various physical dimensions. For conventional microstrip filter dsign, the microstrip resonators are usually housed into a metal box to supress radiation. In such a case, radiation can be ignored, as $Q_r = \infty$. However, in the antenna filter presented here, there is a considerable amount of radiation, which is too large to be ignored in the design process. Therefore, it is necessary to take into account the radiation quality factor of the patch resonator.

The radiation quality factor Q_r, is determined from the simulation of the structure shown in figure 5.4a. The two ports are weakly coupled to the patch through small slots close to the patch edge. Weak coupling implies that $Q_{e1} = Q_{e2} = \infty$. The width of the slot is $W_S = 12$ mm and the length is $L_S = 3$ mm. The simulated frequency response of the structure is shown in figure 5.4b, where S_{21} denotes the S parameter

145

between the two ports. Tiny coupling slots located at the edges of the patch are used in order to weaken the coupling. The loaded quality factor, Q_L, can be calculated directly from the resonant frequency (f_o) and the 3-dB bandwidth (Δf) as given in equation:

$$Q_L = \frac{f_o}{\Delta f} \tag{5.9}$$

The loaded quality factor of the structure can be found by adding the external quality factor Q_e and the unloaded quality factor Q_u.

$$\frac{1}{Q_L} = \frac{1}{Q_e} + \frac{1}{Q_u} \tag{5.10}$$

The external quality factor is the sum of the external quality factors at the input (Q_{e1}) and the output (Q_{e2}).

$$\frac{1}{Q_e} = \frac{1}{Q_{e1}} + \frac{1}{Q_{e2}} \tag{5.11}$$

The total unloaded quality factor of the patch resonator can be found by adding the dielectric, conductor and radiation losses.

$$\frac{1}{Q_u} = \frac{1}{Q_d} + \frac{1}{Q_c} + \frac{1}{Q_r} \tag{5.12}$$

where Q_d, Q_c, and Q_r are the dielectric, conductor, and radiation quality factors respectively.

In the simulation arrangement shown in figure 5.4a, it is assumed that structure is lossless and the metal is modelled as a perfect electronic conductor (PEC). The dielectric material is assumed to be lossless with loss tangent equal to zero. Therefore, the conduction and dielectric quality factors can be ignored as $Q_c = Q_d = \infty$. By substituting these values into equation (5.12), we find out that $Q_u = Q_r$. The two ports are weakly coupled to the patch such that such that $Q_{e1} = Q_{e2} = \infty$. By substituting

these values into equations (5.10), and (5.11), we find out that $Q_L = Q_u = Q_r$. Thus, the radiation quality factor is equal to the loaded quality factor (as arranged) and it can be obtained directly from the figure 5.4b using the equation (5.9).
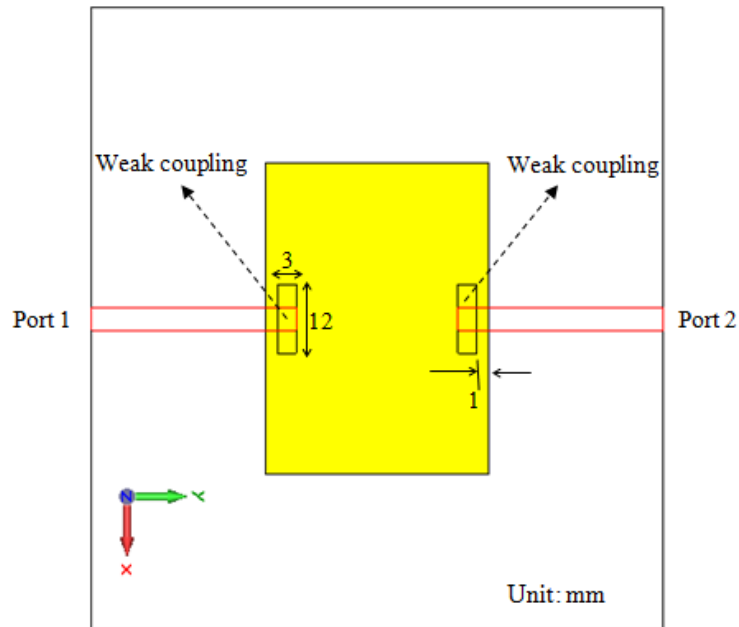
(a)
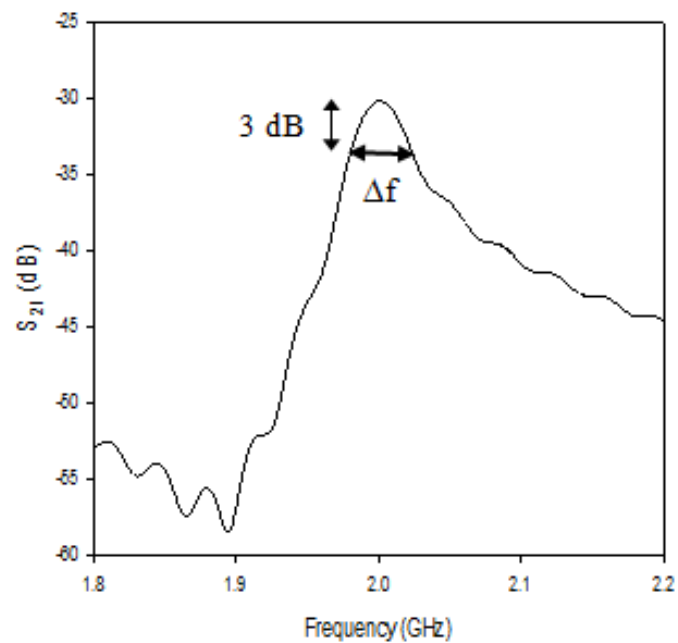
(b)

Figure 5.4: The radiation quality factor calculation: (a) weakly coupled patch; (b) the simulated frequency response of the structure.

The radiation quality factor is calculated and found to be $Q_r = 57$. Design curves to obtain the radiation Q of a rectangular patch were presented by James and Hall in [13]. The Q_r of the patch is calculated using this method and found to be approximately 50, which is in a reasonable agreement with the simulation method.

An arrangement to extract the external quality factor Q_e of the input/output patch resonator is shown in figure 5.5a. The patch, which is assumed to be lossless in the simulation, is excited at port 1 through 50 Ω line as in the overall configuration of figure 5.1. Port 2 is very weakly coupled to the patch, which implies that $Q_{e2} = \infty$, in order to obtain 3-dB bandwidth from the magnitude response of the transmission coefficient S_{21}. The loaded quality factor was calculated from the resonant frequency f_0 and the 3 dB bandwidth as given in equation (5.9). Having obtained the loaded quality factor, the external quality factor was calculated as follows:

$$\frac{1}{Q_{e1}} = \frac{1}{Q_L} - \frac{1}{Q_r} \qquad (5.13)$$

A design curve for Q_e against the slot width W_s was obtained as shown in figure 5.6. In this case as the slot length increases, the coupling from the source increases, and hence Q_e decreases.
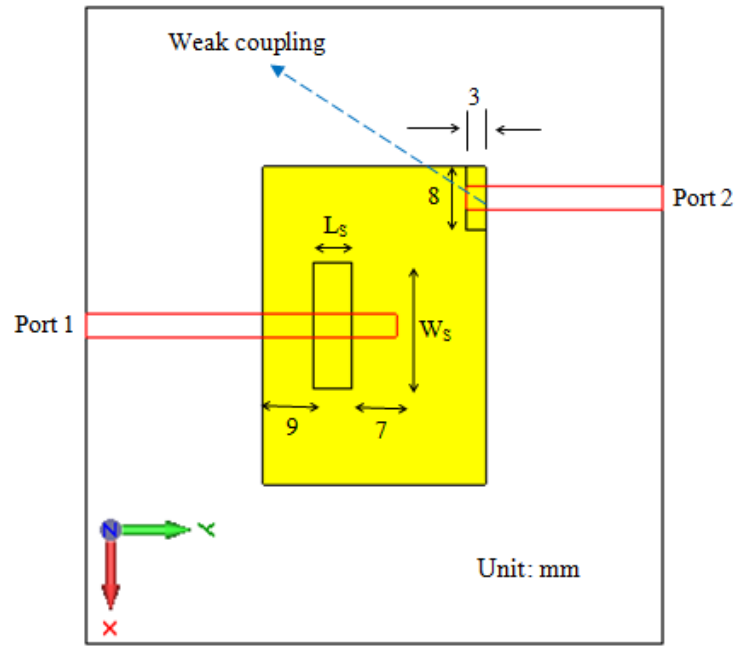
(a)
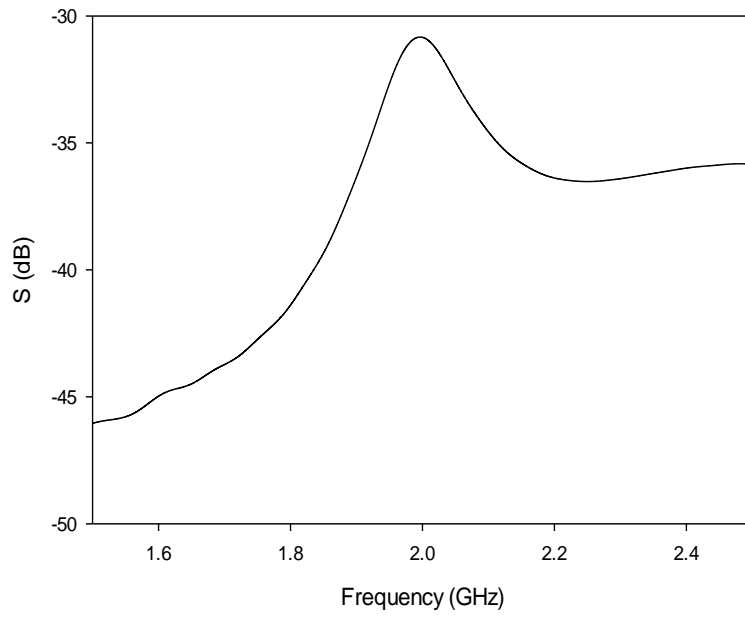
(b)

Figure 5.5: The external quality factor calculation: (a) an arrangement to extract Q_e; (b) simulated frequency response for W_S =4 and L_S =18.
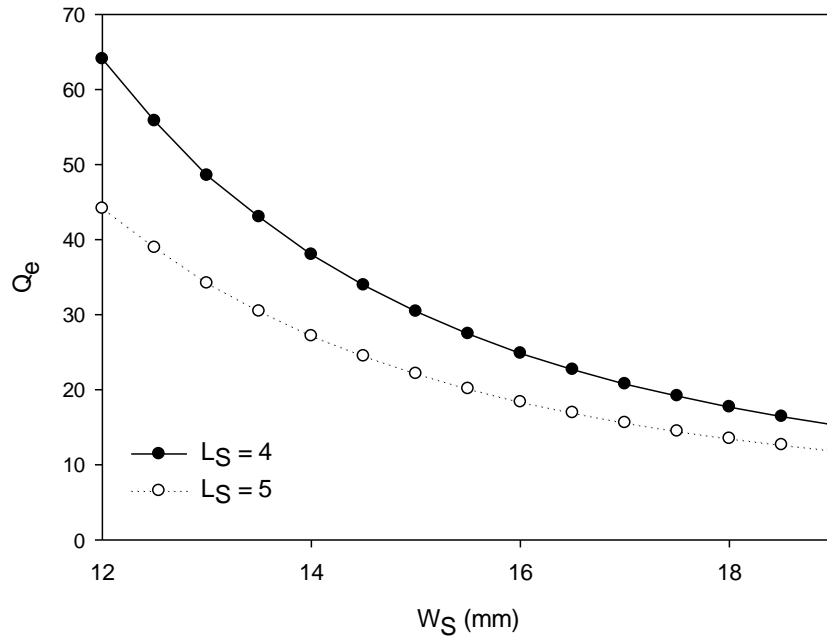
Figure 5.6: The design curve for Q_e against W_S for different values of L_S.

The coupling coefficient between two adjacent resonators, M, was extracted using the arrangement of figure 5.7a. The two coupled patches have the same length and the same operating frequency. The coupling depends on the gap between them. From EM simulations, the coupled resonators are very weakly coupled by the two ports. Figure 5.7b shows the simulated frequency response of the coupled resonators. Two resonant peaks can be clearly observed from the EM simulated response. They correspond to the characterisitic frequencies f_1 and f_2. The coupling coefficient, M, can be extracted using the equation (5.14).

Figure 5.8 shows the design curve for the coupling coefficient M against the spacing g. It can be seen that the coupling decreases as the gap increases. The formula for extracting the coupling coefficient M in terms of the charactersitic frequencies is given by:

$$M_{i,\,i+1} = \frac{{f_2}^2 - {f_1}^2}{{f_2}^2 + {f_1}^2} \qquad (5.14)$$

150
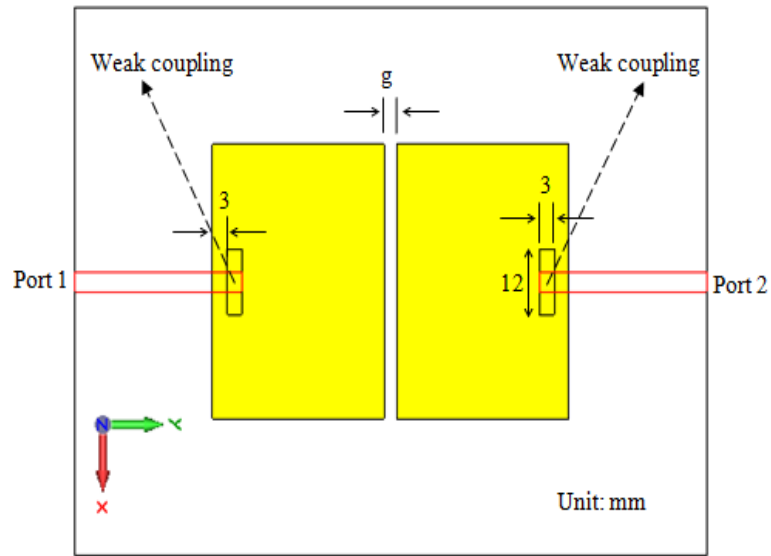
(a)
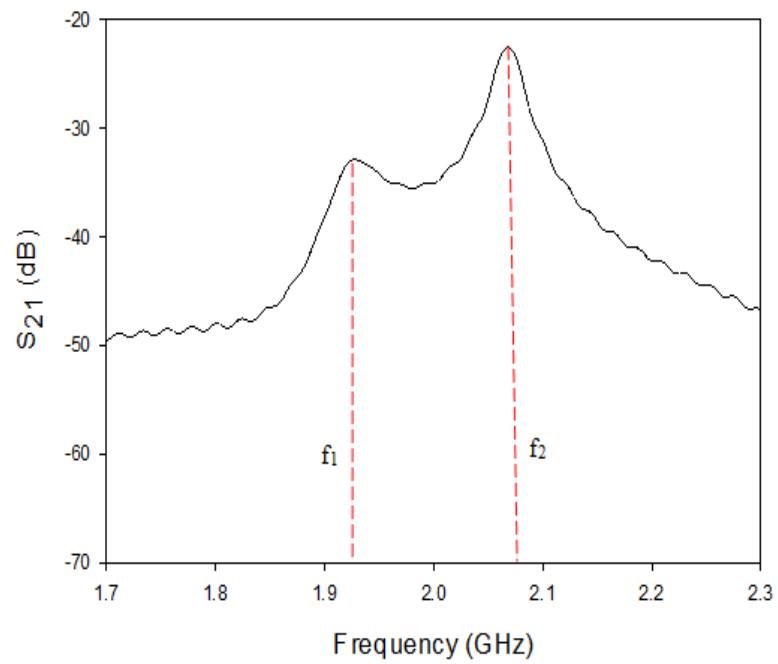
(b)

Figure 5.7: The coupling coefficient calculation: (a) an arrangement for extracting the coupling coefficient M; (b) simulated frequency response for g = 0.5 mm.

151
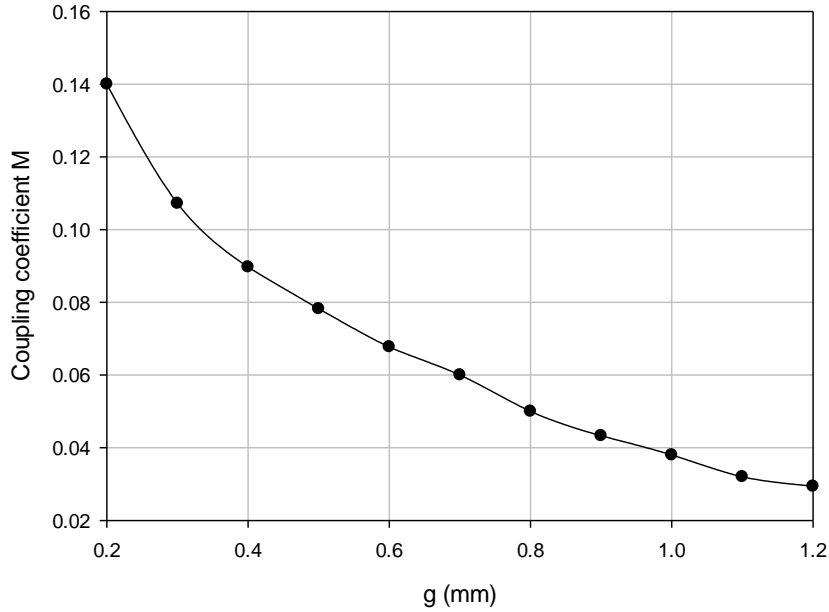
Figure 5.8: The design curve for the coupling coefficient k against the gap g.

The simulations were carried out for range of slot width, W_S, and a fitted curve is obtained. As shown in figure 5.6, the required slot width to achieve the desired external quality factor of $Q_e = 17$ can be read from the curve, which are $W_S = 18$, and $L_S = 4$. Likewise, the required gap g to achieve the desired coupling coefficient of M $= 0.052$ can be directly read from the fitted design curve in figure 5.8, which is g $=$ 0.8 mm. These values are used initially and they result in the performance as shown in figure 5.9. This performance, which does not meet the requirements, can be further improved by using the optimizer in CST software package. The optimizer is run with these initial values with tolerance of $\pm 15\%$. The optimizer goal is $S_{11} <=$ -20 dB from 1.95 to 2.05 GHz. The optimized physical dimensions are determined, which are W_S $=18.76$ mm, $L_S = 3.85$ mm, and g $= 0.72$ mm as referring to the layout in figure 5.1. Since the designed filter needs to be synchronously tuned, all resonators resonate at the same frequency, the middle patch resonator is slightly longer than the I/O

152

resonators. The length of the middle patch was adjusted to improve the result, and found to be L_{P2}= 37 mm.
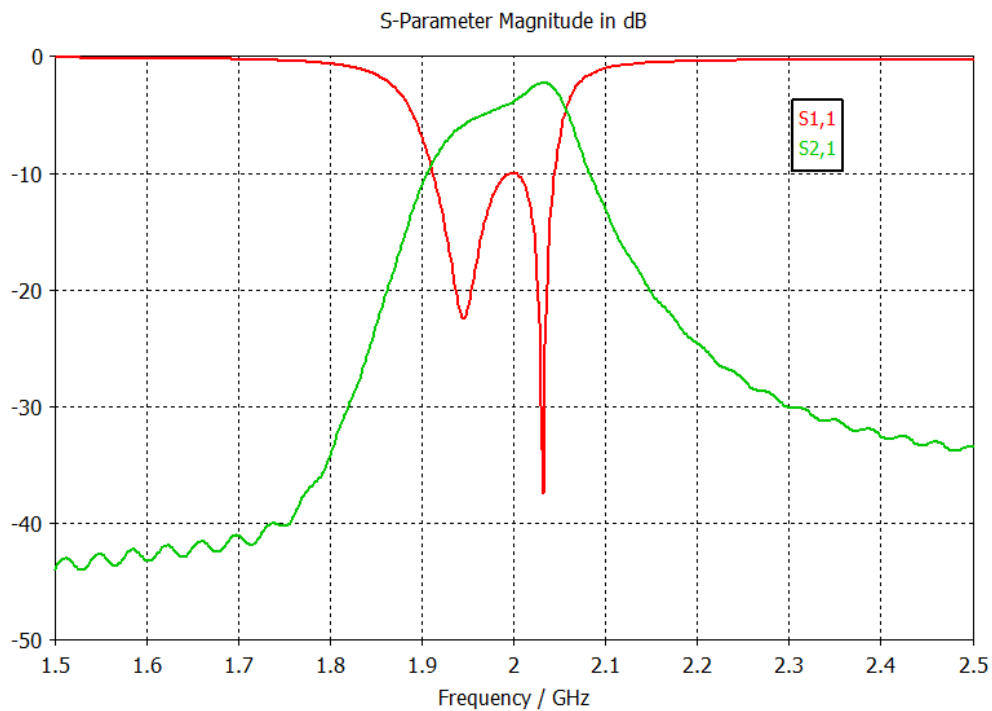
Figure 5.9: The simulated performance of the filter in figure 5.1 using the initial parameters obtained from the design curves: with W_S = 18 mm, L_S = 4.0 mm, and g = 0.8 mm.

5.1.3. Simulation and Measurement Results

Simulations were performed using the commercially available 3D EM solver of CST®. The proposed structure was fabricated and measured as shown in figure 5.10. The simulated and measured return loss and insertion loss are shown in figure 5.11. As can be seen, the measured and simulated midband frequencies are 2.1 and 2.0 GHz respectively. The measured minimum insertion loss is -5.5 dB which is 2.3 dB higher than the simulated one. The measured and simulated 3-dB passbands are 117 and 130 MHz respectively.

The proposed structure exhibits filter-like frequency response with three transmission zeros observed in the S_{11} result. A higher insertion loss is observed in the

measured results because it includes the losses of the feed line and SMA connectors. The dielectric constant tolerance of the substrate material has the most significant effect on the filter performance; it causes a shift in the passband. Etching accuracy can also affect the performance. In addition, stray or unwanted cross couplings generate interactions between different parts of the filter results in degraded performance.
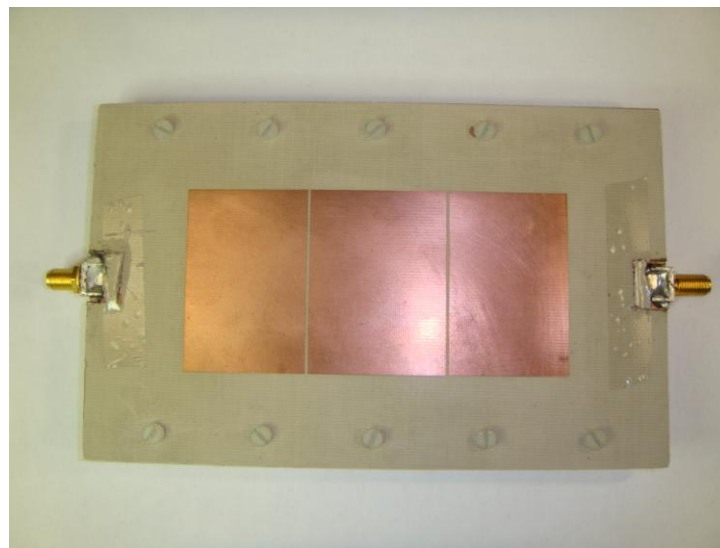
(a)
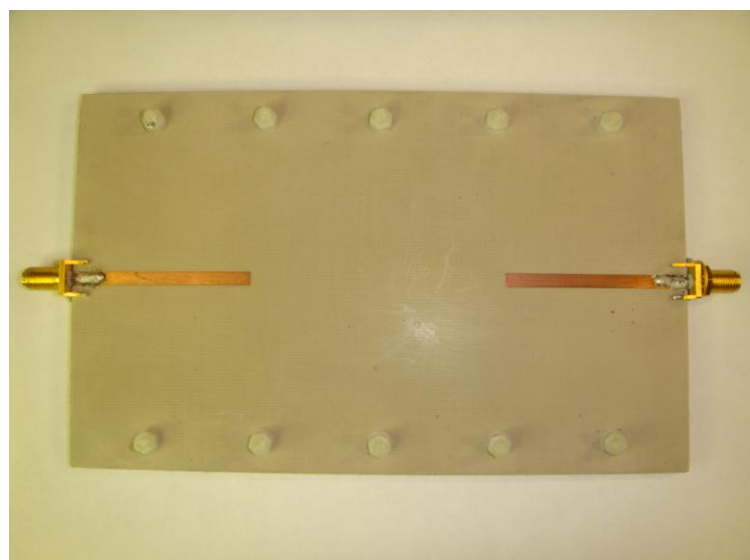
(b)

Figure 5.10: Edge-coupled patches filter (a) top view; (b) bottom view.
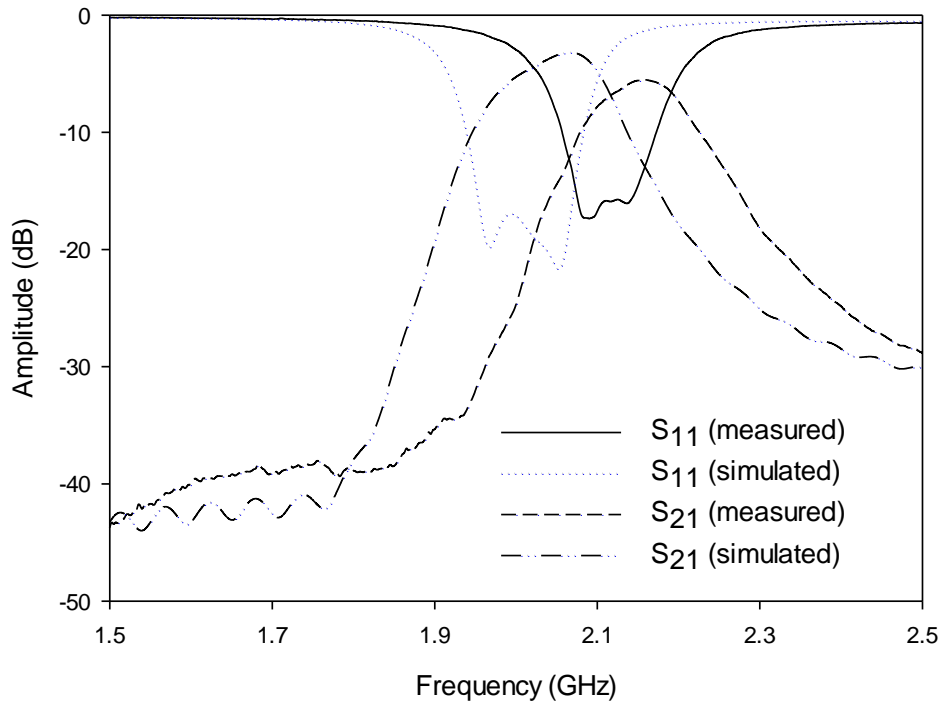
Figure 5.11: The simulated and measured performance of the filter
of figure 5.1 with $W_S = 18.8$ mm,

The simulated and measured realized gain in the broadside direction is shown in figure 5.12a. Good agreement is noted, particularly in the passband around 2.0 GHz. The radiation pattern of the proposed structure has been also simulated and measured. Figure 5.13 illustrates the 3D plot of the simulated radiation pattern. It can be seen that the main beam is slightly tilted and it increases as the frequency increases within the passband. The main lobe direction changes from $\phi = 22^\circ$ at 1.95 GHz to $\phi = 40^\circ$ at 2.05 GHz. The radiation pattern maintains a similar shape within the passband. The simulated and measured radiation patterns are shown in figure 5.14. The radiation pattern is symmetric about the xz (H) plane. A reasonable agreement with the simulation in the co-polarized pattern is obtained. However, the measured cross polarization levels are much higher than the simulation. Nonetheless, their levels remain below -15 dB. Since the filter antenna is composed of patches which are typically low Q resonators, fast roll-off cannot be achieved using this structure.
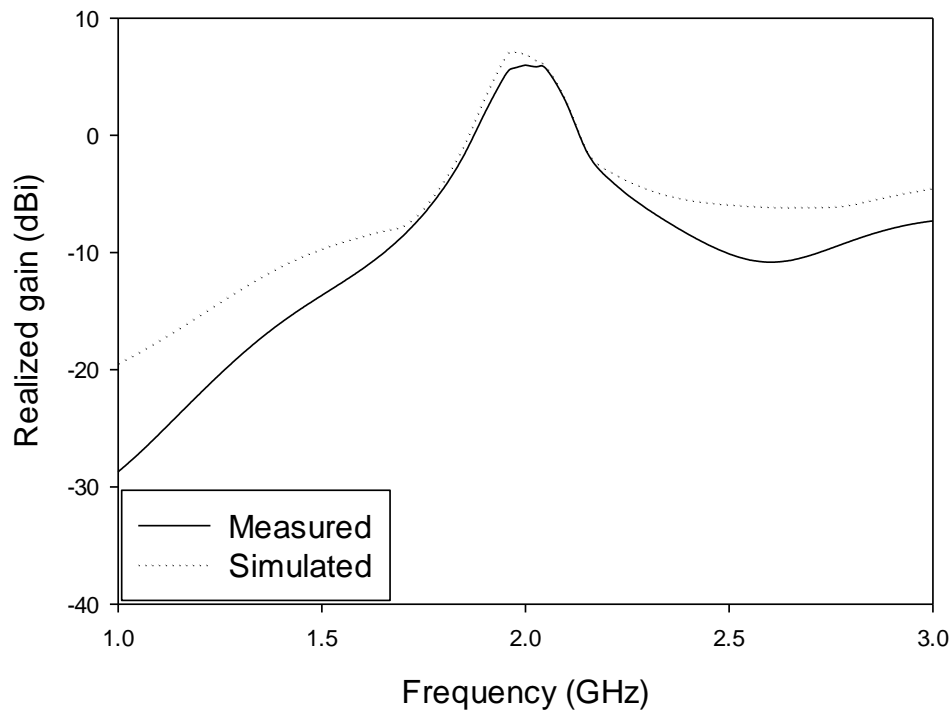
Figure 5.12: The measured and simulated realized gain of the proposed antenna.

As mentioned earlier, the beam is slightly tilted and the direction of the main lobe changes with frequency. This is because the proposed filtering antenna is basically travelling-wave array antenna. For a travelling-wave array, the impedances of the patches and the microstrip lines are well-matched and the separation between the patches can be either a wavelength for broadside radiation or less than wavelength for off broadside radiation. Broadly speaking, the main beam tilts by 1° for 1% of frequency change [14]. Since the separation between the patches is controlled by the mutual coupling, and is found to be much less than a wavelength, the proposed antenna is a travelling-wave antenna, and hence off broadside radiation is obtained.
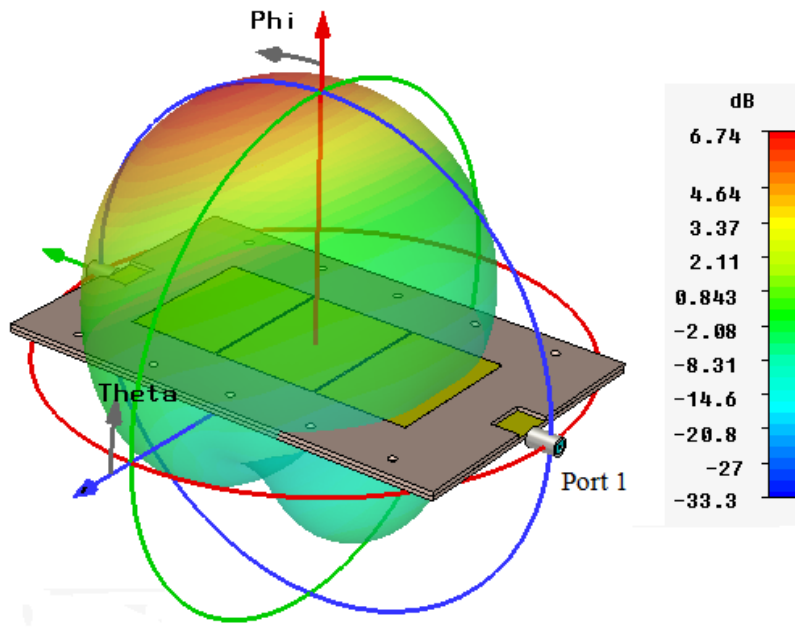
Figure 5.13: 3D plot of the radiation pattern showing the angle phi
at which the beam is tilted.
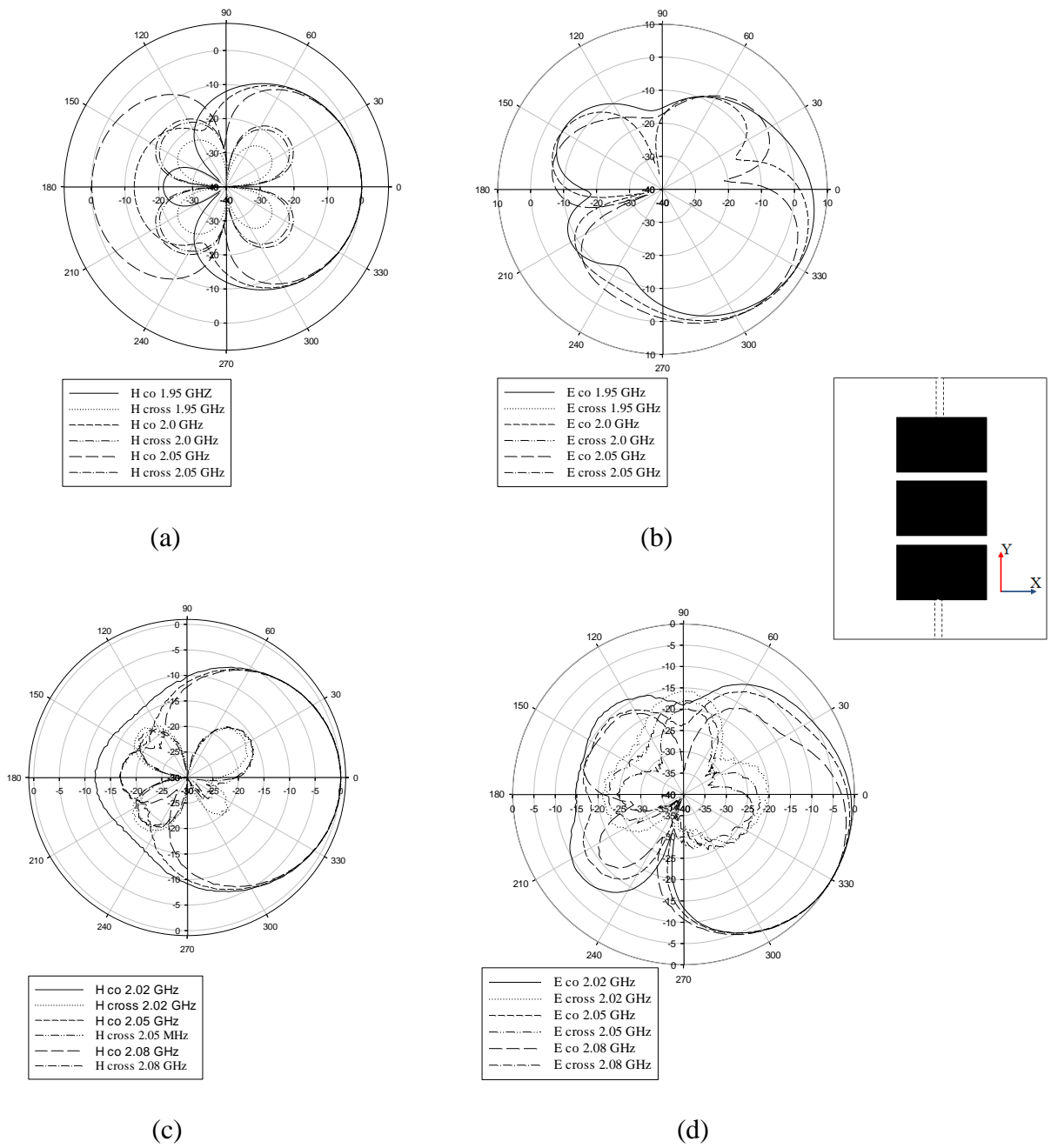
Figure 5.14: The normalized radiation pattern of the edge-coupled patches:
(a) Simulated H plane; (b) simulated E plane; (c) measured H plane; (d) measured E plane.
(Radial units are dB. Circumferential scale is θ, in degrees).

158

5.2. Patch with Hairpin Resonators Filter Antenna

This section presents a novel microstrip antenna with filtering capability that attempts to overcome the difficulty noted in the previous section of current synthesis methods applying only to two port devices. The filtering antenna consists of a coupled line, two hairpin resonators, and a rectangular patch. The proposed structure functions as a three-pole bandpass filter having a bandwidth of 58 MHz centred at a midband frequency of 2.0 GHz. The synthesis process starts with designing microstrip bandpass filter, as described in section 5.2.1. Thereafter, the filter is developed into an antenna by replacing the last resonator and the output line by a rectangular patch. The proposed filtering microstrip antenna exhibits good out-of-band gain suppression, flat in-band gain, good selectivity at the band edges, and a well-shaped radiation pattern.

5.2.1. Hairpin Microstrip Bandpass Filter

Hairpin line bandpass filter is a compact structure which could be realized by folding narrow microstrip resonators into a U shape, known as hairpin resonators. They are approximately half wavelength long at the midband frequency. In order to design this kind of filter accurately, a design method using EM simulations is employed similar to that used in section 5.1.

5.2.1.1 Filter Structure and Design

The bandpass filter is the first step in designing the filtering antenna. Having completed the filter design, the last resonator and the output line of the filter will be replaced by a radiating patch. In order to preserve the filter characteristic, the radiation quality factor of the patch must be equal to the external quality factor of the filter ($Q_{e1} = Q_r$). The bandwidth of the filter is used as a design parameter, and chosen such that the external quality factor of the filter is equal to the radiation quality factor

of the patch which is $Q_r = 30$ as will be shown below in the section 5.2.2. The filter is designed to operate at a midband frequency $f_0 = 2.0$ GHz. A three-pole Chebyshev lowpass prototype with passband ripple of 0.0432 dB is chosen, shown in figure 5.2. The lowpass prototype parameters, given for a normalized cut off frequency $\Omega_c = 1$, $g_0 = g_4 = 1.0$, $g_1 = g_3 = 0.8516$, $g_2 = 1.1032$. Having chosen the external quality factor to be $Q_e = 30$, the fractional bandwidth and the coupling coefficients can be calculated using the equations (5.1) and (5.2):

$$FBW = 0.029$$

$$M_{12} = M_{23} = 0.0303$$

A commercial substrate TRF41 from Taconic® is used for microstrip implementation. The dielectric constant of the material $\varepsilon_r = 4.1$ and the dielectric thickness h = 3.04 mm. The filter is designed to have a coupled line at input and output as shown in figure 5.15. The coupled line is designed to have a characteristic impedance of 50 Ω to match the source impedance. Hence, the coupled line has a width of 5.6 mm. The performance of the filter, which can be plotted based on the coupling matrix as discussed in 5.1.1, is shown in figure 5.16. As expected, three transmission zeros are observed in the return loss result. Two of the poles are located at the edges of the passband at 1.97 and 2.03 GHz and the third one is located at the midband frequency of 2.0 GHz.

The hairpin resonators are approximately half wavelength long at the midband frequency. The total length of the resonator is approximately 47 mm, with line width of 1 mm as shown in figure 5.17. At the resonance of the fundamental mode, the maximum electric field intensity at the open ends of the resonator, and maximum magnetic field intensity is at the centre. The resonators in the proposed filter are electromagnetically coupled because the electric and magnetic fields have

comparative distributions at the coupled arms. Figure 5.17 shows the simulated result for the unloaded quality factor of the resonator.

The currents in the parallel lines of the hairpin resonator have similar magnitudes and opposite directions. Therefore, a resonator with closely spaced arms will have low radiation loss (i.e. high unloaded Q) due to cancelation of the opposing currents. However, closely spaced arms may also function as a pair of coupled lines. A resonator with widely separated arms, on the other hand, will have higher radiation losses and low coupling between the arms. Thus, the geometry of the resonator represents a trade-off in its performance.
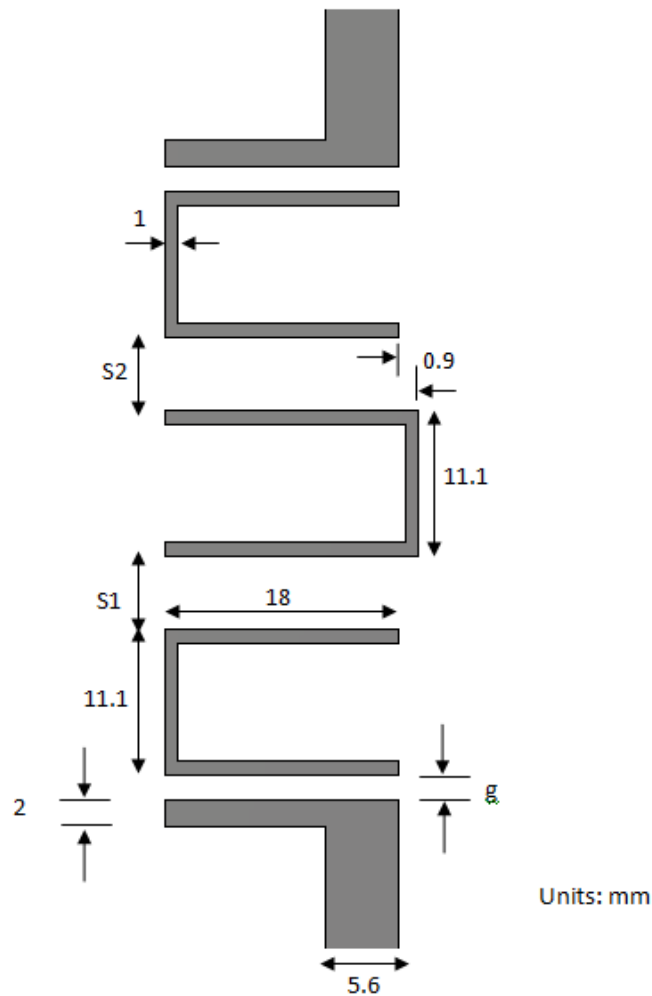
Figure 5.15: Layout of three-pole hairpin microstrip bandpass filter.
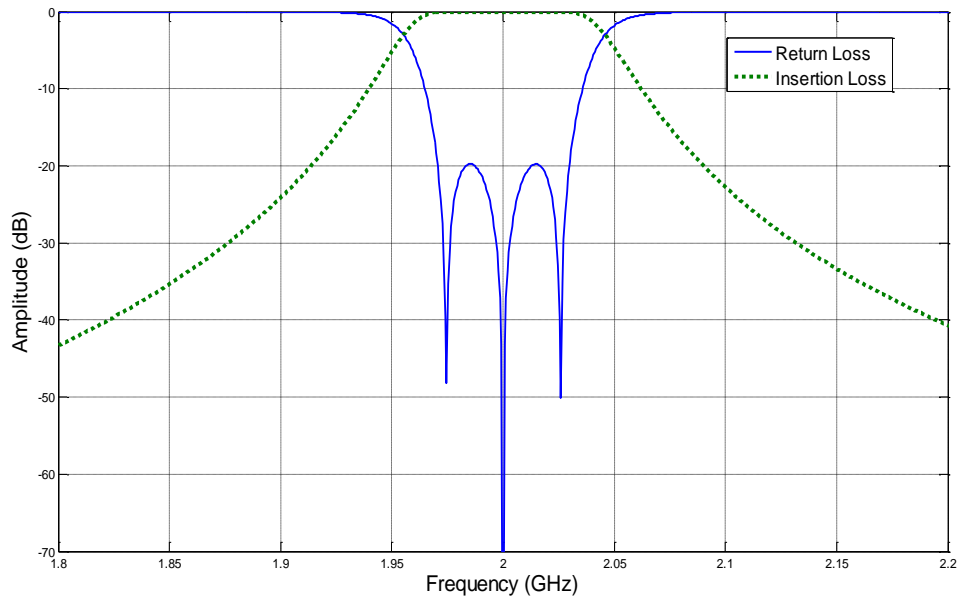
Figure 5.16: The performance of the hairpin bandpass filter based on the coupling matrix calculations.
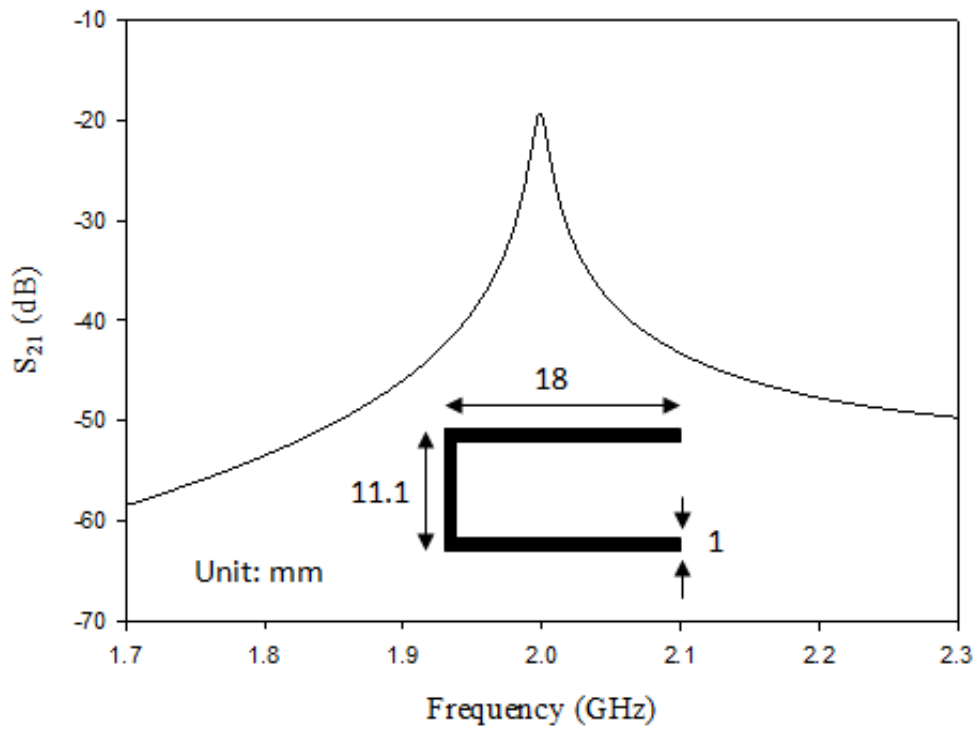
Figure 5.17: The hairpin line resonator: the geometry of the resonator, and the simulated frequency response.

162

5.2.1.2 Extraction of the Design Parameters

Figure 5.18a shows an arrangement to extract the external quality factor of the input/output resonators of the structure shown in figure 5.15. The resonator, which is assumed to be lossless in the simulation, is excited using a coupled line at port 1. Port 2 is weakly coupled to the resonator, which implies that $Q_{e2} = \infty$. The magnitude response of the transmission coefficient S_{21} is used to extract the single-loaded external quality factor Q_e. Q_e can be calculated directly from the resonant frequency f_0 and the 3-dB bandwidth (Δf) as given in the equation (5.9). A design curve of Q_e against the gap g is shown in figure 15.19. In this case, as the gap increases, the coupling from the source decreases, and hence Q_e increases.

The same approach described in 5.1.2 for extracting the inter-resonator coupling is used. The coupling between two adjacent resonators can be extracted using the arrangement of figure 5.20a. The coupling depends on the spacing, S, between them. Figure 5.20b shows the simulated frequency response of the coupled resonators structure for S = 2 mm. The coupling coefficient M can be extracted using equation (5.14). A design curve for M against the spacing S is shown in figure 5.21. It is clear that the coupling decreases as the spacing between the coupled resonators increases. For synchronously tuned filter, where all resonators resonate at the same frequency, the frequency midway the two peaks should be equal to the midband frequency of the filter.
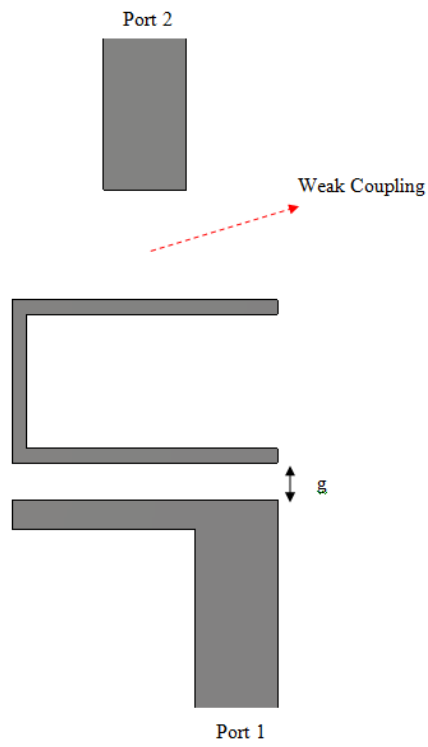
(a)
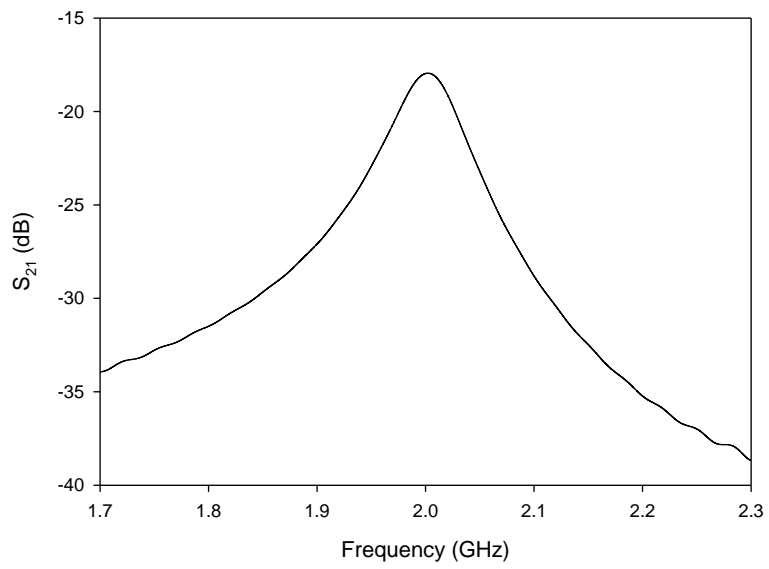
(b)

Figure 5.18: The extraction of the external quality factor: (a) an arrangement to extract Q_e; (b) simulated frequency response for g = 1.2 mm
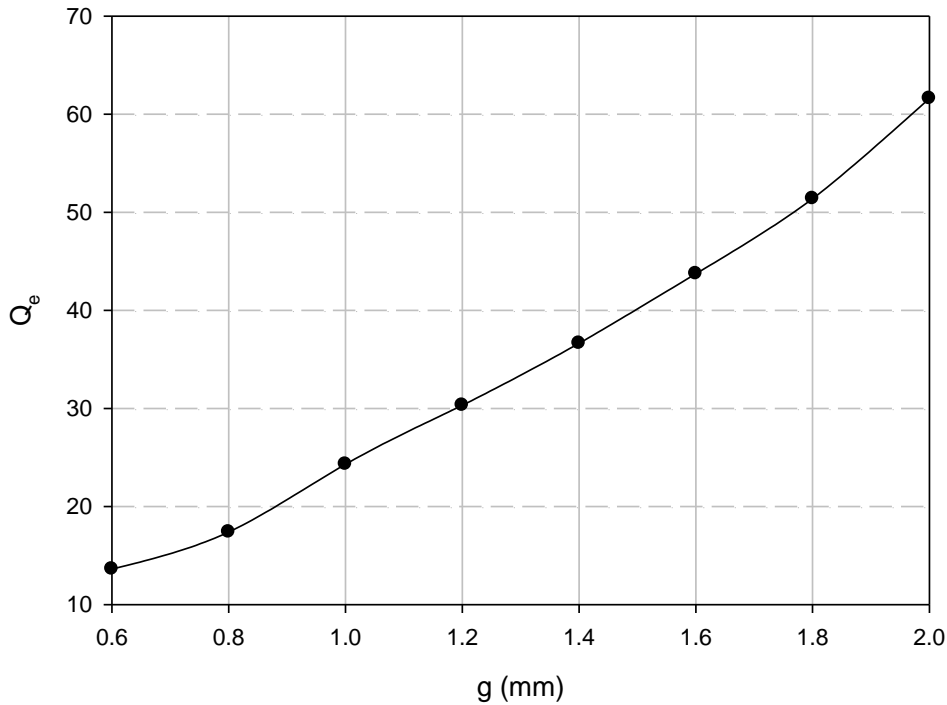
Figure 5.19: The design curve for Q_e against the gap g

From the design curves 5.19 and 5.21, all the physical dimensions, associated with the external quality factor and the coupling coefficients given in equations 5.1 and 5.2, are readily determined, and these are g = 1.2 mm, $S_1 = S_2 = 5.2$ mm as referring to the layout in figure 5.15. The dimensions were rounded off to a resolution of 0.1 mm. The input and output resonators are slightly shorter than the middle resonator in order to compensate for the effect of the coupled line and the adjacent coupled resonator. This simulation based method considers only the couplings along the desired signal path. However, in practice, unwanted or cross couplings cause interactions between non adjacent parts of the filter [12]. Therefore, the inaccuracy inherited in this decomposition method depends on the topology of the filter. In the design of the hairpin bandpass filter it is found to be good accuracy where the values obtained from the design curves resulted in very good performance as will be shown below.
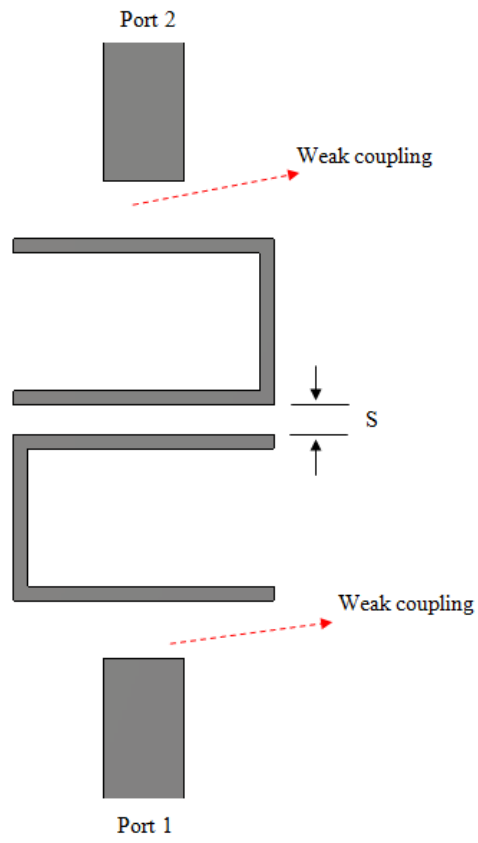
(a)
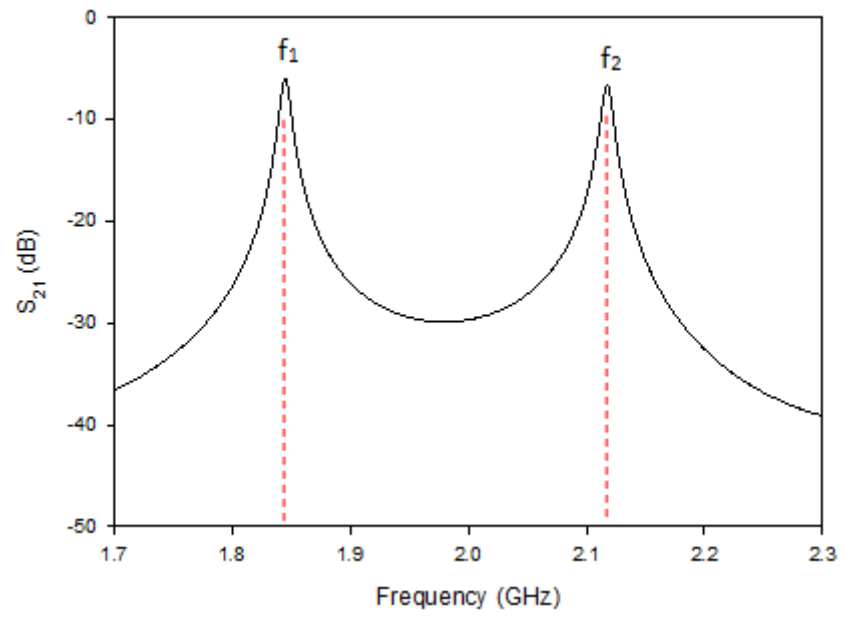
(b)

Figure 5.20: (a) An arrangement for extracting the coupling coefficient K;

(b) simulated frequency response for S = 2 mm.
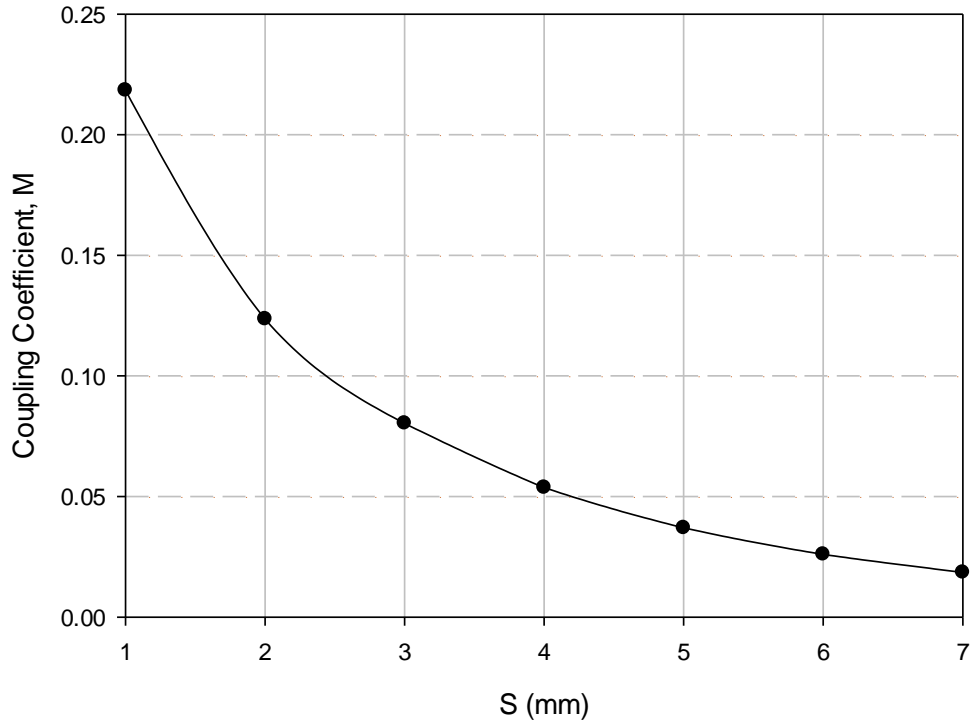
Figure 5.21: Design curve for the coupling coefficient M.

5.2.1.3 Simulation and Measurement Results

The proposed structure has been simulated using the commercially available 3D EM solver of CST Microwave Studio. The proposed structure, shown in figure 5.22, has been fabricated and measured using an HP8722D vector network analyzer in order to verify the performance. Figure 5.23 shows the simulated and measured frequency responses of the filter. The measured and simulated midband frequencies are 2.03 and 2.0 GHz respectively. The simulated midband insertion loss is -0.1 dB whereas the measured one -2.5 dB. The measured return loss is lower than -12 dB. The observed frequency shift towards 2.03 GHz could be due to the variation in the dielectric constant of the substrate which has a tolerance of ±0.15. Other factors may include fabrication tolerance such as soldering and etching accuracies. The simulated and measured 3-dB passbands are 92 and 80 MHz respectively. The higher insertion loss observed in the measured result is mainly due to conductor and dielectric looses of the

material. In addition, the SMA connector used in the printed circuit board (PCB) introduces some additional losses.
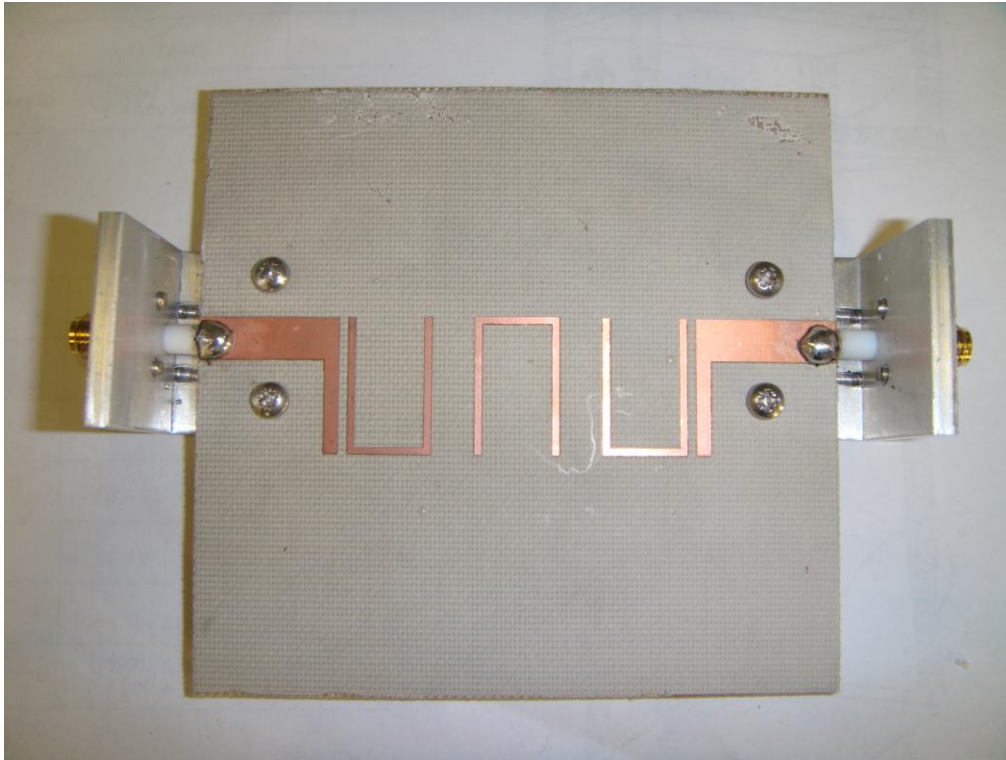
Figure 5.22: Fabricated bandpass filter

Figure 5.24 shows the simulated electric and magnetic fields at the midband frequency of 2.0 GHz. It can be seen that the maximum electric field intensity is at the open ends of the resonator. However, the maximum magnetic field intensity is at the centre of the resonator. The electric and magnetic fields have comparative distributions at the coupled sides of the adjacent resonators. Thus, the coupling in this structure may be referred as electromagnetic (mixed) coupling. The type of coupling depends on the orientation of the coupled resonators. Other couplings such as electric, or magnetic can be used. However, the electromagnetic coupling is found to be stronger, therefore, it is used in the filter design.
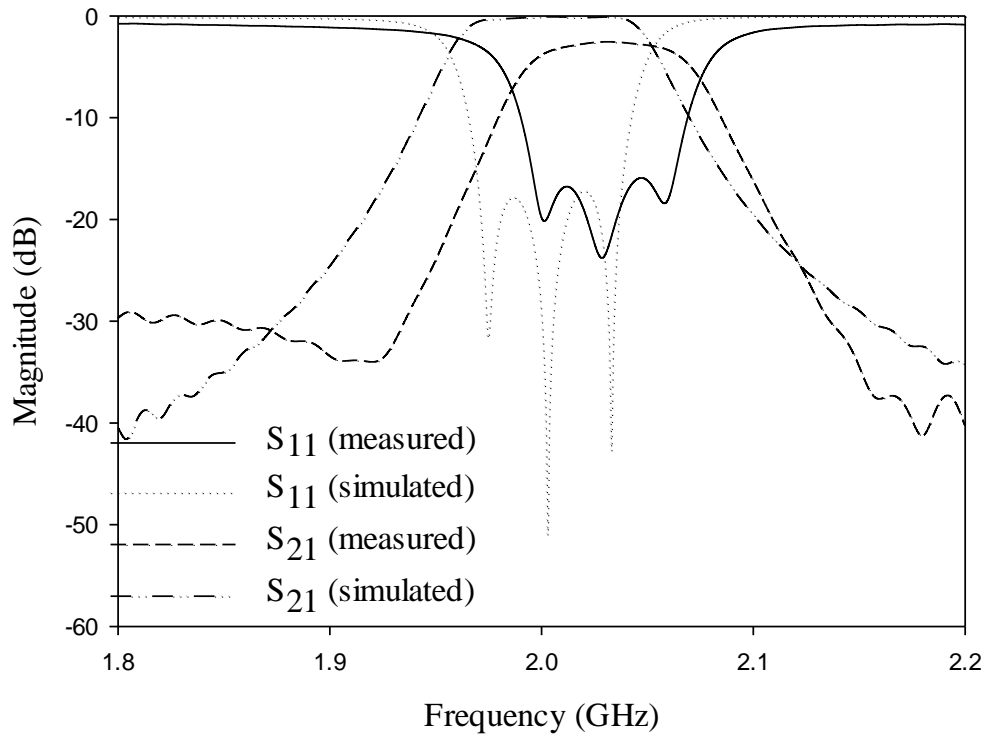
Figure 5.23: Simulated and measured performance of the hairpin microstrip filter in figure 5.15 with g = 1.2 mm, $S_1 = S_2 = 5.2$ mm.
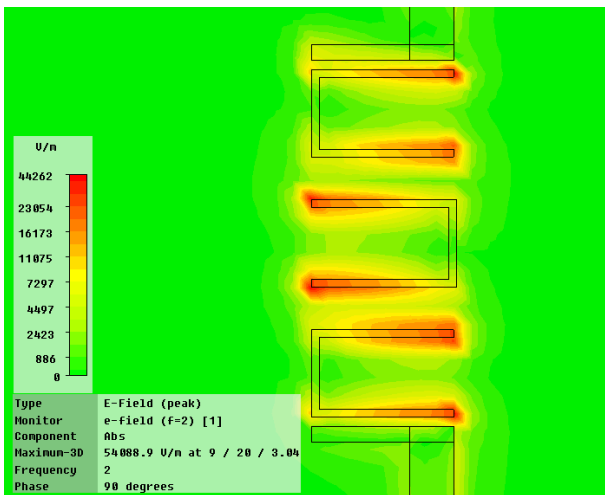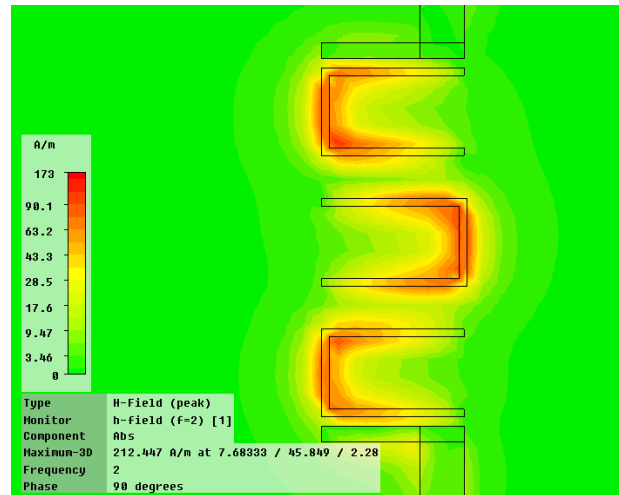
(a)   (b)

Figure 5.24: Simulated field distribution at the midband frequency:

(a) electric field; (b) magnetic field

5.2.2. Filtering Microstrip Antenna

A filtering microstrip antenna is proposed in this section. The antenna is designed based on the filter synthesis approach described in the last section of 5.2.1.

5.2.2.1. Antenna Structure and Design

The proposed filtering antenna is shown in figure 5.25. The rectangular patch replaces the third resonator and the output feed line. In order to preserve the filter characteristics, the radiation quality factor of the patch must be equal to the external quality factor at the input. Thus, the frequency response of the energy radiated by the patch will be similar to that of the insertion loss of the conventional filter. In this design, all the dimensions of the filter are maintained the same apart from the spacing S_2 between the second hairpin resonator and the patch. The spacing S_2 is chosen as to obtain the desirable mutual coupling of $M_{23} = 0.0303$.
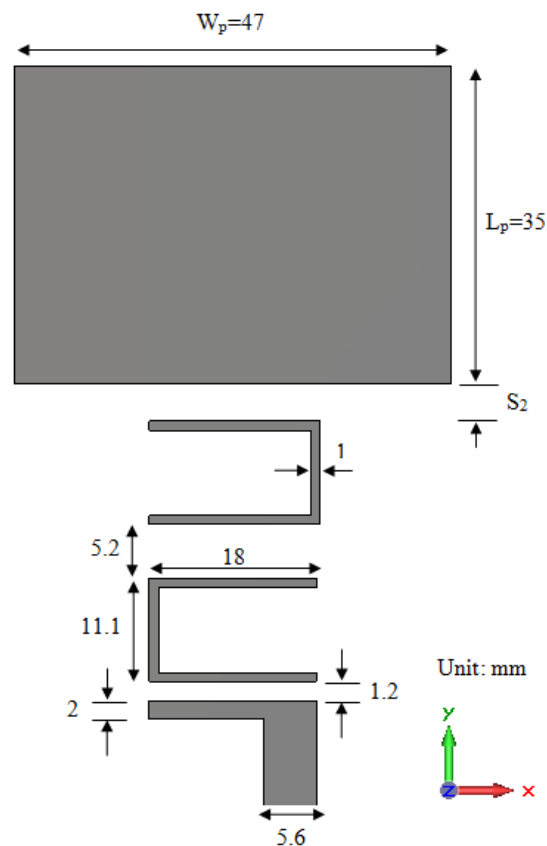
Figure 5.25: Layout of the filtering microstrip antenna

5.2.2.2. Extraction of the Design Parameters

Figure 5.26a shows an arrangement for extracting the radiation quality factor (Q_r) of the patch. The simulated frequency response of this structure is shown in figure 5.26b, where S_{21} is the transmission coefficient between the two ports that are very weakly coupled. Q_r can be calculated from the resonant frequency and the 3-dB bandwidth as given in equation 5.9. Q_r is computed using this method and found to be approximately equal to 30. Thus, $Q_r = Q_{e1}$ and the filter requirement of having the same Q at the two ports is met. The design curves for calculating the Q_r of patch were presented in [13] and gave very close result.

The coupling between the hairpin resonator and the patch can be obtained from the simulations using the setup of figure 5.27a. The coupling is controlled using the spacing S_2 between the patch and the resonator. In the simulations, the coupled resonators are weakly excited by the two ports as arranged. Figure 5.27b shows the typical simulated frequency response of the coupled resonators, where S_{21} denotes the S parameter between the two ports. The two resonant peaks that correspond to the two characteristic frequencies f_1 and f_2 can be clearly observed. The coupling coefficient can be calculated using equation (5.14). Figure 5.28 shows the design curve for M_{23} against S_2. From the design curves obtained in figure 5.28, the spacing S_2 associated with the desired coupling coefficient M_{23}, can be read directly, which is $S_2 = 3.2$ mm.
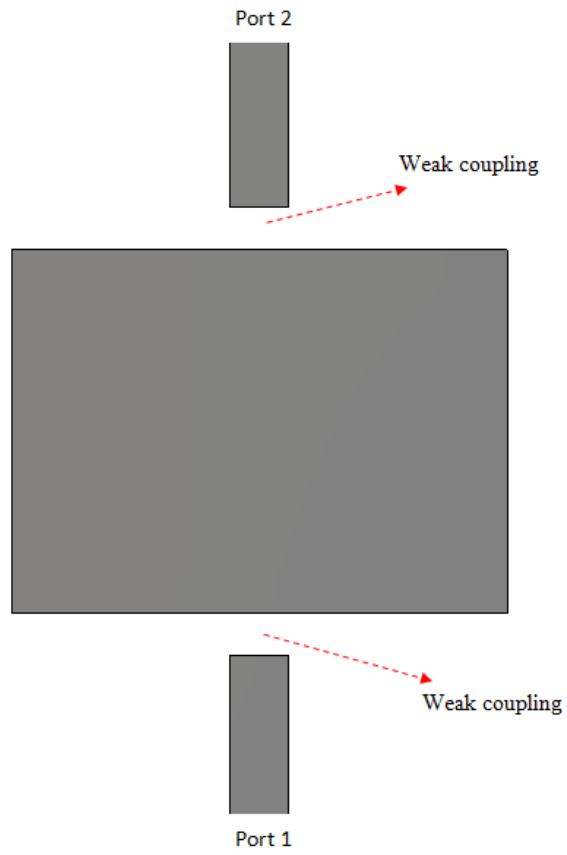
(a)
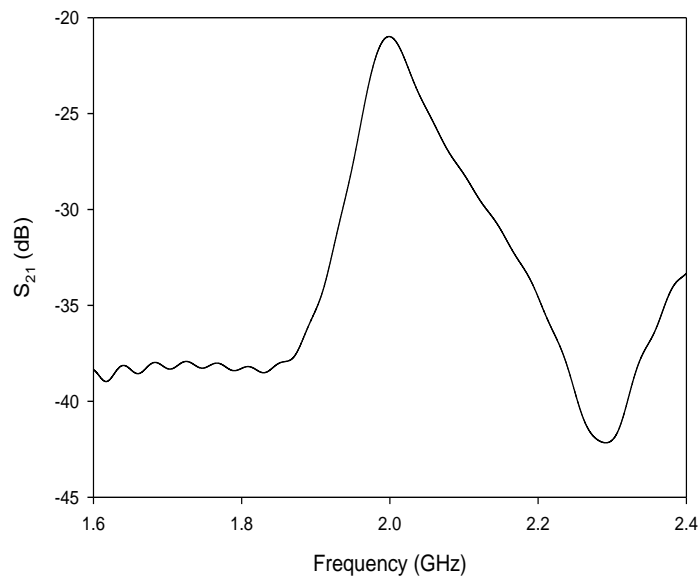
(b)

Figure 5.26: (a) An arrangement for extracting the radiation quality factor of the patch; (b) simulated frequency response
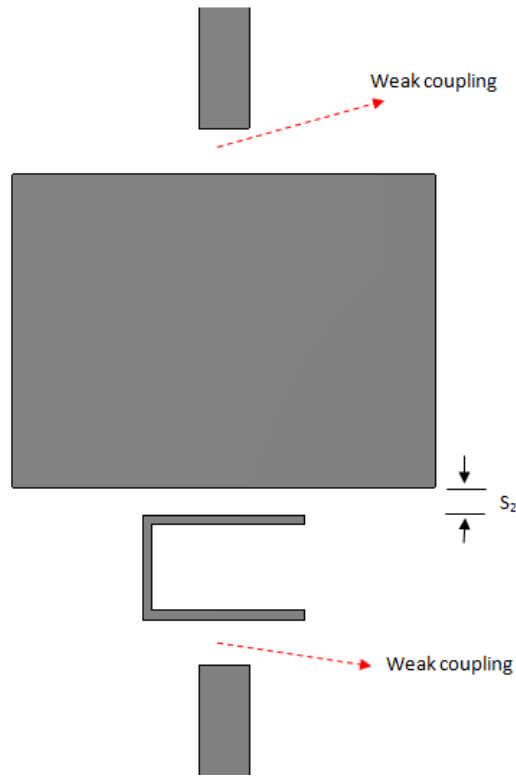
(a)
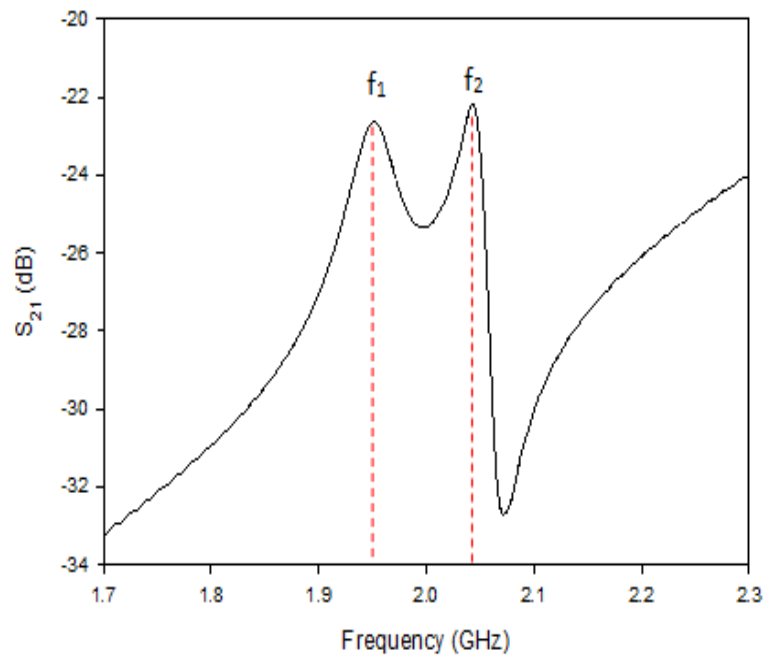
(b)

Figure 5.27: The coupling coefficient calculation: (a) an arrangement for extracting the coupling coefficient M_{23}; (b) simulated frequency response for $S_2 = 2$ mm
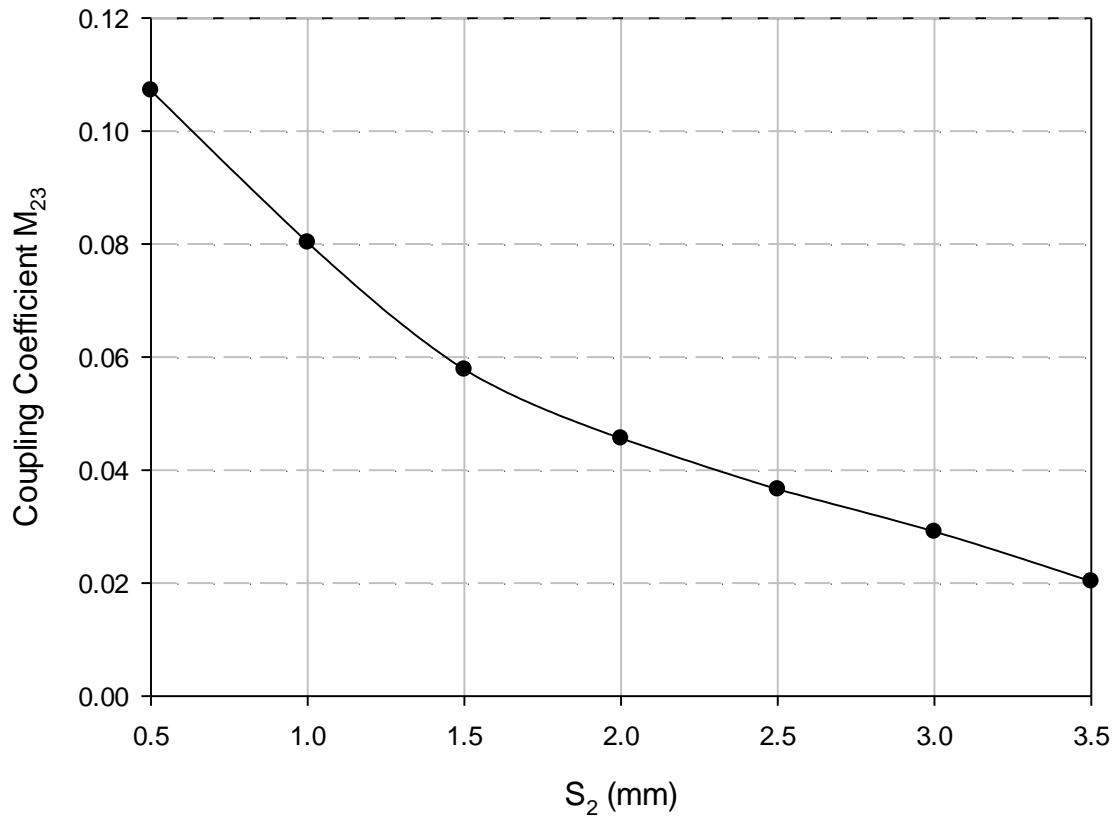
Figure 5.28: Design curve for the coupling coefficient M_{23}

.

5.2.2.3. Simulation and Measurement Results

The proposed filtering microstrip antenna was simulated using CST software package, fabricated, and measured using an HP8722D vector network analyzer VNA. Figure 5.29 shows the simulated and measured reflection coefficient of the structure. The proposed structure exhibits filter-like performance where three reflection zeros are observed. Thus, the patch acts as one resonator of the filter. The simulated midband frequency is 2.0 GHz whereas the measured one is 2.03 GHz. The frequency shift is due to the variation of the dielectric constant which has a tolerance of ± 0.15. The simulated -10 dB bandwidth is 3.64% whereas the measured one is 3.5%.
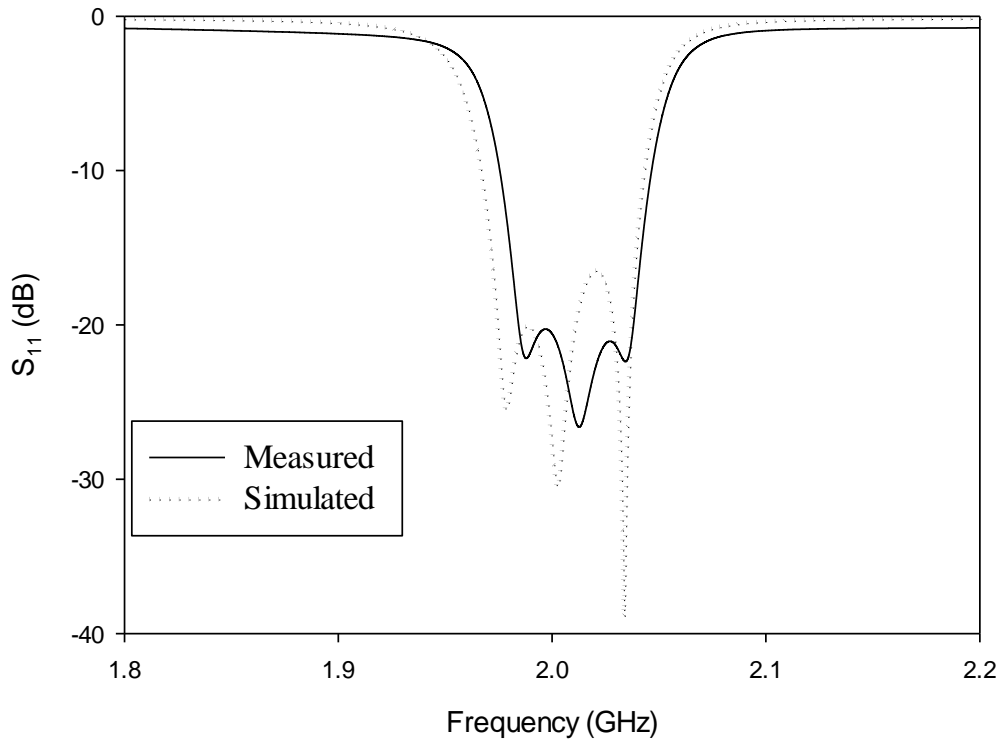
Figure 5.29: The simulated and measured reflection coefficient
of the proposed filtering antenna of figure 5.22 with $S_2 = 3.2$ mm

Figure 5.30 illustrates the simulated and measured radiation pattern of the proposed filtering antenna. The antenna exhibits well-shaped radiation pattern with cross polarization levels well below -20 dB. The antenna maintains similar radiation pattern within the operating bandwidth with maximum power radiated in the broadside direction (+Z). The back lobe radiation may be due to the finite ground plane. The realized gain of the antenna has been simulated and measured. Figure 5.31 shows the simulated and measured realized gain in the broadside direction (+Z). As can be seen the figure, the proposed filtering antenna exhibits flat in-band gain, high out-of-band gain suppression, and high skirt selectivity at the passband edges. The broadside

antenna gain has even better selectivity than the insertion loss of the bandpass filter shown in figure 5.23.

(a)

(b)
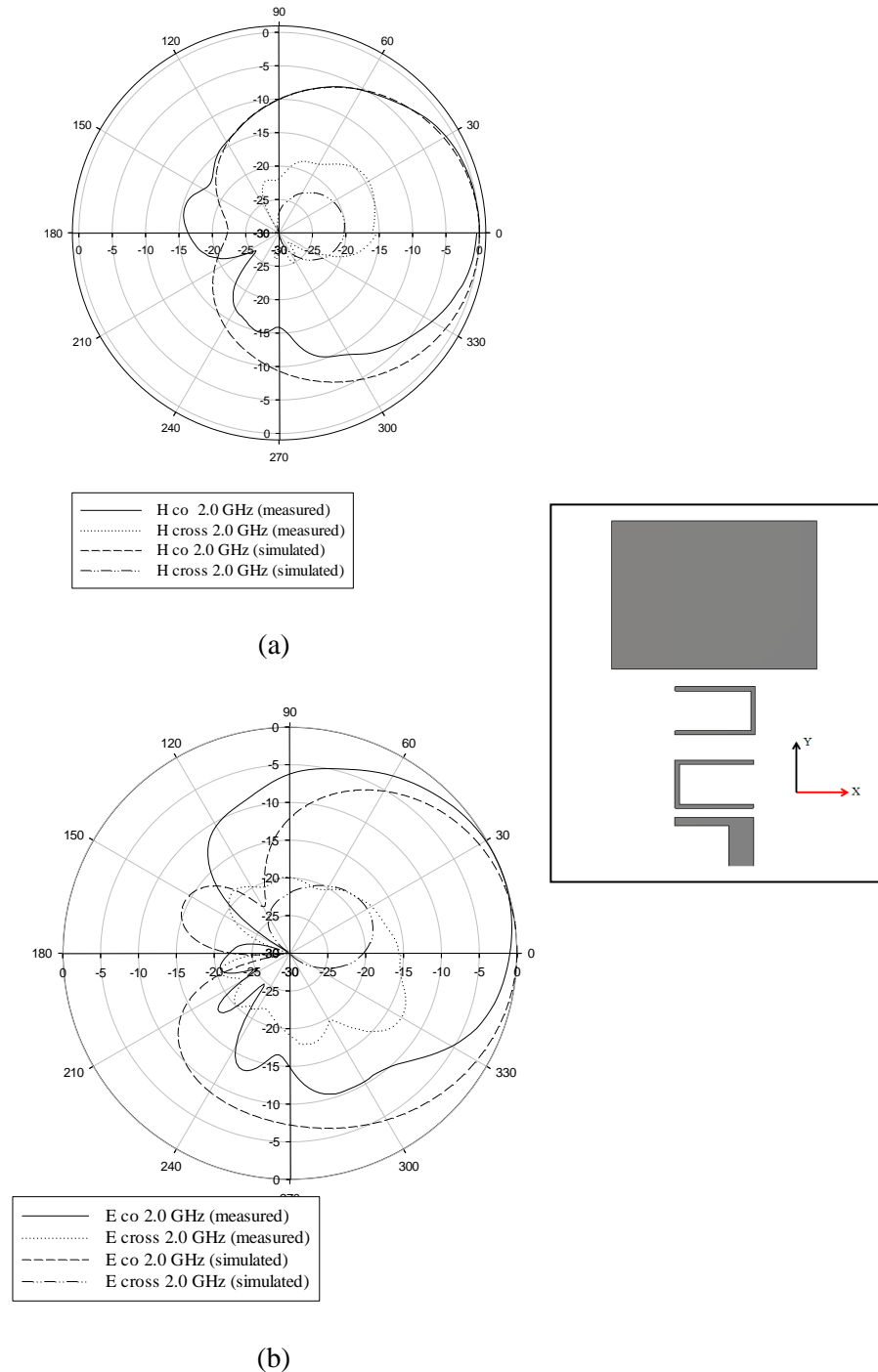
Figure 5.30: The normalized simulated and measured radiation pattern:

(a) H (XZ) plane; (b) E (YZ) plane

(Radial units are dB. Circumferential scale is θ in degrees).
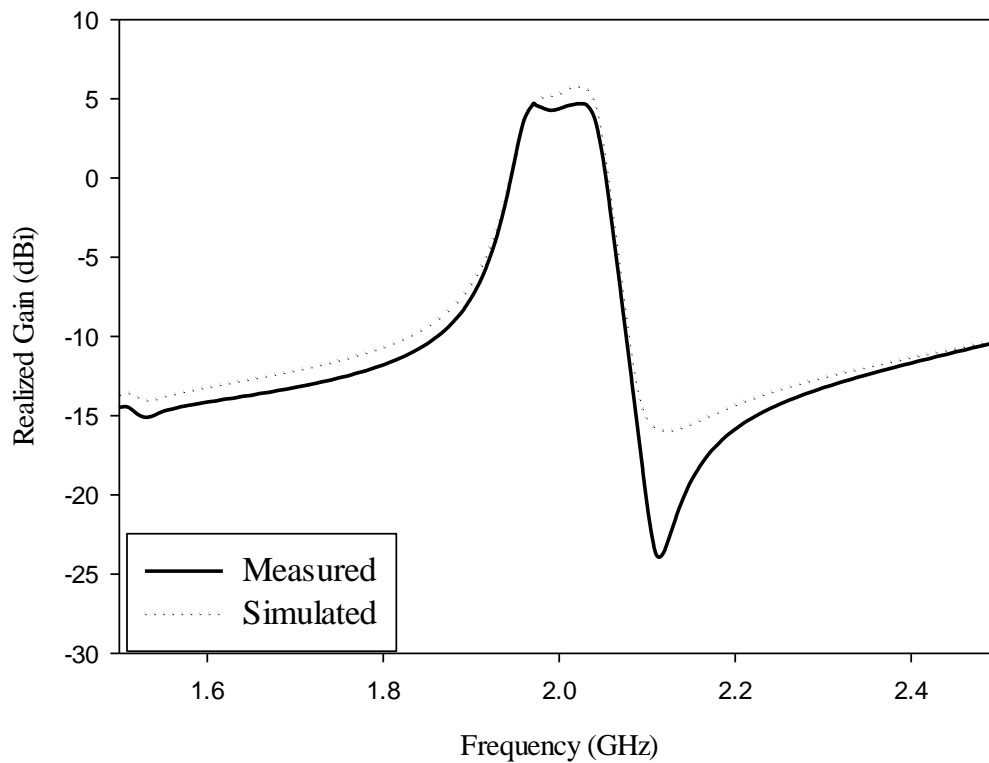
Figure 5.31: The simulated and measured realized gain

In order to demonstrate the advantages of the proposed filtering antenna, its performance is compared with a conventional patch antenna as shown in figure 5.32. The patch is designed to operate at the same midband frequency of the filtering antenna, namely, 2.0 GHz. It can be seen in figure 5.32 that the proposed antenna exhibits a filtering capability with suppressed out-of-band gain. The out-of-band gain suppression can be further improved by increasing the order of the filter (i.e. the number of the coupled resonators). Due to the losses of the coupled resonators, the antenna produces slightly less in-band gain than the conventional one. The fabricated filtering microstrip antenna is shown in figure 5.33.

177
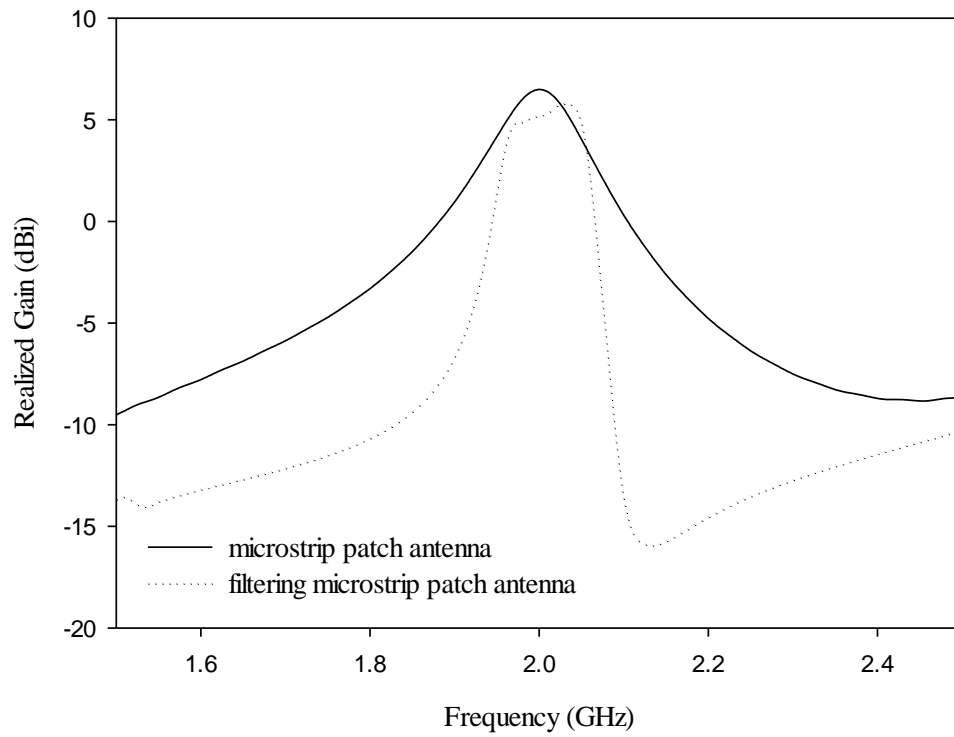
Figure 5.32: The realized gain of the filtering microstrip
antenna vs conventional microstrip antenna

Figure 5.33: The proposed filtering microstrip antenna

178

5.3. Conclusion

Compact microstrip antennas with filtering capabilities are proposed. The proposed antennas are designed based on a filter synthesis approach. The proposed structures combine radiating and filtering functions simultaneously by suppressing out-of-band gain and maintaining flat in-band gain. An edge coupled patches filter antenna is presented. The proposed structure exhibits reasonable filtering performance and radiation properties. Filtering antennas with high Q resonators will have better filtering capability, as is shown in section 5.2. The antenna functions as a third order bandpass filter with equal ripple response. It provides high out-of-band gain suppression, flat-in-band gain, and good skirt selectivity at the band edges.

References:

[1] F. Queudet, I. Pele, B. Froppier, Y. Mahe, and S. Toutain, "Integration of pass-band filters in patch antennas," in Proc. 32nd Eur. Microw. Conf., 2002, pp.685-688.

[2] A. I. Abunjaileh, I. C. Hunter, and A. H. Kemp, "A circuit-theoretic approach to the design of quadruple-mode broadband microstrip antennas," IEEE Trans. Microw. Theory Tech., vol.56, no.4, pp.896-900, Apr.2008.

[3] Chin-Kai Lin and Shyh-Jong Chung, "A filtering microstrip antenna array," IEEE Trans. Microw. Theory Tech., vol.59, no.11, pp.2856-2863, Nov.2011.

[4] Wei-Jun Wu, Ying-Zeng Yin, Shao-Li Zuo, Zhi-Ya Zhang, and Jiao-Jiao Xie, "A new compact filter-antenna for modern wireless communication systems," IEEE Antennas and Wireless Propagation Letters, vol.10, pp.1131-1134, 2011.

[5] S. Oda, S. Sakaguchi, H. Kanaya, R. Pokharel, and K. Yoshida, "Electrically small superconducting antennas with bandpass filters," IEEE Trans. Appl. Supercond., vol.17, no.2, pp.878-881, Jun.2007.

[6] C. T. Chuang and S.J. Chung, "New printed filtering antenna with selectivity enhancement," in Proc. 39th Eur. Microw. Conf., vol.9, pp.747-750.

[7] Chao-Tang Chuang, and Shyh-Jong Chung, "Synthesis and design of new printed filtering antenna," IEEE Transactions on Antennas and Propagation, VOL. 59, No.3, March 2011.

[8] Z. P. Wang, P. S. Hall, and P. Gardner, "Yagi antenna with frequency domain filtering performance," IEEE Antennas and Propagation Society International Symposium APSURSI, pp.1-2, July 2012.

[9] E. H. Lim, and K. W. Leung, "Use of the dielectric resonator antenna as a filter resonator," IEEE Trans. Antennas Propag., vol.56, pp.5-10, Jan. 2008.

[10] Yang Y., and M. J. Lancaster, "Waveguide Slot Antenna with Integrated Filters," the 32 European Space Agency Workshop, 2010.

[11] Constantine A. Balanis, Antenna Theory: Analysis and Design. 2nd Ed. New York, USA: John Wiley & Sons, Inc. 1997.

[12] Jia-Sheng Hong, and M .J. Lancaster, Microstrip Filters for RF/Microwave Applications, New York, USA: John Wiley & Sons, 2001.

[13] J. R. James, P. S. Hall, and C. Wood, Microstrip Antenna: Theory and Design, Peter Pereginus, London, 1981.

[14] Constantine A. Balanis, Modern Antenna Handbook, 2nd ED. New York, USA: John Wiley & Sons, Inc.2008.

CHAPTER VI

CONCLUSIONS AND FUTURE WORK

6.1.   Conclusions

This PhD describes research into multi-frequency and filtering antennas. Several novel antennas are presented, each of which address a specific issue for current and future communication systems, in terms of multi-frequency, wideband coverage, and filtering capability. These antenna designs seem to be promising candidates for implementation in future multiband radios, cognitive radio (CR), and software defined radio (SDR), although specifications for those future systems are not clear.

6.1.1. Conclusions for the Tunable Left Handed Loop Antenna

The tunable left handed loop antenna over a ground plane is presented in chapter 3. The antenna maintains the positive features of left handed wire antennas, such as small size with internal matching. Also, further size reduction is achieved due to the presence of the ground plane underneath. The antenna is a periodic structure which consists of three left handed cells. The resonant frequency of the antenna is controlled using the loading elements and is independent of its size. Each unit cell consists of two series capacitors and one shunt inductor. The loop has a unique feature that the n = 0 mode is excited. This mode has a uniform current distribution both in amplitude and phase. This results in a directional radiation pattern with maximum directivity orthogonal to the ground plane. In order to make the antenna tunable, the inductors are kept fixed at L_L = 10 nH and the capacitors are varied. The n = 0 mode has a -10 dB return loss tuning range of 1.88:1. The tuning range extends from 0.99 GHz to

1.86 GHz. The wide tuning bandwidth is useful to cover a large number of wireless services, such as GSM, GPS, PCS, UMTS, Wi-Fi, and Bluetooth. An electronically tunable loop was developed by replacing the fixed capacitors by varactor diodes. Biasing circuitry was designed to provide the control voltage for the varactors. Finally, a filtering capability was added to investigate the possibility of mode selection using switched filters. The filtering is achieved by integrating a lumped element highpass filter in the loop. The structure maintains the $n = 0$ mode only which can be tuned from 0.9 GHz to 1.5 GHz. Prototypes of the loop with lumped elements, a varactor-tuned loop, and a filtering loop were fabricated and measured. Good agreement between simulation and measurement was obtained.

6.1.2. Conclusions for the Reconfigurable Patch Antenna

The presence of new technologies in communications, such as cognitive radio (CR) and software-defined radio (SDR), add new challenges and opportunities to antenna design. One considerable challenge is covering multiple frequency bands with a single wideband and efficient antenna. A possible solution to this problem is to employ a frequency reconfigurable antenna that tunes to different frequency bands. Such an antenna would not cover all bands simultaneously, but would provide narrow instantaneous bandwidths that are dynamically selectable and would have higher efficiency than a conventional multi band antenna. An intrinsically narrowband antenna with dynamically controlled frequency response achieves the frequency agility and reduces the filtering requirement in the RF front end.

Chapter Four has presented a switchable multi-band reconfigurable patch antenna. The operating frequency can be switched between different frequency bands by activating PIN diodes loading the coupling slot. Three prototypes were designed, simulated, fabricated and measured. The first two prototypes incorporate two switches

and capable of switching between two and four frequency bands over frequency ranges of 1.36:1 and 1.23:1 respectively. The third prototype incorporates four switches and capable of switching between sixteen frequency bands, over frequency range of 1.5:1.The proposed antennas show very good impedance matching, well-shaped radiation patterns and good gain over all operating bands. A tunable patch is also presented in which frequency agility is achieved by employing two PIN diodes and two variable capacitors loaded in the coupling slot. The resonant frequency of the antenna can be shifted over a wide tuning bandwidth. The tuning bandwidth extends from 1.39 GHz to 2.36 GHz. The proposed antenna exhibits stable radiation patterns and reasonable gain within the operating bandwidth. The ability of the proposed antennas to easily select of wide range of discrete frequencies makes them of interest when multiple standards are to be processed by the same receiver. A single passive antenna with multi-resonance or wideband characteristics is a solution. However, this solution suffers from a drawback since the antenna receives other non desired frequencies and some filtering network is required to remove the undesirable frequencies. The narrow instantaneous frequency response makes the antenna good candidate for the cognitive radio applications.

6.1.3. Conclusions for the Filtering Microstrip Antenna

In wireless communication systems, the antenna and the filter are the key components. While the antenna transmits and receives signals, the bandpass filter (BPF) selects signals in the operating band and rejects spurious signals. Due to the increasing trend towards simplicity and miniaturization, it is desirable to integrate the filter and the antenna into a single component that achieves filtering and radiating functions simultaneously, known as a filtering antenna or "filtenna". The filtenna

reduces the pre-filtering requirement and improves the noise performance of the system.

Compact microstrip antennas with filtering capabilities are proposed in Chapter Five. The proposed antennas are designed based on a filter synthesis approach. The proposed structures combine radiating and filtering functions simultaneously by suppressing out-of-band gain and maintaining flat in-band gain. An edge coupled patches filter antenna is presented in Section 5.1. The proposed structure exhibits reasonable filtering performance and radiation properties. Filtering antenna with high unloaded Q resonators will provide better filtering capability, as is shown in Section 5.2. A microstrip antenna consisting of a rectangular patch coupled to two hairpin resonators is presented in Section 5.2. The antenna functions as a third order bandpass filter with equal ripple response. It provides high out-of-band gain suppression (up to 12 dB), flat-in-band gain, and good skirt selectivity at the band edges.

6.2. Future Work

The objective of developing multi-frequency and filtering antennas has been achieved. However, some future work can be done in order to improve the performance of the proposed antennas.

In the case of the tunable left handed loop antenna, the bandwidth of the additional frequency bands achieved at lower frequencies is narrower than the bandwidth of the conventional band. The narrowband performance is unavoidable because a small antenna has a high Q factor which implies a narrow bandwidth. Therefore, a trade-off between size reduction and bandwidth has to be chosen.

Devices such as diodes and transistors are non linear elements. The non linearity is great utility for functions such as amplification, detection, and frequency conversion.

However, non linear devices may cause undesirable responses such as gain suppression and generation of spurious frequency components. These effects may produce increased losses and signal distortion. Future work may focus on the study of undesirable effects, such as inter-modulation distortion (IMD), caused by the use of varactors and switches. Also, the implementation using linear elements such RF MEMS, can be considered.

In the case of the reconfigurable patch, it was shown that the reduction in the antenna resonant frequency by slot lengthening results in increased radiation behind the ground plane. Therefore, the front-to-back (F/B) radiated power ratio decreases. Using a meandered slot could be an effective method to reduce the spurious radiation since it is turned several times to create opposing current directions to cancel the spurious radiation. Therefore, future work may focus in re-designing the antenna using a meandered coupling slot.

In order to meet stringent requirements of RF/Microwave systems, highly selective filters with a single pair of transmission zeros, such as cross coupled filters, can be used. The presence of the transmission zeros near the passband improves the skirt selectivity of the filter. If the selectivity is not high enough, another pair of transmission zeros can be introduced by using cascaded quadruplet (CQ) filter. The filtering antennas presented in Chapter Five are based on Chebyshev equal ripple response. For the Chebyshev response, the resonators are direct-coupled and the transmission zeros are located at ∞. Therefore, the direct-coupled filters (Chebyshev and Butterworth response) exhibit lower selectivity. Future work can focus on designing the filtering antenna using cross coupled filters and CQ filters. In this case, the gain response of the antenna is expected to exhibit transmission zeros which improves the skirt selectivity and the out of band gain suppression. However, such a

filtering antenna might achieve much lower gain as compared with a conventional one. The degradation in the gain is due to the presence of many cross-coupled resonators. Future work should be done to show if the out of band gain suppression offsets the degraded in-band gain.

APPENDIX A

REVIEW OF THE LITERATURE OF FREQUENCY RECONFIGURABLE ANTENNAS
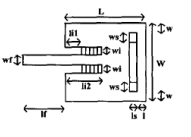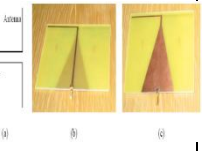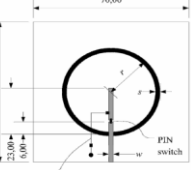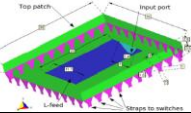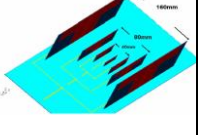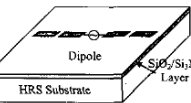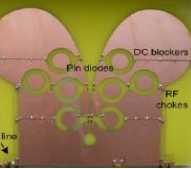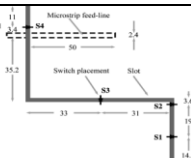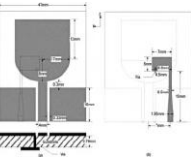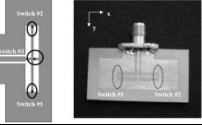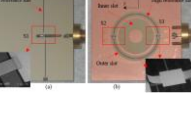
Frequency reconfigurable antennas using different types of switches [1-30] are summarized in Table A.1. Table A.2 shows the reconfigurable antennas utilizing varactor diodes [31-50]. The reconfiguration mechanism and the performance are also discussed.

Table A.1 shows that several antennas employing switches. Antennas reported in Refs. [1, 3, 4, 9, 13, 14, 18, 20, 22, 24, 26, 28, 29, and 30] are utilizing PIN diode switches. The usage of PIN diodes implies designing biasing circuitry to provide the bias voltage to activate/deactivate the diodes.

Reconfigurable antennas utilizing RF Micro Electro-Mechanical System (MEMS) switches presented in [4, 11, 12, 17, 19, 20, 21, and 25] are. Also, antennas using other types of switches such as silicon diode or GaAs FET are presented. The structure of the antenna, the number and type of switches, and the performance are summarized.

Table A.1: Reconfigurable antennas utilizing switches

Ref.	Antenna Figure	Antenna structure	Size (mm)	Switching band (GHz)	Frequency switching technique	Switch type	Number of switch
[1]		Inductively coupled patch	170x120	State 1: 2.96 State 2: 3.24 State 3: 3.76 State 4: 5.28 State 5: 7.96	Altering the length of the coupling slot	PIN diode	8
[2]		PIFA	98×42	Mode 0: 0.85,0.92 and 1.8 Mode 1: 0.85, 0.92, 1.9, and 2.05	Switching feed location	Pin diode	2
						GaAs FET	1
						MEMs	1
		PIFA	100.5×42	Mode 0: 0.8,0.9,1.8,1.9 Mode 1: 1.8,1.9,2.1,2.4	Switching the ground	Pin diode	1
						GaAs FET	1
						MEMs	1
[3]		Stacked square patches	130×130	State 1: 1.75 State 2: 0.69	Switching between stacked square and PIFA antenna	PIN diode	3
[4]		Nested patch	100x100	State 1: 2.4 State 2: 5.6	Activating switches connected inside nested patch	PIN diode	4
[5]		Microstrip planar antenna with a rectangular slot	48×48	Mode1: 3.43 Mode2: 3.11	Altering the length of the path	Switching Diode	2
[6]		Sierpinski fractal antenna	25×20	State 1: 18 State 2: 9.4 State 3: 5.7 & 16.7 State 4: 2.4, 9 & 16.4	RF MEMS used to sequentially activate parts of the sierpinsky antenna	MEMS	6

[7]		Rectangular patch	100x100	State 1: 1.8 State 2: 1.9 State 3: 2.4	Activating switches in the inset fed and across the patch	RF MEMS	4
[8]		Printed dipole	64×64	State 1: 0.9 State 2: 1.1 State 3: 1.21 State 4: 1.5 State 5: 18 State 6: 2.1 State 7: 2.8	Incorporating six ideal switches on each dipole arm	Ideal switch (copper pad)	12
[9]		Annular slot antenna	70×70	Mode 1: 1.6 Mode 2: 2.3	Change the length of the microstrip feed	PIN diode	1
[10]		Patch antenna	30×30	Covers from 1.7 to 2.7	Incorporating switches to connect metal portions to the ground	Ideal switch (copper pad)	8
[11]		Integrated with 7 switches	160×76	State 1: 0.8-0.9 State 2: 1.7-2.5 State 3: 3.3-3.6 State 4: 5.1-5.9	Switching between different length dipoles	MENS	4
[12]		Dipole antenna	16×7	Mode 1: 8.98 Mode 2: 4.86	By activating the switches in the gap of each dipole arm	MEMS	2
[13]		Vivaldi antenna	144×100	States 1 – 3: 1 to 3.2	Four pairs of switchable ring slots are etched to change the wideband operation into narrowband	PIN diode	8
[14]		Slot antenna	76.6×64	State 1: 0.561 State 2: 0.627 State 3: 0.711 State 4: 0.95	Altering the length of the slot using switches	PIN diode	4
[15]		Two ports: PIFA and monopole	54×35	Port 1: 3 to 11 Port 2: 3 matching circuits to obtain resonance at 4, 8, and 10	Port 1 is wideband performance, and port 2 can be tuned be using matching circuits	Not shown	Not shown
[16]		CPW-fed folded dipole antenna	Not shown	state 1: 5.1 state 2: 5.6	By activating the switches	Ideal switch (copper pad)	3
[17]		Annular slot antenna	25×25	State 1: 2.4 State 2: 5.3	Changing the feed line length	MEMS	3

Ref	Figure	Antenna type	Size	Frequency/States	Description	Switch	No.
[18]		Slot-coupled patch	2.6×2.8	Mode 1 to Mode 5: 9.8 to 19	Altering the coupling between the H-shaped patch antenna and two parasitic elements	PIN diode	8
[19]		Printed dipole	Not shown	Cover from 8 to 12	Altering the length of each dipole arm	MEMS	8
[20]		Triangular patch antenna	Not shown	State 1: 1.41 State 2: 1.87	Two spur-lines are etched in the patch. Two PIN diodes are placed to switch the lines on/off	PIN diode	2
[21]		PIFA	100×40	State 1: 0.82-0.96 State 2: 1.7-1.88 State 3: 1.85-1.99 State 4: 1.92-2.17	Switching connection for impedance matching	MEMS	2
		Two PIFAs	100×40	State 1: 0.82-0.849 State 2: 0.88-0.92 State 3: 0.93-0.96 State 4: 0.82-0.89 State 5: 1.71-1.79 State 6: 1.85-1.91 State 7: 1.85-1.99 State 8: 1.92-2.17	Switched connection for impedance matching	MEMS	8
[22]		Two rectangular patches	38.1x38.1	State 1: 10 State 2: 10.5	By controlling PIN diode placed in a thin strip connecting two rectangular patches	PIN diode	1
[23]		Two printed monopoles	50×50	Port 1: 3.1 to 10.6 Port 2: State 1: 5.5 and 9.15 State 2: 4.85 and 8.15 State 3: 4.4, 7.41 and 10.33	The wideband monopole covers from 3 to 11 GHz. The narrowband monopole utilizes two switches to change its length	Ideal Switch (Copper pad)	2
[24]		Slotted rectangular patch	24×20	State 1: 0.67 State 2: 0.85 State 3: 0.95 State 4: 1.18	Switching between different posts	PIN dipole	3
[25]		Microstrip patch antenna	120×120	Mode 1 to Mode 8: (1.8 – 2.4)	Changing the size of the patch	MEMS	4
[26]		Circular patch with sectoral slot	Not shown	State 1: 1.78 State 2: 2.07 State 3: 2.29	Circular patch with sectoral slot which is shunted at different positions using PIN diodes	PIN diode	2

[27]		Slot antenna	Not shown	Mode 1: 8.1 to 11 Mode 2: 2.6 to 11 Mode 3: 4.3 and 10.3	Utilizing six switches to achieve three different frequency bands	Ideal switch (Copper pad)	6
[28]		Stacked patches	39×39	State 1: 1.8-2.1 State 2: 0.6	Switching between two stacked patches	PIN dipole	3
[29]		patch and two parasitic dipoles	100×65	State 1: 10 & 11 State 2: 5 & 15 State 3: 5 & 15 State 4: 14 & 15	Switching the patch and folded dipoles	PIN diode	4
[30]		E-shaped patch	22×13	State 1: 9-15 State 2: 7.5-10.7	Altering the length of E-shaped patch using switches	PIN diode	19

Table A.2 Reconfigurable antennas incorporating varactor diodes

Ref.	Antenna Figure	Antenna structure	Size (mm)	Tuning range (GHz)	Tuning technique	Varactor range (pF)	Number of varactor
[31]		Dual-band bent slot antenna	150×110	Band 1: 1.1 to 1.5 Band 2: 1.7 to 2.9	Dual-frequency operation is achieved by loading a slot antenna with two varactors placed in proper locations along the slot	0.5 to 2.2	2
[32]		Rectangular patch antenna	60×60	1.4 to 2.3	Parallel varactor diodes are placed to connect two rectangular patches	0.1 to 15	6
[33]		Microstrip Patch	Not shown	Two bands: 1.47 to 1.57 1.75 to 1.82	By utilizing a varactor diode in C-shaped slot line	Not shown	1
[34]		Annular slot antenna	300×300	1.9 to 2.5	A varactor is placed at the shorting pin and ground	1.4 to 21	1
[35]		Rectangular patch	77×57	2.6 to 3.3	The varactor is placed on the opposite side of the patch and is connected to the microstrip line at the same position with the feeding probe.	0.4 to 1.5	1

[36]		L-shaped slot	52×52	2.1 – 2.8	Altering the capacitors to reconfigure the slot	0.6 to 4.7	2
[37]		Patch antenna	44×44	1.6 to 1.8	Changing the varactor diodes to alter the capacitance	1.02 to 7.37	2
[38]		Meander line antenna	Not shown	0.4 to 0.7	A varactor diode is placed in series with the upper and lower parts of the meander line	Not shown	1
[39]		PIFA with external matching circuit	44×19.8	0.9 to 2.4	PIFA is connected to an external matching circuit consisting of three capacitors	Capacitor 1: 0.6 to 2.09 Capacitor 2: 0.03 to 3.13 Capacitor 3: 0.33 to 3.47	3
[40]		Micostrip patch	Not shown	Two bands: 0.9 to 1.6 1.58 to 2.2	By inserting a varactor diode in the gap between the patch and parasitic strip	Not shown	1
[41]		Folded slot antenna	40×40	3.2 to 3.3	The resonant frequency of the slot/coplanar patch is tuned using a varactor diode inserted at the radiating slot	1.1 to 1.5	1
[42]		Four sub-Patches	50×50	5 tunable bands to cover 0.92 to 2.98	By inserting a varactor diode at the input of the sub-patches to tune the resonant frequency	2 to 14	4
[43]		Slot antenna	35×20	Mode 1: 0.4 to 0.9 Mode 2: 0.8 to 1.5	A PIN diode and a varactor diode are utilized to tune two resonant modes	Not shown	1
[44]		Quasi-Yagi folded dipole	Not shown	6-6.6	A pair of varactors loaded in the folded dipole	0.1 to 1	2
[45]		IFA	90×40	0.47 to 0.69	A varactor diode is loaded into the IFA element to enable tuning the resonant frequency	0.1 to 1	1
[46]		CPW-fed dipole antenna	50×30	Band 1: 2.06-2.36 Band 2: 3.95-3.50	Two varactors placed at the middle of each arm	Not shown	2

[47]		Printed Loop-Monopole	Not shown	0.7 to 6	The monopole achieves tuning the lower frequency by utilizing an LC tuner while the loop achieves tuning of the upper frequency band by utilizing RF switches	0.2 to 3.8	1
[48]		Capacitively loaded loop	50×50	0.4 to 0.9	Utilizing three varactor diodes and dc isolation capacitors to achieve the frequency tunability	0.1 to 4	3
[49]		Split ring resonator antenna	80×80	1.8 t 2.1	By inserting a varactor diode into a SRR	0.8 to 4.2	1
[50]		PIFA	80×40	1.6 to 2.1	A varactor diode is inserted between the slot and bias	0.2 to 1.2	1

References:

[1] J. M. Laheurte, "Switchable CPW-fed Slot Antenna for Multifrequency Operation", Electron. Lett.6 December 2001, vol37.

[2] A. C. K. Mak, C. R. Rowell, R. D. Murch, and C. – L. Mak, "Reconfigurable multiband antenna designs for wireless communication devices", *IEEE Transaction on Antennas and Propagation*, Vol. 55, Issue 7, 2007, pp. 1919-1928.

[3] M. Ali, T. M. Sayem, and V. K. Kunda, "A reconfigurable stacked microstrip patch antenna for satellite and terrestrial links", *IEEE Transactions on Vehicular Technology*, Vol. 56, Issue 2, 2007, pp. 426-435.

[4] Ibrahim Tekin and Michael Knox, "Reconfigurable dual band microstrip patch antenna for software defined radio applications", *IEEE International Conference on Wireless Information Technology and Systems (ICWIST)*, 2010, pp. 1-4.

[5] K. Sakamoto, E. Nishiyama and M. Aikawa, "Active microstrip planar antenna for frequency switching", *Electronics and Communications in Japan, Part 1*, Vol. 88, No. 11, pp. 1-8, 2005,.

[6] N. Kingsley, D. E. Anagnostou, M. Tentzeris, and J. Papapolymerou, "RF MEMS sequentially reconfigurable sierpinski antenna on a flexible organic substrate with novel DC-Biasing technique", *Journal of Micro electromechanical Systems,* vol. 16, , pp. 1185-1192, 2007.

[7] Sinan Onat, Lale Alatan, and Simsek Demir, "Design of triple-band reconfigurable microstrip antenna emplying RF MEMS switches," *IEE Antennas and Propagation Society International Symposium, vol.2, pp.2812-1815, 2004.*

[8]   A. Mirkamali, P. S. Hall, and M. Soleimani, "Wideband reconfigurable printed dipole antenna with harmonic trap", *IEEE International Workshop in Antenna Technology Small Antennas and Novel Metamaterials,* pp.188-191, 2006.

[9]   Markus Berg, Mikko Komulainen, Erkki Salonen, and Heli Jantunen, "Frequency reconfigurable microstrip-fed annular slot antenna", First European Conference on *Antennas and Propagation., EuCAP,* pp.1-6, 2006.

[10]   Javier Leonardo, A. Quijano, and G. Vecchi, "Optimization of an innovative type of compact frequency-reconfigurable antenna", *IEEE Transactions* on *Antennas and Propagation.,* vol. 57, pp. 9-18, 2009.

[11]   T. Wu, R. L. Li, S. Y. Eom, K. Lim, S. I. Jeon, J. Laskar, and M. M. Tentzeris, "A multiband/scalable reconfigurable antenna for cognitive radio base station", *IEEE International Symposium of Antennas and Propagation Society, AP-S,* pp. 1-4, 2008.

[12]   J. Kiriazi, H. Ghali, H. Ragaie, and H. Haddara, "Reconfigurable dual-band dipole antenna on silicon using series MEMS switches", *IEEE Antennas and Propagation Society International Symposium,* vol.1, pp. 403-406, 2003.

[13]   M. R. Hamid, Peter S. Hall, Peter Gardner, and F. Ghanem, "Frequency reconfigurable Vivaldi antenna", *European Conference in Antennas and Propagation (EuCAP)*, pp. 1-4, *2010.*

[14]   Dimitrios Peroulis, Kamal Sarabandi, and Linda P. B. Katehi, "Design of reconfigurable slot antennas", *IEEE Transactions* on *Antennas and Propagation.,* vol. 53, pp. 645-654, 2005.

[15]   Elham Ebrahimi, James Kelly, and Peter S. Hall, "A reconfigurable narrowband antenna integrated with wideband monopole for cognitive radio

applications", *IEEE International Symposium on Antennas and Propagation Society, APSURSI,* pp. 1-4, *2009.*

[16]   G. H. Huff, and J. T. Bernhard, "Frequency reconfigurable CPW-fed hybrid folded slot/slot dipole antenna", *IEEE International Conference in Wireless Communications and Applied Computational Electromagnetics, ACES,* pp. 574-577, 2005.

[17]   B. A. Cetiner, Q. Xu, and L. Jofre, "Frequency reconfigurable annular slot antenna", *IEEE Antennas and Propagation International Symposium,* pp. 5845-5848, 2007.

[18]   L. Le Garrec, R. Sauleau, and M. Himdif, "A 2:1 band frequency-agile active microstrip patch antenna", *The Second European Conference* on *Antennas and Propagation., EuCAP 2007,* pp. 1-6, *2007.*

[19]   Christos G. Christodoulou, L. F. Feldner, V. Zachou, and D. Anagnostou, "Planar reconfigurable antennas", *European Conference* on *Antennas and Propagation., EuCAP,* pp. 1-7, *2006.*

[20]   Y.J. Sung, B.Y. Kim, T.U. Jang, and Y.S. Kim, "Switchable Triangular Microstrip Patch Antenna for Dual-Frequency Operation," Antennas and Propagation Society International Symposium, 2004, vol.1, pp265-268.

[21]   K. Boyle, P. G. Steeneken, Z. Liu, Y. Sun, A. Simin, T. Huang, E. Spits, O, Kuijken, T. Roedle, and F. Van Straten, "Reconfigurable antennas for SDR and cognitive radio", *European Conference* on *Antennas and Propagation, EuCAP,* pp. 1-6, 2007.

[22]   Manoj Singh, Ananjan Basu, and Shiban K. Koul, "Switchable Frequency Bands Microstrip Antennas," IEEE International Workshop on Antenna Technology, 2009, IWAT 2009,pp.1-4.

[23] M. Al-Husseini, Y. Tawk, C. G. Christodoulou, K. Y. Kabalan, and A. El Hajj, "A reconfigurable cognitive radio antenna design", *IEEE Antennas and Propagation Society International Symposium (APSURSI),* pp. 1-4, *2010.*

[24] Abdel-Fattah Sheta, and Samir F. Mahmoud, "A widely tunable compact patch antenna", *IEEE Antennas and Wireless Propagation Letters,* vol. 7, pp. 40-42, 2008.

[25] T. Y. Han and C. T. Huang, "Reconfigurable monopolar patch antenna", *Electronics Letters*, Vol. 46, pp. 199-200, 2010.

[26] Das Krishna, C. K. Aanandan, P. Mohanan, K. Vasudeban, "Electrically switchable circular microstrip antenna with sector-slot for multiple frequency operation," Antennas and Propagation Society International Symposium 2006, APSURSI 09, pp.4277-4280, 2006.

[27] James Kelly and Peter Hall, "Reconfigurable slot antenna for cognitive radio", *IEEE Antennas and Propagation Society International Symposium (APSURSI),* pp. 1-4, *2009.*

[28] V. Kunda, and M. Ali, "Reconfigurable stacked patch antenna for satellite and terrestrial applications", *IEEE Topical Conference* on *Wireless Communication Technology,* pp. 152-153, 2003.

[29] Elyas Palantei, David V. Thiel, and Steven G. O'Keefe, "Rectangular patch with parasitic folded dipoles: a reconfigurable antenna", *International Workshop* on *Antenna Technology: Small Antennas and Novel Metamaterials, iWAT,* pp. 251-254, *2008.*

[30] B. Z. Wang, S. Xiao and J. Wang, "Reconfigurable patch-antenna design for wideband wireless communication systems", *IET Microwaves, Antennas, and Propagation*, Vol. 1, Issue 2, pp. 414-419, 2007.

[31] N. Behdad, and K. Sarabandi, "Dual-band reconfigurable antenna with a very wide tunability range", *A IEEE Transactions* on *ntennas and Propagation,* vol. 54, pp. 409-416, 2006.

[32] N. Fayyaz, S. Safavi-Naeini, E. Shin, and N. Hodjat, "A novel electronically tunable rectangular patch antenna with one octave bandwidth", *IEEE Canadian Conference* on *Electrical and Computer Engineering,* vol. 1, , pp. 25-28, 1998.

[33] S.V. Shynu, G. Augustin, CK. Aanandan, and K. Vasusevan, "C-Shaped Slot Loaded Reconfigurable Microstrip Antenna," Electronics Letters, vol42, no6, 2006.

[34] P. R. Urwin-Wright, G. S. Hitton, I. K. Graddock, and P. N. Fletcher, "A reconfigurable electrically-small antenna operating in the 'DC' mode", *IEEE Semiannual Vehicular Technology Conference,* vol. 2, pp. 857-861, *2003.*

[35] S. L. S. Yang, A. A. Kishk, and K. F. Lee, "Frequency reconfigurable U-slot microstrip patch antenna", *IEEE Antennas and Wireless Propagation Letters*, Vol. 7, pp. 127-129, 2008.

[36] M. –I. Lai, T. –Y. Wu, J. –C. Hsieh, C. –H. Wang, and S. –K. Jeng, "Design of reconfigurable antennas based on an L-shaped slot and PIN diodes for compact wireless devices", *IET Microwaves, Antennas, & Propagation,* vol. 3, pp. 47-54, 2009.

[37] J. Kishor, P. Kumar, and A. K. Shrivastav, "Designing of varactor tuned microstrip patch antenna", *International Conference* on *Recent Advances in Microwave Theory and Applications, , MICROWAVE*, pp. 907-909, *2008.*

[38] R. J. DeGroot, D. P. Gurney, K. Hutchinson, M. L. Johnson, S. Kuffner, A. Schooler, S. D. Silk, and E. Visotsky, "A cognitive-enabled experimental

system", *IEEE International Symposium* on *New Frontiers in Dynamic Spectrum Access Networks, DySPAN2005,* pp.556-561*, 2005.*

[39]   B. K. Fankem, K. L. Melde, and Z. Zhen, "Frequency reconfigurable planar inverted F antenna (PIFA) with software-defined match control", *IEEE Antennas and Propagation Society International Symposium,* pp. 81-84, *2007.*

[40]   Sung Y. J. "Simple Tunable Dual-band Microstrip Patch Antenna", Electron. Lett., vol.45, pp.666-667, 2009.

[41]   V. Palukuru, M. Komulainen, T. Tick, J. Perantie, and H. Jantunen, "Low-sintering-temperature ferroelectric-thick films RF properties and an application in a frequency-tunable folded slot antenna", *IEEE Antennas and Wireless Propagation. Letters,* vol. 7, pp. 461-464, 2008.

[42]   H. Abutarboush, R. Nilavalan, K. Nasr, H. Al-Raweshidy, and D. Budimir, "Widely tunable multiband reconfigurable patch antenna for wireless applications", *European Conference in Antennas and Propagation (EuCAP),* pp.1-3, *2010.*

[43]   H. Li, J. Xiong, Y. Yu, and S. He, "A simple compact reconfigurable slot antenna with a very wide tuning range", *IEEE Transactions in Antennas and Propagation,* Vol. 58, Issue, 11, pp. 3725-3728, 2010.

[44]   Pei-Yuan Qin, A. Weily, Y. Guo, T. Bird, and Chang-Hong Liang, "Frequency reconfigurable quasi-yagi folded dipole antenna", *IEEE Transactions on Antennas and Propagation,* Vol. 58, Issue 8, pp. 2742-2747, 2010.

[45]   M. Berg, M. Komulainen, V. Palukuru, H. Jantunen, and E. Salonen, "Frequency-tunable DVB-H antenna for mobile terminals", *IEEE Antennas and Propagation Society International Symposium,* pp. 1072-1075, *2007.*

[46]   A. T. Kolsrud, Ming-Yi Li, and K. Chang, "Frequency tunable CPW-fed CPS dipole antenna using varactors", *IEEE Antennas and Propagation Society International Symposium,* Vol. 1, pp. 308-311, *1998.*

[47]   M. Hossain, and T. Yamagajo, "Reconfigurable printed antenna for a wideband tuning", *European Conference in Antennas and Propagation (EuCAP),* pp. 1-4, *2010.*

[48]   Y. Yu, J. Xiong, H. Li, and S. He, "An electrically small frequency reconfigurable antenna with a wide tuning range", *IEEE Antennas and Wireless Propagation Letters,* Vol. 10, pp. 103-106, 2011.

[49]   X. Cheng, D. Senior, J. Whalen, and Y. Yoon, "Electrically small tunable split ring resonator antenna", *IEEE International Symposium on Antennas and Propagation Society (APSURSI),* pp. 1-4, *2010.*

[50]   Se-Keun Oh, Yong-sun Shin, and Seong-ook Park, "A novel PIFA type varactor tunable antenna with U-shaped slot", *International Symposium* on *Antennas, Propagation & EM Theory (ISAPE)*, pp. 1-3, 2006.

APPENDIX B

ANTENNA PARAMETERS AND MEASUREMENTS

The purpose of this section is to provide introductory insights into parameters and measurements of antennas. These parameters include return loss, radiation pattern, polarization, directivity, and gain. This section also describes some antenna measurements.

B.1. Definition

An antenna can be defined as a metallic device that radiates or receives radio waves. The antenna can be considered as a transitional structure between transmission line and free space [1]. Thus, it converts electromagnetic photons into circuit currents and vice versa. The transmission line, which could be a coaxial line, waveguide or planar transmission line is used to transport the electromagnetic energy from the transmitter to the antenna or from the antenna to the receiver. It is required to transmit the energy with minimum attenuation. Therefore, the transmission lines guide energy, antennas radiate (or receive), while resonators store energy [2].

B.1. Input Impedance, Reflection Coefficient and Bandwidth

For circuit theory, the antenna is considered as a load connected to a transmission line as shown in figure B1. The input impedance of an antenna is the ratio between the voltage and the current at its input.

$$Z_{in} = \frac{V_{in}}{I_{in}} = R_a + j\,X_a \qquad \text{(B.1)}$$

Where I_{in} and V_{in} represent the input current and the input voltage of the antenna respectively. The input impedance is a complex number; R_a and X_a are the resistance and reactance of the antenna respectively. The real part of the input impedance consists of two components:

$$R_a = R_r + R_L \qquad \text{(B.2)}$$

Where R_r and R_L are the radiation and loss resistances respectively. In practise, the desired input impedance is 50 Ω or 75 Ω.
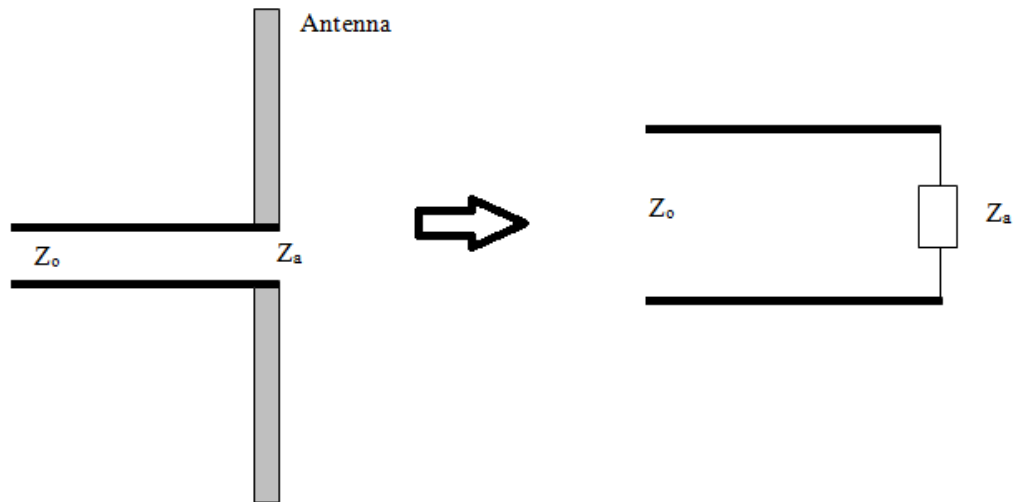

Figure B.1: Antenna input impedance model [3].

Impedance matching is very important since maximum power is delivered when the load is matched to the line and hence power loss in the feed line is minimized. The reflection coefficient, return loss, and standing wave ratio (SWR) can be used to determine if the load is matched to the feed line. The reflection coefficient Γ is the ratio of the reflected voltage to the incident (forward) voltage at the input.

$$\Gamma = \frac{Z_a - Z_o}{Z_a + Z_o} \qquad \text{(B.3)}$$

When the load (antenna) is mismatched, not all available power from the source is delivered to the load. This loss is known as return loss, expressed in dB, is given by:

$$RL = -20 \log_{10} |\Gamma| \tag{B.4}$$

A quantity known as voltage standing wave ratio (VSWR), is measure of mismatch, is given by:

$$VSWR = \frac{1 + |\Gamma|}{1 - |\Gamma|} \tag{B.5}$$

The VSWR is a real number such that $1 \leq VSWR \leq \infty$. A unity VSWR implies perfect match.

The scattering (S) parameters, which can be measured using network analyzer, provide a full description of a microwave network. The S parameters are reflection parameters (S_{ij} for i = j) and transmission parameters (S_{ij} for i # j). The S11 represents the reflection coefficient in db and given by:

$$S_{11} = 10 \log_{10} \Gamma \tag{B.6}$$

The commonly required specification of an antenna is that $S_{11} \leq$ - 10 dB.

B.2. Radiation Pattern and Directivity

The radiation pattern is a plot of the energy radiated by the antenna. Radiation properties of the antenna include radiation intensity, directivity, gain and polarization [1]. There are different types of radiation pattern such as isotropic, omni-directional, and directional pattern.
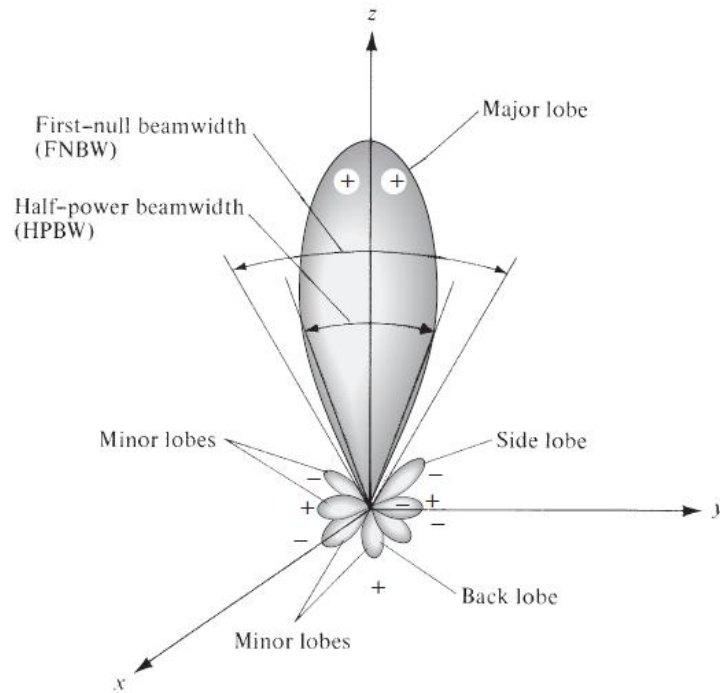
Figure B.2: Radiation pattern of an antenna [1].

The radiation intensity, U, is power radiated (or received) from (or by) the antenna per unit sold angle. The radiation intensity, which is one of the far-field parameters, can be expressed mathematically as

$$U = r^2 W \tag{B.7}$$

Where U is the radiation intensity (W/unit solid angle)

W_{rad} is the radiation density (W/m^2)

The directivity of the antenna is given by the ratio of the radiation intensity in a certain direction to the average radiation intensity [2].

$$D = \frac{U}{U_0} = \frac{4\pi U}{P_{rad}} \tag{B.8}$$

Where P_{rad} is the total power radiated by the antenna and U_0 is the average radiation intensity. The directivity is dimensionless.

B.3. Efficiency and Gain

The total efficiency of the antenna considers the losses at the input and the losses within the antenna. These losses are due to the reflections due to the mismatch, and conductor and dielectric losses. The total efficiency of the antenna is given by

$$e_t = e_r e_c e_d \tag{B.9}$$

where

e_t is the total efficiency

e_r is the reflection efficiency

e_c is the conduction efficiency

e_d is the dielectric efficiency

Another important parameter of the antenna is the gain. The gain is the ratio of the radiation intensity in a certain direction to the radiation intensity that results if the input power was radiated isotropically. The radiation intensity of an isotropic radiator is equal to the accepted power divided by 4Π. Mathematically, this can be expressed as:

$$\text{Gain} = 4\Pi \frac{\text{radiation intensity}}{\text{total input power}} = 4\Pi \frac{U(\theta,\phi)}{P_{in}} \tag{B.10}$$

The gain is related to the directivity as given by:

$$G = D\, e_{cd} \tag{B.11}$$

B.4. Polarization

The polarization of an antenna is the polarization of the wave radiated (received) by the antenna. The polarization of radiated waves is defined as the curve traced by the end of the arrow representing the instantaneous electric field vector [1]. There are

three types of polarization, which are linear, circular, and elliptical polarization. The polarisation is expressed with reference to the electric field. While Co-polarisation represents the polarization that the antenna to radiates (receives), cross-polarisation represents is orthogonal to the co-polarization.

B.5. Measurement Equipments

The vector network analyzer (VNA), shown in Figure B.3, is used to measure the return loss of the antenna.

Figure B.3: The vector network analyzer

The radiation pattern and the realized gain of antenna are measured using the typical instrumentation, shown in Figure B.4. The instrumentation must be designed to cover a wide range of frequencies, and it usually can be classified into five categories [3] as below:

1. transmitting antenna
2. receiving system

3. positioner and recorder

4. data processing unit

For all the antennas design presented in this work, the radiation patterns and gain were measured inside an anechoic chamber in N510, School of Electronic, Electrical and Computer Engineering, University of Birmingham.
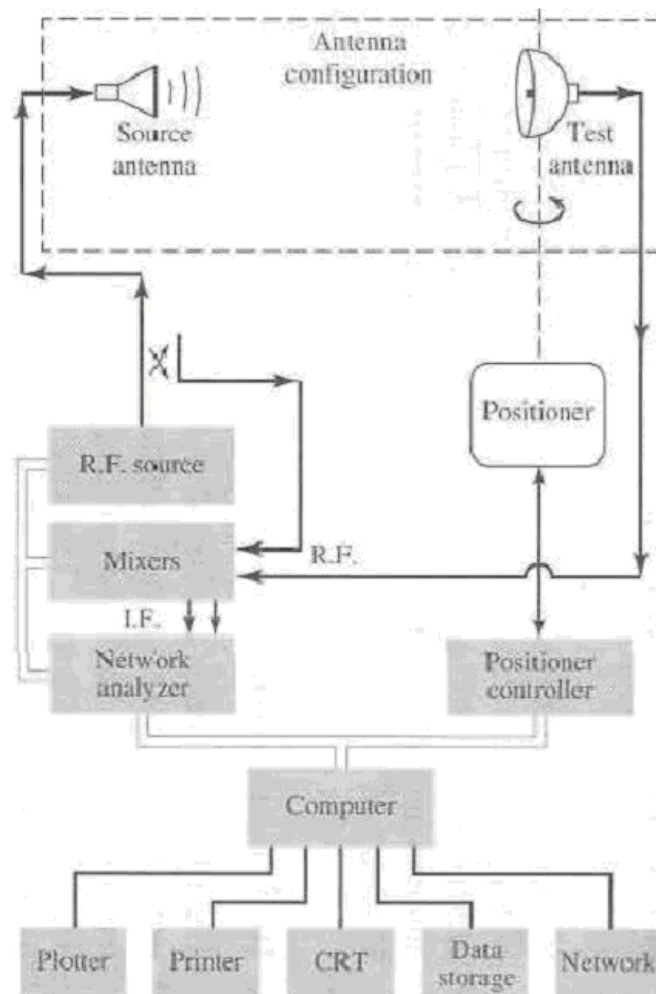

Figure B4: Instrumentations for radiation pattern measurement [1]

References:

[1]   C. A. Balanis, Antenna Theory, Analysis and Design, 3rd ed: John Wiley & Sons, Inc, 2005

[2]   John D. Kraus, Antennas, 2nd edition: McGraw-Hill, 1998

[3]   Yi Huang, and Kevin Boyle, Antennas: From Theory to Practice, Wiley-Blackwell, 2008.

Appendices C-E have been removed from the electronic copy of this thesis due to copyright restrictions